JOURNAL OF FLUID MECHANICS

VOLUME 10 PART 2

MARCH 1961

PUBLISHED BY

CAMBRIDGE UNIVERSITY PRESS

BENTLEY HOUSE, 200 EUSTON ROAD, LONDON, N.W.1

AMERICAN BRANCH: 32 EAST 57TH STREET, NEW YORK 22, N.Y.

Price 30*s.* (*U.S.A.* $5.00)

The JOURNAL OF FLUID MECHANICS exists for the publication of theoretical and experimental investigations of all aspects of the mechanics of fluids, and is issued in four parts per volume.

EDITORS

DR G. K. BATCHELOR, DR T. BROOKE BENJAMIN

Department of Applied Mathematics and Theoretical Physics, University of Cambridge, Free School Lane, Cambridge, England

ASSISTANT EDITORS

DR J. R. A. PEARSON, DR O. M. PHILLIPS

ASSOCIATE EDITORS

PROF. G. F. CARRIER

Pierce Hall, Harvard University, Cambridge 38, *Massachusetts, U.S.A.*

DR W. C. GRIFFITH

Lockheed Missiles and Space Division, Palo Alto, California, U.S.A.

M. J. LIGHTHILL

Royal Aircraft Establishment, Farnborough, Hampshire, England

PROF. R. R. LONG

School of Engineering, The Johns Hopkins University, Baltimore 18, *Maryland, U.S.A.*

DR P. G. SAFFMAN

Department of Mathematics, King's College, London, W.C. 2, *England*

Authors wishing to have papers published in the JOURNAL should communicate them to any one of the persons named above, choosing one in their own country where possible.

Authors are urged to ensure that their papers are written clearly and attractively, in order that their work will be readily accessible to readers.

Manuscripts should be typed in double spacing on one side of the paper only, with references listed at the end in alphabetical order of authors. Drawings should be done on a large scale in Indian ink on tracing cloth or drawing paper, the lettering being shown clearly in pencil for reproduction by the printer; the list of captions should be typed at the end of the manuscript. Proofs of papers from overseas will usually be despatched to authors by airmail. There is no charge for publication. Authors are entitled to receive 50 offprints of a paper in the JOURNAL free of charge, and additional offprints can be purchased if ordered in advance.

SUBSCRIPTIONS

The subscription price for a volume of four parts is £5. 10*s*. net, post free, payable in advance; separate parts 30*s*. net, plus postage. Subscriptions may be sent to any bookseller, or to the Cambridge University Press, Bentley House, 200 Euston Road, London, N.W. 1.

Subscribers in the United States should send their orders to the Cambridge University Press, American Branch, 32 East 57th Street, New York 22, N.Y. The subscription price per volume is $18.50, post free, payable in advance; separate parts $5.00, plus postage.

Quotations for available back volumes and parts may be obtained on application to the Cambridge University Press.

Deposition of a viscous fluid on the wall of a tube

By G. I. TAYLOR
Cavendish Laboratory, Cambridge

(Received 27 September 1960)

Measurements of the amount of fluid left behind when a viscous liquid is blown from an open-ended tube are described.

Introduction

When air is blown into one end of a tube containing a viscous fluid it forms a round-ended column which travels down the tube forcing some of the liquid out at the far end and leaving a fraction m in the form of a layer covering the wall. This fraction has been measured in some cases by Fairbrother & Stubbs (1935), who were interested in the question whether a bubble of air in a capillary tube through which a fluid is flowing is a true index of the velocity of the flow. If U is the velocity of a bubble and U_m the mean velocity of the fluid ahead of it,

$$m = \frac{U - U_m}{U}. \tag{1}$$

Fairbrother & Stubbs's experiments were limited to the case when m is small, and in that case they found as an empirical relationship, which covered experiments made with fluids in which the velocity U, the surface tension T and the viscosity μ all varied,

$$m = 1{\cdot}0(\mu U/T)^{\frac{2}{3}}. \tag{2}$$

As these authors point out, it is to be expected that m should be a function of $\mu U/T$ since that is the only non-dimensional combination of these three symbols, but that m should be proportional to $(\mu U/T)^{\frac{2}{3}}$ has not been explained, nor has the coincidence that the empirically determined constant is 1·0. Fairbrother & Stubbs point out that there are theoretical and experimental reasons for believing that the thickness of the film left on a plane sheet when it is pulled vertically out of a fluid is proportional to $U^{\frac{1}{2}}$. This, however, is not a proper analogy since the existence of the film is due to a balance of viscous and gravitational forces, whereas when the fluid is blown out of a horizontal tube gravity plays little part in the phenomenon.

The empirical relationship (2) can only be valid when m is small; in fact if $\mu U/T$ is greater than 1 so that the corresponding value of m is greater than 1, (2) is meaningless. In the experiments to be described it was found that (2) is a good approximation in the range $0 < \mu U/T < 0{\cdot}09$. The maximum value of $\mu U/T$ obtained in Fairbrother & Stubbs's measurements was 0·014 so that they were well within the range in which (2) holds. When $\mu U/T$ increases beyond 0·09, m is less than would be predicted by (2). The experiments were extended,

using very viscous fluids, to $\mu U/T = 1{\cdot}9$ (i.e. to 135 times Fairbrother & Stubbs's maximum value) when m had reached 0·55. The apparent trend of the curve of experimental points seemed to indicate that m was approaching an asymptotic value at that stage. It seems therefore that if one attempts to blow a very viscous fluid out of a tube more than half may be left behind when the air column breaks through at the far end of the tube.

Experimental details

The method adopted was similar to that used by Fairbrother & Stubbs, but since only one long interface between air and fluid, rather than separate bubbles, was required, the method of introducing the air column needed careful design. The apparatus is shown diagrammatically in figure 1. Since the object of the experiment was to obtain large values of $\mu U/T$ without increasing the speed of flow to such an extent that the stresses due to inertia were comparable with those

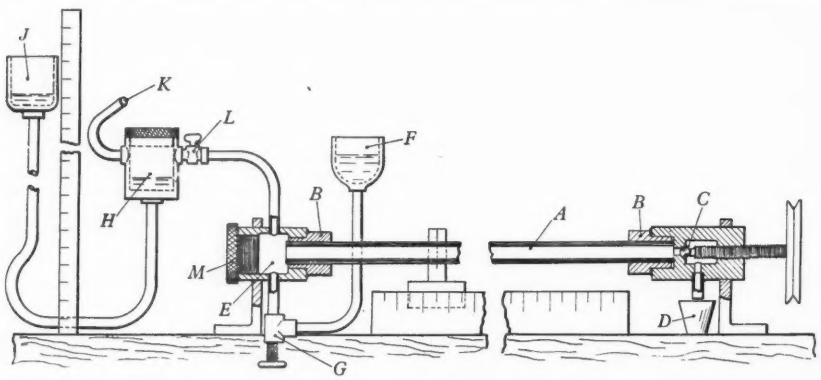

FIGURE 1. Sketch of apparatus.

due to viscosity, most of the experiments were carried out with fluids of large viscosity. Glycerine and strong sucrose solution (golden syrup) diluted with water till its viscosity was 28 poise at 20 °C was used. Glass tubes of accurate bore, known as 'Veridia' tubes, of 2 and 3 mm bore and 4 ft. long were used. The 3 mm tube was slightly conical so that its cross-section varied uniformly through a range of $1\frac{1}{2}$ % over its length. The 2 mm tube had only a quarter of that variation. In figure 1 the tube A has interchangeable brass end pieces B. At the far end these fitted into a fixed ball valve C. The fluid passing the ball passed into a weighed crucible D so that the amount discharged in a measured time could be weighed. At the near end the tube fitted into a chamber E which could be filled with fluid from the container F through the valve G. The air which was forced through the tube was supplied from the Perspex chamber H, and the pressure in H could be raised to 3 atmospheres or more by raising a mercury container J. To maintain the mercury level in H constant the air pressure was raised by means of a subsidiary pump K, while the container J was raised. The pressure vessel could be cut off from the chamber H by turning a tap L.

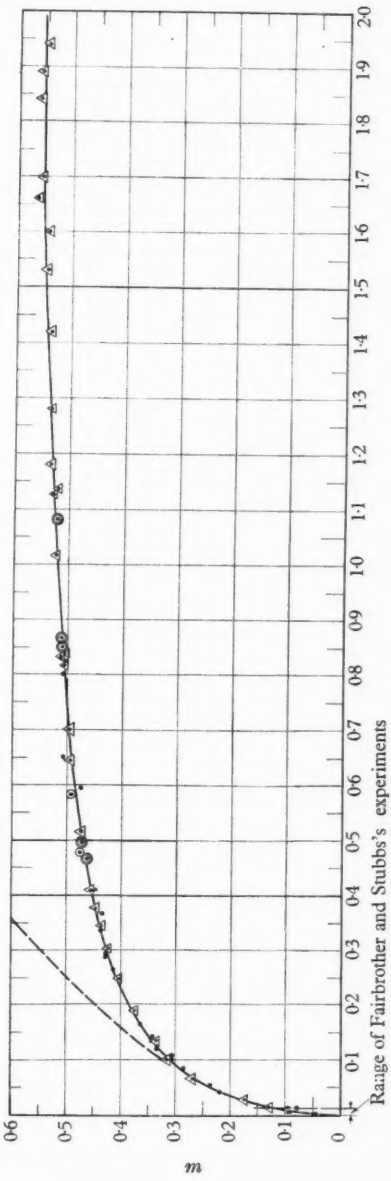

FIGURE 2. Experimental results. •, $\mu = 0{\cdot}79p$ at 20 °C (syrup-water mixture); tube diameters 0·15 and 0·2 cm. △, $\mu = 9{\cdot}3p$ at 20 °C (glycerine); tube diameters 0·2 and 0·3 cm. ◉, $\mu = 28p$ (syrup-water); tube diameter 0·3 cm. ⊙, $\mu = 0{\cdot}3p$ (a lubricating oil); tube diameter 0·15 cm. Broken line: Fairbrother & Stubbs's parabola.

To perform an experiment the tap L was closed and the valves G and C opened. The chamber E and the tube A were then filled, if necessary by applying air pressure to the container F. The valve C was then closed and the crucible D placed in position. By unscrewing a cover M the chamber E was then emptied leaving a meniscus of fluid in the end of the tube. After replacing the cover M the tap L was opened and the air pressure in E raised to about 3 atmospheres.

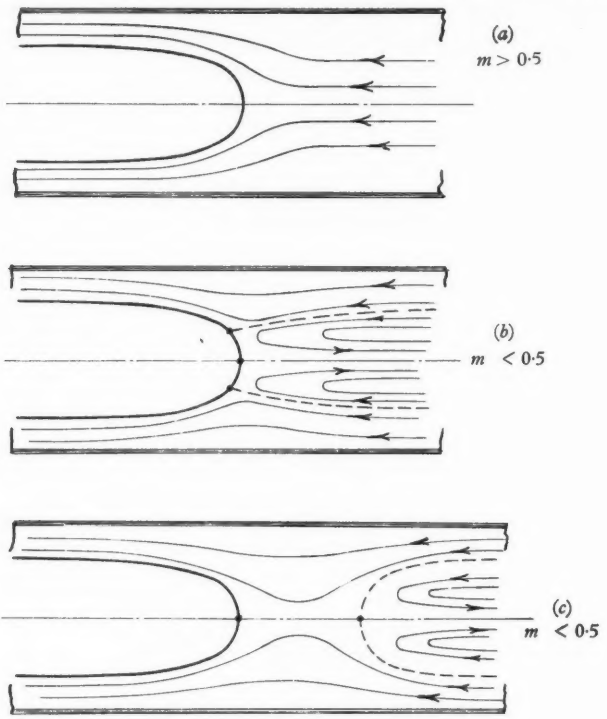

FIGURE 3. Rough sketch of possible streamlines.

The apparatus was then ready for the experiment. The ball valve C was suddenly turned to a previously determined position and at the same moment a stop-watch was started. The meniscus then moved at a nearly uniform speed along the tube. After the meniscus had gone some way along the tube the ball valve C was suddenly closed and simultaneously the stop-watch was stopped. The position of the meniscus was read and the length of the air column in the tube determined. The crucible was weighed and the weight w per unit length of the fluid expelled was measured. The weight per unit length of the fluid in the tube when full was $w_0 = \rho\pi a^2$, where ρ is its density and a the radius of the tube. Evidently

$$1 - m = w/w_0.$$

The viscosity of the fluid used was determined by the capillary-tube method and the surface tensions of glycerine and concentrated solutions of sucrose were taken from physical tables.

Results

The results are shown in figure 2 where m is plotted against $\mu U/T$.

For comparison with the measurements of Fairbrother & Stubbs the parabola $m = (\mu U/T)^{\frac{1}{2}}$ is shown as a broken line, and the range of values of $\mu U/T$ covered by them is also shown. It will be seen that the present experiments are in good agreement with $m = (\mu U/T)^{\frac{1}{2}}$ up to $\mu U/T = 0{\cdot}09$, but that above this value m increases more slowly than $(\mu U/T)^{\frac{1}{2}}$ till at the highest values reached m approaches 0·55. The trend of the curve suggests that m reaches a limiting value above 0·56, when the stresses due to viscosity are much greater than those due to surface tension. It will be noticed that when $m = 0{\cdot}5$ the flow velocity at points far from the meniscus is identical with that of the meniscus, so that if $m > 0{\cdot}5$ the central filament is moving towards the meniscus, whereas if $m < 0{\cdot}5$ the central filament is moving away from it. If the flow is reduced to steady motion by superposing a velocity $-U$ it is only when $m > 0{\cdot}5$ that the flow with only one stagnation point is possible. This is shown by the sketch of figure 3*a*. The two simplest possible types of flow when $m < 0{\cdot}5$ are shown in figures 3*b* and 3*c*. In 3*b* there is one stagnation point on the vertex and a stagnation ring on the meniscus. In figure 3*c* there are two stagnation points on the axis.

REFERENCES

FAIRBROTHER, F. & STUBBS, A. E. 1935 *J. Chem. Soc.* **1**, 527.

The motion of long bubbles in tubes

By F. P. BRETHERTON
Trinity College, Cambridge

(Received 9 November 1960)

A long bubble of a fluid of negligible viscosity is moving steadily in a tube filled with liquid of viscosity μ at small Reynolds number, the interfacial tension being σ. The angle of contact at the wall is zero. Two related problems are treated here.

In the first the tube radius r is so small that gravitational effects are negligible, and theory shows that the speed U of the bubble exceeds the average speed of the fluid in the tube by an amount UW, where

$$W \simeq 1{\cdot}29(3\mu U/\sigma)^{\frac{2}{3}} \quad \text{as} \quad \mu U/\sigma \to 0.$$

(This result is in error by no more than 10% provided $\mu U/\sigma < 5 \times 10^{-3}$.) The pressure drop, P, across such a bubble is given by

$$P \simeq 3{\cdot}58(3\mu U/\sigma)^{\frac{2}{3}}\sigma/r \quad \text{as} \quad \mu U/\sigma \to 0$$

and W is uniquely determined by conditions near the leading meniscus. The interface near the rear meniscus has a wave-like appearance. This provides a partial theory of the indicator bubble commonly used to measure liquid flow-rates in capillaries. A similar theory is applicable to the two-dimensional motion round a meniscus between two parallel plates. Experimental results given here for the value of W agree well neither with theory nor with previous experiments by other workers. No explanation is given for the discrepancies.

In the second problem the tube is wider, vertical, and sealed at one end. The bubble now moves under the effect of gravity, but it is shown that it will not rise at all if

$$\rho g r^2/\sigma < 0{\cdot}842,$$

where ρ is the difference in density between the fluids inside and outside the bubble. If

$$0{\cdot}842 < \rho g r^2/\sigma < 1{\cdot}04, \quad \text{then} \quad \rho g r^2/\sigma - 0{\cdot}842 \simeq 1{\cdot}25(\mu U/\sigma)^{\frac{2}{3}} + 2{\cdot}24(\mu U/\sigma)^{\frac{1}{3}},$$

accurate to within 10%. Experiments are adduced in support of these results, though there is disagreement with previous work.

1. Introduction

In many physical experiments the rate of flow of a liquid is measured by passing it through a capillary tube of radius r, containing an indicator bubble of air, of length several tube diameters. It was pointed out by Fairbrother & Stubbs (1935) that such a bubble moves somewhat faster than the average speed of the liquid in the tube, because it does not behave like a closely fitting piston. Motion

in which the ends of the bubble formed two hemispherical caps filling the tube cross-section would involve infinite viscous stresses at the wall. The only physical forces tending to maintain the shape of the ends against these stresses are those due to the uniform pressure within the bubble, to surface tension, and to gravity. If the tube radius is sufficiently small for gravity to be negligible, it is to be expected that there will be a film of liquid of uniform thickness b between the front and rear menisci, which is in a region of uniform pressure with no tangential stress on the free surface, and therefore at rest. Goldsmith & Mason (1960) have shown experimentally that this is indeed so. The volume swept out by the bubble when moving with speed U must equal the average speed of the liquid in front and behind it, multiplied by the cross-sectional area of the tube. This average speed is thus less than that of the bubble, in the ratio $1-W=(1-b/r)^2$. Measurements or calculation of the film thickness b therefore provide corresponding values for W.

The first problem considered in this paper concerns the balance between surface-tension and viscous forces for a steadily moving interface between an incompressible fluid of viscosity μ and another negligible viscosity, both being contained in a circular tube of radius r. The viscous fluid is assumed to wet the tube wall and the interfacial tension σ is assumed well defined and constant. This implies that the viscous stress tangential to the interface vanishes. The magnitudes of inertial, gravitational and viscous forces, relative to surface-tension force, are given roughly by the dimensionless numbers

$$\rho r U^2/\sigma, \quad \rho g r^2/\sigma, \quad \mu U/\sigma,$$

where ρ is a representative density, and U is the speed of the bubble. We shall assume to begin with that

$$\rho r U/\mu \ll 1, \quad \rho g r^2/\sigma \ll 1.$$

The first condition is that the Reynolds number based on the tube radius is small, and the second that surface-tension forces are much more important than gravitational forces. These requirements will later be somewhat relaxed. The ratios b/r and W must then be determined by consideration of viscous and surface-tension forces alone, and so are functions only of $\mu U/\sigma$. Fairbrother & Stubbs (1935) confirmed this and suggested after several experiments that

$$W = 1{\cdot}0(\mu U/\sigma)^{\frac{1}{2}} \quad \text{for} \quad \mu U/\sigma < 0{\cdot}015. \tag{1}$$

These results have been extended by Taylor (1961) to values of $\mu U/\sigma$ between 0·015 and 2. Equation 1 is valid till $\mu U/\sigma$ reaches 0·09, while for larger values W asymptotes to 0·56. Marchessault & Mason (1960) have proposed the relation

$$W = (\mu/\sigma)^{\frac{1}{2}}\{-0{\cdot}10+1{\cdot}78/U^{\frac{1}{2}}\}$$

for $\mu U/\sigma$ between 7×10^{-6} and 2×10^{-4}. In §2 of this paper a theory is presented which leads to the result

$$W \simeq 1{\cdot}29(3\mu U/\sigma)^{\frac{2}{3}}, \tag{2}$$

accurate to within 5% if $\mu U/\sigma < 0{\cdot}003$. In view of the discrepancies between these values, the author repeated Fairbrother & Stubbs's experiments using a different method. The results are reported in §3.

The second problem considered (§4) concerns a wider tube, vertical and sealed at one end, so that gravity is important. On dimensional grounds the speed of rise U at low Reynolds number must be given by

$$\mu U/\sigma = f(\rho g r^2/\sigma)$$

for some function f, where ρ is now the difference in density between the fluid outside and that inside the bubble. The basic method used to determine f is similar to that of the first problem, but the results are quite different.

It was noticed by Gibson (1913) and independently by Barr (1926) that if $\rho g r^2/\sigma$ is sufficiently small the bubble does not rise at all. Barr gives a critical value of 0·15. Goldsmith & Mason (1960) suggest instead $\rho g r^2/\sigma > 1{\cdot}27$ as a criterion for a rising bubble. The analysis of §4 yields $\rho g r^2/\sigma > 0{\cdot}842$, and this is briefly confirmed by experiment.

The idea behind the theoretical treatment of these two problems is that for sufficiently small $\mu U/\sigma$ the viscous stresses appreciably modify the static profile of the bubble only very near the wall. In this region it turns out that the 'lubrication approximation' gives a good description of the flow and of the profile. In the centre of the tube the static profile is still appropriate and there is a region of overlap in which the two are matched. In §§2.1 and 4.1 the approximate equations are stated without derivation; §§2.2 and 4.2 the self-consistency of this process is examined retrospectively, and an estimate obtained for the range of values of $\mu U/\sigma$ for which it is valid.

2. Bubble in a capillary tube. Theory

2.1. *First approximation*

(i) In this section gravity is assumed negligible. A section of the bubble is given in figure 1 and this is assumed axisymmetric. A gross violation of this symmetry would be visible in practice and does not seem to occur. Also, in this problem, the motion near the wall is essentially determined by a local mechanism, and there is no obvious way in which the interaction between the flow at opposite ends of a diameter can arise, which is a feature of the asymmetric descent under gravity of solid spheres closely fitting in a tube, as considered by Christopherson & Dowson (1959).

For a bubble at rest there are no viscous stresses. The front and rear menisci must assume shapes of constant mean curvature κ_1. The only such axisymmetric shape with no singularity on the axis is a portion of a sphere and, if the angle of contact at the wall is zero, it must be a hemisphere.

For sufficiently small non-zero $\mu U/\sigma$, the interface may be divided into several regions. The front and rear menisci are separated by a region CD, where a uniform film of fluid is at rest on the wall of the tube. This region is taken to be long compared to the film thickness b. The contribution to mean curvature due to axial symmetry is constant and equal to $1/(r-b)$. Also, it is assumed that $b/r \ll 1$. Away from the wall the viscous stresses are $O(\mu U/r)$, whereas stresses due to surface tension are $O(\sigma\kappa_1)$. Thus, in regions AB, EF the fractional change in mean curvature, $\delta\kappa_1/\kappa_1$, due to the motion is $O(\mu U/\sigma)$. However, in regions BC, DE

the viscous stresses are $O(\mu U/b)$ and κ_1 changes from approximately $2/r$ at B, E to approximately $1/r$ at C, D. It cannot be deduced that $b/r = O(\mu U/\sigma)$, for only gradients of stress, rather than the stresses themselves, can be equated. In the regions BC, DE variations of the viscous stress are across the film, in a distance of $O(b)$, but changes in surface-tension stress occur along the tube and may be of larger scale. It will appear later that the relevant value is $O(br)^{\frac{1}{2}}$. In the centre of the tube, however, both variations must be of the same scale $O(r)$.

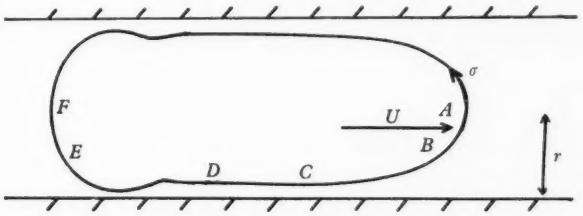

FIGURE 1. Section of a bubble in a horizontal tube.

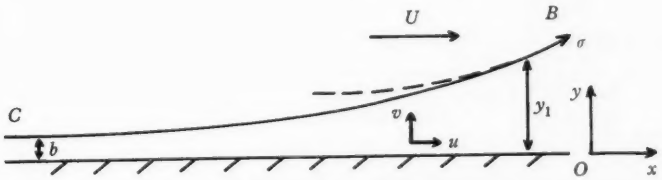

FIGURE 2. The transition region.

(ii) We now consider in detail the transition regions BC, DE using the notation of figure 2. For sufficiently small $\mu U/\sigma$ the interface, $y = y_1$, is almost parallel to the tube wall throughout the region, and the fluid thickness is much less than the tube radius, so it is plausible that the 'lubrication approximation' may describe the flow. Accordingly we make the following approximations.

The fluid motion in the transition region may be treated as if the region were plane, not annular. Further we take $dy/dx \ll 1$ throughout the region. The pressure p_1 within the film is effectively independent of y for given x, and the x-derivatives of velocity u_x, u_{xx}, etc., may be neglected in comparison with the corresponding y-derivatives, u_y, u_{yy}. The condition of zero tangential stress at the interface reduces to

$$u_y = 0, \quad \text{when} \quad y = y_1, \tag{3}$$

and the normal stress condition at the interface,

$$p_1 + \sigma\kappa_1 = -2\mu\{1 + (dy_1/dx)^2\}^{\frac{1}{2}} u_x, \quad \text{when} \quad y = y_1,$$

can be taken as

$$p_1 = -\sigma \frac{d^2 y_1}{dx^2} - \frac{\sigma}{r}. \tag{4}$$

That these approximations are self-consistent will be shown 'a posteriori' in §2.2.

Under these conditions, the Navier–Stokes equations for small Reynolds number become

$$u_{yy} = \frac{1}{\mu}\frac{dp_1}{dx} \tag{5}$$

and the boundary condition at the wall is

$$u = 0 \quad \text{when} \quad y = 0. \tag{6}$$

The volume-flux of fluid in unit time per unit of circumference at any value of x is

$$V = \int_0^{y_1} u\left(1 - \frac{y}{r}\right) dy,$$

or, to the approximation considered in this subsection,

$$V = \int_0^{y_1} u\, dy = -\frac{y_1^3}{3\mu}\frac{dp_1}{dx} \tag{7}$$

from repeated integration of equation (5), using boundary conditions (3) and (6). However, since the motion is steady continuity requires, again approximating,

$$V = U(y_1 - c), \tag{8}$$

for some constant c. Using the pressure boundary condition we obtain

$$\frac{d^3 y_1}{dx^3} = \frac{3\mu U}{\sigma}\frac{y_1 - c}{y_1}. \tag{9}$$

But when $y_1 = b$, $d^3y_1/dx^3 = 0$, so $c = b$. Equation (9) describes the profile of the film throughout the region $BCDE$. It may be put in universal form by the substitutions

$$y_1 = b\eta, \quad x = b(3\mu U/\sigma)^{-\frac{1}{3}}\xi. \tag{10}$$

Then

$$\frac{d^3\eta}{d\xi^3} = \frac{\eta - 1}{\eta^3}. \tag{11}$$

The author is indebted to Sir Geoffrey Taylor, who first drew his attention to this equation.

(iii) The relations (10) show that, for a given solution of equation (11) and for sufficiently small $(3\mu U/\sigma)^{\frac{1}{3}}$, there will exist regions in which

$$\eta = y/b \gg 1 \quad \text{and} \quad y_1/r = b\eta/r \ll 1,$$

but in which

$$\frac{dy_1}{dx} = \left(\frac{3\mu U}{\sigma}\right)^{\frac{1}{3}}\frac{d\eta}{d\xi} \ll 1,$$

so that equation (9) is still valid. Then from equation (11) we see that in these regions $d^3\eta/d\xi^3 \simeq 0$ and

$$\eta \simeq \tfrac{1}{2}P\xi^2 + Q\xi + R,$$

for some constants P, Q, R. This gives

$$y_1 \simeq \tfrac{1}{2}P\left(\frac{3\mu U}{\sigma}\right)^{\frac{2}{3}}\frac{x^2}{b} + Q\left(\frac{3\mu U}{\sigma}\right)^{\frac{1}{3}}x + Rb. \tag{12}$$

However, in this region the mean curvature

$$\kappa_1 \simeq \frac{d^2 y_1}{dx^2} + \frac{1}{r} \simeq \left(\frac{3\mu U}{\sigma}\right)^{\frac{2}{3}}\frac{P}{b} + \frac{1}{r}.$$

Equation (12) thus refers to a region of constant mean curvature and thus describes a profile determined by surface tension alone. This may be extended beyond B, E outside the range of validity of equation (9), $b\eta/r \ll 1$, into the central regions AB, EF of the tube. There the previous analysis does not hold, but viscous stresses must still have a negligible influence on the profile. This is thus a surface of constant mean curvature extending across the tube with tangent nearly parallel to the wall at a distance $O(b/r)$ from it. It is therefore a portion of a sphere of radius r to a first approximation, and the mean curvature of the profile described by equation (12) is to this approximation $2/r$. Thus

$$\frac{b}{r} = \left(\frac{3\mu U}{\sigma}\right)^{\frac{2}{3}} P. \tag{13}$$

The constants P, Q, R, will not, in general, be the same at the two ends B, E. But since they refer to one solution of equation (11), continuous in the whole region $BCDE$, there are relations between their values.

In region CD, $y_1 \simeq b$ and $d^3\eta/d\xi^3 \simeq \eta - 1$. This has the general solution

$$\eta = 1 + \alpha e^{\xi} + \beta e^{-\frac{1}{2}\xi} \cos(\sqrt{3}\xi/2) + \gamma e^{-\frac{1}{2}\xi} \sin(\sqrt{3}\xi/2). \tag{14}$$

All terms on the right-hand side but the first are small compared to unity throughout the region CD. If $(l/b)(3\mu U/\sigma)^{\frac{1}{3}} \gg 1$ where l is the length CD, we have

$$\text{near } C, \quad \eta - 1 \simeq \alpha e^{\xi}, \tag{15}$$

$$\text{near } D, \quad \eta - 1 \simeq \beta e^{-\frac{1}{2}\xi} \cos(\sqrt{3}\xi/2) + \gamma e^{-\frac{1}{2}\xi} \sin(\sqrt{3}\xi/2). \tag{16}$$

These equations indicate that the front and rear menisci may be treated separately, and that there is a fundamental difference between them.

(iv) Equation (15) contains one disposable constant α, but this may be made unity by a suitable change of origin of ξ. There is near C essentially a unique solution of equation (11), and by stepwise integration in the direction of increasing ξ one obtains, relative to this origin, unique values of the constants, P, Q, R. The position of the origin is, however, physically irrelevant. We might equally choose it so that Q vanishes. A different choice yields the same profile shifted laterally, and corresponds to a bubble of the same shape in a slightly different position in the tube.

This integration has been performed for the author by Mr B. M. M. Hardisty, obtaining $P = 0{\cdot}643$, $Q = 0$, $R = 2{\cdot}79$, whence using equation (13)

$$b/r = 0{\cdot}643(3\mu U/\sigma)^{\frac{2}{3}}. \tag{17}$$

The whole of the analysis thus far has hinged on the assumption that b/r is small. This is now seen to be self-consistent for small values of $(3\mu U/\sigma)^{\frac{2}{3}}$. A full discussion of all the approximations made will be found in § 2.2.

Substituting in equation (12), near B, we have

$$y_1 = \tfrac{1}{2}(x^2/r) + 1{\cdot}79(3\mu U/\sigma)^{\frac{2}{3}} r. \tag{18}$$

Now the right-hand side of equation (9) describes the effect of viscous forces on the curvature of the bubble interface in the region where these forces are largest, namely near the wall. The departures from sphericity in regions AB, EF, are of

the same order as the change in the curvature d^2y_1/dx^2 obtained by truncating the integration of equation (9) at the largest value of y_1 for which $dy_1/dx \ll 1$ is valid. Thus, to the approximation considered in this section, equation (18) describes in the region BC an accurate continuation of the spherical region AB. This virtual hemisphere (shown as a dashed curve in figure 2) has a tangent parallel to the wall at a distance $r\{1 - 1{\cdot}79(3\mu U/\sigma)^{\frac{2}{3}}\}$ from the centre of the tube. Thus the true mean curvature of the region AB is $(2/r)\{1 + 1{\cdot}79(3\mu U/\sigma)^{\frac{2}{3}}\}$. The small difference from $2/r$ does not invalidate the identification (13), but this observation does enable us to estimate the pressure drop across a moving front meniscus. This arises partly from viscous stresses in the Poiseuille flow in the capillary and in the unknown motion near the central spherical portion of the meniscus, and partly from the pressure drop across the interface itself, due to surface tension forces. For any given geometrical arrangement, the viscous stresses are proportional to $\mu U/r$, whereas the surface tension stresses are

$$(2\sigma/r)\{1 + 1{\cdot}79(3\mu U/\sigma)^{\frac{2}{3}}\}.$$

Thus the dynamic pressure drop $3{\cdot}58(3\mu U/\sigma)^{\frac{2}{3}}(\sigma/r)$ will dominate for sufficiently small $(\mu U/\sigma)$.

(v) At the rear meniscus the situation is different. In equation (16) are two disposable constants. Change of origin in ξ, which corresponds to lateral displacement of the whole rear meniscus without change of shape, can account for one of these, but it is still possible, by varying the other, to obtain by stepwise integration any value of $P \geqslant 0$ and corresponding values of Q, R. Thus the identification (13) may be carried through for any value of b/r. Given b/r, however, there corresponds a unique profile and a well-defined virtual hemisphere. The profiles all show oscillations in thickness, the minimum value of y/b decreasing as P increases. The pressure drop across a moving rear meniscus exceeds the static value $2\sigma/r$ only if $(b/r)(3\mu U/\sigma)^{-\frac{2}{3}} < 0{\cdot}9$. For larger values it tends to assist rather than hinder the motion. The necessary energy comes from the finite volume of liquid in the film of thickness b at a pressure σ/r higher than the liquid behind the meniscus. For values of $(b/r)(3\mu U/\sigma)^{-\frac{2}{3}} < 0{\cdot}9$ the energy dissipated in the transition region DE exceeds this amount and external work has to be done to make the meniscus move. If b/r is defined by a front meniscus travelling with the same speed U, $(b/r)(3\mu U/\sigma)^{-\frac{2}{3}} = 0{\cdot}643$, the dynamic pressure drop is found to be $-0{\cdot}930(3\mu U/\sigma)^{\frac{2}{3}}\sigma/r$, and the minimum film thickness to be $0{\cdot}716\,b$. Thus the rear meniscus contributes to the total dynamic pressure drop across the bubble, which is $4{\cdot}52\,(\sigma/r)(3\mu U/\sigma)^{\frac{2}{3}}$.

(vi) It remains to calculate the value of W, the fractional velocity correction measured by Fairbrother & Stubbs. This is easily seen to be the proportion of the cross-sectional area of the tube occupied by the film of thickness b, so

$$W = 1{\cdot}29(3\mu U/\sigma)^{\frac{2}{3}} \tag{19}$$

to the approximation considered here.

(vii) A meniscus at rest between two parallel plates in such a way that the radius of curvature in the plane of the plates is large compared to the distance between them must assume an almost semicircular profile when viewed in normal

section in a plane at right angles to the plates. Changes in curvature due to symmetry about the tube axis do not enter into equation (9), so the theory of this subsection can be taken over directly to the almost two-dimensional motion about a moving meniscus between two parallel plates. The only amendment is that the pressure drop across each meniscus should be halved.

2.2. *Justification of the approximations*

In this subsection we review and extend the approximations made in §2.1. These arise in several different ways and will be treated separately.

(i) Consider first the requirement that inertia forces can be neglected in comparison with viscous forces. The previous analysis shows that, provided inertia forces are not so large as to cause appreciable distortion near the centre, this is important only near the walls where the interface profile departs appreciably from the spherical. In nearly parallel flow the appropriate Reynolds number measuring the relative importance of inertial and viscous forces is $\rho U b^2/\mu L$, where L is the length scale of variations downstream, in this case $r(\mu U/\sigma)^{\frac{1}{3}}$. To neglect inertia we require not $\rho U r/\mu \ll 1$, but

$$\rho r U^2/\sigma \ll 1.$$

This is also the condition that inertia forces are negligible in the centre of the tube.

(ii) Secondly, consider the neglect of gravity forces. These can be important both in affecting the flow in the film remaining on the wall, and also in distorting the shape of a static meniscus which we have assumed spherical. The first will not affect the proportion of fluid left behind by the front meniscus; such fluid will merely drain to the lowest generator of the tube. The time scale for this is much longer than the time taken for the meniscus to move a tube diameter if $\rho g b^2/\mu U \ll 1$, i.e. if

$$(\rho g r^2/\sigma)\,(\mu U/\sigma)^{\frac{1}{3}} \ll 1.$$

The change in static profile affects the identification (13). If $\rho g r^2/\sigma$ is appreciable, κ_1 varies from point to point of region AB. Thus $(3\mu U/\sigma)^{\frac{2}{3}}\,(P/b)$ will also vary, and the average value of b over the tube circumference might differ from that given by equation (13). The complete solution of this problem for a horizontal tube is difficult. It is that of finding the surface which touches the wall of a horizontal cylinder, and which has a curvature linearly dependent on the height above the lowest generator. The relevant non-linear partial differential equation has no obvious general solution. However, the author has assumed $(\rho g r^2/\sigma)^2$ to be negligible and obtained the resultant small perturbations of the surface from a hemisphere. To this approximation, the average value of b/r for a horizontal tube is identical with that given by equation (13).

For a vertical tube the problem is easier. The ratio b/r is increased by a factor $1+\frac{2}{3}\rho g r^2/\sigma + O(\rho g r^2/\sigma)^2$ for a rising bubble and by $1-(\frac{2}{3}\rho g r^2/\sigma)+O(\rho g r^2/\sigma)^2$ for a descending one.

(iii) The last and most significant approximations are those made to obtain a solution of the problem in which gravity and inertia are entirely neglected. The value of b/r obtained, which is $O(\mu U/\sigma)^{\frac{2}{3}}$, shows that the contribution of the axial

symmetry to the mean curvature of the interface in the transition regions differs from $1/r$ by an amount of order $(1/r)(\mu U/\sigma)^{\frac{2}{3}}$. The neglect of this in equation (9) is justified, for d^2y_1/dx^2 is of order $1/r$. For similar reasons terms like $2\mu u_x$ in the pressure-boundary condition and corrections to the equations of continuity are all found, when calculated, to be negligible provided $(\mu U/\sigma)^{\frac{2}{3}}$ is sufficiently small. Just how small 'sufficiently' is will be established in the remainder of this subsection, which is devoted to setting up the exact equations and using the results of §2.1 to obtain a closer approximation. Thence the range of validity of these results will become apparent.

(iv) We use the notation of figure 2, remembering that the flow is axisymmetric. Neglecting inertia terms the Navier–Stokes equations become

$$\frac{1}{\mu}p_x = u_{xx}+u_{yy}-\frac{1}{r-y}u_y,$$

$$\frac{1}{\mu}p_y = v_{xx}+v_{yy}-\frac{1}{r-y}v_y-\frac{1}{(r-y)^2}v. \tag{20}$$

The equation of continuity is

$$u_x+v_y-\frac{v}{r-y}=0, \tag{21}$$

and the boundary conditions at the wall are

$$u=v=0, \quad \text{when} \quad y=0. \tag{22}$$

At the surface $y=y_1$, the normal has direction cosines $(-\sin\theta, \cos\theta)$ where $\tan\theta = dy_1/dx$. The components of the stress tensor are

$$p_{xx}: -p+2\mu u_x; \quad p_{yy}: -p+2\mu u_y; \quad p_{xy}: \mu(u_y+v_x).$$

We equate the tangential and normal stresses to 0 and $\sigma\kappa_1$ respectively, giving

$$\mu\{(u_x-v_y)(-2\sin\theta\cos\theta)+(u_y+v_x)(\cos^2\theta-\sin^2\theta)\}=0,$$

$$-p+\mu\{2u_x\sin^2\theta+2v_y\cos^2\theta-2(u_y+v_x)\sin\theta\cos\theta\}=\sigma\kappa_1.$$

At this stage it is an advantage to develop the notation. The suffix 1 attached to any symbol denotes that its value is to be taken on the surface $y=y_1$. The prime $'$ denotes differentiation with respect to x along the surface. We must distinguish carefully between, for example, u_{x1} and u_1'. The former is the value of $\partial u/\partial x$ taken at $y=y_1$; the latter is the derivative of the value of u at the free surface, and is $u_{x1}+u_{y1}y_1'$. Remembering that $\tan\theta = y_1'$ and using equation (21), after some manipulation the surface-boundary conditions may be written

$$u_{y1} = -v_{x1}+\left(2u_{x1}-\frac{v_1}{r-y_1}\right)\frac{2y_1'}{1-y_1'^2} \tag{23}$$

and

$$-\sigma\kappa_1-p_1 = \left(2u_{x1}-\frac{v_1}{r-y_1}\right)(1+y_1'^2)^{\frac{1}{2}}-\frac{v_1}{r-y_1}, \tag{24}$$

where

$$\kappa_1-y_1'' = y_1''\{(1+y_1'^2)^{-\frac{3}{2}}-1\}+(1+y_1'^2)^{-\frac{1}{2}}/r-y_1. \tag{25}$$

The Navier–Stokes equations become

$$u_{yy}-\frac{1}{\mu}p_1' = -u_{xx}+\frac{u_y}{r-y}+\frac{1}{\mu}(p_x-p_1'), \tag{26}$$

and the continuity conditions

$$V-\int_0^{y_1} u\,dy = -\int_0^{y_1} u\frac{y}{r}dy \tag{27}$$

and

$$V-U(y_1-c) = -Uy_1^2/2r \tag{28}$$

complete the exact equations for this problem. We see that in the previous subsection everything on the right-hand side of these equations was neglected. Neglecting these small terms, triple integration of equation (26) with respect to y using boundary conditions (22), (23) and substitution in equation (27) gave an expression for V, equation (7).

We now repeat this procedure—but retaining the neglected terms. Thus,

$$V+\frac{y_1^3}{3\mu}p_1' = \int_0^{y_1}dy\int_0^{y}dy\int_{y_1}^{y}\left\{\frac{1}{\mu}(p_x-p_1')-u_{xx}+\frac{u_y}{r-y}\right\}dy$$
$$+\frac{y_1^2}{2}\left\{-v_{x1}+\left(2u_{x1}-\frac{v_1}{r-y_1}\right)\frac{2y_1'}{1-y_1'^2}\right\}-\int_0^{y_1}u\frac{y}{r}dy. \tag{29}$$

We now manipulate these integrals until they involve solely integrations with respect to y of the x-derivatives of u, y_1. This may always be done, for, from equation (21)

$$v = \frac{1}{r-y}\int_0^{y} -u_x(r-y)\,dy$$

and

$$\frac{1}{\mu}(p_x-p_1') = \frac{\partial}{\partial x}\left\{\int_{y_1}^{y}\frac{1}{\mu}p_y dy\right\}$$
$$= \frac{\partial}{\partial x}\left\{\int_{y_1}^{y}dy\left[v_{xx}+v_{yy}-\frac{1}{r-y}\left(v_y+\frac{v}{r-y}\right)\right]\right\}.$$

The analysis so far is exact. But these integrals are of an order smaller by $(\mu U/\sigma)^{\frac{2}{3}}$ than the terms on the left-hand side of equation (29). For they all involve either x-derivatives to at least second order or products of first order, or a factor y_1/r, and in the last subsection $y_1' = O(\mu U/\sigma)^{\frac{1}{3}}$, and $y_1/r = O(\mu U/\sigma)^{\frac{2}{3}}$. Thus, if we use the values of u obtained in the last subsection by integration of equation (5) to evaluate these integrals, we will obtain an approximation valid to $(\mu U/\sigma)^{\frac{2}{3}}$ higher order.

$$V+\frac{y_1^3}{3\mu}p_1' = -\frac{4}{15\mu}y_1^3p_1''' - \frac{5}{3\mu}y_1^4y_1'p_1'' - \frac{1}{3\mu}y_1^3(y_1y_1''+5y_1'^2)p_1' + \frac{1}{3\mu r}y_1^4p_1'.$$

Using now equations (7), (8) to the same approximation

$$p_1'+3\mu U\frac{y_1-c}{y_1^3} = -\frac{3\mu U}{y_1^3}\left\{\frac{3y_1-7c}{5}y_1y_1''+\frac{y_1-2c}{5}y_1'^2+\frac{y_1}{2r}(y_1-2c)\right\}. \tag{30}$$

Up to this stage we have not used the condition (24) on the normal stress on the interface. Equation (30) is derived only from the equations of motion and

continuity and from the absence of tangential stress. The value of the constant c becomes clear when we substitute for the pressure. To the same approximation then

$$\kappa_1' - \frac{3\mu U}{\sigma}\frac{y_1 - c}{y_1^3} = \frac{3\mu U}{\sigma}\frac{1}{y_1^3}\left\{\tfrac{3}{5}y_1 y_1''(y_1+4c) + \tfrac{1}{5}y_1'^2(y_1+8c) + \frac{y_1}{2r}(y_1-2c)\right\}. \quad (31)$$

When $y_1 = b$, $y_1' = y_1'' = 0$, $\kappa_1 = 1/(r-b)$, so we have $b - c = -b(b-2c)/2r$, i.e.

$$c \simeq b - (b^2/2r).$$

Finally, it should be noted that the exact form of equation (19) expressing W in terms of b is

$$W = \frac{2b}{r}\left(1 - \frac{b}{2r}\right). \quad (32)$$

(v) Equation (31) is the next approximation to equation (9). It is convenient to leave the mean curvature κ_1 in its exact form, equation (25), but otherwise

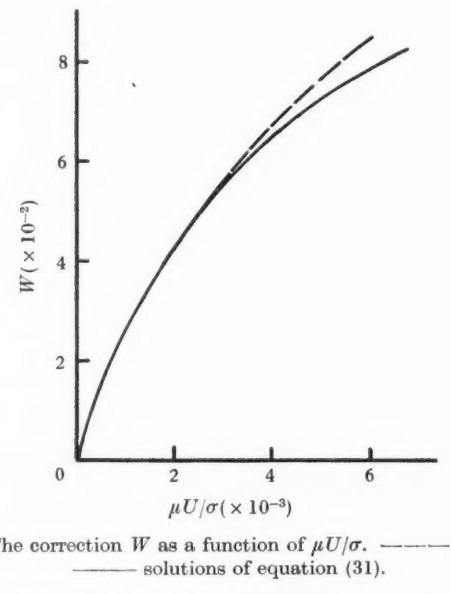

FIGURE 3. The correction W as a function of $\mu U/\sigma$. ——— $1{\cdot}29(3\mu U/\sigma)^{\frac{2}{3}}$; ——— solutions of equation (31).

the only difference is the addition of the terms on the right-hand side. These are all $O(3\mu U/\sigma)^{\frac{2}{3}}$ smaller than those on the left, and it is apparent too, that they are uniformly smaller, except when y_1/b becomes large. When y_1/b becomes large, but y_1/r is still small, the value of κ_1' approaches zero and the profile is approximately a surface of constant mean curvature. As y_1/r increases further κ_1' increases again, and equation (31) is clearly invalid. If, however, $(3\mu U/\sigma)^{\frac{2}{3}}$ is sufficiently small the minimum value of κ_1' can be made arbitrarily near zero, and the matching of the profile at that point to a portion of a sphere extending across the central portions of the tube may be made arbitrarily good. Thus, with the boundary conditions that $y_1 \to b$ as $x \to -\infty$, and that, for large y_1/b, y_1, y_1', y_1''

should be matched to those values appropriate to a spherical region of some curvature centred on $y_1 = r$, equation (31) apparently comprises the first two terms of an asymptotic expansion in powers of $(3\mu U/\sigma)^{\frac{2}{3}}$ of the exact equation describing the profile. It could in principle be used as the basis for obtaining still higher approximations by the same method. The solution of equation (31) presumably provides the first two terms of an asymptotic expansion of the profile itself.

(vi) Solutions of equation (31) have been obtained numerically using a digital computer. The results are shown in figure 3. For values of $\mu U/\sigma$ larger than 5×10^{-3} it was clear from the solutions that the minimum value of κ_1', attained for large values of y_1/b before the terms in $y_1'^2/y_1^2$ on the right-hand side became large again, was insufficiently small for an accurate match to a sphere to be made. This implies that further terms in the asymptotic expansion must be taken for larger values of $\mu U/\sigma$.

(vii) To summarize the results of this subsection: The range of values of $\mu U/\sigma$ for which the calculated values of W are likely to be accurate and yet are appreciably different from the two-thirds power law of § 2.2 is quite small, so the main value of the calculations of the subsection is to delimit accurately the upper limit to the range of validity of that law. It is accurate to within 5%, at $\mu U/\sigma = 3 \times 10^{-3}$. Neglect of inertia forces is permissible if $\rho r U^2/\sigma \ll 1$. The effect of gravity on a horizontal tube is $O(\rho g r^2/\sigma)^2$ but first order in $\rho g r^2/\sigma$ for other orientations.

3. Bubble in a capillary tube. Experiments

3.1. *Method and results*

Fairbrother & Stubbs estimated directly the fractional correction W to the speed of a bubble by measuring the volume of fluid ejected from the tube when the bubble moved a known distance. This method requires an accurate knowledge of the tube radius, and the final correction is obtained from the small difference between two volumes measured in different ways. To avoid gravitational effects the tube diameter must be small, yet if it is too small estimation of volumes becomes difficult. Their experiments were confined, for this reason, to tubes of 2 mm diameter. Their experiments extend down to $\mu U/\sigma = 1 \times 10^{-4}$. Marchessault & Mason (1960) derived the film thickness from the electrical resistance of the tube containing a bubble of known length. Their values for W, mainly for smaller $\mu U/\sigma$, are all somewhat larger than those calculated from the Fairbrother & Stubbs formula. In view of the clear discrepancy between this work and the prediction of this paper (equation 2) the author has repeated these experiments using a different method. Values of W for two different fluids in a 1 mm tube are given in figure 4. The dependence of these curves on the fluid used shows that the physical assumptions made in § 2 are inadequate, but the author is unable to postulate any reason which could, even qualitatively, explain the divergences between different fluids and from the theory.

Because of this it is proposed to give a detailed account of the experimental technique used here and then to conclude with a negative discussion of the causes of the discrepancy.

The apparatus used is shown in figure 5. A column of fluid LM, a few centimetres long, was drawn at constant rate about 100 cm along a carefully cleaned and dried 'Veridia' glass tube of 1 mm diameter. This was achieved by coupling the flow to that of a constant head of viscous oil (Shell Diala) across lengths of hypodermic tubing (providing a higher resistance than the 'Veridia' glass tube).

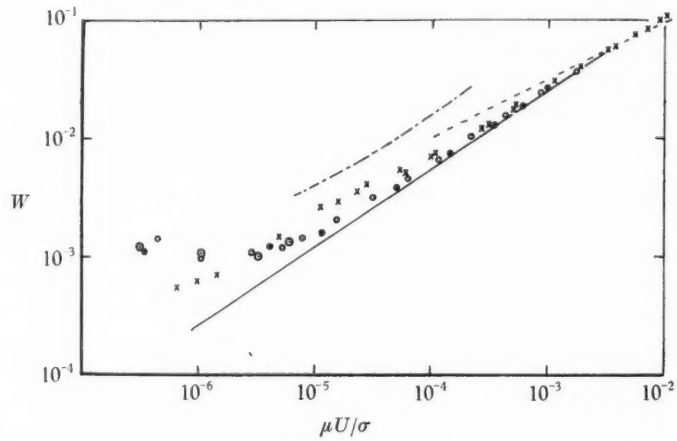

FIGURE 4. ——— Theory; —·— Marchessault & Mason; ––– Fairbrother & Stubbs; × aniline, ○ benzene (horizontal tube), ⊙ benzene (with evaporation precautions), ● benzene (vertical tube).

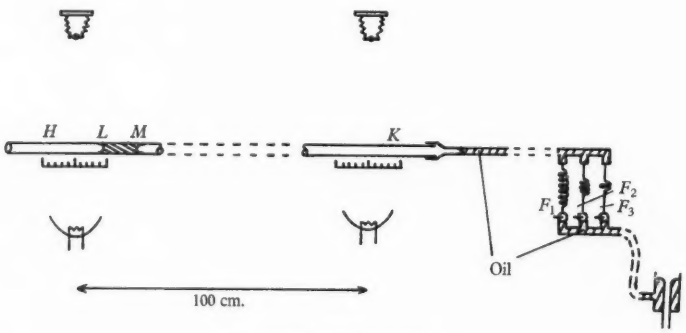

FIGURE 5. The apparatus.

Three such lengths were available, controlled by taps, F_1, F_2, F_3, giving speed ratios for a given head of 50:1. The head could be supplemented, if necessary, using mercury, up to a maximum of 20 cm Hg. Near the points H, K flash photographs of the column gave measurements of its length accurate to $\pm$ 0·001 cm. The average speed U of the rear meniscus of the column was obtained, from the time interval between the flashes, to within 2 % for the fastest run (9·5 sec). The change in length of the column, divided by the length of run, gives the proportion W of fluid left behind.

The advantages of this method are several. It gives a very sensitive method of measuring the very thin film thicknesses involved, down to 2×10^{-5} cm, at which value the probable error is about 6 %. This is independent of the radius of the tube, which, though it should be reasonably constant, need not be accurately known. It may also be used for volatile liquids, provided precautions are taken to saturate the air in the tube. Cleanliness is, however, vital, as a small sample of fluid is involved which touches large areas of tube wall. The apparatus was arranged so that the fluid touched no surface but glass, all of which was cleaned between every run with chromic acid, washed with distilled water, and dried using either acetone and air or by drawing filtered air through a desiccator. This is tedious but effective, and the self-consistency of the results would be improbable in the presence of significant contaminants. Indeed, this is probably the reason for the greater spread of the results for aniline. A check on the diameter of the tube and the accuracy of the length measurements was made by measuring the change in length of a column of mercury in runs in both directions. It returned exactly to its original length, showing that none had been left behind on the wall, but showed that the tube was conical with a change in tube radius of around 1 %. A correction for this (never exceeding 30 %) was applied to the measurements of change in length. W proved to be independent of the length of the columns used, though this was always greater than 4 tube diameters. The speed U varied during the very long runs (up to 36 h) by up to 20 %, because of changes of the viscosity of Diala with room temperature. However, the mean speed was always measured, and the values of μ/σ for the estimated mean temperature obtained from tables.

Finally, the tube was mounted vertically and the same measurements made using benzene. According to §2.2 the values of W so obtained should be larger by the factor $1+\frac{2}{3}\rho g r^2/\sigma$ than the correspnding values for a horizontal tube, provided $(\rho g r^2/\sigma)^2$ can be neglected. For benzene $\rho g r^2/\sigma$ is 0·06, so the values of W have been reduced by 4 % before plotting in figure 4 to make them strictly comparable with the data from the horizontal tube.

3.2. *Discussion*

The results plotted in figure 4 show serious systematic divergences between theory and experiment. These are largest at the slowest speeds, whereas agreement is quite good at the upper end of the range of validity of the theory. Aniline was one of the liquids used by Fairbrother & Stubbs (1935), but their curve lies well outside the spread of points corresponding to aniline in the present measurements. There is no obvious reason for this, though in principle the method used here is probably more accurate for small values of W.

The parameter $\rho r U^2/\sigma$, which was shown in §2.2 to measure the importance of inertia, was never more than 0·1 for either fluid, and, in any case, the main discrepancies occur at much lower speeds and cannot be due to inertia effects. It might be thought that with benzene evaporation could account for the large change in volume of the column at low speeds. This is not so, as was shown by carefully saturating the air in the tube with benzene vapour. No significant difference appeared in the results. The excellent agreement between values for

the horizontal tube and the corrected ones for the vertical tube shows that gravity is satisfactorily accounted for.

The effect was at first thought to be possibly due to roughness of the inside of the tube. Hillocks and hollows of the order of 1μ in height would cause a film to be left behind which was thicker by a constant amount from that predicted by theory, and we would expect W to tend to a constant value for sufficiently small $\mu U/\sigma$, corresponding to all the hollows being full. This does not happen for aniline, and anyhow this hypotheses would not explain the differences for different fluids.

An instability of the meniscus at the lowest speeds would also presumably be a function of $\mu U/\sigma$, and in any case there is no trace of it occurring though it would be difficult to observe visually. It is also difficult to see how a lack of perfect wetting would result in more fluid being left behind at the slower speeds.

It is possible that dissolved impurities or surface charges were present which cause a 'hardening' of the free surface similar to the effect observed in the free rise of small bubbles in large volumes of fluid. These cannot be present in the quantity required to reduce the surface tension by a factor of 4 which varies systematically with time. However, they might conceivably result in the free surface in the transitional region being able to support a tangential stress, and thus make equation (9) invalid. A discussion of various mechanisms which cause 'hardening' has been given by Frumkin & Levich (1947), but it is sufficient here to consider two extreme cases.

If the free surface behaves like a rigid one throughout the transitional region, we may easily obtain the analogue of equation (9). If $b/r \ll 1$ we may neglect the change in surface tension with x from its equilibrium value, but we must replace equation (3) by

$$u = U \quad \text{when} \quad y = y_1.$$

The equation governing the profile then becomes

$$\frac{d^3y_1}{dx^3} = \frac{6\mu U}{\sigma}\frac{y_1 - 2c}{y_1^3}. \tag{33}$$

If we make this dimensionless by

$$y_1 = 2c\eta,$$

$$x = 2c(6\mu U/\sigma)^{-\frac{1}{3}}\xi,$$

we see that

$$2c/a = 2^{\frac{2}{3}}\,0{\cdot}643(3\mu U/\sigma)^{\frac{2}{3}}.$$

When we remember that the quantity actually measured in these experiments was c/a we see that this hypothesis of complete absence of slip actually reduces the value of W by a factor $2^{-\frac{1}{2}}$.

However, if we do not require that equation (33) should hold over effectively the whole transition region, it is possible to obtain an increased value of W. If equation (9) (no tangential stress) holds for $c \leqslant y_1 \leqslant e$ for some e and equation (33) for larger values, the maximum value of P we can obtain is about 0·69 for $e = 3c$, corresponding to an increase of W of only 8 %. Hardening of the surface is thus quite unable to account for the observed results, and they remain a mystery to the author.

The referee has suggested that the discrepancy may be due to the 'disjoining pressure' in thin films of liquid in contact with a solid surface (Frenkel, 1946). A repulsive pressure $f(y_1)$ due to the cohesive forces between molecules appears between the surfaces of all liquid films of small thickness y_1, and f is of order 10^3 dynes/cm^2 when y_1 is $0{\cdot}1\,\mu$. It falls off very rapidly with film thickness, according to an inverse cube or inverse fourth power law. The corrected form of equation (9) is

$$\frac{d^3y_1}{dx^3}+\frac{1}{\sigma}\frac{df}{dy_1}\frac{dy_1}{dx}=\frac{3\mu U}{\sigma}\frac{y_1-c}{y_1^3}.$$

The correction is negligible everywhere if $y_1(df/dy_1) \ll \sigma/r$ in the transition region. These terms are comparable in magnitude when $b = 0{\cdot}25\mu$, corresponding to $W = 1\times10^{-3}$, but the disjoining pressure must be quite negligible when W is an order of magnitude larger. However, when $\mu U/\sigma$ is around 2×10^{-4} systematic divergences between theory and experiment, though smaller, are still apparent, particularly in the case of aniline. Thus though discrepancies at the slowest speeds may possibly be accounted for in this way, this explanation is incomplete.

4. Bubble in a vertical tube

4.1. *Theory. First approximation*

(i) In this section we consider the motion at low Reynolds number of a long bubble in a vertical tube sealed at one end. Gravitation enters into the problem only as a buoyancy force, and always occurs in the equations multiplied by the density difference ρ between the fluid outside and that inside the bubble. When the problem was first attempted it was thought that $\mu U/\sigma$ and $\rho gr^2/\sigma$ should tend to zero together, but the method of §2 produced nonsensical results. Observation of rising bubbles at once suggested the answer, that there is a critical value of $\rho gr^2/\sigma$ below which no rise at all takes place, and application of the lubrication assumptions to flow under small values of $\mu U/\sigma$ and values of $\rho gr^2/\sigma$ slightly greater than the critical gave self-consistent results. This application is given in the remainder of this subsection, together with reasons why no similar theory exists when ρ is slightly subcritical. In §4.2 the range of validity of the theory is considered, and finally in §4.3 some experimental confirmation is mentioned.

(ii) The method of analysis is very similar to that of the previous section. The restriction to cases when the steady speed of rise U is such that $\mu U/\sigma \ll 1$ again implies that the effect of viscous forces on the profile of the bubble will be confined to a region near the wall. Further, in the absence of contrary evidence, axial symmetry will be assumed.

The front and rear menisci are separated by the region CD (figure 6), where a uniform film of fluid is draining under the effects of gravity alone. In regions AB, EF the viscous stresses exert a negligible influence on the film profile, which is determined by static equilibrium between surface tension and gravitational stresses. In the transition regions viscous stresses are important, but the film profiles are everywhere nearly parallel to the tube wall, and the 'lubrication hypothesis' proves to be a self-consistent approximation.

(iii) In the regions AB, EF the profile is determined by the condition

$$\sigma\kappa_1 = \rho gx, \tag{34}$$

where κ_1 is the mean curvature of the surface and x the height above some fixed level. This is the equation which was treated by Bashforth & Adams (1883) in their computations on the profiles on pendent and sessile drops, and into whose results more detail has been interpolated by Fordham (1948). However, for the purpose of this paper the author required a criterion which could not be obtained

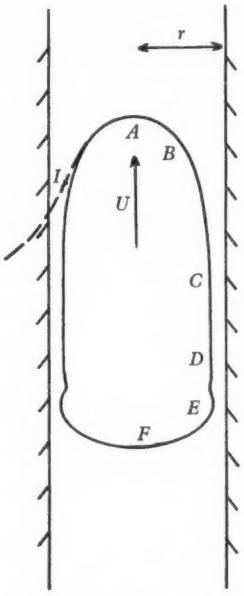

FIGURE 6. Section of a bubble in a vertical tube.

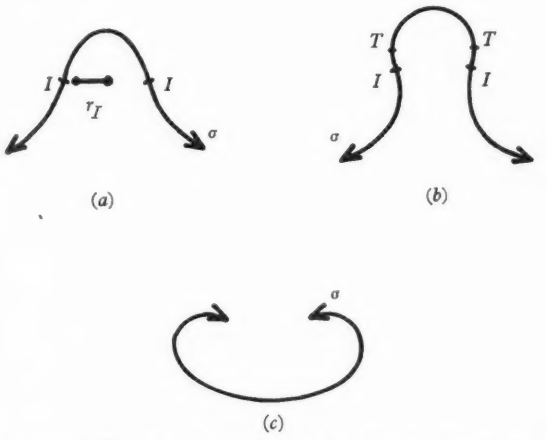

FIGURE 7. Equilibrium profiles under surface tension and gravity forces. (*a*) Top meniscus $\rho g r_I^2/\sigma > 0{\cdot}842$; (*b*) top meniscus $\rho g r_I^2/\sigma < 0{\cdot}842$; (*c*) bottom meniscus.

accurately from these tables, so the digital computer EDSAC II was programmed to give it. The calculated profiles for region AB may be divided into two classes shown diagrammatically in figure 7 (*a*) and (*b*). A member of each of these has a point of inflexion I, at which the radius is r_I, but if $\rho g r_I^2/\sigma > 0{\cdot}842$, as in figure 7 (*a*), there is no point at which the tangent plane is vertical. In figure 7 (*b*) the tangent plane is vertical at a point T. Furthermore, for $|(\rho g r_I^2/\sigma) - 0{\cdot}842| < 0{\cdot}2$, the angle ϕ made with the vertical by the tangent plane at I is given by

$$\phi = 0{\cdot}49\{(\rho g r_I^2/\sigma) - 0{\cdot}842\}. \tag{35}$$

The profile within this range will prove of most interest to us in the following discussion. The profiles for region EF exhibit no point of inflexion, as shown in figure 7 (*c*).

(iv) We now consider the transitional and uniform regions $BCDE$, using the notation of figure 8. If the rate of rise is sufficiently small, the lubrication approximations will describe the flow, and the analysis proceeds exactly as in § 2, except that the pressure everywhere must be modified to account for the gravitational body force, by addition of a term $\rho g x$. Also, the flux V_b in the uniform region is not

zero, but $\rho g b^3/3\mu$ per unit circumference. It is to be expected that, for sufficiently small $\mu U/\sigma$ the ratio of film thickness to tube radius will also be small. This proves to be self-consistent. Equation (9) of § 2.1 is modified to read

$$y_1''' - \frac{\rho g}{\sigma} = \frac{3\mu U}{\sigma}\frac{1}{y_1^3}\left(y_1 - b - \frac{\rho g b^3}{3\mu U}\right). \tag{36}$$

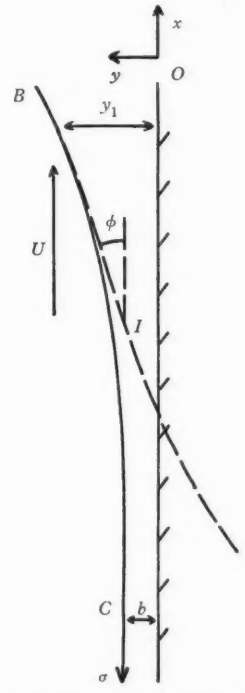

FIGURE 8. The top transition region.

In this problem, however, there is an additional continuity requirement, that all the fluid displaced by the top meniscus of the rising bubble should flow through the uniform region CD to the lower meniscus. Thus

$$-\frac{\rho g b^3}{3\mu} = V_b = -\frac{1}{2\pi r}\{U\pi(r-b)^2\},$$

i.e.

$$\frac{\rho g b^2}{3\mu U} \simeq \frac{r}{2b}, \tag{37}$$

to this order of approximation. Thus, for sufficiently small b/r the last term on the right-hand side of equation (36) greatly exceeds the other two throughout region $BCDE$, and the film profile is given by

$$y_1''' = \frac{\rho g}{\sigma}\left(1 - \frac{b^3}{y_1^3}\right). \tag{38}$$

This may be made dimensionless by the substitution

$$y_1 = b\eta, \quad x = b\,(\rho g b^2/\sigma)^{-\frac{1}{3}}\xi, \tag{39}$$

to give

$$\eta''' = \frac{\eta^3 - 1}{\eta^3}. \tag{40}$$

(v) This equation should be compared with equation (11) of §2.1. In the region CD, $y_1 \simeq b$, $\eta''' \simeq 3(\eta - 1)$. As before this enables us to say that, given b, for a top meniscus there is an essentially unique profile, whereas for a bottom meniscus an infinite family. Also, the relations (39) show that for sufficiently small $\rho g b^2/\sigma$, provided b/r is also small, there exist regions in which

$$\eta = y_1/b \ll 1, \quad y_1/r = b\eta/r \ll 1,$$

and yet

$$y_1' = (\rho g b^2/\sigma)^{\frac{1}{3}}\,\eta \ll 1.$$

Here equation (38) is still valid, but $\eta''' \simeq 1$ and

$$\eta \simeq \tfrac{1}{6}\xi^3 + \tfrac{1}{2}P\xi^2 + Q\xi + R \tag{41}$$

for some constants P, Q, R, which are determined to within a change of origin at a top meniscus. However, in this region $d\kappa_1/dx \simeq y_1''' \simeq \rho g/\sigma$, so equation (41) refers to a region of equilibrium between surface tension and gravity. This is the defining condition of regions AB, EF so the profile there must be identical with that part of one of the profiles shown in figure 7 where the tangent plane is nearly vertical.

But, for a top meniscus, it can fairly easily be shown, and numerical integration confirms, that equation (31) admits of no point where $\eta' = 0$ and the tangent plane is accurately vertical. Thus, no matching at all is possible to a profile of type 7 (b). For a profile of type 7 (a) matching is possible within the assumptions of this section, provided ϕ is small—in other words, provided $\rho g r_I^2/\sigma$ is only slightly greater than 0·842. With origin chosen so that $P = 0$, numerical integration for a top meniscus gives

$$P = 0, \quad Q = 0{\cdot}572, \quad R = 1{\cdot}10.$$

At the point of inflexion I

$$y_1 = 1{\cdot}10b, \quad y_1' = 0{\cdot}572(\rho g b^2/\sigma)^{\frac{1}{3}}, \quad r_I = r - y_1.$$

Insertion in equations (35), (37) gives

$$\begin{aligned}\frac{\rho g r^2}{\sigma} - 0{\cdot}842 &= 1{\cdot}10\left(\frac{b}{r}\right)^{\frac{2}{3}} + 1{\cdot}85\frac{b}{r} \\ &= 1{\cdot}25\left(\frac{\mu U}{\sigma}\right)^{\frac{2}{3}} + 2{\cdot}24\left(\frac{\mu U}{\sigma}\right)^{\frac{1}{3}}.\end{aligned} \tag{42}$$

Near the rear meniscus the film thickness again has a wave-like appearance and a profile can be found matching a meniscus moving with speed U to any small film thickness b.

(iv) The impossibility of matching solutions of equation (38) to a profile of type 7 (a) does not demonstrate that a bubble will not rise in a tube with $\rho g r^2/\sigma < 0{\cdot}842$, for it could do so unsteadily, or under conditions in which the lubrication

approximations do not hold. However, it does indicate a critical radius at which the type of flow changes drastically, and quite simple experiments are sufficient to indicate the nature of the change. These are mentioned in §4.3.

4.2. *Review of approximations*

(i) The importance of inertia forces in the transition region is measured by the ratio $\rho ub^2/\mu L$, where u is a typical velocity, and L the length scale of variation along the streamlines. This latter is $b(\rho gb^2/\sigma)^{-\frac{1}{3}}$, so from continuity the relevant Reynolds number is $(\rho ur/\mu)(\rho gb^2/\sigma)^{\frac{1}{3}}$. For water this becomes of order unity when $\mu u/\sigma$ is around 8×10^{-5}, and $(\rho gr^2/\sigma)-0{\cdot}842 \simeq 0{\cdot}25$, and the neglect of inertia forces is a severe limitation. However, also of importance are the geometrical and related approximations made in deriving equation (42).

(ii) To obtain an estimate of the validity of these results we note that the analysis of §2.2 leading to equation (31) applies directly to this problem, provided we add a 'virtual pressure' ρgx to the true pressure everywhere to account for the gravitational body force. For provided the Reynolds number is small the boundary conditions and equations of motion are otherwise unaltered. Equation (31) now becomes

$$\kappa_1'-\frac{\rho g}{\sigma}-\frac{3\mu U}{\sigma}\frac{y_1-c}{y_1^3}=\frac{3\mu U}{\sigma}\frac{1}{y_1^3}\left\{\tfrac{3}{5}y_1y_1''(y_1+4c)+\tfrac{1}{5}y_1'^2(y_1+8c)+\frac{y_1^2-2cy_1}{2r}\right\}. \quad (43)$$

When $y_1=b$, $y_1'=y_1''=0$, $\kappa_1=1/(r-b)$, so

$$\frac{\rho gb^3}{3\mu U}+b-c=-\frac{b^2-2bc}{2r}.$$

It is also clear from the definition of the constant c of equation (28) that if the bubble surface were to fill completely the cross-section of the tube ($y_1=0$) there would have to be an upward flux $-2\pi rUc$ flowing somehow past the bubble. But in this case the tube is sealed at one end, so $c=\frac{1}{2}r$ exactly. Thus the next approximation to equation (37) is

$$\frac{r}{2}=\frac{\rho gb^3}{3\mu U}+\frac{b}{2}.$$

(iii) Comparison of these equations with equations (37), (38) show that the approximations made in deriving equation (42) have arisen in three ways. The flow in the transition region is not quite undirectional and the terms describing departures from the parabolic velocity profile are the first two on the right-hand side of equation (42), and are smaller than those retained in equation (38) by $O(b/r)^{\frac{2}{3}}$. Terms arising from the film thickness in the transition region being a finite proportion of the radius of the tube are $O(b/r)^{\frac{1}{2}}$. Finally, the neglect of changes in the mean curvature due to axial symmetry is $O(b/r)^{\frac{1}{3}}$ but numerical integration of the relevant equation shows that all these errors are slightly smaller than those contained in equation (35), which approach 10% when

$$(\rho gr^2/\sigma)-0{\cdot}842=0{\cdot}25 \quad \text{and} \quad \mu U/\sigma=8\times10^{-5}.$$

This estimate is for the error in the constants P, Q, R and hence in the profile attained by the meniscus well away from the wall. This profile is identified by the radius at which it would have a point of inflexion if it were continued outwards according to figure 7(*a*). Although the second term in equation (42) is $O(b/r)^{\frac{1}{3}}$ smaller than the first it may still consistently be retained for it arises only in relating r_I to r, once r_I has been correctly identified. Its omission would severely restrict the range of validity of the result.

4.3. *Experimental results*

Complete verification of equation (42) and of the prediction that the bubble will not rise is difficult. One requires, for any given fluid, a tube of constant diameter accurately known and very near the critical value. By chance, however, for water at 20° C and a tube of diameter 0·50 cm (nominal) $\rho g r^2/\sigma = 0{\cdot}842$. The predicted rate of rise at 40 °C is $2{\cdot}1 \times 10^{-3}$ cm/sec. The author immersed such a vertical tube in a water bath with temperature variable between 15 and 40 °C. The results were not completely reproducible. At 15 °C, $\rho g r^2/\sigma = 0{\cdot}834$, the bubble was usually stationary; at 40 °C it was always rising with speeds of the order of a few cm per hour. These speeds depended on the position in the tube and on whether it was accurately vertical. In view of the probable presence of impurities and of variations in the diameter of the tube, these results indicate quantitative agreement with the main conclusion that the bubble will not rise if $\rho g r^2/\sigma < 0{\cdot}842$ and qualitative agreement with equation (42).

5. Conclusion

The theories of this paper form a small contribution to the problem of predicting the profile of a bubble in a capillary tube and the rate of rise of a bubble in a vertical tube. They are limited by the basic physical assumptions made about the properties of the free surface of liquid films under these conditions, that there should be a well-defined surface tension and hence no tangential stress on the surface. Perfect wetting on the tube wall is also essential. But provided inertia forces are negligible, and provided the film left on the wall during the passage of the bubble is sufficiently thin, the effects of viscous forces on the profile of the interface can be described by the lubrication equations, and are confined to a region near the wall. The remainder of the profile is governed by the same relations as if the bubble is stationary, but there is an intermediate region in which the two solutions can be matched. The thickness of fluid left on the wall is in each case determined uniquely by conditions at the front meniscus, whereas at the rear meniscus there is a steady solution matching smoothly onto any film thickness that should previously have been left there. At the rear meniscus also, the profile shows oscillations in thickness in advance of the main curvature. In a capillary tube the bubble moves slightly faster than the mean speed of the fluid in the tube, the fractional correction being $1{\cdot}29(3\mu U/\sigma)^{\frac{2}{3}}$. At the slowest speeds the main pressure drop in such a tube arises from the slight difference in curvature between the front and rear menisci of the bubble, and is $4{\cdot}52(\sigma/r)(3\mu U/\sigma)^{\frac{2}{3}}$. These results are only valid if $\mu U/\sigma < 5 \times 10^{-3}$.

The free rise of a long bubble in a vertical sealed tube is completely inhibited if $\rho g r^2/\sigma < 0{\cdot}842$. This is associated with the existence of a profile in static equilibrium making zero angle of contact with the wall only for smaller radii. For radii up to 12% larger than the critical the rate of rise increases very rapidly, being given by

$$(\rho g r^2/\sigma) - 0{\cdot}842 = 1{\cdot}25(\mu U/\sigma)^{\frac{2}{3}} + 2{\cdot}24(\mu U/\sigma)^{\frac{1}{3}}.$$

From a practical point of view the cases of most interest are when $\mu U/\sigma$ is larger than the very small values discussed here. When surface tension is not dominant, however, none of these methods are appropriate, and a satisfactory method of analysis has yet to be found.

The waves near the rear meniscus predicted in §2.2 are easily observable at larger film thicknesses than those for which theory is valid, and seem to be of quite general occurrence. From the point of view of causality, it is of interest that the values of b/r obtained are in each case determined by consideration of the front meniscus alone. The predictions of the pressure drop across the bubble in a capillary are also of no great practical use, for at the very small values of $\mu U/\sigma$ for which they apply, effects due to the variations in the radius of the tube are likely to be larger. The two-dimensional version of this theory is applicable to the motion of fingers in Hele–Shaw cells considered by Saffman & Taylor (1958), but the restriction to small values of $\mu U/\sigma$ precludes at present an explanation of their results. Experimental verification of this theory is unsatisfactory. For values of $\mu U/\sigma$ larger than 3×10^{-3} the results of this present work, those of Fairbrother & Stubbs (1935), Taylor (1961), and Goldsmith & Mason (1960) are in broad agreement that Fairbrother & Stubbs's formula $1{\cdot}0(\mu U/\sigma)^{\frac{1}{2}}$ is a good estimate for the value of W up to $\mu U/\sigma = 0{\cdot}08$, above which it over estimates the true value. Below 3×10^{-3}, which is also the upper limit of the present theory, there is widespread disagreement, and at the very slowest speeds the divergences between experiment and the two-thirds power law involve a factor of 8. Although in principle the method used by the present author is probably the most accurate in this range, he is unable even to suggest an explanation of this situation. There have also been widely differing estimates of the critical radius below which a long bubble in a vertical tube will not rise. This is surprising, for the phenomenon is striking, and above the critical point the speed of rise increases very rapidly with radius. Provided that adequate precautions are taken about cleanliness, that the cross-section of the tube be circular, and that it be accurately vertical, it should be possible in further experiments to narrow this range considerably.

The author is indebted to Sir Geoffrey Taylor and Dr P. G. Saffman for invaluable help and discussions, to Mr R. G. Wooding and Mr W. E. Thompson for assistance with experiments, to Dr S. G. Mason for commenting on this manuscript, and to the Department of Scientific and Industrial Research for a grant.

REFERENCES

Barr, G. 1926 *Phil Mag.* **1**, 395.

Bashforth, F. & Adams, J. C. 1883 *An Attempt to Test the Theories of Capillary Action.* Cambridge University Press.

Christopherson, D. G. & Dowson, D. 1959 *Proc. Roy. Soc.* A, **251**, 550.

FAIRBROTHER, F. & STUBBS, A. E. 1935 *J. Chem. Soc.* **1**, 527.

FORDHAM, S. 1948 *Proc. Roy. Soc.* A **194**, 1.

FRENKEL, J. 1946 *Kinetic Theory of Liquids*, p. 332. Oxford University Press.

FRUMKIN, A. & LEVICH, V. 1947 *Zh. fiz. khim.* (*J. Phys. Chem., Moscow*), **21**, 1183.

GIBSON, A. H. 1913 *Phil. Mag.* **26**, 952.

GOLDSMITH, H. L. & MASON, S. G. 1960 Private Communication. McGill University, Montreal.

MARCHESSAULT, R. N. & MASON, S. G. 1960 *Ind. Engng Chem.* **52**, 79.

SAFFMAN, P. G. & TAYLOR, G. I. 1958 *Proc. Roy. Soc.* A, **245**, 312.

TAYLOR, G. I. 1961 *J. Fluid Mech.* **10**, 161.

The wave drag of wind over water

By R. W. STEWART

University of British Columbia,† Vancouver, British Columbia

(Received 3 October 1960)

It is shown to be probable that a large proportion of the drag exerted by a water surface on the wind is in the form of wave drag. As a result the usual relation between the wind profile and the surface stress and roughness length are modified. In particular, close to the surface the relation between the transport of momentum and that of heat and water vapour are different from that obtaining over a rough solid surface.

1. Introduction

The interaction between wind and a water surface seems to have been considered from two points of view. In one, favoured by meteorologists, the water surface is regarded as a boundary of the same general nature as solid ground, with negligible velocity relative to that of the wind, which exerts a shearing stress upon the air. From this point of view the principal problem is to determine the characteristic 'roughness length' of the water surface (e.g. see Ellison 1956).

On the other hand there is a growing body of literature (Eckart 1953; Ursell 1956; Phillips, 1957, 1958; Miles 1957, 1959, 1960; Shuleykin 1959) in which the problem of wave generation by wind is treated, the nature of the air flow being taken as given.

An important aspect of this problem seems to have been overlooked. It will be shown below that of the momentum withdrawn from the air by interaction with the water surface, a far from negligible proportion goes into *wave* momentum. It is not difficult to show that the effective height at which the air loses this momentum is not the surface, but is in fact some height at which the wind speed is not less than the phase speed of the waves. We therefore conclude that over water the lowest levels of the atmosphere cannot be considered to be a region of constant turbulent stress, as is usually assumed, but that the turbulent stress must increase with height above the surface. We should thus expect modification of the wind-velocity profile over water and failure of the usual relation between this profile and the surface stress.

2. Momentum input to waves

Although there remains considerable uncertainty about the exact nature of the waves produced by a wind of given strength, duration and fetch, the body of empirical data is now so large that no modern compilation can be very far from the truth. The most convenient presentation is probably that of Groen &

† Now Visiting Professor, Dalhousie University, Halifax, Nova Scotia.

Dorrestein (1958). They have used virtually all the data on wind waves published prior to 1957 to obtain average wave characteristics as a function of wind duration and wind speed. In their Diagram I, wave height H and wave period T is plotted against duration t with wind speed U as a parameter. I have taken from these curves the values for U, t, T and H given in table 1. The curves can be read reliably only to two significant figures, but this accuracy is at least as good as the data upon which they are based.

U (m/sec)	t (hr)	T (sec)	H (m)	E (j/m²)	$C = gT/2\pi$ (m/sec)	$E/C = M$ (kg sec^{-1} m^{-1})	M/t (kg sec^{-2} m^{-1})
10	0·5	1·9	0·32	126	2·96	43	$2{\cdot}4 \times 10^{-2}$
	1·0	2·5	0·53	340	3·9	87	2·4
	2·0	3·2	0·88	950	5·6	190	2·6
	3·0	3·8	1·14	1,590	5·9	270	2·5
	6·0	4·7	1·55	2,940	7·3	462	1·9
15	0·5	2·5	0·54	360	3·9	92	5·1
	1·0	3·2	0·89	970	5·0	194	5·4
	2·0	4·1	1·45	2,570	6·4	40	5·6
	3·0	4·7	1·95	4,650	7·3	64	5·9
	6·0	6·2	2·95	10,600	9·7	109	5·1
	9·0	7·1	3·5	15,000	11·1	135	4·2
20	0·5	2·9	0·77	720	4·5	16	8·9
	1·0	3·8	1·26	1,940	5·9	33	9·2
	2·0	4·9	2·15	5,700	7·65	745	10·4
	3·0	5·8	2·85	9,900	9·05	109	10·0
	6·0	7·5	4·5	24,800	11·7	212	9·8
	9·0	8·6	5·6	38,400	13·4	287	8·9
	12·0	9·4	6·3	48,600	14·7	338	7·8

Table 1

Wind-driven waves are certainly not completely irrotational. On the other hand the relations between wavelength, wave period and phase speed observed for such waves do not differ greatly from those of irrotational waves. It seems unlikely that the momentum associated with the wave motion is greatly different from that of an irrotational wave of the same height and period. If anything, the momentum in the real wave may be somewhat greater than that in the irrotational one.

It is not difficult to show (Lamb 1932, §250) that in an irrotational wave the relation between the wave momentum per unit area M and the wave energy per unit area E is

$$M = \frac{E}{C} = \frac{2\pi E}{g T}. \tag{1}$$

In an actual sea a fairly wide spectral band of wavelengths contributes to the energy, but it is difficult to see how the relations between momentum, energy density and a characteristic wave period could differ greatly from (1).

With these assumptions I have listed in table 1 the wave momentum corresponding to the data shown from Groen & Dorrestein. The average rate of increase of wave momentum can be obtained by dividing by the wind duration t.

An inspection of the last column of table 1 shows that the average rate of momentum increase, M/t, is nearly constant for a very considerable time after the onset of the wind. At later times, of course, saturation effects dominate, and the momentum input must be balanced by losses due to wave breaking, turbulence and viscosity.

The data of table 1, for sufficiently small t, may be summarized by

$$\frac{M}{tU^2} = 2{\cdot}4 \times 10^4 \quad \mathrm{kg\,m^{-3}}. \tag{2}$$

Now $M/tU^2\rho$, where ρ is density of air, has the nature of a drag coefficient, say

$$C_{dW} = 2 \times 10^{-4}, \tag{3}$$

if we define the total drag coefficient C_d by putting the stress

$$\tau = C_d \rho U^2. \tag{4}$$

The total drag coefficient given by Ellison (1956) for winds of about 15 m/sec, using (4) as a definition of C_d, varies only slightly with U and has an average value

$$C_d = 10 \times 10^{-4}. \tag{5}$$

Clearly, then, the contribution of the wave drag (3) to the total drag (5) is far from negligible. Moreover, the estimate of the wave drag given in (3) is really only a lower limit. All the momentum which was originally put into waves, but which has been lost to the drift current because of wave-dissipation mechanisms, is omitted from the estimate. It will be seen below that there are reasons for believing that a majority of the momentum is transferred by wave drag.

3. Interaction height

The energy to momentum ratio of a surface wave is equal to the phase speed C. If an interaction with the air transfers energy and momentum to the waves, then for a given quantity of momentum transferred the energy lost by the air must be at least equal to the energy gained by the waves.

Thus,
$$d(1/2\rho U_i^2) \geqslant C d(\rho U_i), \tag{6}$$

or
$$U_i \geqslant C,$$

where U_i is the wind velocity at the height at which the reaction of the air to the wave drag is effective. Miles (1960) finds that the rate of increase of wave energy depends upon the variation of the velocity profile at the point where $U = C$. This is consistent with (6), as is the reasonance mechanism proposed by Phillips (1957).

4. Energy and momentum transfer

A brief examination of the means by which energy and momentum are transferred from the air to the wave is warranted. In an ordinary turbulent shear flow over a solid surface, momentum is transferred towards the boundary by a Reynolds stress τ. If the boundary is smooth, viscous shear stress ultimately takes over, while if it is rough the force on the boundary is exerted by pressures on the roughness elements. Energy passes towards the boundary by the action of

the Reynolds stress in a term of the form τU. There is also a transfer due to the covariance $-\overline{pv}$ of the pressure fluctuation p and the vertical turbulent velocity $-v$, as well as the 'turbulent energy diffusion' $-\frac{1}{2}\rho\overline{q^2v}$, where q is the local instantaneous speed of the fluctuating motion (Townsend 1955). If the boundary is stationary, no energy goes into it, all the energy being dissipated by the turbulence and the viscous sublayer.

In the case of wave generation the situation is somewhat different. The momentum will be carried right to the surface by the Reynolds stress, as in rough flow. Energy is again transferred to the extent $\tau U - (\overline{pv} + \frac{1}{2}\rho\overline{q^2v})$. However, the energy going into the waves must pass unattenuated through the region where $U < C$. Thus, as τU decreases, $-(\overline{pv} + \frac{1}{2}\rho\overline{q^2v})$ must increase to compensate.

Motions of the required nature must be too highly organized to be called turbulence, particularly since no absorption of energy is involved. Highly organized motions of the required type are involved in Miles's (1960) discussion. They are not described, but must also occur, in the mechanism described by Phillips (1957). In Miles's case the motions are in response to the moving surface, and a Reynolds stress is developed which remains constant with increasing height to the level where $U = C$ and then drops to zero. In Phillips's case the motions must be in response to moving pressure fluctuations in the air at levels $U \geqslant C$, and to movements of the surface caused by these pressures.

5. 'Rough' air flow and wave generation

It is generally believed (e.g. see Ursell 1956, Ellison 1956) that the water surface is at least nearly aerodynamically 'rough' so far as its influence on the motion of the air is concerned. To the extent that this belief is justified, then, the momentum of the air is transmitted into the water because of the correlation between local pressure and local surface slope. Looked at from the point of view of the water, we find that the water is receiving momentum from the air by pressure forces.

Now, in a homogeneous fluid pressure can only produce irrotational motion, and it is difficult to conceive of an irrotational motion carrying momentum which does not have the character of a surface wave, provided water far below the surface is stationary. (The only motion meeting the requirement in the case of a large surface of water seems to be one in which there is a correlation between particle velocity and surface elevation, and it is difficult to see how such a motion would differ from that of a wave.) This argument leads to belief that perhaps most of the momentum from the air enters the water in the form of wave motion. Of course much may go into very small waves or ripples which rapidly decay and lose their momentum to the drift current. The data of Groen & Dorrestein are certainly not inconsistent with this view.

6. Consequences

We have seen above that momentum and energy going into waves of phase velocity C must pass unattenuated through the portion of the air column for which $U < C$. As was remarked, the motions which carry this

stress and energy cannot be described as turbulence. Above the level where $U = C$, however, this stress will be carried by the turbulence. We therefore conclude that the stress carried by the turbulence must *increase* with height above the water surface.

Any discussion of the relation between the turbulent intensity and the mean velocity gradient, whether or not employing the concept of 'eddy viscosity', must lead to the conclusion that the near-surface velocity shear is less in the present case than over a solid boundary. The simple dimensional argument:

$$\frac{\tau_t}{\rho z^2} \propto \left(\frac{\partial U}{\partial z}\right)^2, \tag{7}$$

yields the result that the velocity gradient will be reduced as the square root of the turbulent stress. Here τ_t has been written for the turbulent shear stress.

The usual method of analysis is to assume that the mean velocity will have the form

$$U = \frac{u^*}{K} \ln\left(\frac{z}{z_0}\right), \tag{8}$$

where $u^* = (\tau/\rho)^{\frac{1}{2}}$ and k is von Karman's constant $= 0{\cdot}4$. Measurements of U are made at a variety of heights, so that τ and the roughness length z_0 may be determined.

The consequence of the increase of turbulent stress with height may be expected to be a reduction in $\partial U/\partial z$ at low levels compared with that occurring over a solid surface with the same total stress. The usual interpretation of the data is likely to yield too low a value for the shear stress, and a value for the roughness length which will increase as the height of observation increases.

The most important consequence, however, is likely to be in making estimates of the turbulent transports of heat and water vapour. At the height at which most observations are taken, it is probable that most of the stress is carried by the turbulence, and the error in the calculated total stress may be small, although the significance of the calculated z_0 may be doubtful. However, if the usual interpretation is put upon the data there there will be a large overestimate of the intensity of the turbulence close to the surface. The motions transferring momentum and energy to the water waves will be organized and wave-like, and presumably will contribute little to the transport of sensible heat and water vapour. Thus, in the critical region close to the surface, the transport coefficients for heat and water vapour may be much lower than might be inferred from the momentum transport. It is quite likely, then, that the temperature gradients and humidity gradients close to the water surface will be much larger than would be anticipated from the usual assumptions. It would be useful to have some experimental results to check this conclusion.

This work is a contribution of the Defence Research Board of Canada.

REFERENCES

Eckart, C. 1953 *J. Appl. Phys.* **24**, 1485.

Ellison, T. H. 1956 Article in *Surveys in Mechanics*, edited by G. K. Batchelor and R. M. Davies, Cambridge University Press.

GROEN, P. & DORRESTEIN, R. 1958 *Zeegolven, Kon. Ned. Met. Inst.* report no. 11.

LAMB, H. 1932 *Hydrodynamics*, 6th ed. Cambridge University Press.

MILES, J. W. 1957 *J. Fluid Mech.* **3**, 195.

MILES, J. W. 1959 *J. Fluid Mech.* **6**, 568.

MILES, J. W. 1960 *J. Fluid Mech.* **7**, 469.

PHILLIPS, O. M. 1957 *J. Fluid Mech.* **2**, 417.

PHILLIPS, O. M. 1958 *J. Fluid Mech.* **4**, 426.

SHULEYKIN, V. V. 1959 *Kratkie Kours Fiziky Morya.* Gidrometeoizdat, Leningrad.

TOWNSEND, A. A. 1955 *The Structure of Turbulent Shear Flow.* Cambridge University Press.

URSELL, F. 1956 Article in *Surveys in Mechanics*, edited by G. K. Batchelor and R. M. Davies. Cambridge University Press.

Unsteady interaction of a shock wave with a cellular vortex field

By J. E. WERNER

School of Aeronautics and Astronautics, New York University

(Received 28 May 1960 and in revised form 16 November 1960)

The transient effects generated when a shock wave is suddenly disturbed by a field of cellular vortices have been studied. Both the pressure disturbance on the shock and the local shock velocity are found to be strong functions of the cell geometry. Disturbances are resolved into transient components and sinusoidal components of constant amplitude. The transients are found to die out as $t^{-3/2}$, t being the interaction time, except for one particular case of the cell geometry for which they diminish as $t^{-1/2}$. Furthermore, the analysis indicates that the initial magnitude of the transient components may be quite appreciable in comparison with the sinusoidal component. The theory is extended to treat the convection through the shock of a single column of vortex cells.

1. Introduction

It has been demonstrated (Kovasznay 1953, Chu & Kovasznay 1958) that an arbitrary weak disturbance in a uniform compressible flow can be decomposed into component modes of vorticity, sound and entropy. As a consequence of linearization these fields have the important property of being independent of each other in the absence of natural boundaries. Across a shock-wave, however, the presence of large gradients in the basic flow make it necessary to retain the non-linearity of the fundamental equations. This results in a coupling of modes. In particular a first-order vorticity fluctuation, upon passing through a shock front, generates sound and entropy fields behind the shock (Ribner 1953). At the same time, local displacement of the shock occurs, which means that the analytical problem is of the nature of an unsteady boundary value problem with a free boundary.

The specific model employed here is illustrated in figure 1. A two-dimensional cellular vortex field with a discrete front is convected into an initially plane, normal shock-wave. The objective of the analysis is to investigate the transient behaviour of the shock front and the pressure disturbance generated on the downstream face of the shock.

Interaction studies of a similar nature have been carried out by Ribner (1953), Moore (1953) and Chang (1957). These differ from the present analysis in that they treat the case of a single harmonic disturbance of infinite extent in space. Such a model can be reduced to a steady state problem by a simple translation of the co-ordinate system. It therefore lacks the transient or 'initial' behaviour of the present model. On the other hand, the treatment by Ram & Ribner (1957) of shock interaction with a single vortex exhibits transient

behaviour only. The model considered here occupies a position between the two in that it is comprised of transients which subside, leaving a completely periodic behaviour which may be compared with the results of Ribner (1953), Moore (1953) and Chang (1957). That transient behaviour is significant is borne out by the analysis which indicates that transient components of pressure may in some cases be an order of magnitude larger than the eventual steady-state amplitude. Thus, transients should be considered in any estimates of disturbances generated by an unsteady interaction process.

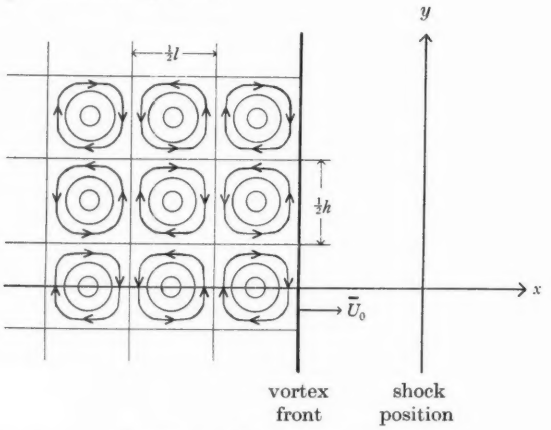

FIGURE 1. Cellular vortex field.

2. Fundamental equations

The flow field is described in co-ordinates fixed at the mean position of the shock as indicated in figure 1. To represent fluctuations, $\delta(\ )$, of pressure P, density ρ_T, velocity $\mathbf{V}$ and entropy Σ the following non-dimensional variables are employed:

$$p = \delta P/\gamma\bar{P},$$
$$\rho = \delta\rho_T/\bar{\rho},$$
$$\sigma = \delta\Sigma/C_P,$$
$$\mathbf{v} = \mathbf{i}u + \mathbf{j}v = \mathbf{i}\frac{\delta U}{a} + \mathbf{j}\frac{\delta V}{a} = \frac{\delta \mathbf{V}}{a},$$

where a is the speed of sound in the basic flow, C_p is the specific heat at constant pressure, and γ is the ratio of specific heats. Basic flow quantities are denoted by $(\bar{\ })$. In terms of these variables the linearized equations of motion for the region behind the shock are, denoting this region by $(\ )_1$,

$$\left.\begin{aligned} &\text{continuity,} && \frac{Dp_1}{D\tau} + \nabla.\mathbf{v}_1 = 0;\\ &\text{momentum,} && \frac{D\mathbf{v}_1}{D\tau} + \nabla p_1 = 0;\\ &\text{energy,} && \frac{D\sigma_1}{D\tau} = 0;\\ &\text{state,} && p_1 - \rho_1 = \sigma_1. \end{aligned}\right\} \tag{2.1}$$

Here $\tau = a_1 t$ and $D/D\tau$ is the linearized Stokes derivative:

$$\frac{D}{D\tau} = \frac{\partial}{\partial \tau} + M_1 \frac{\partial}{\partial x},$$

where $$M_1 = \bar{U}_1/a_1.$$

3. Specification of upstream disturbance

Denoting the region ahead of the shock by $(\ )_0$, the following velocity perturbation in the oncoming flow is assumed:

$$\left.\begin{aligned} u_0(x,y,t) &= |u_0| \sin\kappa(\bar{U}_0 t - x)\sin\lambda y, \\ v_0(x,y,t) &= -\frac{\kappa}{\lambda}|u_0|\cos\kappa(\bar{U}_0 t - x)\cos\lambda y, \end{aligned}\right\} \quad (\bar{U}_0 t - x > 0);$$
$$\left.\begin{aligned} u_0(x,y,t) &= 0, \\ v_0(x,y,t) &= 0, \end{aligned}\right\} \quad (\bar{U}_0 t - x \leqslant 0). \qquad (3.1)$$

The field represented by this perturbation has the cellular structure illustrated in figure 1, which shows the streamlines as they would appear to an observer moving with the basic flow. In the interior of the cellular pattern it can be verified, from the linearized equations of motion, that to the first order

$$p_0 = \rho_0 = \sigma_0 = 0. \qquad (3.2)$$

The region near the leading edge of the vortex field requires special consideration. The pressure on the upstream face of the leading edge is second-order in magnitude. On the downstream face the pressure is identically zero. To maintain this pressure unbalanced a thin plate is imagined held at the leading edge of the vortex field until the time $t = 0$, at which instant it is suddenly removed. Immediately after withdrawal of the plate the vortex field is convected into the shock.

Once the vortex front passes through the shock no further flow modification generated at the front can propagate upstream ahead of the shock. This means that the presence of a vortex front no longer affects the disturbance being convected into the shock from upstream. But at the instant the plate is removed the vortex front is just ahead of the shock. It therefore remains to consider the magnitude of the initial disturbance generated during the infinitesimal time interval before the vortices pass through the shock. That the flow modifications generated in this interval may be neglected can be shown by the following considerations. Locally, the instantaneous removal of the plate and the resulting pressure unbalance are roughly equivalent to the diaphragm shattering in a shock tube. If the pressure difference across such a diaphragm is represented by the non-dimensionalized pressure term $p = \delta P/\gamma P$, it can readily be shown by linearization of the Rankine–Hugoniot equations that, for small values of p, the flow velocity behind the resulting weak shock would be, to the first approximation

$$u = \tfrac{1}{2}p. \qquad (3.3)$$

This indicates that the velocity field generated by removing the plate is initially of the same order of magnitude as the pressure unbalance. Since this latter term

is of second order in magnitude, the initial velocity disturbance is also and may be neglected. The disturbance specified by equations (3.1) and (3.2) is thus correct to the first order.

4. Boundary conditions

Equations (2.1) supply the differential relations satisfied at a point downstream of the shock. To complete the formulation, boundary conditions appropriate to these equations are required. These are provided by the values of p_+, ρ_+, v_+ and σ_+, on the downstream face of the shock, which are in turn related to p_-, ρ_-, v_- and σ_-, on the upstream face, through the Rankine–Hugoniot equations. To arrive at the specific relationships a local element of the shock front is isolated as shown in figure 2. Its displacement from its undisturbed position is denoted by $\psi(y,\tau)$ and its velocity with respect to the upstream flow field by $\mathbf{V}_- + \mathbf{i}a_1\psi_\tau$. The angle between the shock and the y-axis is assumed small and equal to ψ_y. These quantities are substituted into the Rankine–Hugoniot equations which are then linearized. The result is a set of simultaneous equations for $p_+, \rho_+, v_+, \sigma_+$ in terms of $p_-, \rho_-, v_-, \sigma_-$.

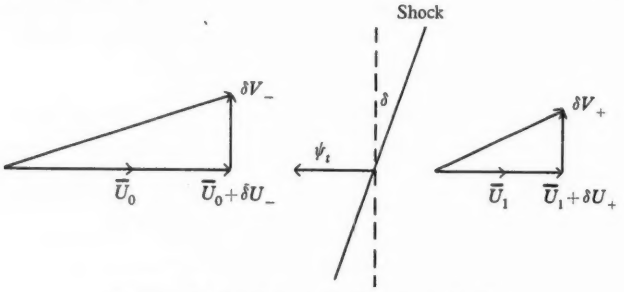

FIGURE 2. Local flow conditions at shock.

The procedure has been carried out by Chang (1957) for the general case of interactions with an oblique shock. Specializing Chang's results for the present case the following equations hold at the shock front:

$$\sigma_+ = \Omega_{13} u_- + \Pi_{11}\psi_\tau, \tag{4.1 A}$$

$$p_+ = \Omega_{23} u_- + \Pi_{21}\psi_\tau, \tag{4.1 B}$$

$$u_+ = \Omega_{33} u_- + \Pi_{31}\psi_\tau, \tag{4.1 C}$$

$$v_+ = \Omega_{44} u_- + \Pi_{41}\psi_y, \tag{4.1 D}$$

where Ω_{ij} and Π_{ij}, as obtained from Chang (1957), are

$$\Omega_{13} = (\gamma-1)(1-\bar{\rho}_1/\bar{\rho}_0)^2 (M_1/M_0)^2,$$

$$\Omega_{23} = -M_1(1-\rho_1/\rho_0)[2+(\gamma-1)(1-\bar{\rho}_1/\bar{\rho}_0) M_1^2](M_1/M_0)/(1-M_1^2),$$

$$\Omega_{33} = (M_1/M_0)[1-(M_1\bar{\rho}_1/\bar{\rho}_0)^2+\gamma(1-\bar{\rho}_1/\bar{\rho}_0)^2 M_1^2]/(1-M_1^2),$$

$$\Omega_{44} = \bar{\rho}_1 M_1/\bar{\rho}_0 M_0,$$

$$\Pi_{11} = -(\gamma-1)(1-\bar{\rho}_0/\bar{\rho}_1)^2(\bar{\rho}_1/\bar{\rho}_0)M_1,$$
$$\Pi_{21} = -M_1(1-\bar{\rho}_0/\bar{\rho}_1)[2+(\gamma-1)(1-\bar{\rho}_1/\bar{\rho}_0)M_1^2]/(1-M_1^2),$$
$$\Pi_{31} = (1-\bar{\rho}_0/\bar{\rho}_1)[1+M_1^2+(\gamma-1)(1-\bar{\rho}_1/\bar{\rho}_0)M_1^2]/(1-M_1^2),$$
$$\Pi_{41} = -(1-\bar{\rho}_1/\bar{\rho}_0)M_1.$$

Along with the specified velocity perturbations at the shock, these equations also include derivatives of the shock displacement. Since displacement is determined only after solution of the flow problem, the shock constitutes a free boundary of the downstream region.

5. The general solution in the region behind the shock

To isolate the pressure p_1 the divergence of the momentum equation, (2.1), is formed and div $\mathbf{v}_1$ eliminated by introducing the continuity relation. The expanded result is

$$\frac{\partial^2 p_1}{\partial\tau^2}+2M_1\frac{\partial^2 p_1}{\partial x\,\partial\tau}-(1-M_1^2)\frac{\partial^2 p_1}{\partial x^2}-\frac{\partial^2 p_1}{\partial y^2}=0. \tag{5.1}$$

In view of the particular time-dependence of the disturbance a solution will be sought by the method of Laplace-transformation. Introducing the pressure transform

$$\tilde{p}_1(x,y,s)=L[p_1(x,y,\tau)]=\int_0^\infty p_1(x,y,\tau)\,e^{-s\tau}\,d\tau, \tag{5.2}$$

the transform of equation (5.1) is

$$s^2\tilde{p}_1+2M_1 s\frac{\partial\tilde{p}_1}{\partial x}-(1-M_1^2)\frac{\partial^2\tilde{p}_1}{\partial x^2}-\frac{\partial^2 p_1}{\partial y^2}=0. \tag{5.3}$$

A general solution of equation (5.3) is obtainable by separation of variables, giving

$$\tilde{p}_1(s)=(A_1\sin\lambda y+A_2\cos\lambda y)$$
$$\times(B_1\exp[\{M_1 s-(s^2+\lambda^2\mu^2)^{\frac{1}{2}}\}x/\mu^2]+B_2\exp[\{M_1 s+(s^2+\lambda^2\mu^2)^{\frac{1}{2}}\}x/\mu^2]), \tag{5.4}$$

where $$\mu^2=1-M_1^2.$$

6. Application of boundary conditions

To satisfy the condition that no disturbances originate in the downstream region we must have

$$B_2=0. \tag{6.1}$$

Additional boundary conditions are furnished by equations (4.1 A–D) which must be satisfied on the shock front. The displacement derivatives ψ_τ, ψ_y are first eliminated by cross-differentiation. Then, with the aid of the fundamental equations (2.1) to eliminate derivatives of u_+ and v_+, the variable p_+ is isolated from the remaining equations to obtain a differential expression for p_+ which must be satisfied by the solution for p_1. This is

$$(1-AM_1)\frac{\partial^2 p_+}{\partial\tau^2}+A(1-M_1^2)\left(\frac{\partial^2 p_1}{\partial x\,\partial\tau}\right)_{x=0}-\frac{AM_1}{C}\frac{\partial^2 p_+}{\partial\tau^2}$$
$$=\frac{AM_1}{C}\left[D\frac{\partial^2 u_-}{\partial y^2}+E\frac{\partial^2 v_-}{\partial\tau\,\partial y}\right]+B\frac{\partial^2 u_-}{\partial\tau^2}$$
$$=\phi(\tau)\sin\lambda y, \tag{6.2}$$

where $$A = \Pi_{21}/\Pi_{31}, \quad B = \Omega_{23} - A\Omega_{33}, \quad C = \Pi_{21}/\Pi_{41},$$
$$D = \Omega_{23}, \quad E = -\Pi_{21}\Omega_{44}/\Pi_{41}.$$

$\phi(\tau)$ is obtained by direct substitution of $u_- = u_0(0, y, \tau)$ etc., into the right-hand side of (6.1), giving

$$\phi(\tau) = |u_0|\,[\phi_0 \sin(\kappa\tau\overline{U}_0/a_1) + \phi_1\delta(\kappa\tau\overline{U}_0/a_1)], \tag{6.3}$$

where $$\phi_0 = (AM_1/C)(D\lambda^2 + E\kappa_1^2\overline{U}_0/a_1) - B\kappa^2(\overline{U}_0/a_1)^2,$$
$$\phi_1 = AM_1D\lambda^2/C - \phi_0,$$

and $\delta(\kappa\tau\overline{U}_0/a_1)$ represents the Dirac delta function arising from discontinuities in the derivatives of u_- and v_-. The absence of cosine terms in equation (6.2) immediately allows us to set $A_2 = 0$. The solution must then be of the form

$$\tilde{p}_1(s) = F(s)\exp[\{M_1 s - (s^2 + \lambda^2\mu^2)^{\frac{1}{2}}\}x/\mu^2]\sin\lambda y, \tag{6.4 A}$$

or in its inverted form

$$p_1(x, y, \tau) = \frac{1}{2\pi i}\int_{c-i\infty}^{c+i\infty} F(s)\exp[\{M_1 s - (s^2 + \lambda^2\mu^2)^{\frac{1}{2}}\}(x/\mu^2) + s\tau]\,ds\sin\lambda y. \tag{6.4 B}$$

Substituting equation (6.4 B) into the boundary condition—equation (6.2)—and setting $x = 0$ an equation is obtained for $F(s)$ which may be put into the form

$$F(s) = \tilde{\phi}(s)\frac{(1+A)s^2 + (AM_1/C)\lambda^2 - AS\{s - (s^2+\lambda^2\mu^2)^{\frac{1}{2}}\}}{(1-A^2)s^4 + \{2(AM_1/C) - \mu^2\}\lambda^2 s^2 + (AM_1/C)^2\lambda^4}. \tag{6.5}$$

From equation (6.4 B) it is evident that $F(s)$ is the transform of $p_+(y\tau)$.

7. Inversion of $F(s)$

With the aid of standard tables and the convolution theorem the inversion of $F(s)$ is achieved in a straightforward manner. The resulting expression however is long and unwieldy. A considerable reduction in the size and number of terms is obtained if we note that over a range of Mach number up to about six, the parameter A is very nearly equal to -1. If this approximation is introduced, equation (6.5) reduces to the simpler form

$$F(s) = -\frac{\mu^2 C}{2M_1 + C\mu^2}\left[\frac{s - (s^2+\lambda^2\mu^2)^{\frac{1}{2}}}{\lambda\mu}\right]\left[\frac{s}{s^2+\beta^2\lambda^2}\right]\frac{\phi(s)}{\lambda\mu} + \left[\frac{M_1}{2M_1 + C\mu^2}\right]\frac{\tilde{\phi}(s)}{s^2+\beta^2\lambda^2}, \tag{7.1}$$

where $\beta^2 = -M_1^2/2C(2M_1 + C\mu^2)$, $\sqrt{\beta^2}$ being positive. Finally, introducing the parameter $\alpha = \overline{U}_0/a_1$ and the explicit form of $\tilde{\phi}(s)$, the inversion of $F(s)$ is found, yielding

$$\frac{p_+}{|u_0|\sin\lambda y} = C_\beta\left[I_\beta(\tau) + \frac{M_1}{C\beta\mu}\sin(\beta\lambda\tau)\right] + C_\alpha\left[I_\alpha(\tau) + \frac{\lambda\mu}{\alpha\kappa}\frac{M_1}{C\mu^2}\sin(\alpha\kappa\tau)\right], \tag{7.2}$$

where

$$I_\beta(\tau) = \int_0^\tau \cos[\beta\lambda(\tau - \tau')]\frac{J_1(\lambda\mu\tau')}{\tau'}\,d\tau',$$
$$I_\alpha(\tau) = \int_0^\tau \cos[\alpha\kappa(\tau - \tau')]\frac{J_1(\lambda\mu\tau')}{\tau'}\,d\tau',$$

$$C_\beta = \frac{\mu^2 C}{2M_1 + C\mu^2}\frac{\alpha\kappa}{\lambda\mu}\left[\frac{\phi_0}{\alpha^2\kappa^2 - \beta^2\lambda^2} + \frac{\phi_1}{\alpha^2\kappa^2}\right], \quad C_\alpha = -\frac{\mu^2 C}{2M_1 + C\mu^2}\frac{\alpha\kappa}{\lambda\mu}\left[\frac{\phi_0}{\alpha^2\kappa^2 - \lambda^2\beta^2}\right].$$

8. Solution for large values of $\lambda\mu\tau$

The asymptotic behaviour of I_α and I_β for $\lambda\mu\tau \gg 1$ may be determined by the method of steepest descents (Jeffreys & Jeffreys 1950). For a line integral in the complex domain of the form

$$I = \int_R \chi(s)\, e^{f(s)} ds, \tag{8.1}$$

where $f(s)$ is analytic with a large positive real part, and R is the path of steepest descent of $f(s)$, a first approximation is given by

$$I = \sum_{\substack{\text{all saddle} \\ \text{points } s_0}} \frac{(2\pi)^{\frac{1}{2}}\, \chi(s_0)\, e^{f(s_0)} e^{i\xi}}{|f''(s_0)|^{\frac{1}{2}}}, \tag{8.2}$$

s_0 being the location of a saddle point of $f(s)$ and ξ the angle with the positive real axis made by R as it passes through s_0.

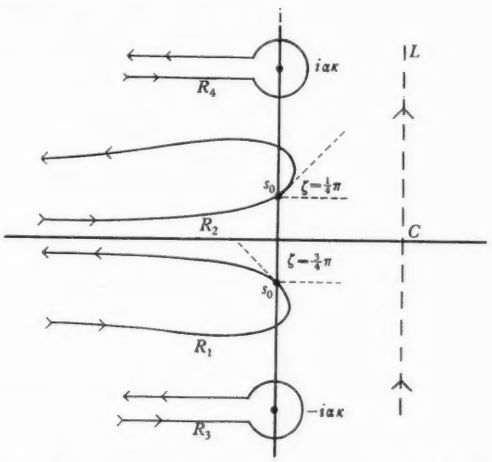

FIGURE 3. Path of steepest descent for evaluation of I_α for $\lambda\mu\tau \gg 1$.

The Laplace representation of I_α may be written in the form of equation (8.1) as follows

$$I_\alpha = \frac{1}{2\pi i} \int_L \frac{s}{s^2 + \alpha^2\kappa^2} \exp\left[s\tau - \ln\left\{\frac{s + (s^2 + \lambda^2\mu^2)^{\frac{1}{2}}}{\lambda\mu}\right\}\right] ds, \tag{8.3}$$

L denoting a line from $C - i\infty$ to $C + i\infty$ with $C > Im[\alpha]$. As shown in figure 3 L may be deformed so that part of it coincides with the paths R_1, R_2 of steepest descent for which equation (8.2) holds. Integration over the remaining parts R_3, R_4 may be carried out exactly by residue theory. The result, valid for large $\lambda\mu\tau$ and $\alpha\kappa/\lambda\mu \neq 1$, is:

$$I_\alpha = \frac{(2/\pi)^{\frac{1}{2}}}{(\alpha\kappa/\lambda\mu)^2 - 1} \frac{\cos\left[\lambda\mu\tau - \cos^{-1}(1/\lambda\mu\tau) + \frac{1}{4}\pi\right]}{(\lambda\mu\tau)^{\frac{3}{2}}} + \nu_1 \sin(\kappa\overline{U}_0 t) + \nu_2 \cos(\kappa\overline{U}_0 t), \tag{8.4}$$

where
$$\left.\begin{aligned} \nu_1 &= (\alpha\kappa/\lambda\mu)\,[1-\{1-(\lambda\mu/\alpha\kappa)^2\}^{\frac{1}{2}}], \\ \nu_2 &= 0, \end{aligned}\right\} \quad \left(\frac{\alpha\kappa}{\lambda\mu} > 1\right);$$
$$\left.\begin{aligned} \nu_1 &= \alpha\kappa/\lambda\mu, \\ \nu_2 &= \{1-(\alpha\kappa/\lambda\mu)^2\}^{\frac{1}{2}}, \end{aligned}\right\} \quad \left(\frac{\alpha\kappa}{\lambda\mu} < 1\right).$$

A similar expression holds for I_β except that β/μ is always greater than unity. Substituting these results into equations (7.2) we obtain the result for $\alpha\kappa/\lambda\mu \neq 1$,

$$\frac{[p_+(y,\tau)]_{\tau\to\infty}}{|u_0|\sin\lambda y} = \sqrt{\frac{2}{\pi}}\left[\frac{C_\beta\mu^2}{\beta^2-\mu^2}+\frac{C_\alpha}{(\alpha\kappa/\lambda\mu)^2-1}\right]\frac{\cos[\lambda\mu\tau-\cos^{-1}(1/\lambda\mu\tau)+\frac{1}{4}\pi]}{(\lambda\mu\tau)^{\frac{3}{2}}}$$
$$+C_\alpha\left\{\left[\nu_1+\frac{M_1}{C\mu^2}\frac{\lambda\mu}{\alpha\kappa}\right]\sin(\kappa\bar{U}_0 t)+\nu^2\cos(\kappa\bar{U}_0 t)\right\}$$
$$= \frac{p_{+\mathrm{trans}}}{|u_0|\sin\lambda y}+\frac{p_{+\infty}}{|u_0|\sin\lambda y}. \tag{8.5}$$

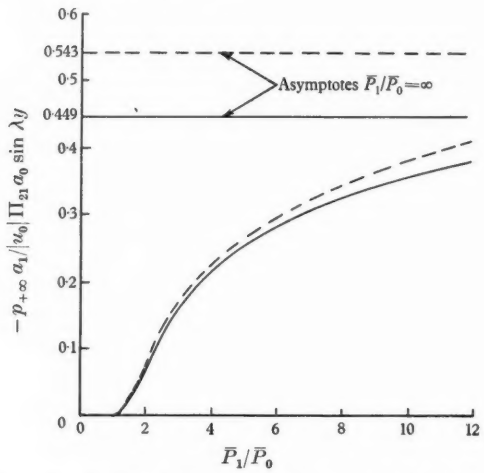

FIGURE 4. Comparison of present theory with Ribner (1953) for determination of amplitude of $p_{+\infty}$, showing $-p_{+\infty}\,a_1/|u_0|\,\Pi_{21}a_0\sin\lambda y$ *vs* shock strength $\bar{P}_1/\bar{P}_0$, for $\lambda=\kappa$. ———, Werner ($A=-1$); – – –, Ribner.

For $\alpha\kappa/\lambda\mu = 1$ the method of steepest descents cannot be applied to I_α. However, it will be shown in §9 that for this case I_α can be expressed in the simple form:

$$I_\alpha = -J_1(\lambda\mu\tau)+\sin(\kappa\bar{U}_0 t), \quad (\alpha\kappa/\lambda\mu = 1). \tag{8.6}$$

Thus, for
$$\alpha\kappa/\lambda\mu = 1,$$
$$[p_+(y,\tau)]_{\tau\to\infty} = \left\{C_\alpha J_1(\lambda\mu\tau)+\sqrt{\frac{2}{\pi}}\left[\frac{C_\beta\mu^2}{\beta^2-\mu^2}\right]\frac{\cos[\lambda\mu\tau-\cos^{-1}(1/\lambda\mu\tau)+\frac{1}{4}\pi]}{(\lambda\mu\tau)^{\frac{1}{2}}}\right.$$
$$\left.+C_\alpha\left[1+\frac{M_1}{C\mu^2}\right]\sin(\kappa\bar{U}_0 t)\right\}. \tag{8.7}$$

As τ approaches ∞, $p_{+\mathrm{trans}}$ dies out as $(\lambda\mu\tau)^{-\frac{3}{2}}$ for $\alpha\kappa/\lambda\mu \neq 1$, and as $(\lambda\mu\tau)^{-\frac{1}{2}}$ for $\alpha\kappa/\lambda\mu = 1$. The remaining term $p_{+\infty}$ varies sinusoidally in time with a fixed

amplitude and a phase which depends on the parameter $\alpha\kappa/\lambda\mu$. The value of $p_{+\infty}$ should be predicted by the quasi-steady theories of Ribner (1953) and Chang (1957). Accordingly, Ribner's theory applied to two vorticity waves oriented at $\pm 45°$ to the mean flow direction is compared with the present theory for the equivalent case of $\kappa = \lambda$ (square vortex cells). For this configuration $\alpha\kappa/\lambda\mu > 1$. In figure 4, the amplitude of $p_{+\infty}a_1/|u_0|\Pi_{21}a_0$ is given as a function of shock strength P_1/P_0 for both Ribner's theory and the present determination. It is evident from this comparison that the approximation $A = -1$ (which aside from the linearization of the problem is the only one made) is applicable even for shock strengths as high as ten.

9. Solutions for small values of $\lambda\mu\tau$

To complete the analysis a representation is sought which describes $p_+(y,\tau)$ near the origin but which can be extended to values of τ for which the asymptotic solutions first become valid.

The case $\alpha\kappa/\lambda\mu > 1$

From the asymptotic results for I_α and I_β it is known that I_α, I_β consist of a transient term which approaches zero as $\tau \to \infty$ and a sine term of fixed amplitude. If two new functions $I_{\alpha t}$, $I_{\beta t}$ are defined by subtracting out the sinusoidal components of I_α and I_β, i.e.

$$I_{\alpha t} = I_\alpha - \frac{\alpha\kappa}{\lambda\mu}\left[1 - \left\{1 - \left(\frac{\lambda\mu}{\alpha\kappa}\right)^2\right\}^{\frac{1}{2}}\right]\sin(\alpha\kappa\tau) \tag{9.1 A}$$

and

$$I_{\beta t} = I_\beta - \frac{\beta}{\mu}\left[1 - \left\{1 - \left(\frac{\mu}{\beta}\right)^2\right\}^{\frac{1}{2}}\right]\sin(\beta\lambda\tau), \tag{9.1 B}$$

then $I_{\alpha t}$, $I_{\beta t}$ are damped oscillatory functions approaching zero as $\tau \to \infty$. For such functions a method of expansion due to Cambi (1956) is particularly well-suited.

A new transform function is defined as follows:

$$\Lambda[f(\tau)] = \lambda\mu\cosh q\int_0^\infty e^{-\tau\lambda\mu\sinh q} f(\tau)\,d\tau. \tag{9.2}$$

If $f(\tau)$ is equal to the nth-order Bessel function $J_n(\lambda\mu\tau)$, we obtain the simple relation

$$\Lambda[J_n(\lambda\mu\tau)] = e^{-nq}. \tag{9.3}$$

This result is applied by first obtaining the Λ transform of $I_{\alpha t}$

$$\begin{aligned}\Lambda[I_{\alpha t}] &= \lambda\mu\cosh q\bar{I}_{\alpha t}(\lambda\mu\sinh q)\\ &= -\frac{b_\alpha e^{4q} + (b_\alpha + 1)e^{2q} + 1}{e^{5q} + d_\alpha e^{3q} + e^q},\end{aligned} \tag{9.4}$$

where

$$b_\alpha = 2\left(\frac{\alpha\kappa}{\lambda\mu}\right)^2\left[1 - \left\{1 - \left(\frac{\lambda\mu}{\alpha\kappa}\right)^2\right\}^{\frac{1}{2}}\right] - 1, \quad d_\alpha = \left(2\frac{\alpha\kappa}{\lambda\mu}\right)^2 - 2.$$

Dividing the denominator of equation (9·4) directly into the numerator, $\Lambda[I_{\alpha t}]$ may be expressed as a series in e^{-nq},

$$\Lambda[I_{\alpha t}] = -\sum_{n\,\text{odd}} f_{\alpha n} e^{-nq}, \tag{9.5}$$

the inversion of which follows from equation (9·3),

$$I_{\alpha t} = -\sum_{n \text{ odd}} f_{\alpha n} J_n(\lambda\mu\tau), \tag{9.6}$$

where

$$f_{\alpha 1} = b_\alpha,$$

$$f_{\alpha 3} = -(d_\alpha f_{\alpha 1} - b_\alpha - 1),$$

$$f_{\alpha 5} = -(d_\alpha f_{\alpha 3} + f_{\alpha 1} - 1),$$

$$f_{\alpha n} = -(d_\alpha f_{\alpha(n-2)} + f_{\alpha(n-4)}) \quad (n \geqslant 7),$$

with corresponding expressions holding for $I_{\beta t}$.

The reason for the particular choice of $I_{\alpha t}$ now becomes more evident. In working with an expansion in $J_n(\lambda\mu\tau)$ it was desired to apply this expansion to a function whose behaviour was not very different from the Bessel function (both $I_{\alpha t}$ and $J_n(\lambda\mu\tau)$ are damped oscillatory functions).

The case $\alpha\kappa/\lambda\mu < 1$

For this case we have found that $[I_\alpha]_{\tau\to\infty}$ approaches a sine wave of unit amplitude but shifted in phase from the original disturbance. For this case then, we construct $I_{\alpha t}$ by subtracting out only the sine component, giving

$$I_{\alpha t} = I_\alpha - \frac{\alpha\kappa}{\lambda\mu}\sin(\alpha\kappa\tau), \tag{9.7}$$

taking note of the fact that now

$$[I_{\alpha t}]_{\tau\to\infty} = \left\{1 - \left(\frac{\alpha\kappa}{\lambda\mu}\right)^2\right\}^{\frac{1}{2}} \cos(\alpha\kappa\tau). \tag{9.8}$$

Repetition of the procedure for $\alpha\kappa/\lambda\mu > 1$ yields an expression for $I_{\alpha t}$ similar to equation (9.6) with

$$b_\alpha = 2\left(\frac{\alpha\kappa}{\lambda\mu}\right)^2 - 1, \quad d_\alpha = 2\left(\frac{\alpha\kappa}{\lambda\mu}\right)^2 - 2.$$

$I_{\beta t}$, of course, remains unchanged since $\beta > \mu$ for all shock strengths. Although $I_{\alpha t}$ no longer goes to zero as before, d_α is sufficiently small to ensure good convergence properties for the expansion.

The case $\alpha\kappa/\lambda\mu = 1$

This case is contained in both the previous cases and we have

$$b_\alpha = 1, \quad d_\alpha = 1, \quad f_{\alpha 1} = 0, \quad f_{\alpha n} = 0 \quad (n > 1).$$

$I_{\alpha t}$ is then simply

$$I_{\alpha t} = -J_1(\lambda\mu\tau), \tag{9.9}$$

and I_α reduces to the form given in equation (8.6).

In terms of $I_{\alpha t}$, $I_{\beta t}$ the pressure disturbance is given by

$$\frac{p_+}{|u_0|\sin\lambda y} = C_\beta I_{\beta t} + C_\alpha[I_{\alpha t} - \nu_2\cos(\kappa\overline{U}_0 t)] + \frac{p_{+\infty}}{|u_0|\sin\lambda y}$$

$$= \frac{p_{+\text{trans}}}{|u_0|\sin\lambda y} + \frac{p_{+\infty}}{|u_0|\sin\lambda y}. \tag{9.10}$$

10. Local shock velocity perturbation

The non-dimensional shock velocity $\psi_t/|\delta U_0|$ may be obtained from the boundary condition equation (4.1 B) written in the form

$$\frac{\psi_t}{|\delta U_0|} = \frac{\delta U_-}{|\delta U_0|} + \frac{p_+}{|u_0|\Pi_{21}a_0/a_1}. \tag{10.1}$$

Substitution of δU_- and p_+ results in the expression

$$\frac{\psi_t}{|\delta U_0|\sin\lambda y} = G\sin(\kappa\overline{U}_0 t+\theta) + \frac{p_{+\mathrm{trans}}}{|u_0|\Pi_{21}(a_0/a_1)\sin\lambda y}, \tag{10.2}$$

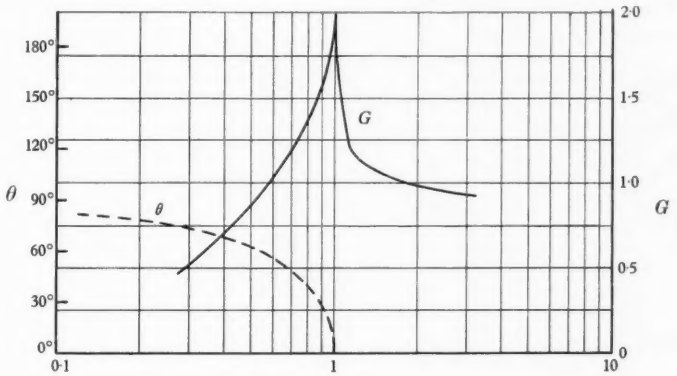

$$\frac{\alpha\kappa}{\lambda\mu} = \frac{h}{l}\frac{\overline{U}_0}{(a_1^2-\overline{U}_1^2)^{\frac{1}{2}}}$$

FIGURE 5. Phase θ and amplitude G of $\psi_t/|\delta U_0|$ *vs* $\alpha k/\lambda\mu$ for shock strength $\overline{P}_1/\overline{P}_0 = 1{\cdot}514$, $\alpha/\mu = 2{\cdot}085$.

where

$$G = \begin{cases} 1+\dfrac{C_\alpha}{\Pi_{21}a_0/a_1}\left[\dfrac{\alpha\kappa}{\lambda\mu}\left\{1-\left[1-\left(\dfrac{\lambda\mu}{\alpha\kappa}\right)^2\right]^{\frac{1}{2}}\right\}+\dfrac{\lambda\mu}{\alpha\kappa}\dfrac{M_1}{C\mu^2}\right] & (\alpha\kappa/\lambda\mu > 1), \\ \left\{\left(1+\dfrac{C_\alpha}{\Pi_{21}a_0/a_1}\left[\dfrac{\alpha\kappa}{\lambda\mu}-\dfrac{\lambda\mu}{\alpha\kappa}\dfrac{M_1}{C\mu^2}\right]\right)^2+\left(\dfrac{C_\alpha}{\Pi_{21}a_0/a_1}\right)^2\left[1-\left(\dfrac{\alpha\kappa}{\lambda\mu}\right)^2\right]\right\}^{\frac{1}{2}} & (\alpha\kappa/\lambda\mu < 1), \end{cases}$$

$$\theta = \begin{cases} 0 & (\alpha\kappa/\lambda\mu > 1), \\ \tan^{-1}\left\{\dfrac{C_\alpha\left\{1-\left(\dfrac{\alpha\kappa}{\lambda\mu}\right)^2\right\}^{\frac{1}{2}}\Big/\Pi_{21}(a_0/a_1)}{1+\dfrac{C_\alpha}{\Pi_{21}(a_0/a_1)}\left[\dfrac{\alpha\kappa}{\lambda\mu}+\dfrac{\lambda\mu}{\alpha\kappa}\dfrac{M_1}{C\mu^2}\right]}\right\} & (\alpha\kappa/\lambda\mu < 1). \end{cases}$$

The amplitude G and phase angle θ are plotted in figure 5 *vs* $\alpha\kappa/\lambda\mu$ for a shock strength of $\overline{P}_1/\overline{P}_0 = 1{\cdot}514$. At this shock strength the time variation of

$$p_{+\mathrm{trans}}a_1/|u_0|\Pi_{21}a_0\sin\lambda y$$

is computed from equations (8.5) and (8.7) for large τ and from equation (9.10) for small τ. The results are plotted in figure 6 for $\alpha\kappa/\lambda\mu = \frac{1}{2}$ and $2{\cdot}085$, and in

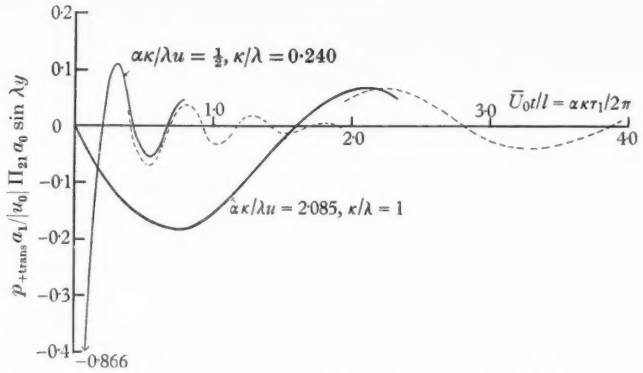

FIGURE 6. Transient component of pressure disturbance immediately behind shock *vs* time for $\alpha k/\lambda u = \frac{1}{2}$, 2·085; $\bar{P}_1/\bar{P}_0 = 1{\cdot}514$, $M_0 = 1{\cdot}2$. ———, Bessel function expansion; - - - -, asymptotic expression.

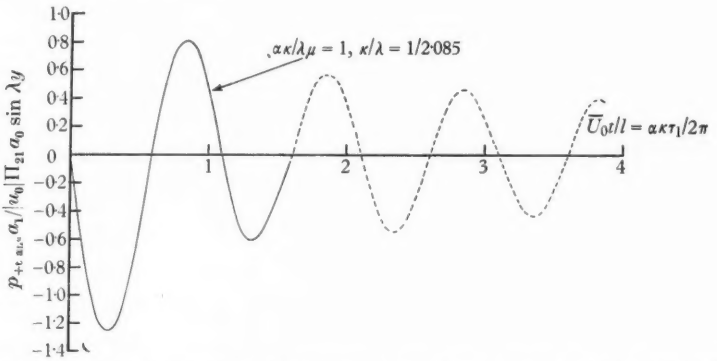

FIGURE 7. Transient component of pressure disturbance immediately behind shock *vs* time for $\alpha k/\lambda u = 1$, $\bar{P}_1/\bar{P}_0 = 1{\cdot}514$, $M_0 = 1{\cdot}2$. ———, Bessel function expansion; - - - -, asymptotic expression.

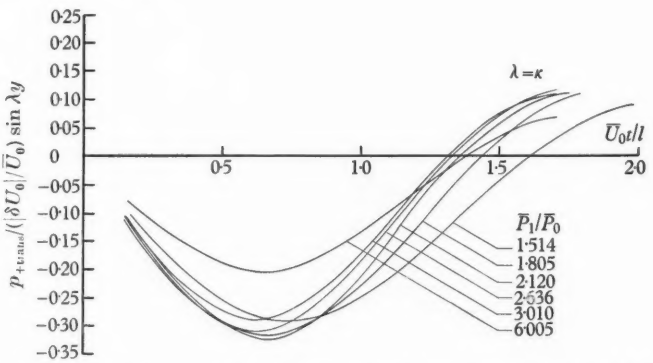

FIGURE 8. Transient component of pressure disturbance immediately behind shock for $\lambda\mu\tau \ll 1$ (initial behaviour), $\lambda = \kappa$, and different shock strengths.

figure 7 for $\alpha\kappa/\lambda\mu = 1$. The value of 2·085 was chosen since at this value $\lambda = \kappa$. It is interesting to note that when $\lambda = \kappa$ (i.e. square vortex cells), the maximum magnitude of $p_{+\text{trans}}$ is an order of magnitude greater than the amplitude of $p_{+\infty}$. In figure 8 the time variation of $p_{+\text{trans}}/(|\delta U_0|/\overline{U}_0)\sin\lambda y$ for $\lambda = \kappa$ at shock strength from 1·514 to 6·005 is plotted. Since $p_{+\text{trans}}$ is normalized with respect to $\overline{P}_1$ we can see from figure 8 that, in this range of shock strengths, the transient pressure component rises in magnitude roughly in proportion to the shock strength.

11. Shock displacement for a single column of vortices

The above solution can be used to solve a second problem which is of some interest, namely the convection through a shock of a single column of vortex cells parallel to the y-axis. For this case the upstream disturbance is specified by

$$\left.\begin{aligned} &u_0 = v_0 = 0 \quad (0 \geqslant \overline{U}_0 t - x, \quad \overline{U}_0 t - x \geqslant (\pi/\kappa) = \tfrac{1}{2}l); \\ &u_0 = |u_0|\sin\kappa(\overline{U}_0 t - x)\sin\lambda y \\ &v_0 = -|u_0|(\kappa/\lambda)\cos\kappa(\overline{U}_0 t - x)\cos\lambda y \end{aligned}\right\} \quad (\pi/\kappa) > \overline{U}_0 t - x > 0. \qquad (11.1)$$

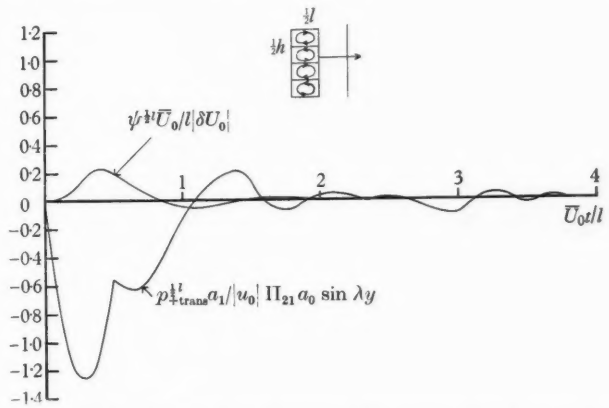

FIGURE 9. Shock displacement and pressure disturbance for a single column of vortices, with $\alpha\kappa/\lambda\mu = 1$, $\lambda/\kappa = 2{\cdot}085$, $\overline{P}_1/\overline{P}_0 = 1{\cdot}514$, $M_0 = 1{\cdot}2$.

Calling the shock displacement for this case $\psi^{\frac{1}{2}l}$ we have by simple superposition

$$\psi^{\frac{1}{2}l}_l = \psi_l(y,t) + \psi_l(y, t - l/2\overline{U}_0), \qquad (11.2)$$

ψ_l being the displacement velocity found previously for the semi-infinite vortex field. Integration of equation (11.2) yields the displacement $\psi^{\frac{1}{2}l}$ which is plotted in figure 9 together with $p^{\frac{1}{2}l}_{+\text{trans}} a_1/|u_0|\,\Pi_{21} a_0 \sin\lambda y$ as a function of time for $\alpha\kappa/\lambda\mu = 1$, $\overline{P}_1/\overline{P}_0 = 1{\cdot}514$.

This work was completed at the Johns Hopkins University and was supported by the United States Air Force under contract AF 18(600)-757. A more detailed discussion of the problem appears in Werner (1959).

REFERENCES

CAMBI, E. 1956 *J. Math. Phys.* **35**, 114.

CHANG, C. T. 1957 *J. Aero. Sci.* **24**, 675.

CHU, B. T. & KOVASZNAY, L. S. G. 1958 *J. Fluid Mech.* **3**, 494.

JEFFREYS, H. J. & JEFFREYS, B. S. 1950 *Methods of Mathematical Physics.* Cambridge University Press.

KOVASZNAY, L. S. G. 1953 *J. Aero. Sci.* **20**, 657.

MOORE, F. K. 1953 *N.A.C.A., Tech. Note*, no. 2879.

RAM, G. S. & RIBNER, H. S. 1957 *Proceedings of Heat Transfer and Fluid Mechanics Institute.* Stanford University Press.

RIBNER, H. S. 1953 *N.A.C.A. Tech. Note*, no. 2864.

WERNER, J. E. 1959 *Air Force Office of Scientific Research, Tech. Rep.*, no. 59-46.

A non-linear theory for oscillations in a parallel flow

By D. J. BENNEY

Department of Mathematics, Massachusetts Institute of Technology

(Received 21 April 1960 and in revised form 10 August 1960)

Three-dimensional periodic oscillations in the shear flow region between two parallel streams are considered up to that second order of the oscillation amplitude. It is shown that, as an integral part of the oscillation, there is a mean secondary flow in the nature of a longitudinal vortex. Despite the dissimilarity in the profile of the basic flows, several of the principal features of the calculated results can be compared with those observed for the Blasius flow by Schubauer and Klebanoff & Tidstrom at the National Bureau of Standards.

1. Introduction

One of the most basic and challenging problems in fluid mechanics is to obtain an understanding of the various physical mechanisms involved during the transition from laminar to turbulent flow. It could be called the missing link between the two régimes of fluid motion. This problem has been subject to a great deal of theoretical and experimental research, especially over the last decade, and considerable progress has been made to bridge the gap. However, there remains a vast amount of work still to be done before our knowledge of the transition phenomenon is complete. One may anticipate that the final answer will include many simultaneous effects.

In order to study the breakdown of laminar flow it is necessary to follow the growth of a disturbance superposed on the basic flow. If this disturbance is of very small amplitude, the equations can be linearized and one can develop the linear theory of hydrodynamic stability. This theory has been investigated in great detail and a survey of the subject is given in the monograph by Lin (1955). There can be no doubt that the initial trend of a small disturbance will be described adequately by the results of the linearized theory. Indeed there is now ample experimental evidence to support this fact (Schubauer & Skramstead 1948). However, as the oscillation grows the non-linear terms in the equations become important, and must be included in the investigation.

It has long been recognized that the inclusion of the non-linear terms adds two important new features to the problem. First, there is the effect of the Reynolds stresses in producing a redistribution of momentum and so a distortion of the original velocity profile, and secondly, the excitation of higher harmonics of the original oscillation. For finite-amplitude oscillations the modification of the basic flow through the action of the Reynolds stresses can be quite appreciable, and this will in turn modify the rate of transfer of energy from the mean flow to the disturbance, and so the rate of growth of the disturbance. Meksyn &

Stuart (1951) have calculated these modifications for the case of flow between parallel plates, and have given some calculations showing that the production of higher harmonics plays a less important role. Their results show that an increase in the amplitude of the oscillation produces a lower critical Reynolds number. More recently Stuart (1958, 1959) has given a somewhat simpler analysis based on energy methods and has obtained good agreement with experiment for the case of flow between rotating circular cylinders. Both these discussions consider only two-dimensional disturbances. The importance of the critical layer region as the 'weak spot' of instability has been stressed by Lin (1957). He has shown that for disturbances in a parallel flow all the harmonic components of the oscillation simultaneously become important around the critical layer, before the amplitude of the fundamental is large enough to cause any significant distortion of the mean flow, sufficiently large for experimental observation.

The search for a suitable mechanism to describe the onset of turbulence has aroused much interest. Several plausible theories have been proposed and all possess some element of truth, although no single one appears to be the complete answer. Landau's concept (1944) of successive instabilities seems intuitively reasonable, and enables one to picture the appearance of additional modes of oscillation corresponding to a sequence of critical Reynolds numbers. Görtler & Witting (1957) have proposed a theory, in line with Landau's conjecture, based on the curvature of the streamlines causing a periodic vortex structure. There is experimental evidence to support the existence of secondary vortices, although there has not been any definite confirmation of the phase relationships involved.

A horseshoe vortex structure as the fundamental element of transition has been proposed by Theodorson (1952), who also suggested that strictly two-dimensional disturbances are unimportant for causing transition. This latter conjecture is strongly supported by the recent experiments of Schubauer (1957) and Klebanoff & Tidstrom (1958), which we shall discuss briefly below.

The presence of longitudinal vortices during transition has been reported by many experiments. These can be observed using dye and china-clay techniques.

Mention must be made of the relative importance of two- and three-dimensional disturbances. This is a current issue that has attracted much attention. On the basis of linearized theory, Squire's result (1933), namely, that three-dimensional disturbances are equivalent to two-dimensional ones at a lower Reynolds number is applicable, and so to estimate the onset of instability one need only consider two-dimensional disturbances. However, once the flow is above the critical Reynolds number, oblique waves also become unstable. Therefore it must be anticipated that the initially two-dimensional waves will become progressively three-dimensional as the Reynolds number is increased. This point has been emphasized in earlier work by Lin (1957). Indeed, since turbulence is an essentially three-dimensional phenomenon there must be a stage during development when the three-dimensional disturbances tend to dominate. Two-dimensional theory cannot be expected to suffice. This simple observation suggests the necessity of a theoretical investigation of three-dimensional effects.

Recent experiments also point strongly to the desirability of such an investigation. Notable among the vast array of experiments probing the phenomena of transition, is the work of Schaubauer (1957) and Klebanoff & Tidstrom (1958) at the National Bureau of Standards. Most of their work has concerned boundary-layer transition on a flat plate. Perhaps the most startling and significant fact revealed by these experiments is the almost periodic spanwise variations of intensity with peaks and valleys occuping fixed positions and forming streets of high and low intensity. This periodic spanwise variation causes a warping of the velocity profile, the turbulence appearing to originate at these peaks and to spread into the valleys. More recently, further experimental work on this spanwise variation has been done and we shall have occasion to refer to it at a later stage.

This brief introduction points to the multitude of effects observed and predicted during transition. If it serves no other purpose, at least it does pose the question as to whether there is any advantage in a theoretical approach which does not include all the non-linear terms. The complete solution of the non-linear equations should automatically include all of these effects. A consideration of all the non-linear terms has been advocated by von Kármán, and it is in this spirit that we have undertaken the present investigation.

Our task is to examine finite-amplitude disturbances, paying special attention to the three-dimensional oscillations. It is to be stressed that this will be done by setting up a systematic perturbation from the linear theory and that a purely formal mathematical approach is adopted, although much of the motivation for this work stems from recent experimental evidence.

It is difficult to give a detailed explanation of the conclusions before the actual calculations have been made. Therefore at this stage only brief comment will be made on the interpretation of the results. A detailed description will be given later.

The quantity found to be of prime importance is the mean secondary vorticity in the downstream direction. This vorticity has a periodic spanwise variation and produces a redistribution of momentum in planes perpendicular to the direction of flow. It is this momentum exchange that is responsible for an alternate steepening and flattening of the velocity profile, causing a warping or crumbling effect on the basic flow. Explicit formulas are obtained for the rate of growth of the second-order mean motion. Superposed on these secondary vortices there is the vorticity of the primary oscillation itself. This is periodic in the downstream direction, and so the two effects combined should produce alternately partial reinforcement and cancellation over each wavelength.

The results obtained are applicable to a general parallel flow; but for illustrative purposes we have restricted the detailed calculations to the case of a shear profile. It is to be noted that, although our interests are chiefly with the three-dimensional nature of the motion, we do not discount two-dimensional effects. The results found by Meksyn & Stuart (1951) are in fact included in the analysis. It is believed, however, that in most situations the spanwise profile distortion will be the more important mechanism during transition.

2. Mathematical formulation

We now proceed to give the mathematical formulation on which the subsequent calculations will be based. The symbols p, $\mathbf{q}$, $\boldsymbol{\omega}$ and R will be used to denote the fluid pressure, velocity, vorticity and Reynolds number, respectively. As mentioned in §1, the calculation of the second-order vorticity will play a key role in this development. For this purpose it would suffice to use the vorticity equation, namely,

$$\frac{\partial \boldsymbol{\omega}}{\partial t} + (\mathbf{q}.\nabla)\,\boldsymbol{\omega} = (\boldsymbol{\omega}.\nabla)\,\mathbf{q} + \frac{1}{R}\Delta\boldsymbol{\omega}. \tag{2.1}$$

This will be referred to at the end of this section. But in order to calculate the second-order velocities it is convenient to proceed directly from the equations of motion, together with the continuity equation, that is,

$$\frac{\partial \mathbf{q}}{\partial t} + (\mathbf{q}.\nabla)\,\mathbf{q} = -\nabla p + \frac{1}{R}\Delta\mathbf{q}, \tag{2.2}$$

$$\nabla.\mathbf{q} = 0, \tag{2.3}$$

where we have supposed the fluid to be incompressible and all quantities are expressed in dimensionless form.

We may suppose that $\mathbf{q}$, p and $\boldsymbol{\omega}$ are expanded as perturbation series of the form

$$\mathbf{q} = \mathbf{q}^{(0)} + a\mathbf{q}^{(1)} + a^2\mathbf{q}^{(2)} + \ldots, \tag{2.4}$$

$$p = p^{(0)} + ap^{(1)} + a^2p^{(2)} + \ldots, \tag{2.5}$$

$$\boldsymbol{\omega} = \boldsymbol{\omega}^{(0)} + a\boldsymbol{\omega}^{(1)} + a^2\boldsymbol{\omega}^{(2)} + \ldots, \tag{2.6}$$

where $\mathbf{q}^{(0)}$ is the undisturbed basic flow and $\mathbf{q}^{(1)}$ the primary oscillation, etc. The symbol a is used to denote a perturbation amplitude, and $p^{(0)}$ is the pressure distribution associated with the basic flow.

Taking (x, y, z) as rectangular co-ordinates, and a given parallel basic flow $\mathbf{q}^{(0)} = \{u_0^{(0)}(y), 0, 0\}$, we wish to trace the growth of a wave of small amplitude propagating in the x-direction, having a possible z-variation of amplitude, which will for the moment remain unspecified.

Successive perturbations are determined by sets of equations of the type

$$\frac{\partial \mathbf{q}^{(n)}}{\partial t} + \sum_{r=0}^{n} (\mathbf{q}^{(n-r)}.\nabla)\,\mathbf{q}^{(r)} = -\nabla p^{(n)} + \frac{1}{R}\Delta\mathbf{q}^{(n)}, \tag{2.7}$$

$$\nabla.\mathbf{q}^{(n)} = 0 \quad (n = 1, 2, \ldots). \tag{2.8}$$

We now proceed to derive the equations relevant for a determination of $\mathbf{q}$ and $\boldsymbol{\omega}$ up to terms $O(a^2)$, and in particular to find the second-order mean motion induced by the primary oscillation.

Let

$$\mathbf{q} = (u, v, w), \tag{2.9}$$

$$\mathbf{q}^{(n)} = (u^{(n)}, v^{(n)}, w^{(n)}), \tag{2.10}$$

and so

$$\boldsymbol{\omega} = (\xi, \eta, \zeta) = \left(\frac{\partial w}{\partial y} - \frac{\partial v}{\partial z}, \frac{\partial u}{\partial z} - \frac{\partial w}{\partial x}, \frac{\partial v}{\partial x} - \frac{\partial u}{\partial y}\right), \tag{2.11}$$

$$\boldsymbol{\omega}^{(n)} = (\xi^{(n)}, \eta^{(n)}, \zeta^{(n)}) = \left(\frac{\partial w^{(n)}}{\partial y} - \frac{\partial v^{(n)}}{\partial z}, \frac{\partial u^{(n)}}{\partial z} - \frac{\partial w^{(n)}}{\partial x}, \frac{\partial v^{(n)}}{\partial x} - \frac{\partial u^{(n)}}{\partial y}\right). \tag{2.12}$$

If α is the wave-number of the primary oscillation associated with the x-direction, we take,

$$\left.\begin{aligned} u^{(1)} &= u_1^{(1)}(y,z,t)\,e^{i\alpha x} + u_1^{(1)*}(y,z,t)\,e^{-i\alpha x},\\ v^{(1)} &= v_1^{(1)}(y,z,t)\,e^{i\alpha x} + v_1^{(1)*}(y,z,t)\,e^{-i\alpha x},\\ w^{(1)} &= w_1^{(1)}(y,z,t)\,e^{i\alpha x} + w_1^{(1)*}(y,z,t)\,e^{-i\alpha x},\\ p^{(1)} &= p_1^{(1)}(y,z,t)\,e^{i\alpha x} + p_1^{(1)*}(y,z,t)\,e^{-i\alpha x},\\ \xi^{(1)} &= \xi_1^{(1)}(y,z,t)\,e^{i\alpha x} + \xi_1^{(1)*}(y,z,t)\,e^{-i\alpha x},\\ \eta^{(1)} &= \eta_1^{(1)}(y,z,t)\,e^{i\alpha x} + \eta_1^{(1)*}(y,z,t)\,e^{-i\alpha x},\\ \zeta^{(1)} &= \zeta_1^{(1)}(y,z,t)\,e^{i\alpha x} + \zeta_1^{(1)*}(y,z,t)\,e^{-i\alpha x}, \end{aligned}\right\} \tag{2.13}$$

where

$$\left.\begin{aligned} \xi_1^{(1)} &= \frac{\partial w_1^{(1)}}{\partial y} - \frac{\partial v_1^{(1)}}{\partial z},\\ \eta_1^{(1)} &= \frac{\partial u_1^{(1)}}{\partial z} - i\alpha w_1^{(1)},\\ \zeta_1^{(1)} &= i\alpha v_1^{(1)} - \frac{\partial u_1^{(1)}}{\partial y}, \end{aligned}\right\} \tag{2.14}$$

and where an asterisk is used to denote a complex conjugate.

The equations governing the first-order motion are

$$\left.\begin{aligned} \frac{\partial u_1^{(1)}}{\partial t} + i\alpha u_0^{(0)} u_1^{(1)} + v_1^{(1)}\frac{\partial u_0^{(0)}}{\partial y} &= -i\alpha p_1^{(1)} + \frac{1}{R}\left(\frac{\partial^2}{\partial y^2} + \frac{\partial^2}{\partial z^2} - \alpha^2\right) u_1^{(1)},\\ \frac{\partial v_1^{(1)}}{\partial t} + i\alpha u_0^{(0)} v_1^{(1)} &= -\frac{\partial p_1^{(1)}}{\partial y} + \frac{1}{R}\left(\frac{\partial^2}{\partial y^2} + \frac{\partial^2}{\partial z^2} - \alpha^2\right) v_1^{(1)},\\ \frac{\partial w_1^{(1)}}{\partial t} + i\alpha u_0^{(0)} w_1^{(1)} &= -\frac{\partial p_1^{(1)}}{\partial z} + \frac{1}{R}\left(\frac{\partial^2}{\partial y^2} + \frac{\partial^2}{\partial z^2} - \alpha^2\right) w_1^{(1)},\\ i\alpha u_1^{(1)} + \frac{\partial v_1^{(1)}}{\partial y} + \frac{\partial w_1^{(1)}}{\partial z} &= 0. \end{aligned}\right\} \tag{2.15}$$

The secondary flow $\mathbf{q}^{(2)}$, $p^{(2)}$, $\boldsymbol{\omega}^{(2)}$, can be written as the sum of a mean motion and a second-harmonic oscillation. Thus,

$$\left.\begin{aligned} u^{(2)} &= u_0^{(2)}(y,z,t) + u_2^{(2)}(y,z,t)\,e^{2i\alpha x} + u_2^{(2)*}(y,z,t)\,e^{-2i\alpha x},\\ v^{(2)} &= v_0^{(2)}(y,z,t) + v_2^{(2)}(y,z,t)\,e^{2i\alpha x} + v_2^{(2)*}(y,z,t)\,e^{-2i\alpha x},\\ w^{(2)} &= w_0^{(2)}(y,z,t) + w_2^{(2)}(y,z,t)\,e^{2i\alpha x} + w_2^{(2)*}(y,z,t)\,e^{-2i\alpha x},\\ p^{(2)} &= p_0^{(2)}(y,z,t) + p_2^{(2)}(y,z,t)\,e^{2i\alpha x} + p_2^{(2)*}(y,z,t)\,e^{-2i\alpha x},\\ \xi^{(2)} &= \xi_0^{(2)}(y,z,t) + \xi_2^{(2)}(y,z,t)\,e^{2i\alpha x} + \xi_2^{(2)*}(y,z,t)\,e^{-2i\alpha x},\\ \eta^{(2)} &= \eta_0^{(2)}(y,z,t) + \eta_2^{(2)}(y,z,t)\,e^{2i\alpha x} + \eta_2^{(2)*}(y,z,t)\,e^{-2i\alpha x},\\ \zeta^{(2)} &= \zeta_0^{(2)}(y,z,t) + \zeta_2^{(2)}(y,z,t)\,e^{2i\alpha x} + \zeta_2^{(2)*}(y,z,t)\,e^{-2i\alpha x}, \end{aligned}\right\} \tag{2.16}$$

where

$$\xi_0^{(2)} = \frac{\partial w_0^{(2)}}{\partial y} - \frac{\partial_{\prime} {}_0^{(2)}}{\partial z},$$

$$\eta_0^{(2)} = \frac{\partial u_0^{(2)}}{\partial z},$$

$$\zeta_0^{(2)} = -\frac{\partial u_0^{(2)}}{\partial y},$$

and

$$\xi_2^{(2)} = \frac{\partial w_2^{(2)}}{\partial y} - \frac{\partial v_2^{(2)}}{\partial z},$$

$$\eta_2^{(2)} = \frac{\partial u_2^{(2)}}{\partial z} - 2i\alpha w_2^{(2)},$$

$$\zeta_2^{(2)} = 2i\alpha v_2^{(2)} - \frac{\partial u_2^{(2)}}{\partial y}.$$

The notation used is such that superscripts refer to the order of the motion and subscripts give the harmonic.

The equations to determine the mean secondary flow are

$$\left.\begin{aligned}
&\frac{\partial u_0^{(2)}}{\partial t} + v_0^{(2)}\frac{du_0^{(0)}}{dy} + \frac{\partial}{\partial y}(u_1^{(1)}v_1^{(1)*} + u_1^{(1)*}v_1^{(1)}) + \frac{\partial}{\partial z}(u_1^{(1)}w_1^{(1)*} + u_1^{(1)*}w_1^{(1)}) \\
&\qquad = \frac{1}{R}\left(\frac{\partial^2}{\partial y^2} + \frac{\partial^2}{\partial z^2}\right) u_0^{(2)}, \\
&\frac{\partial v_0^{(2)}}{\partial t} + 2\frac{\partial}{\partial y}(v_1^{(1)}v_1^{(1)*}) + \frac{\partial}{\partial z}(v_1^{(1)}w_1^{(1)*} + v_1^{(1)*}w_1^{(1)}) = -\frac{\partial p_0^{(2)}}{\partial y} + \frac{1}{R}\left(\frac{\partial^2}{\partial y^2} + \frac{\partial^2}{\partial z^2}\right) v_0^{(2)}, \\
&\frac{\partial w_0^{(2)}}{\partial t} + \frac{\partial}{\partial y}(v_1^{(1)}w_1^{(1)*} + v_1^{(1)*}w_1^{(1)}) + 2\frac{\partial}{\partial z}(w_1^{(1)}w_1^{(1)*}) = -\frac{\partial p_0^{(2)}}{\partial z} + \frac{1}{R}\left(\frac{\partial^2}{\partial y^2} + \frac{\partial^2}{\partial z^2}\right) w_0^{(2)}, \\
&\qquad \frac{\partial v_0^{(2)}}{\partial y} + \frac{\partial w_0^{(2)}}{\partial z} = 0.
\end{aligned}\right\} \tag{2.17}$$

The second-order oscillation satisfies

$$\left.\begin{aligned}
&\frac{\partial u_2^{(2)}}{\partial t} + v_2^{(2)}\frac{du_0^{(0)}}{dy} + 2i\alpha u_0^{(0)}u_2^{(2)} + i\alpha u_1^{(1)2} + v_1^{(1)}\frac{\partial u_1^{(1)}}{\partial y} + w_1^{(1)}\frac{\partial u_1^{(1)}}{\partial z} \\
&\qquad = -2i\alpha p_2^{(2)} + \frac{1}{R}\left(\frac{\partial^2}{\partial y^2} + \frac{\partial^2}{\partial z^2} - 4\alpha^2\right) u_2^{(2)}, \\
&\frac{\partial v_2^{(2)}}{\partial t} + 2i\alpha u_0^{(0)}v_2^{(2)} + i\alpha u_1^{(1)}v_1^{(1)} + v_1^{(1)}\frac{\partial v_1^{(1)}}{\partial y} + w_1^{(1)}\frac{\partial v_1^{(1)}}{\partial z} \\
&\qquad = -\frac{\partial p_2^{(2)}}{\partial y} + \frac{1}{R}\left(\frac{\partial^2}{\partial y^2} + \frac{\partial^2}{\partial z^2} - 4\alpha^2\right) v_2^{(2)}, \\
&\frac{\partial w_2^{(2)}}{\partial t} + 2i\alpha u_0^{(0)}w_2^{(2)} + i\alpha u_1^{(1)}w_1^{(1)} + v_1^{(1)}\frac{\partial w_1^{(1)}}{\partial y} + w_1^{(1)}\frac{\partial w_1^{(1)}}{\partial z} \\
&\qquad = -\frac{\partial p_2^{(2)}}{\partial z} + \frac{1}{R}\left(\frac{\partial^2}{\partial y^2} + \frac{\partial^2}{\partial z^2} - 4\alpha^2\right) w_2^{(2)}, \\
&\qquad 2i\alpha u_2^{(2)} + \frac{\partial v_2^{(2)}}{\partial y} + \frac{\partial w_2^{(2)}}{\partial z} = 0.
\end{aligned}\right\} \tag{2.18}$$

From the set (2.17), or from (2.1), it is readily seen that the component $\xi_0^{(2)}$ of the mean second-order vorticity satisfies the equation

$$\frac{\partial \xi_0^{(2)}}{\partial t} + \left(\frac{\partial^2}{\partial y^2} - \frac{\partial^2}{\partial z^2}\right)(v_1^{(1)}w_1^{(1)*} + v_1^{(1)*}w_1^{(1)}) + 2\frac{\partial^2}{\partial y\,\partial z}(w_1^{(1)}w_1^{(1)*} - v_1^{(1)}v_1^{(1)*}) = \frac{1}{R}\left(\frac{\partial^2}{\partial y^2} + \frac{\partial^2}{\partial z^2}\right)\xi_0^{(2)}. \tag{2.19}$$

The momentum transfer associated with this longitudinal vorticity will be of prime importance in later discussions.

3. Distortion effects at high Reynolds numbers

For flows at high Reynolds numbers the velocity field will conform to the inviscid equations as a first approximation, except within the critical layer region, where viscous corrections would be needed. A discussion of the subtleties involved in this limiting process can be found in Chapter 8 of Lin's book (1955). Indeed the inviscid limit is justifiable for the case of amplified disturbances and for neutral disturbances as a limiting case. If the complex wave velocity is $c = c_r + ic_i$, then c_r represents the wave speed, $c_i > 0$ implies amplified, $c_i = 0$ neutral, and $c_i < 0$ damped disturbances. It is convenient to introduce the amplitude functions for the primary oscillation; these are denoted by a circumflex. Thus,

$$u_1^{(1)}(y,z,t) = \hat{u}_1^{(1)}(y,z)\, e^{-i\alpha ct}, \tag{3.1}$$

and similarly for $v_1^{(1)}, w_1^{(1)}$, and $p_1^{(1)}$.

In studying the growth or decay of an oscillation we are interested in the case when c_i is close to zero. For the case of large Reynolds numbers we can find quite simple explicit formulas for the rates of growth of the second-order mean velocity modifications. To this purpose it is convenient to rewrite equations (2.17). Dropping the viscous terms, we have

$$\frac{\partial v_0^{(2)}}{\partial y} + \frac{\partial w_0^{(2)}}{\partial z} = 0, \tag{3.2}$$

$$\frac{\partial w_0^{(2)}}{\partial y} - \frac{\partial v_0^{(2)}}{\partial z} = \xi_0^{(2)}, \tag{3.3}$$

$$\frac{\partial u_0^{(2)}}{\partial t} + v_0^{(2)} \frac{du_0^{(0)}}{dy} - \hat{r}_0^{(2)}(y,z)\, e^{2\alpha c_i t} = 0, \tag{3.4}$$

$$\frac{\partial \xi_0^{(2)}}{\partial t} = \hat{\xi}_0^{(2)}(y,z)\, e^{2\alpha c_i t}, \tag{3.5}$$

where
$$\hat{r}_0^{(2)}(y,z) = -\frac{\partial}{\partial y}(\hat{u}_1^{(1)}\hat{v}_1^{(1)*} + \hat{u}_1^{(1)*}\hat{v}_1^{(1)}) - \frac{\partial}{\partial z}(\hat{u}_1^{(1)}\hat{w}_1^{(1)*} + \hat{u}_1^{(1)*}\hat{w}_1^{(1)}), \tag{3.6}$$

and
$$\hat{\xi}_0^{(2)}(y,z) = \left(\frac{\partial^2}{\partial z^2} - \frac{\partial^2}{\partial y^2}\right)(\hat{v}_1^{(1)}\hat{w}_1^{(1)*} + \hat{v}_1^{(1)*}\hat{w}_1^{(1)}) + 2\frac{\partial^2}{\partial y\, \partial z}(\hat{v}_1^{(1)}\hat{v}_1^{(1)*} - \hat{w}_1^{(1)}\hat{w}_1^{(1)*}). \tag{3.7}$$

Integrating (3.5), we have

$$\xi_0^{(2)} = \hat{\xi}_0^{(2)}(y,z)\left(\frac{e^{2\alpha c_i t} - 1}{2\alpha c_i}\right) + \hat{C}(y,z), \tag{3.8}$$

where the form of the solution is so written that the limiting case $c_i \to 0$ can readily be discussed. Clearly the arbitrary function of integration gives the initial value of $\xi_0^{(2)}$, which we may take as zero for the purpose at hand. The interpretation of the solution for $t = 0$ is to be taken more in the formal rather than the physical sense. The solution is supposed to be valid for a range of t, $t_1 < t < t_2$.†

† When the manuscript was shown to Dr J. T. Stuart and Mr J. Watson, they pointed out that the method they have developed for two-dimensional disturbances can be adopted here to modify the solution so as to make it valid for $t \to -\infty$.

In using this result for $\xi_0^{(2)}$, the time dependence of the corresponding velocity components can easily be found. The results are

$$u_0^{(2)} = \hat{s}_0^{(2)}(y,z)\frac{(e^{2\alpha c_i t} - 1 - 2\alpha c_i t)}{(2\alpha c_i)^2} + \hat{r}_0^{(2)}(y,z)\left(\frac{e^{2\alpha c_i t} - 1}{2\alpha c_i}\right), \tag{3.9}$$

$$v_0^{(2)} = \hat{v}_0^{(2)}(y,z)\left(\frac{e^{2\alpha c_i t} - 1}{2\alpha c_i}\right), \tag{3.10}$$

$$w_0^{(2)} = \hat{w}_0^{(2)}(y,z)\left(\frac{e^{2\alpha c_i t} - 1}{2\alpha c_i}\right), \tag{3.11}$$

$$\xi_0^{(2)} = \hat{\xi}_0^{(2)}(y,z)\left(\frac{e^{2\alpha c_i t} - 1}{2\alpha c_i}\right), \tag{3.12}$$

where

$$\frac{\partial \hat{v}_0^{(2)}}{\partial y} + \frac{\partial \hat{w}_0^{(2)}}{\partial z} = 0, \tag{3.13}$$

$$\frac{\partial \hat{w}_0^{(2)}}{\partial y} - \frac{\partial \hat{v}_0^{(2)}}{\partial z} = \hat{\xi}_0^{(2)}(y,z), \tag{3.14}$$

$$\hat{s}_0^{(2)}(y,z) = -\hat{v}_0^{(2)}(y,z)\frac{du_0^{(0)}}{dy}, \tag{3.15}$$

and $\hat{r}_0^{(2)}(y,z)$, $\hat{\xi}_0^{(2)}(y,z)$ are given by (3.6) and (3.7).

A knowledge of the primary oscillation is sufficient to determine $\hat{r}_0^{(2)}(y,z)$ and $\hat{\xi}_0^{(2)}(y,z)$, thence the solution of a Poisson equation gives the second-order mean velocities. The equations also show that the second-order mean velocities grow exponentially in time, or in the case of neutral oscillations as powers of t; for

$$\lim_{c_i \to 0}\left(\frac{e^{2\alpha c_i t} - 1}{2\alpha c_i}\right) = t,$$

$$\lim_{c_i \to 0}\left\{\frac{e^{2\alpha c_i t} - 1 - 2\alpha c_i t}{(2\alpha c_i)^2}\right\} = \tfrac{1}{2}t^2.$$

Therefore even for neutral disturbances the secondary flow will build up and eventually dominate.

One of the most interesting features of this analysis is that a three-dimensional primary oscillation induces a mean second-order vorticity into the flow, having a component $\xi_0^{(2)}$ in the downstream direction. It is this mechanism which produces a spanwise momentum exchange and causes a warping of the original velocity profile.

Thus far the analysis has been kept quite general and the equations would apply to a general type of parallel flow. To be more definite we now prescribe the primary oscillation. The initial oscillation must be expected to be two-dimensional. However, as mentioned earlier in §1, three-dimensional waves must appear at some stage during the development. We assume this to occur before the oscillation leaves the linear range. There is a strong experimental support for this conjecture. Schubauer and Klebanoff in their experiments report that transition never occurs without first being preceded by a strong warping of the wave.

A more general infinitesimal oscillation can be compounded of a purely two-dimensional component together with a standing wave in the spanwise direction.

Of course, in the practical situation this latter component must be present to some degree, for undoubtedly there will always be some spanwise irregularity in the amplitude of the oscillation. The question then arises as to which component will be dominant as transition is approached. This will depend on which component has the higher amplification rate and so would require the details of the stability for the flow under consideration.

We now revert to a less cumbersome notation and consider in detail the case of a sinusoidal spanwise variation of amplitude (wave-number β) associated with the three-dimensional wave. We write

$$\left.\begin{aligned}
u_0^{(0)}(y) &= u_0(y),\\
u_1^{(1)}(y,z,t) &= \hat{u}_1^{(1)}(y,z)\,e^{-i\alpha ct} = [\lambda\hat{u}_1(y)\cos\beta z + \mu\hat{U}_1(y)]\,e^{-i\alpha ct},\\
v_1^{(1)}(y,z,t) &= \hat{v}_1^{(1)}(y,z)\,e^{-i\alpha ct} = [\lambda\hat{v}_1(y)\cos\beta z + \mu\hat{V}_1(y)]\,e^{-i\alpha ct},\\
w_1^{(1)}(y,z,t) &= \hat{w}_1^{(1)}(y,z)\,e^{-i\alpha ct} = [\lambda\hat{w}_1(y)\sin\beta z]\,e^{-i\alpha ct},\\
p_1^{(1)}(y,z,t) &= \hat{p}_1^{(1)}(y,z)\,e^{-i\alpha ct} = [\lambda\hat{p}_1(y)\cos\beta z + \mu\hat{P}_1(y)]\,e^{-i\alpha ct},\\
\xi_1^{(1)}(y,z,t) &= \hat{\xi}_1^{(1)}(y,z)\,e^{-i\alpha ct} = [\lambda\hat{\xi}_1(y)\sin\beta z]\,e^{-i\alpha ct},
\end{aligned}\right\} \tag{3.16}$$

where the ratio μ/λ is a measure of the relative importance of two- and three-dimensional oscillations, and will be taken to be real. There is then no loss of generality in taking this ratio to be positive. The reality of μ/λ corresponds to taking the two- and three-dimensional oscillations to be in phase. This corresponds to the situation in the experiments of Schubauer and Klebanoff. Also it appears to be the most likely physical situation if one regards the three-dimensionality developing as a perturbation from the two-dimensional waves.†

The two sets of equations governing the primary oscillations then become

$$\left.\begin{aligned}
i\alpha\hat{u}_1 + \frac{d\hat{v}_1}{dy} + \beta\hat{w}_1 &= 0,\\
i\alpha(u_0-c)\,\hat{u}_1 + \frac{du_0}{dy}\hat{v}_1 &= -i\alpha\hat{p}_1,\\
i\alpha(u_0-c)\,\hat{v}_1 &= -\frac{d\hat{p}_1}{dy},\\
i\alpha(u_0-c)\,\hat{w}_1 &= +\beta\hat{p}_1,
\end{aligned}\right\} \tag{3.17}$$

and

$$\left.\begin{aligned}
i\alpha\hat{U}_1 + \frac{d\hat{V}_1}{dy} &= 0,\\
i\alpha(u_0-c)\,\hat{U}_1 + \frac{du_0}{dy}\hat{V}_1 &= -i\alpha\hat{P}_1,\\
i\alpha(u_0-c)\,\hat{V}_1 &= -\frac{d\hat{P}_1}{dy}.
\end{aligned}\right\} \tag{3.18}$$

Also, the function $\hat{\xi}_1(y)$ is determined by

$$\hat{\xi}_1 = \frac{d\hat{w}_1}{dy} + \beta\hat{v}_1. \tag{3.19}$$

† If μ/λ is complex the subsequent analysis suffers some slight modifications. These will not be considered in this paper.

Corresponding to this primary oscillation, the mean secondary flow has components which we write as

$$\left.\begin{aligned}
\hat{v}_0^{(2)}(y,z) &= \lambda^2\hat{v}_a(y)\cos 2\beta z + \lambda\mu\hat{v}_b(y)\cos\beta z + \lambda^2\hat{v}_c(y) + \mu^2\hat{v}_d(y),\\
\hat{w}_0^{(2)}(y,z) &= \lambda^2\hat{w}_a(y)\sin 2\beta z + \lambda\mu\hat{w}_b(y)\sin\beta z + \lambda^2\hat{w}_c(y) + \mu^2\hat{w}_d(y),\\
\hat{\xi}_0^{(2)}(y,z) &= \lambda^2\hat{\xi}_a(y)\sin 2\beta z + \lambda\mu\hat{\xi}_b(y)\sin\beta z + \lambda^2\hat{\xi}_c(y) + \mu^2\hat{\xi}_d(y),\\
\hat{r}_0^{(2)}(y,z) &= \lambda^2\hat{r}_a(y)\cos 2\beta z + \lambda\mu\hat{r}_b(y)\cos\beta z + \lambda^2\hat{r}_c(y) + \mu^2\hat{r}_d(y),\\
\hat{s}_0^{(2)}(y,z) &= \lambda^2\hat{s}_a(y)\cos 2\beta z + \lambda\mu\hat{s}_b(y)\cos\beta z + \lambda^2\hat{s}_c(y) + \mu^2\hat{s}_d(y),\\
\hat{p}_0^{(2)}(y,z) &= \lambda^2\hat{p}_a(y)\cos 2\beta z + \lambda\mu\hat{p}_b(y)\cos\beta z + \lambda^2\hat{p}_c(y) + \mu^2\hat{p}_d(y).
\end{aligned}\right\} \tag{3.20}$$

The subscript a refers to that part of the mean secondary flow induced by the purely three-dimensional part of the oscillation, and the subscript b to the part due to the interaction of the two components of the primary oscillation. Both these secondary a and b flows are periodic in z and will produce three-dimensional distortions of the original flow profile. Quantities with subscripts c and d are merely two-dimensional distortions due to the three- and two-dimensional components of the fluctuation respectively. If $\lambda = 0$ the mean secondary flow would reduce to the d flow, corresponding to the case of a purely two-dimensional oscillation which has been considered earlier by Meksyn & Stuart (1951).

On referring to the general equations for the mean secondary flow derived at the beginning of this section we can now obtain, using the assumed primary oscillation, sets of equations to determine the a, b, c, and d flows.

The a flow is determined by

$$\left.\begin{aligned}
\hat{s}_a &= -\hat{v}_a\frac{du_0}{dy},\\
\hat{r}_a &= -\frac{1}{2}\frac{d}{dy}(\hat{u}_1\hat{v}_1^* + \hat{u}_1^*\hat{v}_1) - \beta(\hat{u}_1\hat{w}_1^* + \hat{u}_1^*\hat{w}_1),\\
\hat{\xi}_a &= -\left(\frac{1}{2}\frac{d^2}{dy^2} + 2\beta^2\right)(\hat{v}_1\hat{w}_1^* + \hat{v}_1^*\hat{w}_1) - 2\beta\frac{d}{dy}(\hat{v}_1\hat{v}_1^* + \hat{w}_1\hat{w}_1^*),\\
\frac{d\hat{v}_a}{dy} + 2\beta\hat{w}_a &= 0,\\
\frac{d\hat{w}_a}{dy} + 2\beta\hat{v}_a &= \hat{\xi}_a.
\end{aligned}\right\} \tag{3.21}$$

The b flow is determined by

$$\left.\begin{aligned}
\hat{s}_b &= -\hat{v}_b\frac{du_0}{dy},\\
\hat{r}_b &= -\frac{d}{dy}(\hat{u}_1\hat{V}_1^* + \hat{u}_1^*\hat{V}_1 + \hat{U}_1\hat{v}_1^* + \hat{U}_1^*\hat{v}_1) - \beta(\hat{U}_1\hat{w}_1^* + \hat{U}_1^*\hat{w}_1),\\
\hat{\xi}_b &= -\left(\frac{d^2}{dy^2} + \beta^2\right)(\hat{V}_1\hat{w}_1^* + \hat{V}_1^*\hat{w}_1) - 2\beta\frac{d}{dy}(\hat{V}_1\hat{v}_1^* + \hat{V}_1^*\hat{v}_1),\\
\frac{d\hat{v}_b}{dy} + \beta\hat{w}_b &= 0,\\
\frac{d\hat{w}_b}{dy} + \beta\hat{v}_b &= \hat{\xi}_b.
\end{aligned}\right\} \tag{3.22}$$

The c and d flows are independent of z and so $\hat{\xi}_c = \hat{\xi}_d = 0$. Also

$$\frac{d\hat{v}_c}{dy} = \frac{d\hat{v}_d}{dy} = \frac{d\hat{w}_c}{dy} = \frac{d\hat{w}_d}{dy} = 0.$$

Hence, for the case of a fluid in the presence of a solid boundary or of a fluid extending to infinity, these four velocity components must be zero.

Therefore the c flow is given by

$$\left.\begin{aligned} \hat{s}_c &= 0, \\ \hat{r}_c &= -\frac{1}{2}\frac{d}{dy}(\hat{u}_1\hat{v}_1^* + \hat{u}_1^*\hat{v}_1), \\ \hat{\xi}_c &= 0, \\ \hat{v}_c &= 0, \\ \hat{w}_c &= 0. \end{aligned}\right\} \tag{3.23}$$

Similarly the d flow is given by

$$\left.\begin{aligned} \hat{s}_d &= 0, \\ \hat{r}_d &= -\frac{1}{2}\frac{d}{dy}(U_1V_1^* + U_1^*V_1), \\ \hat{\xi}_d &= 0, \\ \hat{v}_d &= 0, \\ \hat{w}_d &= 0. \end{aligned}\right\} \tag{3.24}$$

Thus these two-dimensional distortions contribute to $u_0^{(2)}$ through the gradient of the Reynolds stress, but do not contribute to $v_0^{(2)}$ or $w_0^{(2)}$.

For the sake of completeness we list the equations for the analogous contributions (e, f, g, h) to the oscillatory secondary flow. We write

$$\left.\begin{aligned} u_2^{(2)}(y,z,t) &= \hat{u}_2^{(2)}(y,z)\,e^{-2i\alpha ct} \\ &= [\lambda^2\hat{u}_e(y)\cos 2\beta z + \lambda\mu\hat{u}_f(y)\cos\beta z + \lambda^2\hat{u}_g(y) + \mu^2\hat{u}_h(y)]\,e^{-2i\alpha ct}, \\ v_2^{(2)}(y,z,t) &= \hat{v}_2^{(2)}(y,z)\,e^{-2i\alpha ct} \\ &= [\lambda^2\hat{v}_e(y)\cos 2\beta z + \lambda\mu\hat{v}_f(y)\cos\beta z + \lambda^2\hat{v}_g(y) + \mu^2\hat{v}_h(y)]\,e^{-2i\alpha ct}, \\ w_2^{(2)}(y,z,t) &= \hat{w}_2^{(2)}(y,z)\,e^{-2i\alpha ct} \\ &= [\lambda^2\hat{w}_e(y)\sin 2\beta z + \lambda\mu\hat{w}_f(y)\sin\beta z + \lambda^2\hat{w}_g(y) + \mu^2\hat{w}_h(y)]\,e^{-2i\alpha ct}, \\ p_2^{(2)}(y,z,t) &= \hat{p}_2^{(2)}(y,z)\,e^{-2i\alpha ct} \\ &= [\lambda^2\hat{p}_e(y)\cos 2\beta z + \lambda\mu\hat{p}_f(y)\cos\beta z + \lambda^2\hat{p}_g(y) + \mu^2\hat{p}_h(y)]\,e^{-2i\alpha ct}. \end{aligned}\right\} \tag{3.25}$$

The e flow is then determined by the equations

$$\left.\begin{aligned} 2i\alpha(u_0-c)\,\hat{u}_e + \frac{du_0}{dy}\hat{v}_e + \frac{1}{2}\left(\hat{v}_1\frac{d\hat{u}_1}{dy} - \hat{u}_1\frac{d\hat{v}_1}{dy}\right) &= -2i\alpha\hat{p}_e, \\ 2i\alpha(u_0-c)\,\hat{v}_e &= -\frac{d\hat{p}_e}{dy}, \\ 2i\alpha(u_0-c)\,\hat{w}_e + \frac{1}{2}\left(\hat{v}_1\frac{d\hat{w}_1}{dy} - \hat{w}_1\frac{d\hat{v}_1}{dy}\right) &= 2\beta\hat{p}_e, \\ 2i\alpha\hat{u}_e + \frac{d\hat{v}_e}{dy} + 2\beta\hat{w}_e &= 0, \\ \hat{\xi}_e &= \frac{d\hat{w}_e}{dy} + 2\beta\hat{v}_e. \end{aligned}\right\} \tag{3.26}$$

For the f flow

$$\left.\begin{aligned} 2i\alpha(u_0-c)\,\hat{u}_f+\frac{du_0}{dy}\hat{v}_f+2i\alpha\hat{u}_1\hat{U}_1+\hat{v}_1\frac{d\hat{U}_1}{dy}+\hat{V}_1\frac{d\hat{u}_1}{dy}&=-2i\alpha\hat{p}_f,\\ 2i\alpha(u_0-c)\,\hat{v}_f-\beta\hat{w}_1\hat{V}_1&=-\frac{d\hat{p}_f}{dy},\\ 2ia(u_0-c)\,\hat{w}_f+\hat{V}_1\frac{d\hat{w}_1}{dy}-\hat{w}_1\frac{d\hat{V}_1}{dy}&=\beta\hat{p}_f,\\ 2i\alpha\hat{u}_f+\frac{d\hat{v}_f}{dy}+\beta\hat{w}_f&=0,\\ \hat{\xi}_f=\frac{d\hat{w}_f}{dy}+\beta\hat{v}_f.& \end{aligned}\right\} \tag{3.27}$$

For the g flow

$$\left.\begin{aligned} 2i\alpha(u_0-c)\,\hat{u}_g+\frac{du_0}{dy}\hat{v}_g+\frac{1}{2}\left(\hat{v}_1\frac{d\hat{u}_1}{dy}-\hat{u}_1\frac{d\hat{v}_1}{dy}\right)-\beta\hat{u}_1\hat{w}_1&=-2i\alpha\hat{p}_g,\\ 2i\alpha(u_0-c)\,\hat{v}_g-\beta\hat{v}_1\hat{w}_1&=-\frac{d\hat{p}_g}{dy},\\ \hat{w}_g&=0,\\ 2i\alpha\hat{u}_g+\frac{d\hat{v}_g}{dy}&=0,\\ \hat{\xi}_g&=0. \end{aligned}\right\} \tag{3.28}$$

Finally, the h flow is given by

$$\left.\begin{aligned} 2i\alpha(u_0-c)\,\hat{u}_h+\frac{du_0}{dy}\hat{v}_h+\hat{V}_1\frac{d\hat{U}_1}{dy}-\hat{U}_1\frac{d\hat{V}_1}{dy}&=-2i\alpha\hat{p}_h,\\ 2i\alpha(u_0-c)\,\hat{v}_h&=-\frac{d\hat{p}_h}{dy},\\ \hat{w}_h&=0,\\ 2i\alpha\hat{u}_h+\frac{d\hat{v}_h}{dy}&=0,\\ \hat{\xi}_h&=0. \end{aligned}\right\} \tag{3.29}$$

We shall now perform the calculations for a particular case. Such a calculation will shed considerable light on the mechanism involved.

4. Application to the case of a shear flow between parallel streams

In this section detailed calculations are given for the case of the shear profile $u_0(y) = \tanh y$ (cf. Esch 1957, and Drazin 1958). Such a shear flow can be readily approximated experimentally by mixing two parallel streams, and so the theoretical predictions should be capable of direct confirmation. At the time of performing these calculations no experimental results for a shear flow, with special attention to spanwise variations, appear to be available. Such experiments would be highly desirable.

From the set of equations (3.17), governing the standing wave component of the primary oscillation, it can be shown by a simple elimination that $\hat{v}_1$ satisfies the equation

$$(u_0-c)\left(\frac{d^2}{dy^2}-\alpha^2-\beta^2\right)\hat{v}_1-\frac{d^2u_0}{dy^2}\hat{v}_1=0. \tag{4.1}$$

For $u_0(y) = \tanh y$, we have a point of inflexion at $y = 0$, and Curle (1956) has shown there is a neutral oscillation given by

$$\hat{v}_1 = \operatorname{sech} y; \quad \alpha^2 + \beta^2 = 1; \quad c = 0. \tag{4.2}$$

In fact one can set up a regular perturbation in c about this solution using the method of variation of constants. As our interest centres on the case of c_i small, we shall be content with the first term of this perturbation.

A complete solution of the linear system (3.17) corresponding to this neutral oscillation is

$$\left.\begin{aligned} \hat{u}_{1i} &= \frac{i}{\alpha}[\beta^2 \operatorname{cosech} y - \operatorname{sech} y \tanh y], \\ \hat{v}_{1i} &= \operatorname{sech} y, \\ \hat{w}_{1i} &= \beta \operatorname{cosech} y, \\ \hat{p}_{1i} &= i\alpha \operatorname{sech} y. \end{aligned}\right\} \tag{4.3}$$

For the two-dimensional component of the primary oscillation we take the known neutral solution of the set of equations† (3.18), namely,

$$\left.\begin{aligned} \hat{U}_{1i} &= -i \operatorname{sech} y \tanh y, \\ \hat{V}_{1i} &= \operatorname{sech} y, \\ \hat{P}_{1i} &= i \operatorname{sech} y. \end{aligned}\right\} \tag{4.4}$$

These will be reliable solutions for fairly slow spanwise variations of amplitude and for c_i small. Again the solutions could be improved by perturbation techniques; but for the range of interest the above approximations will be taken as adequate. As was mentioned in § 3, in practice one part of the second-order mean flow (the b flow) may be of a quasi-steady nature, corresponding to slightly different downstream wave-numbers for the two- and three-dimensional parts of the primary oscillations.

In the solutions (4.3) and (4.4), the subscript i has been added to emphasize the fact that these solutions are purely inviscid solutions, and therefore will be reliable solutions for the flow of a real fluid at high Reynolds number, provided we are not close to the critical layer ($y = 0$). It is important to note that the amplitude functions $\hat{u}_{1i}$ and $\hat{w}_{1i}$ exhibit singularities at $y = 0$, which would be absent in any real fluid. That is, when viscosity is included these poles would not be present.

On the basis of a purely inviscid analysis, we obtain, from (3.21) to (3.24),

$$\left.\begin{aligned} \hat{\xi}_{ai} &= -\frac{16\beta}{\sinh^3 2y}[(1-\beta^2)\cosh 2y - \beta^2], \\ \hat{r}_{ai} &= 0, \end{aligned}\right\} \tag{4.5}$$

$$\left.\begin{aligned} \hat{\xi}_{bi} &= -\frac{2\beta}{\sinh^3 2y}[16\cosh 2y + \beta^2 \cosh 4y - \beta^2], \\ \hat{r}_{bi} &= 0, \end{aligned}\right\} \tag{4.6}$$

$$\left.\begin{aligned} \hat{\xi}_{ci} &= \hat{r}_{ci} = 0, \\ \hat{\xi}_{di} &= \hat{r}_{di} = 0. \end{aligned}\right\} \tag{4.7}$$

† Strictly, this solution would have to be modified due to the difference in the value of α; but the logarithmic singularity is believed to be unimportant compared to the higher-order singularities present in the inviscid oscillation.

It is seen that the functions ξ_{ai} and ξ_{bi} have poles of order three at the critical layer. Thus the singularities in the primary flow give rise to more serious difficulties for the secondary flow. Clearly this singular behaviour can be corrected by using a viscous correction near $y = 0$.

Corresponding to the neutral oscillation $\hat{v}_{1i} = \operatorname{sech} y$, the equivalent two-dimensional component of this oscillation is given by $i\alpha\hat{u}_{1i} + \beta\hat{w}_{1i} = \operatorname{sech} y \tanh y$. However, the cross-wave component is $\hat{\phi}_i = \beta\hat{u}_{1i} + i\alpha\hat{w}_{1i} = +(i\beta/\alpha)\operatorname{sech}^3 y \coth y$, and has a pole at $y = 0$. The complete differential equation for $\hat{\phi}$ is obtained by taking a suitable combination from the set (2.15). It is

$$\frac{d^2\hat{\phi}}{dy^2} - [i\alpha R \tanh y + 1]\hat{\phi} = \beta R \operatorname{sech}^3 y. \tag{4.8}$$

Formally putting R infinite, we have the inviscid solution

$$\hat{\phi}_i = -\frac{\beta}{i\alpha}\operatorname{sech}^3 y \coth y. \tag{4.9}$$

It is well known that the critical layer has a thickness of order $(\alpha R)^{-\frac{1}{3}}$ and it is within this region that the solution $\hat{\phi}_i$ will be modified by a correction of the boundary-layer type.

A formal method of dealing with a homogeneous second-order differential equation, involving a large parameter αR, whose coefficient has a turning point, has been given by Langer (1949). The extension to the non-homogeneous problem is very simple. We sketch the method as it applies to the problem at hand.

First consider the general solution $\hat{\psi}$ of the homogeneous equation

$$\frac{d^2\hat{\psi}}{dy^2} - [i\alpha R \tanh y + 1]\hat{\psi} = 0. \tag{4.10}$$

Let
$$T(y) = \int_0^y \sqrt{(\tanh y)}\, dy = \tanh^{-1}\sqrt{(\tanh y)} - \tan^{-1}\sqrt{(\tanh y)}, \tag{4.11}$$

$$Z(y, \alpha R) = iY(y, \alpha R) = i(\alpha R)^{\frac{1}{3}}(3T/2)^{\frac{2}{3}}, \tag{4.12}$$

$$Q(y) = (3T/2)^{\frac{1}{6}}\left(\frac{dT}{dy}\right)^{-\frac{1}{2}}, \tag{4.13}$$

$$\hat{\psi}_1(y) = Q(y)\, h(Z), \tag{4.14}$$

where
$$\frac{d^2h}{dZ^2} + Zh = 0. \tag{4.15}$$

A straightforward substitution then shows that $\hat{\psi}_1$ satisfies the equation

$$\frac{d^2\hat{\psi}_1}{dy^2} - \left[i\alpha R \tanh y + \frac{1}{Q}\frac{d^2Q}{dy^2}\right]\hat{\psi}_1 = 0, \tag{4.16}$$

$Q^{-1}d^2Q/dy^2$ being regular and non-zero in a neighbourhood of $y = 0$. Equation (4.16) is considered as the approximating differential equation for (4.10) and correct to order $(\alpha R)^{-\frac{1}{3}}$ we may write $\hat{\psi} \equiv \hat{\psi}_1$.

The solutions of equation (4.15) are the modified Hankel functions of order one-third. That is, in the usual notation,

$$h_1(Z) = (\tfrac{2}{3}Z^{\frac{3}{2}})^{\frac{1}{3}} H^{(1)}_{\frac{1}{3}}(\tfrac{2}{3}Z^{\frac{3}{2}}), \tag{4.17}$$

$$h_2(Z) = (\tfrac{2}{3}Z^{\frac{3}{2}})^{\frac{1}{3}} H^{(2)}_{\frac{1}{3}}(\tfrac{2}{3}Z^{\frac{3}{2}}). \tag{4.18}$$

As $Q(y)$ is a known function of y, we can write the general solution of equation (4.10) as

$$\hat{\psi} = \{A_1 h_1(Z) + A_2 h_2(Z)\} Q(y), \tag{4.19}$$

where A_1 and A_2 are arbitrary constants.

Returning now to the non-homogeneous problem, the solution $\hat{\phi}(y)$ is required to approach the inviscid solution $\hat{\phi}_i(y)$ for $(\alpha R)^{\frac{1}{3}} y$ large. An application of the method of variation of constants readily shows that this solution is

$$\hat{\phi} = -\frac{\beta}{i\alpha} \operatorname{sech}^3 y \coth y \, Z L(Z), \tag{4.20}$$

where $L(Z)$ is a Lommel function, and is the solution of the differential equation $d^2L/dZ^2 + ZL = 1$, which behaves like Z^{-1} for $|Z|$ large. $L(Z)$ can easily be checked to be expressible in the form

$$L(Z) = \frac{h_2(Z) \int_{i\infty}^{Z} h_1(\zeta)\, d\xi - h_1(Z) \int_{-i\infty}^{Z} h_2(\zeta)\, d\zeta}{W\{h_1(Z), h_2(Z)\}}, \tag{4.21}$$

provided $-\frac{2}{3}\pi < \arg(Z) < \frac{2}{3}\pi$. In the above application $\arg(Z) = \pm \frac{1}{2}\pi$. $W\{h_1(Z), h_2(Z)\}$ denotes the Wronskian of the functions $h_1(Z)$ and $h_2(Z)$. In the usual normalization for the Hankel functions, we have

$$W\{h_1(Z), h_2(Z)\} = -\frac{4i}{\pi} \left(\frac{3}{2}\right)^{\frac{1}{3}}. \tag{4.22}$$

The above method of approximate solution can be systematically extended to higher approximations by using perturbation series in $(\alpha R)^{-\frac{1}{3}}$.

In dealing with the case of high Reynolds numbers we shall retain only the leading terms in αR for all quantities in the subsequent work. The viscous corrections, which apply for $Y = O(1)$, or $y = O(\alpha R)^{-\frac{1}{3}}$, remove the singularities obtained by the inviscid analysis.

The Lommel function plays an important role in the problem and it is useful to list a few of its properties. We write

$$L(Z) = L_r(Y) + iL_i(Y), \tag{4.23}$$

where

$$Y = (\alpha R)^{\frac{1}{3}} y. \tag{4.24}$$

From the differential equation we have

$$\frac{d^2 L_r}{dY^2} + Y L_i = -1, \tag{4.25}$$

$$\frac{d^2 L_i}{dY^2} - Y L_r = 0. \tag{4.26}$$

Also, using the result that $[h_1(Z^*)]^* = h_2(Z)$, it can be shown, from (4.21), that L_r is an even and L_i an odd function of Y. For Y large,

$$L_r = -\frac{2}{Y^4} + \frac{2240}{Y^{10}} - \ldots, \tag{4.27}$$

$$L_i = -\frac{1}{Y} + \frac{40}{Y^7} - \ldots. \tag{4.28}$$

The graphs of $L_r(Y)$ and $L_i(Y)$ are shown in figure 1.

Dropping the subscripts i for the corrected solution, a little manipulation yields

$$\left.\begin{aligned}\hat{u}_1 &= -\frac{\beta^2(\alpha R)^{\frac{1}{3}}}{\alpha} L_r(Y) - \frac{i}{\alpha}(\beta^2 \operatorname{cosech} y - \operatorname{sech} y \tanh y)\, Y L_i(Y),\\ \hat{v}_1 &= \operatorname{sech} y,\\ \hat{w}_1 &= -\beta \operatorname{cosech} y\, Y L_i(Y) + i\beta(\alpha R)^{\frac{1}{3}} L_r(Y),\end{aligned}\right\} \tag{4.29}$$

$$\left.\begin{aligned}\hat{U}_1 &= -i \operatorname{sech} y \tanh y,\\ \hat{V}_1 &= \operatorname{sech} y.\end{aligned}\right\} \tag{4.30}$$

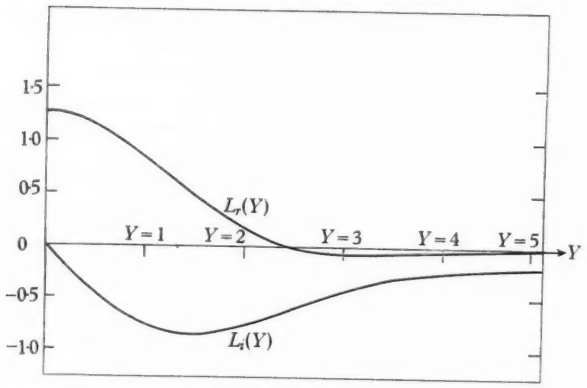

FIGURE 1. Graphs of $L_r(Y)$ and $L_i(Y)$.

The corresponding second-order quantities are

$$\left.\begin{aligned}\hat{\xi}_a &= -\frac{16\beta}{\sinh^3 2y}[(1-\beta^2)\cosh 2y - \beta^2]\, G(Y),\\ \hat{r}_a &= \frac{\beta^2(\alpha R)^{\frac{2}{3}}}{\alpha}\frac{dL_r}{dY},\end{aligned}\right\} \tag{4.31}$$

where

$$G(Y) = \frac{Y^3}{2(1-2\beta^2)}\left[2\beta^2\frac{d}{dY}(L_r^2 + L_i^2) - Y L_r\right];$$

$$\left.\begin{aligned}\hat{\xi}_b &= -\frac{2\beta}{\sinh^3 2y}[16\cosh 2y + \beta^2 \cosh 4y - \beta^2]\, H(Y),\\ \hat{r}_b &= \frac{2\beta^2(\alpha R)^{\frac{2}{3}}}{\alpha}\frac{dL_r}{dY},\end{aligned}\right\} \tag{4.32}$$

where $H(Y) = -\frac{1}{2}Y^4 L_r$. Also,

$$\left.\begin{aligned}\hat{\xi}_c &= 0,\\ \hat{r}_c &= \frac{\beta^2(\alpha R)^{\frac{2}{3}}}{\alpha}\frac{dL_r}{dY},\end{aligned}\right\} \tag{4.33}$$

$$\left.\begin{aligned}\hat{\xi}_d &= 0,\\ \hat{r}_d &= 0.\end{aligned}\right\} \tag{4.34}$$

For Y large

$$G(Y) = 1 - \frac{16(70 - 19\beta^2)}{(1 - 2\beta^2)\, Y^6} + \ldots, \tag{4.35}$$

$$H(Y) = 1 - \frac{1120}{Y^6} + \ldots. \tag{4.36}$$

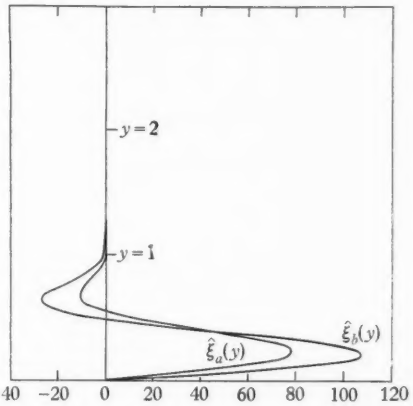

FIGURE 2. Mean secondary vorticity amplitude functions.

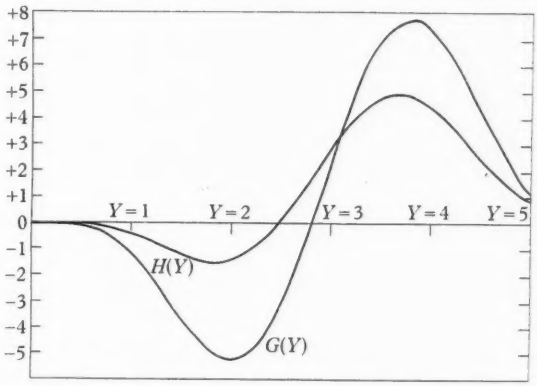

FIGURE 3. Correction functions $G(Y)$ and $H(Y)$.

The actual calculations have been performed for $\beta = \frac{1}{2}$, $\alpha R = 125$, which have been taken as typical of the behaviour of the functions. Both $\hat{\xi}_a$ and $\hat{\xi}_b$ are odd functions of y. Figure 2 shows these functions. Figure 3 shows the graphs of the correction functions $G(Y)$ and $H(Y)$.

We now apply these results and calculate the mean secondary motion.

5. The mean secondary motion

First we discuss the a flow contribution to the mean secondary motion. This has a spanwise period π/β, and is induced by the three-dimensional standing wave part of the primary oscillation. From (3.21) we have

$$\frac{d^2\hat{v}_a}{dy^2} - 4\beta^2\hat{v}_a = -2\beta\hat{\xi}_a, \tag{5.1}$$

$$\hat{w}_a = -\frac{1}{2\beta}\frac{d\hat{v}_a}{dy}, \tag{5.2}$$

where, from (4.31),

$$\hat{\xi}_a(y) = \hat{\xi}_{ai}(y)\,G(Y). \tag{5.3}$$

We require the solution of (5.1), for $y > 0$, subject to the conditions $\hat{v}_a(0) = 0$, and $\hat{v}_a(y) \to 0$ as $y \to \infty$. For $y < 0$, $\hat{v}_a(y)$ and $\hat{w}_a(y)$ are defined as odd and even functions respectively. Thus

$$\hat{v}_a(-y) = -\hat{v}_a(y); \quad \hat{w}_a(-y) = \hat{w}_a(y). \tag{5.4}$$

It is to be noted in passing that the solution of (5.1) with $\hat{\xi}_a = 0$ gives two-dimensional potential type motions.

The solution of (5.1) satisfying the condition at infinity can be written down in explicit form by the method of variation of constants. We have

$$\hat{v}_a(y) = A\,e^{-2\beta y} - \int_{\infty}^{y} \hat{\xi}_a(t)\sinh 2\beta(y-t)\,dt, \tag{5.5}$$

$$\hat{w}_a(y) = A\,e^{-2\beta y} + \int_{\infty}^{y} \hat{\xi}_a(t)\cosh 2\beta(y-t)\,dt, \tag{5.6}$$

where both integrals are clearly convergent. For $\hat{v}_a(0) = 0$, A is determined from

$$A = \int_0^{\infty} \hat{\xi}_a(t)\sinh 2\beta t\,dt, \tag{5.7}$$

and so

$$w_a(0) = -\int_0^{\infty} \hat{\xi}_a(t)\,e^{-2\beta t}dt. \tag{5.8}$$

Using this value for A, we can rewrite $\hat{v}_a(y)$ and $\hat{w}_a(y)$ in an alternative form, convenient for small values of y, namely,

$$\hat{v}_a(y) = \left(\int_0^{\infty} \hat{\xi}_a(t)\,e^{-2\beta t}dt\right)\sinh 2\beta y - \int_0^{y} \hat{\xi}_a(t)\sinh 2\beta(y-t)\,dt, \tag{5.9}$$

$$\hat{w}_a(y) = -\left(\int_0^{\infty} \hat{\xi}_a(t)\,e^{-2\beta t}dt\right)\cosh 2\beta y + \int_0^{y} \hat{\xi}_a(t)\cosh 2\beta(y-t)\,dt. \tag{5.10}$$

Approximate values for the constants A and $\hat{w}_a(0)$ can be obtained in the following way. $\hat{\xi}_{ai}(t)$ can be expanded as a Laurent series about $t = 0$ of the form

$$\hat{\xi}_{ai}(t) = \frac{a_0}{t^3} + \frac{a_1}{t} + \ldots, \tag{5.11}$$

where, for the case at hand,

$$a_0 = -2\beta(1-2\beta^2). \tag{5.12}$$

Putting $T = (\alpha R)^{\frac{1}{3}} t$, and $Y = (\alpha R)^{\frac{1}{3}} y$, we have from equations (5.7), (5.8)

$$A = -4\beta^2(1-2\beta^2)(\alpha R)^{\frac{1}{3}} \int_0^\infty \frac{1}{T^2} G(T)\, dT + O(\alpha R)^{-\frac{1}{3}}, \tag{5.13}$$

and

$$\hat{w}_a(0) = 2\beta(1-2\beta^2)(\alpha R)^{\frac{2}{3}} \int_0^\infty \frac{1}{T^3} G(T)\, dT + O(\alpha R)^{\frac{1}{3}}. \tag{5.14}$$

On using the value for $G(T)$ from equation (4.31) we find, after some simplification,

$$A = 4(\alpha R)^{\frac{1}{3}} \beta^4 \int_0^\infty (L_r^2 + L_i^2)\, dT + O(\alpha R)^{-\frac{1}{3}}, \tag{5.15}$$

$$\hat{w}_a(0) = -(\alpha R)^{\frac{2}{3}} \beta \left[2\beta^2 L_r^2(0) - \frac{dL_i}{dY}(0) \right] + O(\alpha R)^{\frac{1}{3}}. \tag{5.16}$$

So for R large, $A > 0$, and $\hat{w}_a(0) < 0$.

Also from equation (5.9), using the same transformations, we have

$$\hat{v}_a(y) = \left\{ \int_0^\infty \xi_a \left[\frac{T}{(\alpha R)^{\frac{1}{3}}} \right] \exp\left[-\frac{2\beta T}{(\alpha R)^{\frac{1}{3}}} \right] \frac{1}{(\alpha R)^{\frac{1}{3}}}\, dT \right\} \sinh\left[\frac{2\beta Y}{(\alpha R)^{\frac{1}{3}}} \right]$$
$$- \int_0^Y \xi_a \left[\frac{T}{(\alpha R)^{\frac{1}{3}}} \right] \sinh\left[\frac{2\beta(Y-T)}{(\alpha R)^{\frac{1}{3}}} \right] \frac{1}{(\alpha R)^{\frac{1}{3}}}\, dT, \tag{5.17}$$

and so for Y large,

$$\hat{v}_a(y) \to -4\beta^2(1-2\beta^2)(\alpha R)^{\frac{1}{3}} \int_0^\infty \frac{1}{T^2} G(T)\, dT. \tag{5.18}$$

Thus $\hat{v}_a(y)$ tends to a constant value of order $(\alpha R)^{\frac{1}{3}}$ as we approach the outer edge of the critical layer. On comparing (5.13) and (5.18), it is seen that it is this term that induces the external potential motion $A e^{-2\beta y}$.

The preceding analysis shows very clearly the importance of the critical layer. Although viscous forces are negligible outside the small region $y = O(\alpha R)^{-\frac{1}{3}}$, we see that they are indeed responsible for inducing a potential component to the secondary motion, which is dominant far away from the critical layer. This two-dimensional secondary flow, induced by the purely three-dimensional part of the original oscillation, may be described as being due to a source distribution at the critical layer of strength $\sigma(z) = (A/\pi)\cos 2\beta z$ per unit length. This source distribution is of $O\{a^2\lambda^2(\alpha R)^{\frac{1}{3}}\}$, and determines the direction of the circulation for the a motion at infinity.

In figure 4 we show the graphs of $\hat{v}_a(y)$, $\hat{w}_a(y)$, $\hat{r}_a(y)$, and $\hat{s}_a(y)$.

By the same method we can discuss the b flow contribution to the mean secondary motion. This has a spanwise period $2\pi/\beta$ and is induced by the non-linear interaction of the two- and three-dimensional parts of the oscillation. From (3.22), we have

$$\frac{d^2\hat{v}_b}{dy^2} - \beta^2 \hat{v}_b = -\beta \xi_b, \tag{5.19}$$

$$\hat{w}_b = -\frac{1}{\beta} \frac{d\hat{v}_b}{dy}, \tag{5.20}$$

$$\xi_b(y) = \xi_{bi}(y)\, H(Y). \tag{5.21}$$

These equations are of the same form as (5.1), (5.2), (5.3), with a, G, and 2β, replaced by b, H, and β, respectively.

Hence we find, for $y > 0$,

$$\hat{v}_b(y) = Be^{-\beta y} - \int_\infty^y \hat{\xi}_b(t) \sinh \beta(y-t)\, dt, \tag{5.22}$$

$$\hat{w}_b(y) = Be^{-\beta y} + \int_\infty^y \hat{\xi}_b(t) \cosh \beta(y-t)\, dt. \tag{5.23}$$

As before,

$$B = \int_0^\infty \hat{\xi}_b(t) \sinh \beta t\, dt, \tag{5.24}$$

$$\hat{w}_b(0) = -\int_0^\infty \hat{\xi}_b(t)\, e^{-\beta t}\, dt. \tag{5.25}$$

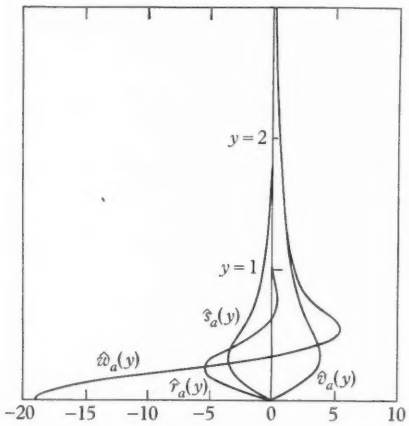

FIGURE 4. Amplitude functions for the a flow.

On using this value for B, the expressions for $\hat{v}_b(y)$ and $\hat{w}_b(y)$ can be rewritten in the alternative form

$$\hat{v}_b(y) = \left(\int_0^\infty \hat{\xi}_b(t)\, e^{-\beta t} dt\right) \sinh \beta y - \int_0^y \hat{\xi}_b(t) \sinh \beta(y-t)\, dt, \tag{5.26}$$

$$\hat{w}_b(y) = -\left(\int_0^\infty \hat{\xi}_b(t)\, e^{-\beta t} dt\right) \cosh \beta y + \int_0^y \hat{\xi}_b(t) \cosh \beta(y-t)\, dt. \tag{5.27}$$

Near $t = 0$,

$$\hat{\xi}_{bi}(t) = -\frac{4\beta}{t^3} + O\left(\frac{1}{t}\right), \tag{5.28}$$

and so

$$B = -4\beta^2(\alpha R)^{\frac{1}{3}} \int_0^\infty \frac{1}{T^2} H(T)\, dT + O(\alpha R)^{-\frac{1}{3}}, \tag{5.29}$$

$$\hat{w}_b(0) = 4\beta(\alpha R)^{\frac{2}{3}} \int_0^\infty \frac{1}{T^3} H(T)\, dT + O(\alpha R)^{\frac{1}{3}}. \tag{5.30}$$

On using the fact that $H(T) = -\frac{1}{2}T^4 L_2(T)$, we find

$$B = O(\alpha R)^{-\frac{1}{3}}, \tag{5.31}$$

$$\hat{w}_b(0) = 2\beta(\alpha R)^{\frac{2}{3}} \frac{dL_i(0)}{dY} + O(\alpha R)^{\frac{1}{3}}. \tag{5.32}$$

Thus the interaction flow, or b flow, produces a potential component $O\{a^2\lambda\mu(\alpha R)^{-\frac{1}{3}}\}$, in contrast to the a flow. The same strong spanwise momentum exchange is present near the critical layer. Figure 5 shows the graphs of $\hat{v}_b(y)$, $\hat{w}_b(y)$, $\hat{r}_b(y)$ and $\hat{s}_b(y)$.

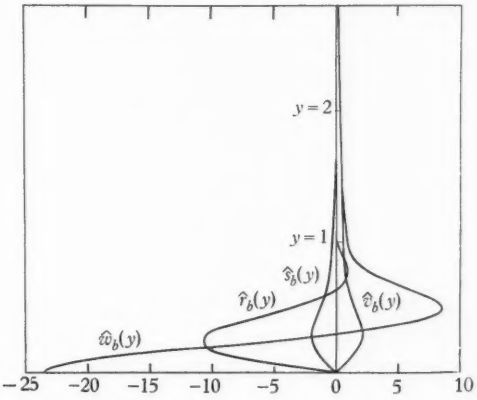

FIGURE 5. Amplitude functions for the b flow.

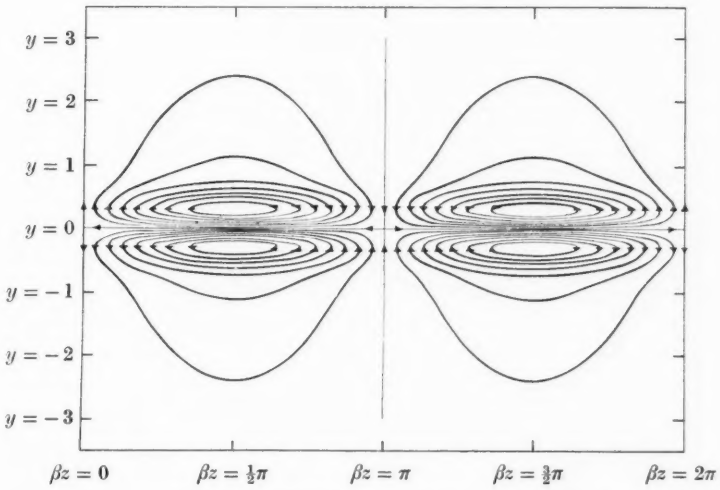

FIGURE 6. Streamline pattern for secondary motion, $\mu/\lambda \gg 1$.

The c flow part of the mean secondary flow is a purely two-dimensional distortion due, however, to the three-dimensionality of the original oscillation. The only non-zero second-order term is $\hat{r}_c(y) = \hat{r}_a(y)$, relating to the downstream velocity component. This tends to produce a defect in x-momentum close to the critical layer at all points across the profile, and a very slight excess at the outer edge of the critical layer. The effect is confined to the region $y = O(\alpha R)^{-\frac{1}{3}}$.

To the order of the approximation used in the present analysis, the d flow, due to the two-dimensional oscillation, does not affect the mean flow.

In order to interpret these results, it is desirable to plot the projections, on the (y, z)-plane, of the streamlines for the entire second-order mean motion. These will be obtained by solving the differential equation

$$\frac{dy}{v_0^{(2)}(y, z, t)} = \frac{dz}{w_0^{(2)}(y, z, t)}, \tag{5.33}$$

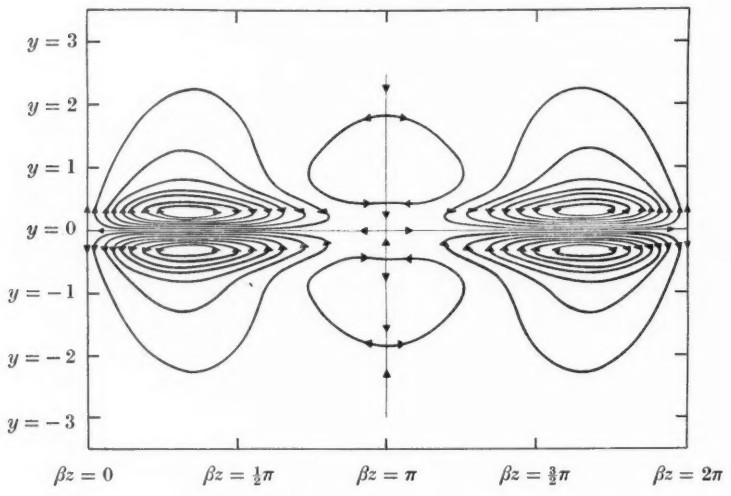

FIGURE 7. Streamline pattern for secondary motion, $\mu/\lambda = 2$.

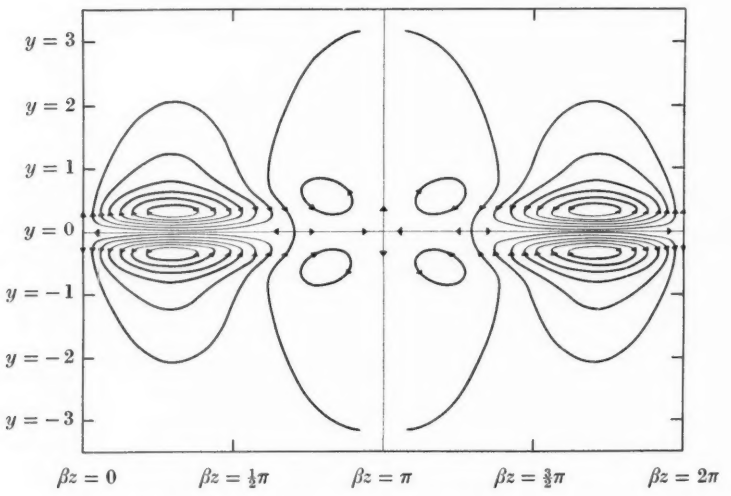

FIGURE 8. Streamline pattern for secondary motion, $\mu/\lambda = 1$.

that is, from

$$\frac{dy}{\lambda^2\hat{v}_a\cos 2\beta z+\lambda\mu\hat{v}_b\cos\beta z}=\frac{dz}{\lambda^2\hat{w}_a\sin 2\beta z+\lambda\mu\hat{w}_b\sin\beta z}, \tag{5.34}$$

and so, on integration, the streamlines are given by

$$\frac{\lambda^2}{2\beta}\hat{v}_a\sin 2\beta z+\frac{\lambda\mu}{\beta}\hat{v}_b\sin\beta z=\text{const.} \tag{5.35}$$

Figures 6, 7, 8, 9, 10 show these streamline patterns for various ratios of μ/λ. These streamlines have been plotted using equal increments of the stream-function

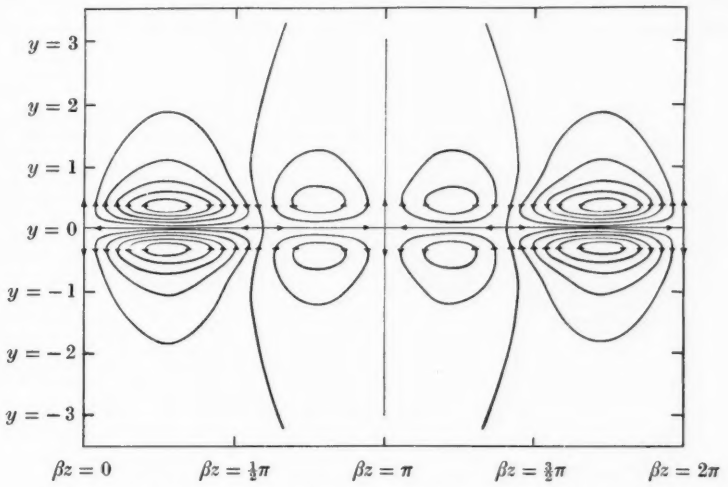

FIGURE 9. Streamline pattern for secondary motion, $\mu/\lambda = \frac{1}{2}$.

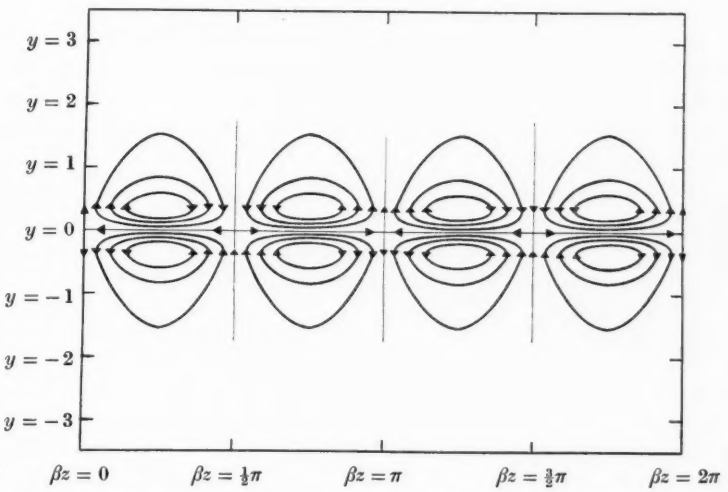

FIGURE 10. Streamline pattern for secondary motion, $\mu/\lambda = 0$.

from $y = 0$, and show clearly the steady longitudinal vortex structure of the secondary flow.

This completes the formal mathematical calculations for the mean flow. It remains to interpret these results and to discuss the physical mechanisms involved. To this purpose it is necessary to make a few simple observations on the primary oscillation.

6. The primary oscillation

It is to be anticipated that the effect of the secondary motion will be diminished or intensified by the downstream periodicity of the primary oscillation. The longitudinal vorticity associated with the three-dimensionality of the oscillation

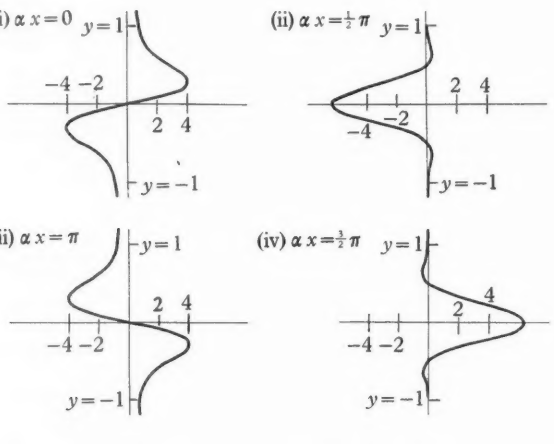

FIGURE 11. Amplitude of $w^{(1)}$ at spanwise position, $\beta z = \frac{1}{2}\pi$.

is of particular interest. Therefore we list the relevant fluctuations. They are, putting $c = 0$,

$$w^{(1)} = 2\lambda\Big[-\frac{\beta^2(\alpha R)^{\frac{1}{3}}}{\alpha} L_r(Y)\cos\alpha x + \frac{1}{\alpha}(\beta^2\operatorname{cosech} y - \operatorname{sech} y\tanh y)\, Y L_i(Y)\sin\alpha x\Big]\cos\beta z + 2\mu[\operatorname{sech} y\tanh y\sin\alpha x], \tag{6.1}$$

$$v^{(1)} = 2\lambda[\operatorname{sech} y\cos\alpha x]\cos\beta z + 2\mu[\operatorname{sech} y\cos\alpha x], \tag{6.2}$$

$$w^{(1)} = 2\lambda[-\beta\operatorname{cosech} y\, Y L_i(Y)\cos\alpha x - \beta(\alpha R)^{\frac{1}{3}} L_r(Y)\sin\alpha x]\sin\beta z, \tag{6.3}$$

$$\xi^{(1)} = 2\lambda\Big[-\beta\operatorname{cosech}^2 y\operatorname{sech} y\, Y^2\frac{dL_i(Y)}{dY}\cos\alpha x - \beta(\alpha R)^{\frac{2}{3}}\frac{dL_r(Y)}{dY}\sin\alpha x\Big]\sin\beta z. \tag{6.4}$$

It is seen, therefore, that $w^{(1)}$ and $\xi^{(1)}$ have spanwise maxima where βz is an odd multiple of $\frac{1}{2}\pi$. The distributions for $w^{(1)}$ and $\xi^{(1)}$, at the position $\beta z = \frac{1}{2}\pi$, are shown

in figures 11 and 12, for different downstream positions. It will be noticed that when $\alpha x = \frac{1}{2}\pi$, the oscillation will lend support to the vortex distribution of the b flow. This corresponds to the convex part of the streamline. When $\alpha x = 3\pi/2$ the vorticity due to the oscillation tends to cancel that of the b flow. We shall return to this point in the next section.

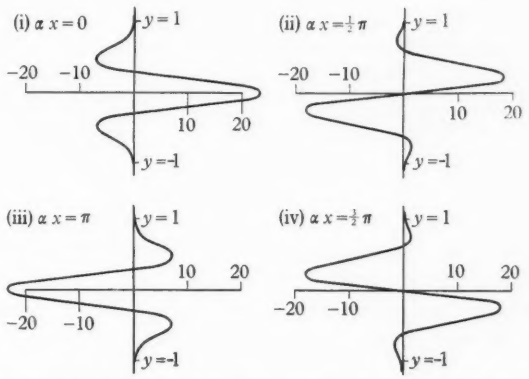

FIGURE 12. Amplitude of $\xi^{(1)}$ at spanwise position, $\beta z = \frac{1}{2}\pi$.

7. Physical interpretation of the results

In previous sections calculations have been made for the second-order velocities induced by oscillations of finite amplitude. It is clear that this mechanism in which the secondary vorticity produces a spanwise redistribution of momentum will apply to non-linear oscillations in any parallel flow, although the phase relationships may differ from case to case. Therefore, in this discussion, we shall restrict ourselves to an interpretation in the case of the profile $u_0(y) = \tanh y$. Also, in this report we shall neglect the effect of the second and higher harmonics.

Initially one must expect that the oscillation will be mainly two-dimensional, that is $\mu/\lambda \gg 1$, and so the steady secondary flow will be essentially the b flow. This b flow induces a steady cellular vortex structure on the motion as indicated in figure 6. Momentum is extracted from the viscous region at spanwise positions $\beta z = 0, \pm 2\pi, \pm 4\pi, \ldots$, where the amplitude of the $w^{(1)}$ oscillation is a maximum, and fed back into this region at intermediate spanwise positions $\beta z = \pm\pi, \pm 3\pi, \ldots$. This large-scale exchange process produces an alternate defect and excess of x-momentum at these points respectively. In turn it is responsible for a spanwise alternate thinning and bulging of the original velocity profile. From figure 5, it is seen that this effect should be most pronounced at the outer edges of the critical layer, the profile gradually becoming more and more warped.

This picture is somewhat modified by the primary oscillation itself. The oscillation is periodic in x and has the same spanwise period as that of the b flow. The vorticity distribution of the oscillation is an even or odd function of y according to whether αx is an even or odd multiple of $\frac{1}{2}\pi$. Clearly from figures 11 and 12 this vortex system will tend to reinforce and cancel that of the secondary b flow once each downstream wavelength. This vortex intensification will take

place when $\alpha x = \frac{1}{2}\pi, \frac{5}{2}\pi, \frac{9}{2}\pi, \ldots$, corresponding to longitudinal vortices having their centres at spanwise positions $\beta z = \frac{1}{2}\pi, \frac{3}{2}\pi, \ldots$. At such points the streamline is convex, the maximum cancellation occurring where the streamline is concave, contrary to the Görtler & Witting model (1957). This does not mean that the Görtler & Witting mechanism is not present, but it does show that there are other effects beyond those indicated by their theory. Existing experimental evidence lends support to the idea of vortex intensification at the convex part of the streamline, as predicted by the present theory.

If the three-dimensionality of the oscillation increases, then the a flow contribution to the secondary motion will become more prominent. The extreme case for an entirely standing wave oscillation is shown in figure 10. This a flow also induces a cellular vortex structure on the motion, the spanwise period being π/β. The vorticity is again an odd function of y. However, this motion is unlikely to be observed without a considerable b flow contribution being superposed.

We now trace growth of the secondary motion as the three-dimensionality of the oscillation becomes stronger. The secondary flow goes through the stages sketched in figures 6 to 10. The original vortices move closer towards the velocity defect regions, and much weaker vortices begin to appear outside the critical layer near the excess positions. The centres of these latter vortices gradually move down closer to the critical layer as the motion becomes more three-dimensional. It is to be recalled that the a flow has a dominant potential component $O\{a^2\lambda^2(\alpha R)^{\frac{1}{3}}\}$. For the stronger vortices the same periodic intensification will be present at the downstream stations $\alpha x = \frac{1}{2}\pi, \frac{5}{2}\pi, \ldots$; but in the case of the weaker newly formed vortices, which may be difficult to observe, the reinforcement will be less marked. However, any such detectable intensification should now take place at $\alpha x = \frac{3}{2}\pi, \frac{7}{2}\pi, \ldots$.

This longitudinal vortex structure and the associated mechanism of momentum transfer produces spanwise alternate excesses and defects in the x-momentum. The directions of the a and b vortices is such as to accentuate the spanwise points of velocity defect, which should therefore be quite sharply defined at $\beta z = 0$, $\pm 2\pi, \pm 4\pi, \ldots$. The c flow adds a two-dimensional defect to the profile at all spanwise positions. Although the thinning of the profile should be quite pronounced, the bulging at the intermediate positions $\beta z = \pm\pi, \pm 3\pi, \ldots$ will be more evenly distributed about these points. In fact, as the wave becomes more warped, these regions of excess may show a small defect region at their centres. These conclusions can readily be seen by referring to the streamline patterns.

8. Concluding remarks

In this paper we have used formal mathematical methods to investigate finite-amplitude oscillations during the breakdown of laminar flow. It is to be emphasized that while we do not discount ordinary two-dimensional distortions, it is felt that in many situations the formation of secondary vortices and the associated crumbling of the profile will be more strongly evident. Certainly this mechanism must be present to some degree during transition. In recent experimental literature there is repeated reference to the formation of this vortex structure.

Clearly the theory presented here could be improved in accuracy by a slightly more sophisticated approach. For instance, no account has been taken of the small differences in the values of α, αc_r, and αc_i for the two- and three-dimensional oscillations. The difference in amplification rates could have been included very easily and is, in any case, compensated for by the disposable ratio μ/λ. The differences in α and αc_r have been neglected on the grounds that their effects over the few wavelengths of practical interest would be small. Indeed, one might anticipate that in the non-linear range a synchronization phenomenon would occur, similar to that encountered in the study of periodic solutions of ordinary differential equations. Another point to be mentioned is that the principal three-dimensional mean flow distortion (the b flow) is linear in the three-dimensional component of the primary oscillation, and so for the purposes of calculation any value of β will yield a typical secondary-flow structure.

Doubtless the most important practical situation is that of boundary-layer transition. Here the Reynolds number depends on the downstream position (as opposed to the case of channel flow), and experimentally the waves develop as a space amplification rather than as a time amplification. Thus a more realistic approach to this problem would be to follow a wave of given frequency (αc real), and to examine its amplification with x (α complex). This would require some modifications of the present theory. In the non-linear problem one would then have a second-order mean flow growing in x rather than in t.

During completion of this work Dr G. B. Schubauer and Mr P. S. Klebanoff, in a private communication, have very kindly forwarded the results of some recent unpublished experimental work on a Blasius profile, performed at the National Bureau of Standards. Despite the vast difference between the case of shear-flow and boundary-layer instability, there is a very distinct agreement with the present theory. A theoretical study of the non-linear effects during boundary-layer instability is planned in the near future. This will enable a detailed comparison of theory and experiment to be made.

The author wishes to express his gratitude to Professor C. C. Lin of the Massachusetts Institute of Technology for his help and encouragement during this investigation. The general results in the first few sections of this paper were obtained jointly with Professor Lin, and have been summarized elsewhere (Benney & Lin 1960). My thanks also to Dr G. B. Schubauer and Mr P. S. Klebanoff of the National Bureau of Standards for several pleasant and informative discussions, and to Dr J. T. Stuart and Mr J. Watson of the National Physical Laboratory for reading the manuscript. This work was supported in part by the Office of Naval Research.

REFERENCES

Benney, D. J. & Lin, C. C. 1960 *Phys. Fluids*, **3**, 656.
Curle, N. 1956 *Aero. Res. Coun.* **18**, 426.
Drazin, P. G. 1958 *J. Fluid Mech.* **4**, 214.
Esch, R. E. 1957 *J. Fluid Mech.* **3**, 289.
Görtler, H. & Witting, H. 1957 *Boundary Layer Research Symposium, Freiburg*, p. 110.
Klebanoff, P. S. & Tidstrom, K. D. 1958 *Nat. Bur. Stand. Rep.* 5741.

LANDAU, L. 1944 *C.R. Acad. Sci., U.R.S.S.*, **44**, 311.
LANGER, R. E. 1949 *Trans. Amer. Math. Soc.* **67**, 461.
LIN, C. C. 1955 *Hydrodynamic Stability.* Cambridge University Press.
LIN, C. C. 1957 *Boundary Layer Research Symposium, Freiburg*, p. **144**.
MEKSYN, D. & STUART, J. T. 1951 *Proc. Roy. Soc.* A, **208**, 517.
SCHUBAUER, G. B. 1957 *Boundary Layer Research Symposium, Freiburg*, p. 85.
SCHUBAUER, G. B. & SKRAMSTEAD, H. K. 1948 *NACA Rep.* 909.
SQUIRE, H. B. 1933 *Proc. Roy. Soc.* A, **142**, 621.
STUART, J. T. 1958 *J. Fluid Mech.* **4**, 1.
STUART, J. T. 1959 *Aero. Res. Coun.* **21**, 188.
THEODORSEN, T. 1952 *Proc. 2nd Midwest Conf. on Fluid Mech., Ohio.*

The theory of the jet-flap for unsteady motion

By D. A. SPENCE*
Graduate School of Aeronautical Engineering, Cornell University

(Received 12 September 1960)

Linearized methods developed in earlier papers (Spence 1956, 1961) are used to discuss the non-stationary flow of a wing with a jet-flap. We consider a thin two-dimensional wing at zero incidence in a steady stream of speed U, with a thin jet emerging parallel to the chord at the trailing edge, and study the motion following an instantaneous deflexion of the jet through an angle τ_0. If the momentum-flux coefficient C_J of the jet is $\ll 4$, the governing equations can be put in a form in which C_J does not appear explicitly, and a similarity solution then gives the shape of the jet at small times t from the start of the motion as a function of $(x-c)\mu^{-\frac{1}{3}}t^{-\frac{2}{3}}$, where $x=c$ is the trailing edge and $\mu=\frac{1}{4}C_J$. The solution is obtained from a certain third-order integro-differential equation, by constructing the Mellin transform of the non-dimensional shape. When t is large the jet near the wing approaches the shape given by the known results for steady flow, but its shape at distances of the order of Ut downstream changes diffusively under the action of the starting vortex. A similarity solution is also found for the flow in this region in terms of $(x-Ut)\mu^{-\frac{1}{3}}t^{-\frac{2}{3}}$, without restriction to small μ. Expressions for the lift coefficient at small and large times are found, and the case of an oscillating deflexion angle is treated by the same methods.

1. Introduction

In a paper published some years ago (Spence 1956; this will be referred to as I) the author used the methods of thin aerofoil theory to discuss the flow past a two-dimensional wing with a jet emerging from the trailing edge at a small angular deflexion τ relative to the chordline, into fluid moving with undisturbed speed U and constant density ρ. This represents the mathematical idealization of a jet blowing over a small flap. Numerical solutions were given in the paper for the lift derivatives with respect to the wing-incidence α and to the jet-deflexion τ as functions of the jet momentum coefficient C_J; more recently (Spence 1961, referred to as II) these have been replaced, using an analytic solution of the singular integro-differential equation for the slope of the jet, by expansions in powers of C_J and $\ln C_J$ valid for $\frac{1}{4}C_J$ ($=\mu$ say) less than 1—which range of momentum coefficients covers most practical applications.

In the present paper attention is turned to the unsteady motion of such a wing, and in particular to that which would follow a time-dependent change in the flap-angle τ. This problem can be formulated in linearized approximation using the model introduced in I, and the analytic methods of II can be used to obtain

* On leave from the Royal Aircraft Establishment, Farnborough, Hants.

closed solutions of the resulting flow problem in a number of limiting cases. We restrict ourselves here to motions in which the wing remains at zero incidence, and τ is a prescribed function of the time t; the same methods could, however, be used to discuss more general types of motion—for instance, flight through a sharp-edged gust, or following a sudden change of incidence. For such motions the theory of aerofoils without jets is well developed, and a synthesis of the results found here with those of the classical unsteady aerofoil theory will be given later by J. C. Erickson.

The problem is formulated in § 2 in terms of a distribution of vorticity representing the wing and jet. In linearized approximation this is located in the plane of the wing, and suitable boundary conditions are applied on the normal component of the velocity induced by it at this plane. In § 2.4 the lift coefficient in unsteady flow is expressed as the time-derivative of a certain integral of the stated vortex distribution, to be evaluated for particular cases in later sections. The derivation depends on the fact that the total vorticity inside a sufficiently large contour enclosing the aerofoil remains zero for all time if it is so initially, positive vorticity on and near the wing being balanced by an equal amount of opposite sign which is swept back at stream speed. This negative distribution is analogous to the starting vortex of classical theory, but differs in that it spreads diffusively over a growing region as a result of changes induced in the curvature of the jet. The constancy of circulation around a large contour cannot be deduced in the usual way from Kelvin's theorem, since in the presence of a jet extending to infinity a large circuit surrounding the wing and moving with the fluid could deform in such a way as not to close across the jet; but nevertheless it follows from the governing equations, as is shown in § 2.3.

Two particular types of time-dependence have been examined in the remainder of the paper: first, that of a sudden change in deflexion, described by

$$\tau(t) = \begin{cases} 0 & (t \leqslant 0), \\ \tau_0 & (t > 0), \end{cases} \tag{1}$$

(a non-zero value for $t \leqslant 0$ would be taken care of by the steady solution of II) and second, steady oscillation with reduced frequency n, i.e.

$$\tau(t) = \tau_0 \exp(inUt/c), \tag{2}$$

where c is the chord length. The second is closely related to the operational solution of the first and is therefore treated rather briefly in § 5. The remarks just made about the constancy of circulation in a large circuit do not of course apply in this case unless the motion is assumed to have been in existence only for a finite time. From the solution of the first case, that for an arbitrary transient $\tau(t)$ can be written down as a convolution integral, so these two are sufficient for a fairly full discussion of the problem. The solution for the sudden-deflexion case is developed in detail in §§ 3 and 4 for small and large times, respectively. For small times, the transformation used in II to introduce the jet-strength parameter $\mu = \frac{1}{4}C_J$ into the co-ordinates in such a way as to magnify the trailing edge region results in a great simplification of the equations, which then possess a similarity solution in terms of $x/t^{\frac{3}{2}}$ when μ is small. With the aid

of a similar transformation of the co-ordinates in the neighbourhood of the point $x = Ut$ it is also possible to discuss the flow at large times, in this case without restriction on the value of μ, and again a 'similarity' solution is found for the downwash distribution over the jet far from the wing.

2. Formulation of the problem

We suppose as before that the jet is a thin two-dimensional curved sheet of high velocity gas in irrotational motion, with time-dependent streamline boundaries as in figure 1, and are again able to write the pressure difference Δp between points immediately above and immediately below the jet, and lying on the same normal to the internal streamlines, as the product of the mean local curvature κ and the jet momentum-flux J.

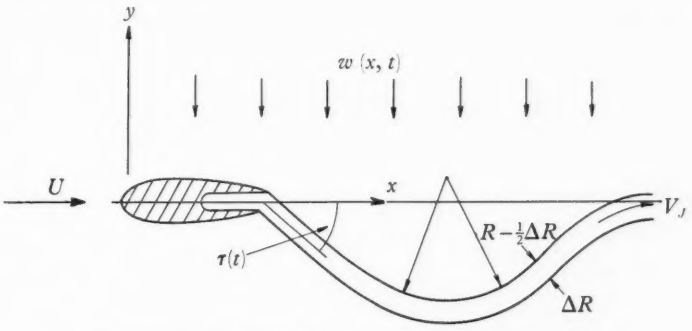

FIGURE 1. Flow in an element of the jet (schematic).

2.1. *Pressure rise across a thin jet*

This property, first pointed out by Erickson (1959), follows from the fact that the normal is an equipotential of the flow within the jet, along which $p+\frac{1}{2}\rho_J V^2$ is therefore constant at any instant, where p, V and ρ_J are the pressure, velocity and density within the jet. Hence to the first order in small quantities

$$\Delta p+\rho_J \overline{V}\Delta V = 0,$$

where Δ represents the difference between the values of a quantity on the upper and lower boundaries, and $\overline{V}$ is the mean value of V across the jet. The condition of irrotationality within the jet may likewise be expressed as

$$(\Delta V/\Delta R)+(\overline{V}/R) = 0,$$

where $R\mp\frac{1}{2}\Delta R$ are the radii of curvature of upper and lower boundaries. Hence, eliminating ΔV,

$$\Delta p = -(\rho_J \overline{V}^2\Delta R)/R = -\kappa J, \tag{3}$$

and in the limit $\Delta R \to 0$, an extension of the argument used in I again shows that J is constant along the jet.

2.2. *Linearized form of equations*

The pressure difference given by (3) may be set equal to that in the outside stream, in which the velocity potential is $\phi(x, y, t)$ say. Again we linearize the

problem by applying the boundary conditions on the line $y = 0$, and using the unsteady form of Bernoulli's equation, are able to write

$$\rho\left(\frac{\partial}{\partial t} + U\frac{\partial}{\partial x}\right)\Delta\phi + \Delta p = 0, \tag{4}$$

where $$\Delta\phi(x,t) = \phi(x,+0,t) - \phi(x,-0,t).$$

Replacing Δp in this equation by (3), and writing the curvature as $-\partial^2 h_0/\partial x^2$, where $h_0(x,t)$ is the displacement of the jet below the real axis, we then have

$$x > c: \quad \left(\frac{\partial}{\partial t} + U\frac{\partial}{\partial x}\right)\Delta\phi = -\tfrac{1}{2}cC_J U^2 \frac{\partial^2 h_0}{\partial x^2}, \tag{5}$$

the momentum-flux coefficient C_J being defined as $J/\frac{1}{2}\rho U^2 c$. If now the wing and jet are represented by a distribution of vorticity on the x-axis, of magnitude $\gamma(x,t) = (\partial/\partial x)\Delta\phi$, then the downward velocity $w(x,t) = -\phi_y(x,0,t)$ at the axis is related to γ as before by

$$w(x,t) = -\frac{1}{2\pi}\int_0^\infty \frac{\gamma(\xi,t)\,d\xi}{\xi - x}, \tag{6}$$

but the condition that the flow should be tangential to the jet becomes

$$x > c: \quad \left(\frac{\partial}{\partial t} + U\frac{\partial}{\partial x}\right) h_0(x,t) = w(x,t), \tag{7}$$

where $x = 0$ and $x = c$ represent the leading and trailing edges of the wing. An equation of the same form as the last must also be satisfied at the wing, $h_0(x,t)$ then being a prescribed function describing the applied motion. But as stated in the introduction, the present paper is restricted to consideration of cases in which the wing is at zero incidence to the stream, and only the jet-deflexion is time-dependent. Accordingly, we set

$$0 < x < c: \quad w(x,t) = 0 \tag{8}$$

on the wing, and specify the initial slope of the jet by means of

$$w(c,t) = U\left(\frac{\partial h_0}{\partial x}\right)_{x=c} = U\tau(t). \tag{9}$$

The first of these boundary conditions can be absorbed into the integral relating downwash to vorticity exactly as in the steady case, II § 2.2 (this form of reference to sections in II will be used throughout), so that (6) is again replaced by

$$x > c: \quad w(x,t) = -\frac{1}{2\pi}\left(\frac{x-c}{x}\right)^{\frac{1}{2}}\int_c^\infty \left(\frac{\xi}{\xi - c}\right)^{\frac{1}{2}} \frac{\gamma(\xi,t)\,d\xi}{\xi - x}, \tag{10}$$

and the problem is now specified on the interval $c < x < \infty$ by the last two equations together with (5) and (7). The latter may be combined, by cross-differentiation to eliminate h and $\Delta\phi$, into a single auxiliary equation between w and γ, namely

$$\left(\frac{\partial}{\partial t} + U\frac{\partial}{\partial x}\right)^2 \gamma(x,t) = -\tfrac{1}{2}cC_J U^2 \left(\frac{\partial}{\partial x}\right)^3 w(x,t), \tag{11}$$

so that (10) and (11) are now the governing equations on $c < x < \infty$, subject to the remaining boundary condition (9). To find the position of the jet, as is done for small times in § 3, it is also necessary to specify its initial position by means of $h(x, 0) = 0$. Information about this is lostin the differentiation leading to (11), so this equation is not used in the short-time discussion; it is, however, the more useful form for treating the motion after times long enough for it to have become independent of the precise starting conditions.

2.3. *Circulation round a contour far from the wing*

In showing that $\Delta\phi(x, t) \to 0$ as $x \to \infty$ for all time, it will be assumed for the present that sufficiently far from the wing the jet returns to its undisturbed position along the axis, so that with increasing x the curvature finally vanishes.

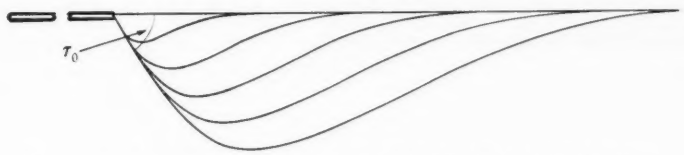

FIGURE 2. Successive jet shapes at small times after initial deflexion (equal intervals of $t^{\frac{3}{2}}$) (schematic).

Intuitively this seems clear, for if the final position were displaced vertically an infinite amount of work would have been done to the fluid in finite time; moreover, the assumption will be confirmed from the solutions for the jet shape to be found in later sections. To prove the result concerning $\Delta\phi$ we may solve equation (4) in terms of Δp in the form

$$\Delta\phi(x,t) = -(1/\rho U)\int_{\max(0,\,x-Ut)}^{x} \Delta p\left(\xi, t+\frac{\xi-x}{U}\right)d\xi + F(x-Ut),$$

where F is arbitrary. Since this solution holds for all positive or negative x and t (although the integrand vanishes when either of its arguments is less than zero) the initial conditions show that $F \equiv 0$. Then if $x - Ut > c$ we can replace Δp in the integrand by the jet curvature, by (3), obtaining

$$\Delta\phi(x,t) = -(J/\rho U)\int_{x-Ut}^{x} \kappa\left(\xi, t+\frac{\xi-x}{U}\right)d\xi.$$

If $$\mathrm{K}(x,t) = \max\left|\kappa\left(\xi, t+\frac{\xi-x}{U}\right)\right| \quad \text{for} \quad x-Ut \leqslant \xi \leqslant x,$$

the absolute value of the integral is $\leqslant (J/\rho U)\,Ut\,\mathrm{K}(x,t)$, and, for a fixed t,

$$\mathrm{K}(x,t) \to 0 \quad \text{as} \quad x \to \infty.$$

Therefore as stated $$\lim_{x\to\infty} \Delta\phi(x,t) = 0,$$

the limit being approached non-uniformly with respect to t—i.e. as indicated in figure 2, the larger the time, the further from the wing must one go before $|\Delta\phi(x,t)|$ becomes less than a chosen small quantity.

The result can be written in a number of equivalent ways. Using (6) and (10),

$$0 = \Delta\phi(\infty,t) = \int_0^\infty \gamma(\xi,t)\,d\xi = \lim_{x\to\infty} 2\pi x w(x,t) = \int_c^\infty \left(\frac{\xi}{\xi-c}\right)^{\frac{1}{2}} \gamma(\xi,t)\,d\xi. \quad (12)$$

It may be noted in passing that the last result in (12) is equivalent to the so-called 'Wagner condition' of classical unsteady aerofoil theory, when with a suddenly applied downwash $U\alpha$ at the wing the integral instead of vanishing would equal $-\pi U\alpha$ for all time. In the absence of a jet γ is a function of $Ut-x$ only, and is readily obtained in terms of Hankel functions on inversion of this integral condition (von Kármán & Sears 1938).

2.4. *Lift coefficient in unsteady flow*

The lift force L on the wing is the sum of the integrated normal presures over the chord and the direct component $J\sin\tau$ of the jet momentum at exit. Writing τ for $\sin\tau$,

$$L = -\int_0^c \Delta p\,dx + J\tau(t) = \rho\frac{\partial}{\partial t}\int_0^c \Delta\phi\,dx + \rho U\Delta\phi(c,t) + J\tau(t), \quad (13)$$

using (4) for the pressure difference at the wing. The last term on the right is ρ times the integral of the right-hand side of (5) from $x=c$ to $x=\infty$, so (13) can be replaced by the single integral

$$C_L = L/\tfrac{1}{2}\rho U^2 c = (2/U^2c)\int_0^\infty dx\left(\frac{\partial}{\partial t} + U\frac{\partial}{\partial x}\right)\Delta\phi \quad (14)$$

for the lift coefficient. In the transient case in which $\Delta\phi(\infty,t)$ is zero, the second term makes no contribution, leaving

$$C_L = (2/U^2c)\frac{\partial}{\partial t}\int_0^\infty \Delta\phi\,dx = -(2/U^2c)\frac{\partial}{\partial t}\int_0^\infty x\gamma(x,t)\,dx \quad (15)$$

on integration by parts. $\int_0^\infty \Delta\phi\,dx$ may be identified as ρ^{-1} times the 'impulse' of the system. Since the integral equation for $\gamma(x,t)$ has been formulated on the interval $c<x<\infty$, it is convenient to eliminate the integration from 0 to c in (15). To do so, use equation (7) of II, to write the vorticity distribution on the wing in terms of that on the jet as

$$0 \leqslant x \leqslant c: \quad \gamma(x,t) = \frac{1}{\pi}\left(\frac{c-x}{x}\right)^{\frac{1}{2}}\int_c^\infty \left(\frac{\xi}{\xi-c}\right)^{\frac{1}{2}}\frac{\gamma(\xi,t)\,d\xi}{\xi-x}. \quad (16)$$

Then
$$-\int_0^c x\gamma(x,t)\,dx = \int_c^\infty \left(\frac{\xi}{\xi-c}\right)^{\frac{1}{2}}\gamma(\xi,t)\left[\frac{1}{\pi}\int_0^c \frac{x^{\frac{1}{2}}(c-x)^{\frac{1}{2}}}{x-\xi}\,dx\right]d\xi$$

and from a well-known result (see, for example, I, equation 66) the integral in square brackets is found to equal $[\xi^{\frac{1}{2}}(\xi-c)^{\frac{1}{2}} - \xi + \tfrac{1}{2}c]$; combining this with $\int_c^\infty \xi\gamma(\xi,t)\,d\xi$ and making use of (12) enables one finally to write the lift coefficient as

$$C_L = -(2/U^2c)\frac{\partial}{\partial t}\int_c^\infty \xi^{\frac{1}{2}}(\xi-c)^{\frac{1}{2}}\gamma(\xi,t)\,d\xi. \quad (17)$$

3. Sudden change in deflexion: small-time solution

In this section a solution valid for small times will be found for the first case mentioned in the introduction, that in which the wing is at zero incidence throughout, and at $t = 0$ the angular deflexion of the jet at the trailing edge changes instantaneously from 0 to τ_0. The motion in the region $x > c$ is then described by the equations of § 2.2, subject to the boundary conditions

$$h_0(c,t) = h_0(x,0) = 0, \quad \left(\frac{\partial h_0}{\partial x}\right)_{x=c} = \tau_0. \tag{18}$$

Physically one might expect the jet to deform somewhat in the manner indicated in figure 2, and a similarity solution showing this behaviour can in fact be found for its shape near the trailing edge. As a preliminary step the governing equations may be simplified, provided the jet-strength parameter $\mu = \frac{1}{4}C_J$ is sufficiently small, less than $\frac{1}{4}$ say—this is not a severe restriction on C_J—by absorbing μ into the co-ordinates near the trailing edge. As in II, write

$$\left.\begin{aligned} h_0(x,t) &= \mu c\tau_0 (x/c)^{-\frac{1}{2}} h(x',t'), \\ \gamma(x,t) &= 2U\tau_0 (x/c)^{-\frac{1}{2}} g(x',t'), \\ \text{where} \qquad x' &= \frac{x-c}{\mu c}, \quad t' = \frac{Ut}{\mu c}, \end{aligned}\right\} \tag{19}$$

and excluding terms of order μ, equations (5), (7) and (10) become

$$\frac{\partial h}{\partial t'} + \frac{\partial h}{\partial x'} = -\frac{1}{\pi}\int_0^\infty \left(\frac{x'}{\xi'}\right)^{\frac{1}{2}} \frac{g(\xi',t')\,d\xi'}{\xi'-x'}, \tag{20}$$

$$\frac{\partial g}{\partial t'} + \frac{\partial g}{\partial x'} = -\frac{\partial^3 h}{\partial x'^3}, \tag{21}$$

with boundary conditions derived from (18)

$$h(x',0) = h(0,t') = 0, \quad h_{x'}(0,t') = 1. \tag{22}$$

If $t' \ll 1$ an approximation to these equations may be made by omitting the derivatives with respect to x' on the left-hand side of (20) and (21), since they are smaller than those with respect to t' except at points so close to the trailing edge that $x'/t' = O(1)$. Cross-differentiation of the approximate equations gives

$$h_{t't'} = \frac{1}{\pi}\int_0^\infty \left(\frac{x'}{\xi'}\right)^{\frac{1}{2}} \frac{h_{\xi'\xi'\xi'}\,d\xi'}{\xi'-x'}. \tag{23}$$

A similarity solution for (23), satisfying the boundary conditions (22), is found by writing

$$h(x',t') = t'^{\frac{3}{2}} f(x'/t'^{\frac{3}{2}}) = t'^{\frac{3}{2}} f(z) \tag{24}$$

say, when the equation becomes

$$f - zf' - 2z^2 f'' = -(9/2\pi)\int_0^\infty \left(\frac{z}{\zeta}\right)^{\frac{1}{2}} \frac{f'''(\zeta)\,d\zeta}{\zeta - z}. \tag{25}$$

The first boundary condition is automatically satisfied and the remaining two become

$$f(0) = 0, \quad f'(0) = 1. \tag{26}$$

The solution for this equation is found in § 3.1. The existence of the solution justifies *a posteriori* the omission of the x'-derivatives from (20) and (21), since

$$(\partial/\partial x')/(\partial/\partial t') \ll O(t'^{\frac{1}{3}}) \ll 1$$

for small t'. The solution is not, however, uniformly valid, but applies only when $x'/t' \ll 1$; when the reverse inequality holds the time derivatives disappear from the equations, leaving the equation for steady motion that was solved in II. The latter therefore correctly describes the singular behaviour of the vortex distribution very close to the trailing edge, with validity in a neighbourhood that grows linearly with time.

Equation (23) can also be derived in another way which displays its region of validity more clearly. If $t = t'$ and $y = x' - t'$, say, are treated as the independent variables, $\partial/\partial t' + \partial/\partial x'$ is replaced by $\partial/\partial t$, and $\partial/\partial x'$ by $\partial/\partial y$, so that (20) and (21) become

$$\frac{\partial h}{\partial t} = -\frac{1}{\pi}\int_{-t}^{\infty}\left(\frac{y+t}{\eta+t}\right)^{\frac{1}{3}}\frac{g(\eta,t)\,d\eta}{\eta-y}, \quad \frac{\partial g}{\partial t} = -\frac{\partial^3 h}{\partial y^3}.$$

For small t the first of these can be approximated provided $y/t \gg 1$ by setting $t = 0$ in the kernel and at the lower limit, after which (23) is recovered on cross-differentiation.

3.1. *Similarity solution for the jet-shape*

Equation (25) may be solved by the method used by Lighthill (1959)—see also II § 3.2—for the basic equation of steady motion. Write

$$f(z) = \frac{1}{2\pi i}\int_{c-i\infty}^{c+i\infty} z^{-s}F(s)\,ds \tag{27}$$

for some real c, where $F(s)$ is the Mellin transform $\int_0^\infty z^{s-1}f(z)\,dz$. Differentiation gives

$$-\tfrac{2}{9}(f - zf' - 2z^2 f'') = \frac{1}{2\pi i}\int_{c-i\infty}^{c+i\infty}\left(\frac{2s+2}{3}\right)\left(\frac{2s-1}{3}\right)z^{-s}F(s)\,ds,$$

$$f''' = -\frac{1}{2\pi i}\int_{c-i\infty}^{c+i\infty} z^{-s-3}s(s+1)(s+2)F(s)\,ds.$$

If $s(s+1)(s+2)F(s)$ is regular in the strip $c-3 < \mathscr{R}s < c$, the contour in the last integral can be changed to $\mathscr{R}s = c-3$, whence on writing $s-3$ for s the integral becomes

$$f''' = -\frac{1}{2\pi i}\int_{c-i\infty}^{c+i\infty} z^{-s}(s-3)(s-2)(s-1)F(s-3)\,ds. \tag{28}$$

Then, using the result $\quad \dfrac{1}{\pi}\displaystyle\int_0^\infty\left(\frac{z}{\zeta}\right)^{\frac{1}{3}}\frac{\zeta^{-s}}{\zeta - z}\,d\zeta = -\tan\pi s$

which holds for $|\mathscr{R}s| < \frac{1}{2}$ to evaluate the Cauchy integral in (25), we obtain the functional equation

$$\left(\frac{2s+2}{3}\right)\left(\frac{2s-1}{3}\right)F(s) = (s-3)(s-2)(s-1)(\tan\pi s)F(s-3), \tag{29}$$

provided $|c| < \frac{1}{2}$. To simplify the equation write $F(s) = P(s)\,Q(s)$ where

$$P(s) = \frac{(s-1)!}{\frac{1}{3}(2s+2)!} \frac{\left(\sin\frac{\pi s}{3}\right)\left(\sin\pi\frac{s-1}{3}\right)}{\left(\sin\pi\frac{s-\frac{1}{2}}{3}\right)}, \tag{30}$$

when it becomes

$$Q(s) = -(\tan\pi s)\,Q(s-3) = \left(\tan\pi\frac{s-1}{3}\right)\left(\tan\pi\frac{s}{3}\right)\left(\tan\pi\frac{s+1}{3}\right)Q(s-3). \tag{31}$$

Clearly one solution of (31) is

$$G_0\left(\frac{s-1}{3}\right)G_0\left(\frac{s}{3}\right)G_0\left(\frac{s+1}{3}\right) = \Psi(s), \quad \text{say}, \tag{32}$$

where $G_0(s)$ is the Lighthill function defined in II (equation 38), which satisfies

$$G_0(s) = (\tan\pi s)\,G_0(s-1), \quad G_0(0) = G_0(-\tfrac{1}{2}) = 1, \tag{33}$$

and has poles of order n at $s = -n$ and at $s = n - \frac{1}{2}$, where n is a positive integer.

The general solution must be $\Psi(s)$ multiplied by a function of period 3, and to decide whether any such further factor is necessary we must see whether the conditions imposed on $F(s)$ in deriving the functional equation (29) are satisfied. The function $P(s)$ has a simple pole at $s = -1$ with residue $\frac{3}{4}$ and is otherwise regular in $\mathscr{R}s < \frac{1}{2}$, the remaining poles being those of $\operatorname{cosec}\frac{1}{3}\pi(s-\frac{1}{2})$ at $s = 3n+\frac{1}{2}$ ($n = 0, 1, 2, \ldots$). The three factors of $\Psi(s)$ have simple poles at $s = -2, -3, -4$ and at $\frac{5}{2}, \frac{3}{2}, \frac{1}{2}$, respectively. Therefore if we choose $0 < c < \frac{1}{2}$,

$$s(s+1)\,(s+2)\,P(s)\,\Psi(s)$$

is regular as required in the strip $c-3 < \mathscr{R}s < c$.

Finally, $F(s)$ must be integrable as $|\mathscr{I}s| \to \infty$ on $\mathscr{R}s = c$ in order for the integral (27) to exist. It was shown in II § 3.3 that $G_0(s) \sim \exp(-\frac{1}{2}\pi\,|\mathscr{I}s|)$, so by (31)

$$\Psi(s) \sim \exp(-\tfrac{1}{2}\pi\,|\mathscr{I}s|).$$

Also

$$P(s) \sim \exp(\tfrac{1}{6}\pi\,|\mathscr{I}s|).$$

The product of these factors $\sim \exp(-\frac{1}{3}\pi\,|\mathscr{I}s|)$, and the inclusion of a further periodic factor would either introduce poles into the strip $c-3 < \mathscr{R}s < c$ or prevent the convergence of $F(s)$ as $|\mathscr{I}s| \to \infty$. Therefore the solution is completed by writing

$$Q(s) = A\Psi(s), \tag{34}$$

where A is a constant to be determined from the second boundary condition (26). (The first has been satisfied by choosing $P(s)$ regular at $s = 0$.) Since

$$f'(z) = -\frac{1}{2\pi i}\int_{c-i\infty}^{c+i\infty} sF(s)\,z^{-s-1}\,ds,$$

the first term in the expansion of $f'(z)$ for small z is the residue of $-sF(s)$ at its pole at $s = -1$. The boundary condition is therefore satisfied if $F(s)$ has residue 1 at this point, where $P(s)$ has a simple pole with residue $\frac{3}{4}$ and $\Psi(s)$ is regular. Therefore

$$A = \frac{4}{3\Psi(-1)} = \tfrac{4}{3}[G_0(-\tfrac{2}{3})\,G_0(-\tfrac{1}{3})]^{-1}. \tag{35}$$

3.2. *Lift coefficient*

Inserting the co-ordinate transformation (19) into the expression (17) for the lift coefficient, we obtain

$$C_L = -4\tau_0\mu^{\frac{1}{2}}\frac{\partial}{\partial t'}\int_0^\infty \xi^{\frac{1}{2}}g(\xi,t')\,d\xi.$$

This may be evaluated from the solution of the last section, since $\partial g/\partial t' = -\partial^3 h/\partial x'^3$ in the small-time approximation; thus in terms of the similarity variable defined by (24)

$$C_L = 4\tau_0\mu^{\frac{1}{2}}t'^{-\frac{1}{3}}\int_0^\infty z^{\frac{1}{2}}f'''(z)\,dz. \tag{36}$$

To evaluate this expression invert (28), obtaining

$$\int_0^\infty z^{s-1}f'''(z)\,dz = -(s-3)(s-2)(s-1)F(s-3).$$

The required integral is the value of the right-hand side when $s = 3$, namely

$$-\frac{(\frac{1}{2})!\,(-\sin\frac{1}{2}\pi)\,(-\sin\frac{5}{6}\pi)}{(-\frac{1}{3})!\,(-\sin\frac{2}{3}\pi)}\begin{vmatrix} G_0(-\frac{5}{6})\,G_0(-\frac{1}{6}) \\ (\frac{3}{4})\,G_0(-\frac{2}{3})\,G_0(-\frac{1}{3}) \end{vmatrix}.$$

Since $G_0(s) = G_0(-\frac{1}{2}-s)$, (by II, equation 35), $G_0(-\frac{1}{6}) = G_0(-\frac{1}{3})$ and

$$G_0(-\tfrac{5}{6}) = (\cot\tfrac{1}{6}\pi)\,G_0(\tfrac{1}{6}) = \sqrt{3}\,G_0(-\tfrac{2}{3}),$$

so that finally

$$C_L = \frac{8\tau_0(\pi\mu)^{\frac{1}{2}}}{3(-\frac{1}{3})!}t'^{-\frac{1}{3}} = 3{\cdot}4905\tau_0\mu^{\frac{1}{6}}\left(\frac{Ut}{c}\right)^{-\frac{1}{3}}. \tag{37}$$

Thus in a sudden deflexion the lift force is infinite initially. Physically this implies that an infinite rate of working is required to start the motion impulsively. If the deflexion were described more generally by some function $\tau(t)$ the lift coefficient for small times could be written as a Stieltjes integral

$$C_L = 3{\cdot}4905\mu^{\frac{1}{6}}\left(\frac{U}{c}\right)^{-\frac{1}{3}}\int_0^{\tau(t)}(t-u)^{-\frac{1}{3}}\,d\tau(u),$$

showing that infinite values of C_L occur only if $d\tau/dt$ is singular at $t = 0$, as is the case with the delta-function representation of equation (1).

3.3. *Jet shape*

The shape of the jet for small and large values of z is found by moving the contour $\mathscr{R}s = c$ in (27) over successive poles of the integrand. The residues are evaluated in the same way as in II § 3.4 using the properties of the G_0 function listed there. Those at the poles $s = -n$, where n is a positive integer, give the expansion for $z < 1$, and those at $s = n - \frac{1}{2}$ that for $z > 1$. The double pole at $s = \frac{1}{2}$ produces a logarithmic leading term in the asymptotic expansions

$$f(z) \sim \left\{\begin{array}{l} z - \dfrac{2z^2}{3^{\frac{2}{3}}(\frac{1}{3})!} - \dfrac{2z^3}{27(-\frac{1}{3})!} + O(z^4\ln z) \quad \text{for} \quad z < 1, \\ \dfrac{1}{(\pi z)^{\frac{1}{2}}}\left[\dfrac{3}{\pi}\ln(4z) + C - \dfrac{3}{5(-\frac{1}{3})!}\dfrac{1}{z} - \dfrac{3}{28(\frac{1}{3})!}\dfrac{1}{z^2}\right] + O\left(\dfrac{\ln z}{z^3}\right) \quad \text{for} \quad z > 1. \end{array}\right\} \tag{38}$$

where
$$C = \frac{\gamma+3}{\pi} - \frac{4}{3^{\frac{3}{2}}} = 0{\cdot}3689,$$

γ being Euler's constant. The function $f(z)$ is plotted in figure 3, the neighbourhood of $z = 1$ having been supplied by eye, and plots of

$$h(x', t') = t'^{\frac{2}{3}} f(x'/t'^{\frac{2}{3}})$$

confirm that the shape of the jet for small times is as indicated in figure 2. In physical co-ordinates the leading terms are

$$h(x,t) = \begin{cases} x' + O(x'^2/t'^{\frac{2}{3}}) & \text{for} \quad x < t^{\frac{2}{3}}, \\ \dfrac{t'}{(\pi x')^{\frac{1}{2}}} \left(\dfrac{3}{\pi} \ln x'\right) & \text{for} \quad x > t^{\frac{2}{3}}, \end{cases} \tag{39}$$

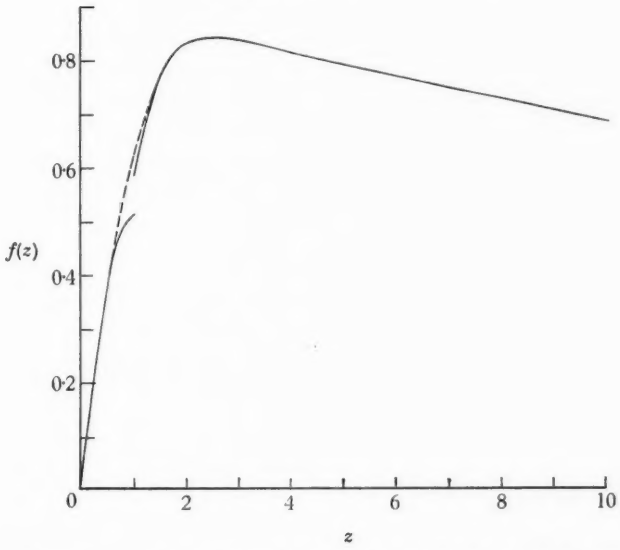

FIGURE 3. Non-dimensional shape-function $f(z)$ for small times.

according to (38), but in fact, for $x' \ll t'$, the steady solution of II in which $h(x) = x + O(x^2 \ln x)$ should apply; the term of order $x'^2/t'^{\frac{2}{3}}$ in (39) is valid only when $t' \ll x' \ll t'^{\frac{2}{3}}$.

4. Sudden change in deflexion: large-time solution

When the time from the instant of jet deflexion is long, the flow in the neighbourhood of the wing approaches that described by the steady solution of II. The integral of the vorticity on the wing and in its neighbourhood therefore approaches the value $\Gamma_\infty = \frac{1}{2}UcC_L^{(\infty)}$ say, where $C_L^{(\infty)}$ is the lift coefficient in steady flow with the final deflexion. But since the total circulation about the system, $\Delta\phi(\infty, t)$, is zero initially, it remains so for all time, a balance being brought about by negative vorticity which is swept downstream and causes the jet far from the

wing to deform as indicated in figure 4. After a sufficiently long time, this negative vorticity acts on the wing as would a line vortex of magnitude $-\Gamma_\infty$ at a distance Ut downstream, producing a downwash $\Gamma_\infty/(2\pi Ut)$ at the wing. This is equivalent to a reduction in incidence of amount $(c/4\pi Ut)\,C_L^{(\infty)}$. In the opposite direction, at distances large compared with Ut, the combined distribution is seen as a doublet of strength $-\Gamma_\infty Ut$ at the origin.

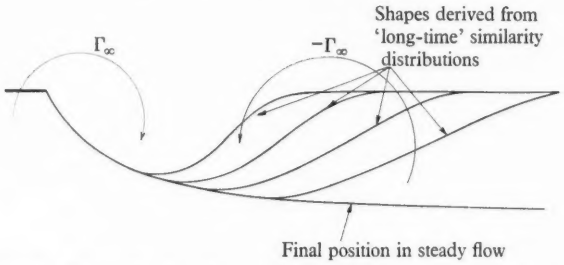

FIGURE 4. Successive jet-shapes at long times from start (schematic).

4.1. *Final form of the jet far from the wing*

To discuss the flow mathematically, we may write the distributions of vorticity and downwash as

$$\left.\begin{aligned}\gamma(x,t) &= \gamma_\infty(x)+\gamma_1(y,t),\\ w(x,t) &= w_\infty(x)+w_1(y,t),\end{aligned}\right\} \tag{40}$$

where $$y = x - Ut,$$

$\gamma_\infty(x)$ and $w_\infty(x)$ being the distributions in steady flow with deflexion τ_0. The Wagner condition $\Delta\phi(\infty,t)=0$ is

$$0 = \int_c^\infty \left(\frac{\xi}{\xi-c}\right)^{\frac{1}{2}} \gamma(\xi,t)\,d\xi = \Gamma_\infty + \int_{c-Ut}^\infty \left(\frac{\eta+Ut}{\eta+Ut-c}\right)^{\frac{1}{2}} \gamma_1(\eta,t)\,d\eta$$

by (12), and subtracting the corresponding steady equations (II, equations 8 and 5) from (10) and (11), the equations connecting w_1 and γ_1 are obtained as

$$w_1(y,t) = -\frac{1}{2\pi}\left(\frac{y+Ut-c}{y+Ut}\right)^{\frac{1}{2}} \int_{c-Ut}^\infty \left(\frac{\eta+Ut}{\eta+Ut-c}\right)^{\frac{1}{2}} \frac{\gamma_1(\eta,t)\,d\eta}{\eta-y}$$

and

$$\frac{\partial^2\gamma_1}{\partial t^2} = -\tfrac{1}{2}cC_J U^2 \frac{\partial^3 w_1}{\partial y^3}. \tag{41}$$

From these it appears that for large t, γ_1 and w_1 approach the functions $\gamma_0(y,t)$ and $w_0(y,t)$ say, which satisfy the equations obtained by allowing t to tend to infinity wherever it occurs explicitly in the last three equations, namely

$$\int_{-\infty}^\infty \gamma_0(\eta,t)\,d\eta = -\Gamma_\infty \tag{42}$$

and

$$w_0(y,t) = -\frac{1}{2\pi}\int_{-\infty}^\infty \frac{\gamma_0(\eta,t)\,d\eta}{\eta-y}, \tag{43}$$

respectively, together with (41) which is unaffected. Note that two separate steps have been made in deriving (43): first, the kernel

$$\left(\frac{y+Ut-c}{y+Ut}\,\frac{\eta+Ut}{\eta+Ut-c}\right)^{\frac{1}{2}}$$

has been set equal to unity, which is equivalent to disregarding the boundary condition $w_1(y,t)=0$, $-Ut<y<-Ut+c$, obtained from (8), and is justifiable provided $w_0(y,t)$ is small enough on this interval for large t; secondly, the lower limit of integration has been changed from the trailing edge $y=-Ut+c$ to $y=-\infty$, which is justifiable provided $\gamma_0(\eta,t)$ dies out sufficiently rapidly for large negative η. The solution found below is shown in § 4.3 to meet both these requirements.

4.2. *Similarity solutions for the downwash distribution*

The last three equations can be solved for γ_0 and w_0 in terms of a similarity parameter proportional to $y/t^{\frac{2}{3}}$. As in the small time solution the jet strength parameter $\mu=\frac{1}{4}C_J$ can be adsorbed into the co-ordinate system, but by contrast with that case there is no need here to restrict μ to small values, since the transformed equations are exactly independent of μ.

Write

$$y=\mu c y', \quad t=\frac{\mu c t'}{U}$$

and set

$$\gamma_0(y,t)=\frac{\Gamma_\infty}{\mu c}t'^{-\frac{2}{3}}g(z), \qquad (44)$$

$$w_0(y,t)=\frac{\Gamma_\infty}{2\mu c}t'^{-\frac{4}{3}}f(z),$$

where

$$z=y'/t'^{\frac{2}{3}}.$$

Then equations (41) to (43) become

$$\tfrac{10}{9}g+2zg'+\tfrac{4}{9}z^2g''=-f''', \qquad (45)$$

$$\int_{-\infty}^{\infty}g(\zeta)\,d\zeta=-1, \qquad (46)$$

and

$$f(z)=-\frac{1}{\pi}\int_{-\infty}^{\infty}\frac{g(\zeta)\,d\zeta}{\zeta-z}. \qquad (47)$$

To solve these equations by the Mellin transform technique used earlier, we first change to the semi-infinite interval $0<z<\infty$ by defining for $z>0$

$$\left.\begin{aligned} f_1(z)&=\tfrac{1}{2}f(z)-\tfrac{1}{2}f(-z),\\ f_2(z)&=\tfrac{1}{2}f(z)+\tfrac{1}{2}f(-z),\\ g_1(z)&=\tfrac{1}{2}g(z)+\tfrac{1}{2}g(-z),\\ g_2(z)&=\tfrac{1}{2}g(z)-\tfrac{1}{2}g(-z). \end{aligned}\right\} \qquad (48)$$

Then, for $z > 0$, f_1 is related to g_1, and f_2 to g_2 by (45), and the two remaining equations become

$$\int_0^\infty g_1(\zeta)\,d\zeta = -\tfrac{1}{2}, \quad \int_0^\infty g_2(\zeta)\,d\zeta \quad \text{exists}, \tag{49}$$

and

$$f_1(z) = -\frac{2z}{\pi}\int_0^\infty \frac{g_1(\zeta)\,d\zeta}{\zeta^2 - z^2}, \tag{50}$$

$$f_2(z) = -\frac{2}{\pi}\int_0^\infty \frac{\zeta g_2(\zeta)\,d\zeta}{\zeta^2 - z^2}. \tag{51}$$

The solution of (50) is carried out in the Appendix, and it is also shown that the only solution of (51) such that $\int_0^\infty g_2(\zeta)\,d\zeta$ exists as required by (49) is the trivial solution

$$f_2(z) \equiv g_2(z) \equiv 0. \tag{52}$$

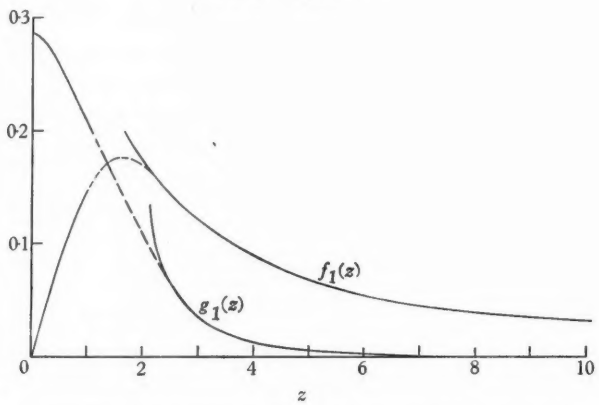

FIGURE 5. Distributions of downwash (f_1) and vorticity (g_1) from long-time solution.

Therefore, for $z > 0$,

$$\left.\begin{aligned} f(z) &= -f(-z) = f_1(z), \\ g(z) &= g(-z) = g_1(z), \end{aligned}\right\} \tag{53}$$

and the solutions for $f_1(z)$, $g_1(z)$ found in the Appendix are

$$\left.\begin{aligned} z < 1: \quad f_1(z) &= -\frac{2}{3\pi}\sum_{n=0}^{\infty}(-1)^n\left(\frac{4n+1}{3}\right)!\,\frac{z^{2n+1}}{(2n+1)!}, \\ g_1(z) &= -\frac{2}{3\pi}\sum_{n=0}^{\infty}(-1)^n\left(\frac{4n-1}{3}\right)!\,\frac{z^{2n}}{(2n)!}, \end{aligned}\right\} \tag{54}$$

$$\left.\begin{aligned} z > 1: \quad f_1(z) &\sim -\frac{1}{\pi z}\left\{1 + \frac{3}{4z}\sqrt{\frac{\pi}{2z}} + \frac{315}{64z^3}\sqrt{\frac{\pi}{2z}} + \ldots\right\}, \\ g_1(z) &\sim -\frac{3}{4z^2\sqrt{2\pi z}}\left\{1 + \frac{4}{z\sqrt{2\pi z}} - \frac{315}{48z^3} + \ldots\right\}. \end{aligned}\right\} \tag{55}$$

The two latter are the leading terms of asymptotic expansions in which the full series are divergent for all $z \geqslant 1$. These functions are plotted in figure 5.

4.3. *Limiting forms of the downwash distribution*

It is easy to confirm from (55) that the downwash at distances $x \gg Ut$ from the wing has, as expected, the distribution produced by a doublet $-\Gamma_\infty Ut$ at the origin, since for large positive values of $y = x - Ut$, from (44) and (55)

$$w_0 = \frac{\Gamma_\infty}{2\mu c} t'^{-\frac{3}{2}} f\left(\frac{y'}{t'^2}\right) \sim -\frac{\Gamma_\infty}{2\pi\mu c y'} = -\frac{\Gamma_\infty}{2\pi(x-Ut)},$$

whereas $w_\infty \sim \Gamma_\infty/2\pi x$, so that altogether

$$x \gg Ut: \quad w(x,t) \sim \frac{\Gamma_\infty}{2\pi}\left(\frac{1}{x} - \frac{1}{x-Ut}\right) = -\frac{\Gamma_\infty Ut}{2\pi x^2} + O\left(\frac{t^2}{x^3}\right). \tag{56}$$

The leading term is that produced by the stated doublet. The equation also shows that the jet shape sufficiently far from the wing will be undisturbed at any given time, thereby justifying the argument used in § 2.3 to show that

$$\lim_{x\to\infty} \Delta\phi(x,t) = 0.$$

Close to the wing, on the other hand, $y = x - Ut \sim -Ut$, in which case we find in the same way

$$x \ll Ut: \quad w_0 \sim \frac{\Gamma_\infty}{2\pi Ut}. \tag{57}$$

The last two results could of course have been written down at once on the physical grounds mentioned at the beginning of § 4, but the mathematical discussion is unavoidable if one is to seek higher approximations in $1/t$ to the flow near the wing. The fact that the downwash due to γ_0 dies out at the wing like $1/t$ justifies the first step in forming equation (43), and the justification for the second step follows from the fact that the contribution from the tail of the γ_0 distribution, namely

$$\int_{-\infty}^{-Ut} \frac{\gamma_0(\eta,t)\,d\eta}{\eta - y},$$

behaves like

$$-\frac{3\Gamma_\infty(\mu c)^{\frac{1}{2}}\sqrt{Ut}}{4(2\pi)^{\frac{1}{2}}} \int_{-\infty}^{-Ut} \frac{d\eta}{(-\eta)^{\frac{5}{2}}(\eta - Ut + x)} = O\left[\left(\frac{Ut}{c}\right)^{-\frac{3}{2}} \ln\frac{Ut}{x}\right] \tag{58}$$

for large t (using the asymptotic expansion for $g(z)$), and consequently is an order of magnitude smaller than the leading term.

4.4. *Lift coefficient at large times*

To discuss the flow near the wing at times $t \gg c/U$ say, we may expand the time-dependent part $\gamma_1(y,t)$ of the full vorticity distribution, equation (40), in the form

$$\gamma_1(x-Ut,t) = \gamma(x,t) - \gamma_\infty(x) = \gamma_0(y,t) - \frac{c}{Ut}\gamma_2(x) + o\left(\frac{c}{Ut}\right) \tag{59}$$

say, for $x \ll Ut$. The corresponding downwash is

$$w_1 = w(x,t) - w_\infty(x) = w_0(y,t) + \frac{c}{Ut} w_2(x) + o\left(\frac{c}{Ut}\right)$$

say, where
$$w_2(x) = -\frac{1}{2\pi}\int_0^\infty \frac{\gamma_2(\xi)\,d\xi}{\xi - x}. \tag{60}$$

Then since both w_0, γ_0 and w_∞, γ_∞ satisfy (11) separately, on equating terms of order $1/t$ in that equation we find

$$\gamma_2(x) = -\tfrac{1}{2}cC_J w_2'(x). \tag{61}$$

The condition that the downwash w_1 vanishes over the wing (where $w_\infty(x)$ is also zero) is, to order $1/t$,

$$0 \leqslant x \leqslant c: \quad w_0 + \frac{c}{Ut} w_2 = \frac{c}{Ut}\left(\frac{\Gamma_\infty}{2\pi c} + w_2\right) = 0. \tag{62}$$

The last three equations show that $w_2(x)$ is precisely the distribution of downwash in steady flow past a wing at incidence $\alpha = -\Gamma_\infty/2\pi cU$ with a tangential (i.e. undeflected) jet at the trailing edge, and from the results for that problem (see I or II, or Thwaites 1960, pp. 500 *et seq.*) we can deduce in particular that

$$\int_0^c \gamma_2(\xi)\,d\xi = -\tfrac{1}{2}Uc\alpha\left(\frac{\partial C_L^{(\infty)}}{\partial \alpha} - C_J\right), \tag{63}$$

$\partial C_L^{(\infty)}/\partial\alpha$ being the lift derivative with respect to incidence for the value of C_J in question. From equation (13) it is seen that to order $1/t$ the lift coefficient differs from $C_L^{(\infty)}$ only by reason of the contribution of $\gamma_2(x)$ to $(\Delta\phi)_{x=c}$, which is c/Ut times (63); thus since

$$\alpha = -\Gamma_\infty/2\pi cU = -C_L^{(\infty)}/4\pi,$$

$$\frac{C_L}{C_L^{(\infty)}} = 1 - \frac{1}{4\pi}\left(\frac{\partial C_L^{(\infty)}}{\partial \alpha} - C_J\right)\left(\frac{c}{Ut}\right) + o\left(\frac{c}{Ut}\right). \tag{64}$$

For small values of C_J, $\partial C_L^{(\infty)}/\partial\alpha \to 2\pi$, so in the limit we recover the result

$$C_L/C_L^{(\infty)} = 1 - c/(2Ut) + \ldots$$

of the classical unsteady aerofoil theory for a sudden change of incidence.

From (58) it appears that the next term in the expansion will be of order $t^{-\frac{3}{2}}\ln t$; to calculate this however it would be necessary to derive an expression for $\gamma_0 - \gamma_1$ far from the wing and this has not been attempted. It is possible to show that $C_L/C_L^{(\infty)} = 1 + O(c/Ut)$ simply by inserting the limiting distribution $\gamma_0(y,t)$ in the integral (17), since the contribution from $\gamma_\infty(x)$ disappears on differentiation with respect to t, but the precise coefficient of $1/t$ cannot be found by this means.

5. Oscillating flap-angle

In this section the solution of the problem presented by a steady harmonic variation of the initial angle τ will be outlined. For simplicity it will be assumed that $\mu = \frac{1}{4}C_J$ is small enough to permit the co-ordinate-stretching transformation which renders the equations independent of μ to first order. We set

$$\tau(t) = \tau_0 e^{inUt/c} \tag{2}$$

and seek a solution
$$\left.\begin{aligned} h_0(x,t) &= \mu c\tau_0 e^{inUt/c}(x/c)^{-\frac{1}{2}}h(x'),\\ \gamma(x,t) &= 2U\tau_0 e^{inUt/c}(x/c)^{-\frac{1}{2}}g(x'),\end{aligned}\right\} \tag{65}$$
where as before
$$x' = \frac{x-c}{\mu c}.$$

Then excluding terms of order μ and omitting the primes, (5), (7) and (10) become
$$i\nu h + h' = -\frac{1}{\pi}\int_0^\infty \left(\frac{x}{\xi}\right)^{\frac{1}{2}} \frac{g(\xi)\,d\xi}{\xi - x} \tag{66}$$
and
$$i\nu g + g' = -h'', \tag{67}$$
where $\nu = \mu n$, and the boundary conditions are
$$h(0) = 0, \quad h'(0) = 1. \tag{68}$$

Iterative solutions to these equations can be found in the cases $\nu \ll 1$, $\nu \gg 1$, which we now treat in turn.

5.1. *Low-frequency oscillation*

If $\nu < 1$, which is the case for small μ if the physical reduced frequency n is of order 1, the first approximation is found by setting $\nu = 0$, when the basic steady equation
$$Lh'(x) \equiv h'(x) - \frac{1}{\pi}\int_0^\infty \left(\frac{x}{\xi}\right)^{\frac{1}{2}} \frac{h''(\xi)\,d\xi}{\xi - x} = 0, \quad h'(0) = 1 \tag{69}$$
studied in II is obtained. The solution will be denoted here by $h_\infty(x)$ so that in the notation of II
$$h'_\infty(x) = f_0(x) = \frac{1}{2\pi i}\int_{c-i\infty}^{c+i\infty} x^{-s}(s-1)!\,G_0(s)\,ds,$$
$G_0(s)$ being the Lighthill function defined by equation (33) of the present paper. Since $h_\infty(0) = 0$,
$$h_\infty(x) = \int_0^x f_0(\xi)\,d\xi. \tag{70}$$

Putting this back in (66) and (67), we can write
$$h(x) = h_\infty(x) + i\nu h_1(x) + \ldots, \tag{71}$$
where $h_1(x)$ satisfies $h_1(0) = h'_1(0) = 0$, and
$$Lh'_1(x) = -h_\infty(x) - \frac{1}{\pi}\int_0^\infty \left(\frac{x}{\xi}\right)^{\frac{1}{2}} \frac{h'_\infty(\xi)\,d\xi}{\xi - x}. \tag{72}$$

By the methods of II § 3.5 the solution is found to be
$$h'_1(x) = -2\int_0^x \xi h''_\infty(\xi)\,d\xi = -2\int_0^x \xi f'_0(\xi)\,d\xi. \tag{73}$$

The first term in (71) represents a slow oscillation of the basic steady solution, and the second a small correction 90° out of phase; this will be modified in turn by higher terms. The solution is not valid for large x, since $h_\infty(x) \sim 2(x/\pi)^{\frac{1}{2}}$ and the term νh which is excluded in forming the first approximation dominates

over that retained if we go far enough from the wing. Moreover it is physically unrealistic to imagine the jet oscillating with an amplitude that tends to infinity far downstream. In fact since the motion must have started at some large negative time $-T$, at distances of the order of UT from the wing the jet will be described by the long-time transient solution of § 4.

5.2. *High-frequency oscillation*

In the other extreme case, $\nu \gg 1$, a first approximation $h_0(x)$ say is obtained by omitting $h'(x)$ and $g'(x)$ from (66) and (67), respectively, leaving the equation

$$-\nu^2 h_0(x) = \frac{1}{\pi}\int_0^\infty \left(\frac{x}{\xi}\right)^{\frac{1}{2}} \frac{h_0'''(\xi)\,d\xi}{\xi - x}, \tag{74}$$

with boundary conditions given by (68). In the same way as the low-frequency oscillation is closely related to the long-time solution, this case is related to the small-time solution: in fact (74) differs from the equation satisfied by the Fourier transform of the jet-shape for small times only in the absence of a term $g_\xi(\xi, 0)$ from the numerator in the integrand, arising from the initial value of the vorticity distribution. The solution of (74) can be carried out by the method used in § 3, and we find

$$H_0(s) = \int_0^\infty x^{s-1} h_0(x)\,dx = -A\nu^{-\frac{2}{3}(s+1)}(s-1)!\left(\sin\frac{\pi s}{3}\right)\left(\sin\pi\frac{s-1}{3}\right)\Psi(s), \tag{75}$$

where $\Psi(s)$ is the product defined by (32) and A the constant $4/3\Gamma(-1)$ given by (35). $h_0(x)$ is therefore $\nu^{-\frac{2}{3}}$ times a function of $\nu^{\frac{2}{3}}x$.

In this case the expansion can be continued by writing

$$\left.\begin{aligned} h(x) &= h_0(x) + i\nu^{-\frac{1}{3}} h_1(x) + \ldots, \\ g(x) &= g_0(x) + i\nu^{-\frac{1}{3}} g_1(x) + \ldots, \end{aligned}\right\} \tag{76}$$

where h_1 and g_1 are given by

$$-\nu^{\frac{1}{3}} h_1 + h_0' = -\frac{i\nu^{-\frac{1}{3}}}{\pi}\int_0^\infty \left(\frac{x}{\xi}\right)^{\frac{1}{2}} \frac{g_1(\xi)\,d\xi}{\xi - x},$$

$$-\nu^{\frac{2}{3}} g_1 + g_0' = -i\nu^{-\frac{1}{3}} h_1'''(\xi).$$

These equations may be combined to eliminate g_1 in the form

$$\begin{aligned} \nu^2 h_1 + \frac{1}{\pi}\int_0^\infty \left(\frac{x}{\xi}\right)^{\frac{1}{2}} \frac{h_1'''(\xi)\,d\xi}{\xi - x} &= \nu^{\frac{4}{3}} h_0' - \frac{\nu^{-\frac{2}{3}}}{\pi}\int_0^\infty \left(\frac{x}{\xi}\right)^{\frac{1}{2}} \frac{h_0^{(\mathrm{iv})}(\xi)\,d\xi}{\xi - x} \\ &= 2\nu^{\frac{4}{3}} h_0'(x). \end{aligned} \tag{77}$$

(The last step follows on differentiation of (74), since

$$\int_0^\infty \xi^{-\frac{1}{2}} h_0^{(\mathrm{iv})}(\xi)\,d\xi = (\tfrac{1}{2})!\,\Gamma(-\tfrac{7}{2}) = 0.)$$

The solution of (77) can be found by the same methods; again we find a third-order difference equation for the Mellin transform

$$H_1(s) = \int_0^\infty x^{s-1} h_1(x)\,dx.$$

The equation is not homogeneous like (29), but has a term from the right-hand side of (77) involving $H_0(s-1)$, and after some analysis which will be omitted here, the solution obtained is

$$H_1(s) = \frac{2}{3}\left(\operatorname{cosec}\frac{\pi s}{3}\right)\left[(s+1)\left(\cos\pi\frac{s-2}{3}\right) - \frac{1}{\sqrt{3}}\left(\sin\pi\frac{s-2}{3}\right)\right]H_0(s). \quad (78)$$

5.3. *Lift coefficient with an oscillating jet*

Equation (17) which gives the lift coefficient in terms of the vorticity distribution on the jet depends on the fact that $\Delta\phi$ tends to zero far from the wing. This holds in a steady oscillation too, if it is assumed that the motion started at some large but finite negative time $-T$, in which case the flow remains undisturbed at distances from the wing that are large compared with UT. In the low-frequency case however the equation cannot be applied directly, since when the expression for the transformed vorticity $g(x')$ obtained from the analysis of § 5.1 is inserted in (17) the integral in that equation is divergent. This is because of the invalidity of the solution for large x' that was mentioned earlier. To get round the difficulty we now obtain an expression for C_L in which the lowest order terms in μ can be found as finite integrals of $g(x')$. Equation (13) can be rearranged to give

$$C_L = \frac{2}{Uc}\int_0^c \gamma(\xi,t)\,d\xi + \frac{2}{U^2c}\frac{\partial}{\partial t}\int_0^c (c-\xi)\,\gamma(\xi,t)\,d\xi + C_J\tau(t).$$

Using the identity (16) to replace the integrals from 0 to c by integrals from c to ∞, we obtain

$$C_L = \frac{2}{Uc}\int_c^\infty \left\{\left(\frac{\xi}{\xi-c}\right)^{\frac{1}{2}} - 1\right\}\gamma(\xi,t)\,d\xi$$
$$+ \frac{1}{U^2}\frac{\partial}{\partial t}\int_c^\infty \left\{\left(\frac{\xi}{\xi-c}\right)^{\frac{1}{2}} + 2\left(\frac{\xi-c}{c}\right) - 2\left(\frac{\xi}{c}\right)^{\frac{1}{2}}\left(\frac{\xi-c}{c}\right)^{\frac{1}{2}}\right\}\gamma(\xi,t)\,d\xi + C_J\tau(t). \quad (79)$$

Inserting the expression (65) for $\gamma(\xi,t)$, this becomes simply

$$C_L = 4\tau_0\mu^{\frac{1}{2}}e^{inUt/c}\left(1+\frac{in}{2}\right)\int_0^\infty \xi'^{-\frac{1}{2}}g(\xi')\,d\xi' + o(\mu^{\frac{1}{2}}). \quad (80)$$

If n is of order unity, ν is of order μ and the low frequency solution of § 5.1 applies. $g(\xi)$ is equal to $f_0'(\xi)$ and the integral in (80) is therefore known from II to be $\pi^{\frac{1}{2}}$, whence

$$C_L = 4\tau_0(\pi\mu)^{\frac{1}{2}}\exp(inUt/c - \epsilon), \quad (81)$$

where the phase angle $\epsilon = \tan^{-1}(\frac{1}{2}n)$, showing that the lift coefficient oscillates with a phase lag increasing with frequency about the value $4\tau_0(\pi\mu)^{\frac{1}{2}}$ which corresponds to a steady deflexion τ_0. The effect of the higher-frequency terms will be to change both phase and amplitude by amounts of order ν.

In the high-frequency case, on the other hand, the difficulties with the integral in (17) do not arise. Substituting from (65), the expression for the lift coefficient is found to be

$$C_L = -4\mu^{\frac{1}{2}}\tau_0 e^{inUt/c}\int_0^\infty \xi^{\frac{1}{2}}ivg(\xi)\,d\xi.$$

The first approximation to $ivg(\xi)$ is $-h_0'''(\xi)$, on insertion of which the integral may be evaluated as $\frac{3}{8}H_0(-\frac{3}{2})$, yielding the expression

$$C_L = 4\tau_0(\pi\mu/3)^{\frac{1}{2}}\nu^{\frac{1}{2}}e^{inUt/c}. \tag{82}$$

This shows the amplitude to be frequency-dependent in a way that fits neatly with the $t^{-\frac{1}{2}}$ dependence found in the related short-time discussion of § 3.2, and also that the phase-lag has decreased to zero.

6. Discussion

The analysis shows that a first approximation for small times to the flow with a suddenly deflected jet can be found in the 'similarity' form used in § 3. The same solution can also be found by writing equation (23) operationally in terms of the Laplace transform with respect to time. The author has not found a way of improving this solution by a higher term, as was done for the high-frequency oscillating case in § 5.2, on account of its invalidity near $x' = 0$. The conclusion that the lift-coefficient varies for small times as $t^{-\frac{1}{2}}$ would not be altered by a more exact analysis, since there is always a region to which the similarity solution applies. The lift coefficient comes entirely from the apparent mass terms in the limit, and it appears that the force required to deflect the jet impulsively must be infinite. The 'impulse' of the fluid $\int_0^t L\,dt$ is however finite (and zero initially).

It may be noted that the long-time solution for the motion far from the wing is independent of the precise way in which the flow was started, depending only on the total circulation in the final steady flow near the wing and therefore on the final deflexion of the jet. This solution would also apply if the wing were at incidence. The similarity solution for $\gamma_0(y,t)$ found in § 4 actually describes the way a jet extending from $y = -\infty$ to $y = +\infty$ would deform if at time $t = 0$ it lay wholly along the axis and a vortex of magnitude $-\Gamma_\infty$ was concentrated at the origin.

I am grateful to Professor W. R. Sears and Mr J. C. Erickson for calling my attention to the problem and for many helpful discussions, and also to Mr Erickson for verifying the analysis in the manuscript. This work was carried out under the sponsorship of the Mechanics Division, Office of Scientific Research, USAF (Contract AF 49(638)-544).

REFERENCES

Erickson, J. C. 1959 Private communication.
von Kármán, Th. & Sears, W. R. 1938 *J. Aero. Sci.* **5**, 379–90.
Lighthill, M. J. 1959 *Aero. Res. Coun., Lond., Rep.* no. 20,793.
Spence, D. A. 1956 (referred to as I) *Proc. Roy. Soc.* A, **238**, 46–68.
Spence, D. A. 1961 (referred to as II) *Proc. Roy. Soc.* A (in the Press).
Thwaites, B. (editor) 1960 *Incompressible Aerodynamics.* Oxford University Press.

Appendix. Integral equations for the downwash far from the wing

The equations derived in § 4 connecting f_1 (the anti-symmetric part of the downwash distribution) and g_1 (the symmetric part of the vorticity distribution) are

$$f_1(x) = -\frac{2x}{\pi}\int_0^\infty \frac{g_1(\xi)\,d\xi}{\xi^2 - x^2} \tag{A 1}$$

and

$$\tfrac{2}{9}(5g_1 + 9xg_1' + 2x^2g_1'') = -f_1''', \tag{A 2}$$

with the condition

$$\int_0^\infty g_1(\xi)\,d\xi = -\tfrac{1}{2}. \tag{A 3}$$

To solve we construct the Mellin transforms

$$F_1(s) = \int_0^\infty x^{s-1}f_1(x)\,dx, \quad G_1(s) = \int_0^\infty x^{s-1}g_1(x)\,dx, \tag{A 4}$$

from which on inversion f_1 and g_1 will be found as

$$f_1(x) = \frac{1}{2\pi i}\int_{c-i\infty}^{c+i\infty} F_1(s)\,x^{-s}ds, \quad g_1(x) = \frac{1}{2\pi i}\int_{c-i\infty}^{c+i\infty} G_1(s)\,x^{-s}ds, \tag{A 5}$$

where c is some real constant such that $x^{c-1}f_1(x)$, $x^{c-1}g_1(x) \in L(0,\infty)$. Since, provided $|\mathscr{R}s| < 1$,

$$-\frac{2x}{\pi}\int_0^\infty \frac{\xi^{-s}d\xi}{\xi^2 - x^2} = x^{-s}\tan\frac{\pi s}{2}, \tag{A 6}$$

we obtain from (A 1), multiplying both sides by x^{s-1} and integrating from 0 to ∞,

$$F_1(s) = (\tan\tfrac{1}{2}\pi s)\,G_1(s), \tag{A 7}$$

provided $-1 < c < 1$. Differentiating (A 5), the left-hand side of (A 2) becomes

$$\frac{1}{2\pi i}\int_{c-i\infty}^{c+i\infty} \tfrac{2}{9}\{5 - 9s + 2s(s+1)\}\,G_1(s)\,x^{-s}ds \tag{A 8}$$

and the right-hand side

$$\frac{1}{2\pi i}\int_{c-i\infty}^{c+i\infty} (-s)(-s-1)(-s-2)\,F_1(s)\,x^{-s-3}ds.$$

If $s(s+1)(s+2)\,F_1(s)$ is regular in $c-3 < \mathscr{R}s < c$, the contour of integration can be moved to $\mathscr{R}s = c-3$ in this integral. Then writing $s-3$ for s it may be rewritten

$$-\frac{1}{2\pi i}\int_{c-i\infty}^{c+i\infty} (s-3)(s-2)(s-1)\,F_1(s-3)\,x^{-s}ds. \tag{A 9}$$

Equating the integrands of (A 8) and (A 9), and using (A 7), we get

$$\left(\frac{5-2s}{3}\right)\left(\frac{2-2s}{3}\right)G_1(s) = -(s-1)(s-2)(s-3)(\cot\tfrac{1}{2}\pi s)\,G_1(s-3). \tag{A 10}$$

Writing

$$G_1(s) = \left(-\frac{2s+1}{3}\right)!\,(s-1)!\,\phi(s), \tag{A 11}$$

the functional equation is simplified to

$$(\sin\tfrac{1}{2}\pi s)\,\phi(s) + (\cos\tfrac{1}{2}\pi s)\,\phi(s-3) = 0. \tag{A 12}$$

One solution is $$\phi(s) = A\cos\tfrac{1}{2}\pi s, \tag{A 13}$$

where A is constant, and the possibility that this would be multiplied by some further function of period 3 is excluded by the same type of argument as used in § 3, since already $\phi(s) \sim \exp(-\frac{1}{3}\pi|\mathscr{I}s|)$ for large $|\mathscr{I}s|$, so this is the only solution. A is fixed from (A 3), since

$$\int_0^\infty g_1(\xi)\,d\xi = G(1) = A\lim_{s\to 1}\left(-\frac{2s+1}{3}\right)!\,\left(\cos\frac{\pi s}{2}\right) = -\tfrac{1}{2}.$$

The limit is $\frac{3}{4}\pi$, so $A = -2/3\pi$. Therefore

$$\left.\begin{matrix}F_1(s)\\ G_1(s)\end{matrix}\right\} = -\left(\frac{2}{3\pi}\right)\left(-\frac{2s+1}{3}\right)!\,(s-1)\left.\begin{matrix}\cos\\ \sin\end{matrix}\right\}\frac{\pi s}{2} \tag{A 14}$$

and $s(s+1)(s+2)F_1(s)$ is regular as required in $c-3 < \mathscr{R}s < c$ if we choose $0 < c < 1$. The inversion formulae (A 5) can now be used to obtain series expansions for $f_1(x)$ and $g_1(x)$.

For $0 < x < 1$ the integrals are evaluated by moving the contour to the left over successive poles, namely those of $(s-1)!\,(\sin\frac{1}{2}\pi s) = 2\pi/(-s)!\,(\cos\frac{1}{2}\pi s)$ and of $(s-1)!\,(\cos\frac{1}{2}\pi s) = 2\pi/(-s)!\,(\sin\frac{1}{2}\pi s)$ at odd and even negative integers, whence

$$f_1(x) = -\frac{2}{3\pi}\sum_{n=0}^{\infty}(-1)^n\left(\frac{4n+1}{3}\right)!\,\frac{x^{2n+1}}{(2n+1)!} \tag{A 15}$$

and

$$g_1(x) = -\frac{2}{3\pi}\sum_{n=0}^{\infty}(-1)^n\left(\frac{4n-1!}{3}\right)!\,\frac{x^{2n}}{(2n)!}. \tag{A 16}$$

These series are absolutely convergent for $0 \leqslant x \leqslant 1$.

Asymptotic expansions are obtained as minus the sums of residues at the poles of $\{-(2s+1)/3\}!$, i.e. $s = 1, \frac{5}{2}, 4, \ldots$, to the right of $\mathscr{R}s = c$:

$$\left.\begin{matrix}f_1(x)\\ g_1(x)\end{matrix}\right\} \sim \frac{1}{\pi}\sum_{n=0}^{p}(-1)^n\left.\begin{matrix}\sin\\ \cos\end{matrix}\right\}\left(\frac{3n-1}{4}\pi\right)\frac{[\frac{1}{2}(3n-3)]!}{(n-1)!}\,x^{\frac{1}{2}(3n-1)} + o(x^p) \tag{A 17}$$

with the leading terms quoted in § 4.

In exactly the same way as above, the equations connecting the symmetric part f_2 of the downwash distribution and the antisymmetric part g_2 of the vorticity, namely

$$f_2(x) = -\frac{2}{\pi}\int_0^\infty \frac{\xi g_2(\xi)\,d\xi}{\xi^2 - x^2} \tag{A 18}$$

together with (A 2) with changed suffix, can be solved to give

$$G_2(s) = B\left(-\frac{2s+1}{3}\right)!\,(s-1)!\left(\sin\frac{\pi s}{2}\right). \tag{A 19}$$

But since $\{-\frac{1}{3}(2s+1)\}!$ has a pole at $s = 1$, the other two factors being unity there, the requirement that $G_2(1) = \int_0^\infty g_2(\xi)\,d\xi$ should exist can only be satisfied with the trivial choice $B = 0$, i.e.

$$f_2(x) \equiv g_2(x) \equiv 0. \tag{A 20}$$

On the behaviour of liquid dispersions in mixing vessels

By REUEL SHINNAR

Department of Chemical Engineering, Technion-Israel Institute of Technology, Haifa

(Received 8 March 1960 and in revised form 26 November 1960)

The present paper is concerned with the conditions of flow in tanks containing stirred fluids. An attempt is made to apply the theoretical concepts of local isotropy to explain the behaviour of liquid in liquid dispersions, subjected to turbulent agitation. Relations describing quantitatively the influence of turbulence on both break-up and coalescence of individual droplets are derived and are compared with experimental evidence. A special type of dispersion is described in which droplet size is controlled by the prevention of coalescence due to turbulence. The dependence of droplet size on energy dissipation per unit mass, as predicted by the theory of local isotropy, is put to an experimental test using geometrically similar vessels of different sizes.

Though the results are not entirely conclusive, experimental evidence suggests that the hypothesis of locally isotropic flow may be applicable to the flow conditions described in the paper, and that statistical theories of turbulence can be of practical value in estimating droplet sizes in agitated dispersions.

Introduction

The mixing or agitation of fluids in cylindrical tanks is a common operation in chemical industry, and as such has been studied extensively. A wide variety of agitator designs is used, while conditions of flow may vary from laminar flow to fully-developed turbulence. The following discussion is limited to turbine agitators and conditions of turbulent flow only.

The behaviour of liquid-liquid dispersions in such tanks is of special interest. If two immiscible liquids are agitated, a dispersion is formed, in which continuous break-up and coalescence of droplets occur simultaneously. If the agitation is continued over a sufficiently long time, a local dynamical balance between break-up and coalescence is established. The average size of the droplets at equilibrium will then depend on the conditions of agitation, which affect the dispersion in several ways:

(*a*) droplets will be broken up in regions of high shear stress near the agitator blades;

(*b*) turbulent velocity and pressure variations along the surface of a single droplet may cause break-up;

(*c*) the turbulent flow may accelerate or slow down the coalescence of the droplets.

In an actual dispersion all three processes occur simultaneously. Break-up in

regions of high shear stress should be important in very dilute dispersions, and in cases where coalescence is negligible. In cases in which coalescence is important, the influence of the local turbulent flow on the equilibrium state of the dispersion should predominate.

The phenomena mentioned under (*b*) and (*c*) are on a microscale, and the average droplet size of the dispersion is determined by what happens in a very small volume of fluid around the individual droplet. Thus the direct influence of the large-scale flow may be comparatively small. Now, a hypothesis put forward by Kolmogoroff is that, if the Reynolds number of the flow is high, the statistical properties of the flow-field in a very small volume of liquid can be estimated from a concept of local isotropy. The possibility of applying Kolmogoroff's theory to predict the droplet sizes in such dispersions is investigated here. This investigation should be of wider interest for the study of locally isotropic turbulence in general, especially as conditions of flow in stirred tanks allow the realization of very high degrees of turbulence. Such conditions are hard to obtain in wind tunnels.

A rule for the scaling-up of mixing plants from experimental results on the basis of a criterion of specific power input has been used empirically for a long time by chemical engineers. The theory of local isotropy is qualitatively closely related to such a criterion. Thus it should be expected that this theory, by putting the criterion on a more solid analytical basis, would shed new light on the range of its applicability.

For completeness, a short review of the basic concepts of local isotropy will be given, before the possibility of locally isotropic flow in a stirred tank is considered.

Kolmogoroff's theory of local isotropy

The theory of local isotropy (Kolmogoroff 1941) has been reviewed extensively (Batchelor 1947, 1953). Therefore only a short summary will be given in what follows.

Kolmogoroff has put forward the hypothesis that in any turbulent flow at sufficiently high Reynolds numbers the small-scale components of the turbulent velocity fluctuations are statistically independent of the main flow and of the turbulence-generating mechanism. The small-scale velocity fluctuations are determined by the local rate of energy dissipation per unit mass of fluid ϵ and the kinematic viscosity ν. Otherwise put, the spectrum of turbulent velocity fluctuations includes a range of high wave-numbers called the 'universal equilibrium range', which is uniquely determined by ϵ and ν. Kolmogoroff defines a length scale by

$$\eta = (\nu^3/\epsilon)^{\frac{1}{4}}, \tag{1}$$

and a velocity scale by

$$v = (\nu\epsilon)^{\frac{1}{4}}. \tag{2}$$

These parameters can be used to define conditions of flow in the equilibrium range instead of ϵ and ν.

For local isotropy to exist, the linear scale L of the energy-containing eddies must be large compared to the scale of the small energy-dissipating eddies η.

This implies that the Reynolds number of the flow must be high, or alternatively (cf. Batchelor 1953) that $(Lu'/\nu)^{\frac{3}{4}} \gg 1$, where u' is the root-mean-square of one component of the turbulent velocity fluctuation. If the conditions mentioned above for the existence of local isotropy are met, then in any small volume of characteristic dimension r ($\ll L$) all velocity correlations must be functions of v and η, or of ϵ and ν, only. Thus the mean-square of relative velocity $u(r)$ between any two points distance r apart† is a universal function of v and η. Furthermore, if $L \gg r \gg \eta$, then $\overline{u^2(r)}$ is independent of viscosity, and is a function of ϵ only.

In this case, and for very small values of r as well, the form of the universal function can be obtained from dimensional analysis.

$$\overline{u^2(r)} = C_1 \epsilon^{\frac{2}{3}} r^{\frac{2}{3}} \quad \text{for} \quad L \gg r \gg \eta, \tag{3}$$

$$\overline{u^2(r)} = C_2 \epsilon r^2/\nu \quad \text{for} \quad L \gg \eta \gg r. \tag{4}$$

The range of values of r for which (3) applies is called the 'inertial subrange'. In order for an inertial subrange to exist, $(Lu'/\nu)^{\frac{3}{4}}$ must be large compared to unity. Under the experimental conditions generally used for the study of turbulence in the laboratory, it is very difficult to satisfy the above conditions, and therefore few data proving the existence of local isotropy in the inertial subrange are available. The possibility of obtaining very high values of ϵ and of $u'L/\nu$ in a mixing tank should therefore be of interest for the study of locally isotropic turbulence.

Conditions of flow in stirred tanks

Local isotropy is possible with different types of agitators. However, the discussion will be limited to paddle and turbine agitators, because of their simple design and wide application. A typical agitator of this type is shown in figure 1. The mixing vessel is equipped with flow baffles to prevent the establishment of a vortex around the agitator shaft (avoidance of the influence of Froude number). The same effect can be obtained by excluding air from the vessel and filling it completely with liquid. The conditions of turbulence in such a mixing vessel can be predicted from a modified Reynolds number ND^2/ν, where D is the diameter of the agitator and N is its speed in revolutions per second. Fully developed turbulence (in the region of the agitator) exists with such agitators if this modified Reynolds number is higher than 10^4. It has been shown experimentally that for high Reynolds numbers the energy input of the mixing impellor per unit mass of liquid in the vessel is independent of the properties of the liquid, and a function only of the geometrical design of the agitator and its speed (Rushton *et al.* 1950). In geometrically similar vessels the average energy dissipation $\bar{\epsilon}$ in the liquid must therefore be a function of N and D only, and by dimensional analysis one can derive

$$\bar{\epsilon} = KN^3D^2. \tag{5}$$

Here K is a dimensionless constant dependent on the geometry of the vessel and the agitator only.

† u can be taken as the component of relative velocity parallel to the line joining the two points; similar results can be stated for other components of the relative velocity.

The knowledge of the average energy dissipation is not sufficient to determine the dependence of local values of ϵ on N and D, unless the distribution of the main flow velocity in the tank is universal. That means that the ratio of the average flow velocities at any two points is constant, and independent of Reynolds

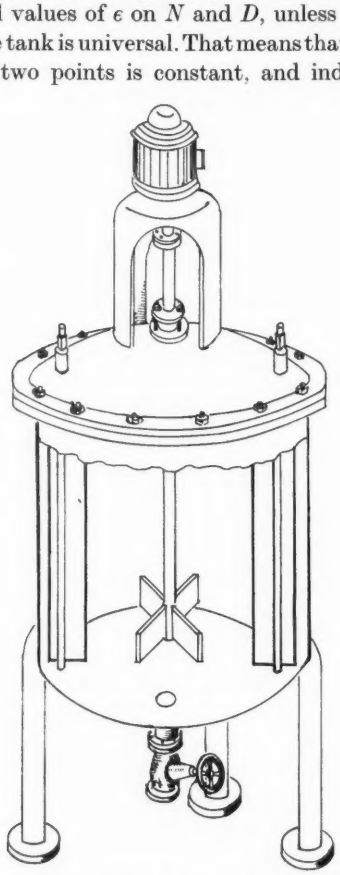

FIGURE 1. Sketch of a turbine mixer.

number and fluid properties. In this case only can it be assumed that the distribution in space of ϵ is universal also, and all local values of ϵ are then directly proportional to $\bar{\epsilon}$. Thus

$$\epsilon(x, y, z) = K'(x, y, z)\, N^3 D^2. \tag{6}$$

The dimensionless factor K' is an experimentally determinable function of the co-ordinates of any point in the vessel.

The velocity distribution in mixing tanks of this type has been experimentally investigated by Rushton & Sachs (1954) and by Aiba Schuichi (1958), and was found to be universal at Reynolds numbers above 10^4 with the equipment used. It is of particular interest to note that the velocity distribution in the liquid jets leaving the agitator blades was also found to be universal, whereas in a free jet the distribution becomes universal only at large distances from the origin.

Though the mixing action of a turbine agitator has often been compared to that of a free jet in stagnant surroundings, there is a basic difference between the two cases. While liquid entering the agitator is already highly turbulent, in a jet fully developed turbulence exists only at a comparatively large distance from the origin.

Taking into consideration the above discussion, it is permissible to conclude that, in an agitated fluid, statistical equilibrium is possible at any location in the liquid.

The requirements for the existence of local isotropy in a mixing tank can be fulfilled, though the flow is definitely non-isotropic. Experimentally, the realization of Reynolds numbers of several millions and local values of ϵ above 10^6 are feasible. Thus, for $\bar{\epsilon} = 10^6\,\mathrm{cm^3/sec^2}$ and $\nu = 1$ centistoke, η becomes equal to 10 microns. The Reynolds number of turbulence (Lu'/ν) in this case will be approximately 8500 for $L = 5\,\mathrm{cm}$, and 75,000 for $L = 25\,\mathrm{cm}$. Thus even for relatively small L, L/η will be very large.†

The flow around a turbine agitator should therefore furnish experimental evidence as to the validity of the concepts of local isotropy. However, one practical difficulty is that a reliable instrument for the detection and measurement of turbulent velocity fluctuations is not yet available for use with liquids.

Some indirect experimental evidence, however, can be obtained by measuring the droplet size distribution of agitated dilute dispersions of two immiscible liquids.

Break-up and coalescence of liquid dispersions in turbulent flow

If a dilute liquid-liquid dispersion is exposed to turbulent flow conditions, simultaneous coalescence and break-up occur. If the dispersion remains in a quasi-stationary flow-field for a sufficient duration, a dynamical equilibrium between coalescence and break-up is established. It is possible to predict from simple theoretical considerations the influence of the turbulent velocity fluctuations on both break-up and coalescence. The case of break-up has been treated previously by Kolmogoroff (1949) and Hinze (1955). The equations for prevention of coalescence were derived by Shinnar & Church (1960).

(*a*) *Break-up of droplets*

Consider a small volume of fluid in which turbulence is locally isotropic. Any of the droplets in this volume will be exposed to both inertial forces due to velocity fluctuations and to viscous shear forces. If the droplet is much larger than the microscale η, viscous forces can be neglected. In this case the droplet will oscillate about its spherical equilibrium shape concurrently with the surrounding fluid, provided the densities and viscosities of both liquids are not much different. If the deformations are large, the droplets become unstable and break up into two or more smaller fragments. But in order to become unstable, the kinetic energy of the oscillations must be sufficient to provide the gain in surface energy

† In order to calculate the Reynolds number of turbulence defined above, the macroscale of turbulence L must be known. Though L has not been determined, its order of magnitude should be comparable to the width of the agitator blades.

due to the break-up. The kinetic energy of the oscillating droplet may be assumed proportional to $\rho\overline{u^2(d)}\,d^3$, where $\overline{u^2(d)}$ is the mean-square of the relative velocity fluctuations between two diametrically opposite points on the surface of the droplet. The minimum gain in surface energy is approximately proportional to σd^2. The value of the ratio between these two energies ($\rho\overline{u^2(d)}\,d/\sigma$) is called the Weber number. The critical value of this ratio at which break-up occurs is dependent on the number of droplets formed as a result of the break-up. This critical value should be constant for any given system, though it may vary for different liquids.

In locally isotropic flow the average mean-squared velocity between two points is given by equations (3) and (4), and therefore the Weber number of a droplet, the diameter of which is much larger than η, becomes

$$We = \frac{\rho\overline{u^2(d)}\,d}{\sigma} = \frac{\rho C_1 \bar{\epsilon}^{\frac{2}{3}} d^{\frac{5}{3}}}{\sigma}. \tag{7}$$

The relation $\bar{\epsilon} = KN^3D^2$, which was obtained from other evidence, has been discussed in connexion with equation (5). Thus the value of the maximum stable droplet diameter can be obtained from the relation

$$\rho C_1 K^{\frac{2}{3}} N^2 D^{\frac{4}{3}} d^{\frac{5}{3}} \sigma^{-1} = \text{constant}. \tag{8}$$

Equation (8) should apply only to cases in which the maximum diameter obtained is larger than η.

In contrast to the above, if σ is very small or ν is rather large, as for instance for some emulsions, the maximum stable droplet diameter will be smaller than the microscale η. In this case the viscous shear forces cannot be neglected any longer, as the stresses due to viscous shear will be much larger than those due to inertial effects. The corresponding equation for the break-up of a droplet, due to viscous shear only, was derived by Taylor (1932):

$$\mu_c \frac{\partial u}{\partial r}\frac{d}{\sigma} = \Phi\left(\frac{\mu_d}{\mu_c}\right), \tag{9}$$

where Φ is a certain function, and the suffices c and d refer to the continuous and dispersed phases. In locally isotropic flow $(\partial u/\partial r)^2 = 2\epsilon/15\nu$. Therefore equation (9) now becomes

$$\frac{\mu_c \bar{\epsilon}^{\frac{1}{2}} d}{\nu_c^{\frac{1}{2}}\sigma} = \frac{\mu_c K^{\frac{1}{2}} N^{\frac{3}{2}} D d}{\nu_c^{\frac{1}{2}}\sigma} = \Phi\left(\frac{\mu_d}{\mu_c}\right). \tag{10}$$

This equation should describe the breakup of droplets in emulsions, whenever $d < \eta$.†

† Kolmogoroff has suggested for this case, in analogy with equation (7), that

$$\frac{\rho\overline{u^2(d)}\,d}{\sigma} = \frac{\rho C_2 \bar{\epsilon} d^3}{\nu\sigma} = \phi\left(\frac{\mu_d}{\mu_c}\right),$$

where ϕ is an unknown function. It should be pointed out, however, that, if $d \ll \eta$, then the viscous shear forces should be *much* larger than the inertial forces, which are given by $\rho\overline{u^2(d)}$.

(*b*) *Coalescence of droplets*

In an agitated dispersion, the rate of coalescence of droplets may be accelerated or slowed down by turbulence, depending on the physical properties of the constituents of the system.

Local velocity fluctuations will increase the rate of collisions between droplets and thereby increase the chance of coalescence. However, it is well known that only a small number of collisions result in immediate coalescence. This is so because a thin film of liquid, trapped between two colliding droplets, acts as an elastic cushion and may cause the droplets to recoil. If the two droplets adhere to each other, the thickness of the film separating them will gradually decrease due to diffusion. When the film has thinned down sufficiently, the boundary between the two droplets may collapse. However, turbulent velocity fluctuations may meanwhile communicate sufficient energy to the two droplets to cause re-separation, before coalescence has occurred. This effect will be enhanced if the time needed for the thinning down of the film is artificially increased, for instance by adding a protective colloid to the dispersion. This may be pushed to the point of complete prevention of coalescence in turbulent flow. Coalescence of such a dispersion will, of course, take place rapidly if agitation is stopped.

The effectiveness of the prevention of coalescence as described above is found to be a function of individual droplet diameters, since the forces of adhesion and those of inertia are different functions of droplet diameter. Hence, for very small droplets, turbulent energy input into a droplet pair may be insufficient to overcome the adhesion energy barrier.

The droplet diameter $d_{\min}$, for which the energy due to turbulent velocity fluctuations is equal to the energy of adhesion, depends on the intensity of agitation defined by $\bar{\epsilon}$, and also, naturally, on the physical properties of the constituents. This droplet diameter can be estimated as follows.

The force of adhesion between any two droplets of respective diameters d_1 and d_2 is given by

$$F(h_0) = \frac{\pi d_1 d_2}{d_1 + d_2} \int_{h_0}^{\infty} f(h)\, dh. \tag{11}$$

Here h_0 is the smallest distance between the two droplets, i.e. h_0 is actually the thickness of the 'films' separating them; h_0 is zero when the droplets touch each other; $f(h)$ is the force of attraction per square centimetre between two infinite parallel surfaces separated by a distance h (Bradley 1932; Deryaguin *et al.* 1934). The energy of adhesion E_a can be calculated from equation (11) by

$$E_a = \int_{h_0}^{\infty} F(h')\, dh' = \pi \int_{h_0}^{\infty} \int_{h}^{\infty} \frac{d_1 d_2}{d_1 + d_2} f(h)\, dh\, dh', \tag{12}$$

$$= 2 \frac{d_1 d_2}{d_1 + d_2} A(h_0), \tag{12a}$$

where $A(h_0)$ is defined by

$$\tfrac{1}{2}\pi \int_{h_0}^{\infty} \int_{h}^{\infty} f(h)\, dh\, dh'$$

and is the energy necessary to separate completely two droplets of unit diameter initially separated by the minimum distance h_0. If the two droplets are of equal diameter, equation (12*a*) simplifies to

$$E_a = A(h_0)\, d. \tag{13}$$

The kinetic energy of two droplets of diameter d in movement relative to each other is proportional to $\rho \overline{u^2(d)}\, d^3$. As already stated, this must be larger than the energy of adhesion in order to prevent coalescence. The drop diameter for which separation is still possible in a given fluid is therefore given implicitly by

$$\frac{\rho \overline{u^2(d)}\, d^2}{A(h_0)} = \text{constant}. \tag{14}$$

In locally isotropic flow $\overline{u^2(d)} = C(\epsilon d)^{\frac{2}{3}}$ [see equation (3)], and so (14) may be written as

$$C_1 \rho \epsilon^{\frac{2}{3}} d^{\frac{8}{3}} / A(h_0) = \text{constant}. \tag{15}$$

For fluid stirred in a tank at constant power number, this is equivalent to

$$C_1 \rho K^{\frac{2}{3}} N^2 D^{\frac{4}{3}} d^{\frac{8}{3}} / A(h_0) = \text{constant}. \tag{16}$$

Both $A(h_0)$ and h_0 are constant and independent of the droplet diameter d in any given dispersion as long as h_0/d is small. However, the numerical values of these constants are difficult to estimate from the properties of the system. For a given pair of fluids, $A(h_0)$ is constant, and equations (15) and (16) may be applied to predict the dependence of $d_{\min}$ on $\bar{\epsilon}$.

The considerations set out above do not apply if the maximum diameter defined by equation (8) is *smaller* than the diameter as given by equation (16), for then separation of adhering droplets by turbulent agitation becomes insignificant. Thus droplets in the dispersion fuse rapidly until the diameter of the drop formed reaches the unstable size for *break-up*, and then fragmentation into several smaller droplets becomes probable. The process restarts with coalescence. The size distribution is determined by the state of dynamical equilibrium reached.

In figure 2 the maximum stable droplet diameter as determined by the process of break-up, and the minimum stable droplet diameter as determined by the process of coalescence, are plotted against agitator speed. This latter quantity is proportional to $\epsilon^{\frac{1}{3}}$.

From this figure it is apparent that prevention of coalescence due to turbulent velocity fluctuations in the bulk liquid is of importance in the region to the left of the point of intersection between the two lines plotted on the graph, while being relatively unimportant to the right of this point. The value of $\bar{\epsilon}$ at which the two lines intersect depends on the physical properties of the constituents. The existence of such a critical value has been confirmed experimentally as will be seen later.

(*c*) *Simultaneous break-up and coalescence*

In practice, the size distribution of droplets in an agitated dispersion is determined by both break-up and coalescence occurring simultaneously. The diameters defined in equations (8) and (16) are in reality statistical averages; in the case of

(8), of the droplet size for which break-up most probably occurs, and in the case of (16), of the droplet size above which prevention of coalescence becomes effective. From the plots of the dependence of d on ϵ some conclusions as to which of the two processes predominates in the dispersion can be drawn. In addition, it is possible to conclude that in cases where locally isotropic flow may be assumed to exist, droplet size distribution is a function of energy dissipation and the physical properties of the constituents only.

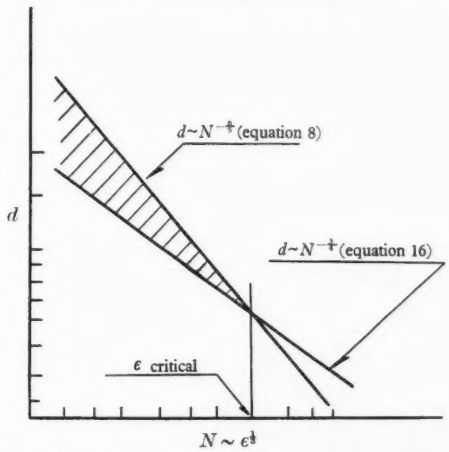

FIGURE 2. Logarithmic plot of droplet diameter as a function of agitator speed. Equation (8): d controlled by breakup; equation (16): d controlled by prevention of coalescence.

The reasoning set out above provides the limitations to the empirical engineering rule of scaling-up mixing plants. As already mentioned above, this rule is based on a specific energy input per unit mass criterion. Thus this criterion, which of course applies only approximately, can safely be applied to all those cases where (*a*) local isotropy is expected to exist, (*b*) the main influence of turbulent agitation is confined to the vicinity of a small particle or droplet, and (*c*) the influence of the large-scale flow (gross mixing) may be neglected.

There exist some special dispersions in which prevention of coalescence is the factor determining droplet size; this can be shown by experimental evidence unrelated to the above. As already mentioned, the addition of a protective colloid to the dispersion may slow down coalescence. Dispersions can be prepared in which no break-up or coalescence will occur as long as constant agitation is maintained, and individual droplets are completely stable for many hours of agitation. This effect can be shown very convincingly by colouring part of the droplets: it will be found that under these special conditions the coloured droplets will retain their original colour without sharing this with other droplets. Also, droplet sizes will be distributed in a relatively narrow band. The sizes will again depend on agitation, and a reduction in agitator speed will lead to a different size distribution in equilibrium. If a stable equilibrium is again attained at the reduced agitator speed, the colour tracer method may again be used to show that no further intermixing does occur.

For these special dispersions, the term 'turbulence-stabilized dispersions' has been suggested by the author, and a detailed discussion of the properties of such dispersions has been given (Shinnar & Church 1961).

Experimental evidence

Several authors have studied experimentally the behaviour of two immiscible liquids when agitated together (Magnusson 1954; Vermeulen, Williams & Langlois 1955; Shinnar 1957; Shinnar & Church 1961). Their results will be discussed below. In addition, some new experimental evidence obtained by the author is given.

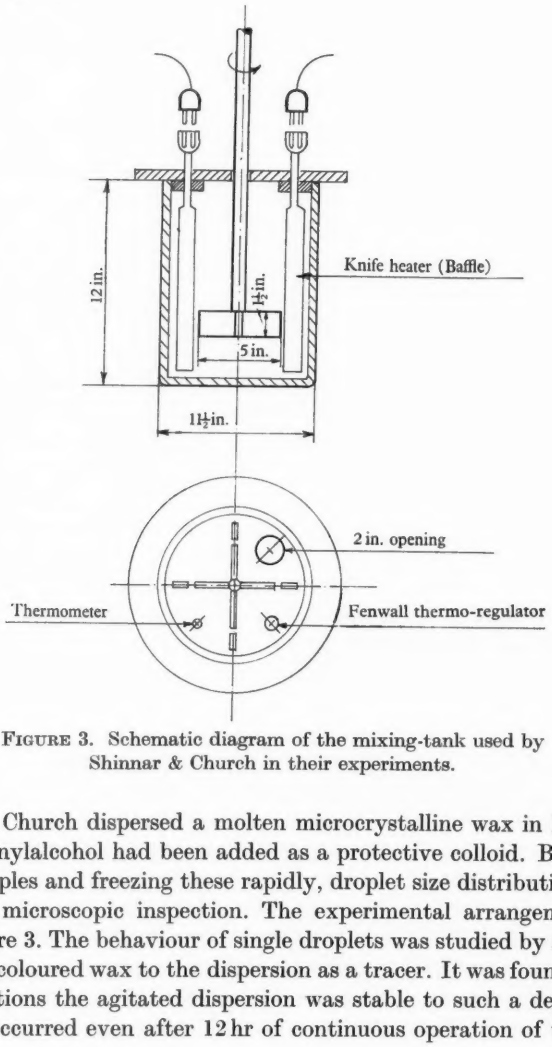

FIGURE 3. Schematic diagram of the mixing-tank used by Shinnar & Church in their experiments.

Shinnar & Church dispersed a molten microcrystalline wax in hot water to which polyvinylalcohol had been added as a protective colloid. By syphoning off small samples and freezing these rapidly, droplet size distributions could be obtained by microscopic inspection. The experimental arrangement used is shown in figure 3. The behaviour of single droplets was studied by adding small quantities of coloured wax to the dispersion as a tracer. It was found that under certain conditions the agitated dispersion was stable to such a degree that no intermixing occurred even after 12 hr of continuous operation of the agitator.

However, whenever agitator speed was reduced, coalescence took place at once, and proceeded until after about 2 hr a new stable equilibrium was established, and no further intermixing and coalescence occurred. This was taken to indicate that droplet size in such dispersions is determined by the prevention of coalescence by turbulence; thus (16) should apply to these dispersions. Figure 4 shows the appearance of samples of dispersions stabilized at different agitator speeds. Samples were taken from various points in the mixing tank, and no variation of droplet size with location could be detected.

In figures 5 and 6 average droplet sizes are plotted against agitator speed for some typical experiments with two different protective colloids. The droplet diameter given in these figures is the Sauter mean diameter defined by $d_{32} = \Sigma nd^3/\Sigma nd^2$, where d is the diameter of each droplet and n is the number of droplets in each size group. The use of a mean diameter instead of a maximum or minimum diameter as employed above appears permissible, as the spread of the size distribution curves is small and the curves are all of similar shape. Table 1 lists all size distributions for the experimental points plotted in figure 6. The ratio of d_{max} and d_{min}, which are defined so that 90 % of the cumulative volume of all droplets have a diameter smaller than d_{max} and 10 % are smaller than d_{min}, is fairly constant and its value is about two. It is only at 627 r.p.m. that this ratio increases slightly to a value of about three, but as will be explained later the dispersion was not 'stable' at this agitator speed.

All points plotted on figures 5 and 6 were tested for stability by the tracer method and the results are indicated in the figure. The assumption that prevention of coalescence by turbulence controls droplet size is of course justified only for those points for which no intermixing of the tracer wax occurred. For these points the results are in reasonable agreement with (16). One of the stabilizers tested (figure 6) gave rise to dispersions in which the existence of a critical agitator speed could be experimentally checked. Thus at 627 r.p.m. the dispersion behaved as if no protective colloid were present and the tracer wax became completely dispersed after only 10 min of agitation, even though at lower agitator speeds no intermixing could be detected after as long as 12 hr of continuous agitation. When the concentration of the protective colloid was increased by as much as fivefold, rapid intermixing was not prevented, though analysis of the water phase showed that a large excess of free colloid was present. It may therefore be assumed that 627 r.p.m. was above the critical agitator speed in these dispersions and for the experimental arrangement used.

All experimental results given by Shinnar & Church were obtained from tests carried out with the same equipment. To test the validity of (16) for scaling-up purposes another series of experiments with turbulence-stabilized dispersions was carried out by the author. Two sets of similar tanks and impellors were employed, the dimensions of which are given in figure 7. A Pfaudler type turbine-agitator was used instead of the flat-blade turbine shown in figure 3 as two sets of such agitators were available. Test results are plotted in figure 8 where droplet sizes are given as functions of N^3D^2. The agreement with theory is seen to be quite good.

It should be pointed out that in the experiments described above the agitator

chosen was large in comparison with the mixing vessel. Thus the influence of agitation extended to all parts of the mixing tank. Smaller agitators may be expected to give much less uniform agitation, and in such cases droplet sizes

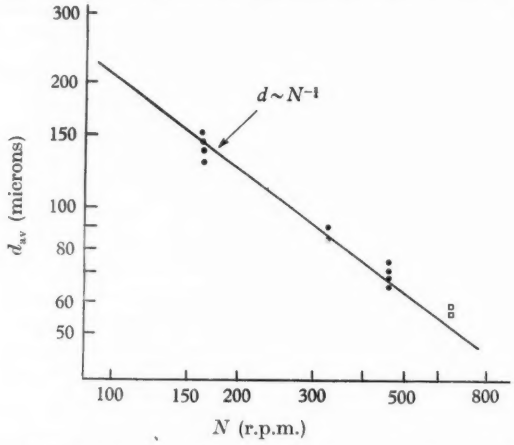

FIGURE 5. Average droplet size as a function of agitator speed in a turbulence-stabilized dispersion (droplet size controlled by prevention of coalescence). Experimental arrangement shown in figure 3. Dispersion used: 5% molten wax (Shellwax 700) in hot water containing 0·1% polyvinylalcohol (Du Pont Elvanol 51–05 low molecular weight). Viscosity $\nu_c = 0{\cdot}35$ centistokes; $\nu_d = 22{\cdot}5$ centistokes. Results of colour tracer test indicated on plot as follows: ●, no visible intermixing after 2 hr; □, partial intermixing after 2 hr.

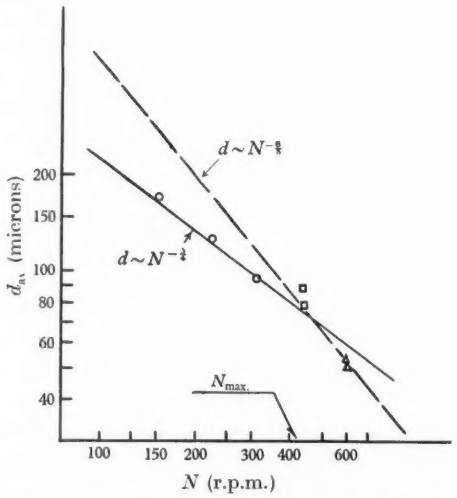

FIGURE 6. As in figure 5. Dispersion used: 5% molten wax (Shellwax 700) in hot water containing 0·1% polyvinylalcohol (Du Pont Elvanol 50–42 high molecular weight). Viscosity $\nu_c = 0{\cdot}4$ centistokes, $\nu_d = 22{\cdot}5$ centistokes. Results of colour tracer test indicated on plot as follows: ○, no visible intermixing after 2 hr; □, partial intermixing after 2 hr; △, rapid intermixing.

r.p.m. ...	156		220		312		440		440		627		627	
d_{av} (microns)	*A*	*B*	*A*	*B*	*A*	*B*	*A*	*B*	*A*	*B*	*A*	*B*	*A*	*B*
15	—	—	10	0·002	14	0·005	65	0·035	95	0·10	410	1·90	334	1·6
30	61	0·07	25	0·038	75	0·205	135	0·605	183	1·55	297	11·30	310	12·0
45	—	—	47	0·240	87	0·81	175	2·51	179	5·15	210	27·0	199	26·0
60	67	0·81	79	0·97	171	3·83	195	6·9	255	17·40	95	29·2	98	30·4
75	—	—	115	2·77	258	11·35	164	11·2	121	16·05	21	12·6	24	14·5
90	83	2·43	165	6·85	281	21·2	211	25·2	114	26·1	7	7·2	11	11·5
105	—	—	201	13·1	293	35·1	141	26·6	55	20·0	3	4·9	1	1·6
120	127	8·80	177	17·3	101	18·1	65	18·4	18	9·75	1	2·44	1	2·4
135	—	—	127	17·7	21	5·3	15	6·2	1	0·78	1	3·46	—	—
150	171	23·1	113	21·6	8	2·8	3	1·65	3	3·12	—	—	—	—
165	—	—	35	8·9	3	1·3	1	0·70	—	—	—	—	—	—
180	111	26·0	20	6·6	—	—	—	—	—	—	—	—	—	—
195	—	—	8	3·4	—	—	—	—	—	—	—	—	—	—
210	34	12·6	1	0·53	—	—	—	—	—	—	—	—	—	—
225	—	—	—	—	—	—	—	—	—	—	—	—	—	—
240	23	12·7	—	—	—	—	—	—	—	—	—	—	—	—
255	—	—	—	—	—	—	—	—	—	—	—	—	—	—
270	16	12·4	—	—	—	—	—	—	—	—	—	—	—	—
285	—	—	—	—	—	—	—	—	—	—	—	—	—	—
300	1	1·09	—	—	—	—	—	—	—	—	—	—	—	—
$d_{3,2}$	177		127		97		91		79		53		51	
d_{max}	265		174		135		130		115		98		92	
d_{min}	128		96		75		68		57		34		35	
d_{max}/d_{min}	2·07		1·82		1·80		1·91		2·02		2·88		2·63	

TABLE 1. Size distribution of dispersion of figure 6

A, number of particles in size group; *B*, volume percentage of particle class; d_{av}, average diameter in size group.

may not be independent of location in the tank. Furthermore, complete prevention of coalescence due to turbulence may no longer be possible. No quantitative criteria for a minimum agitator size (compared with tank size) have as yet been established. The problem is currently under investigation.

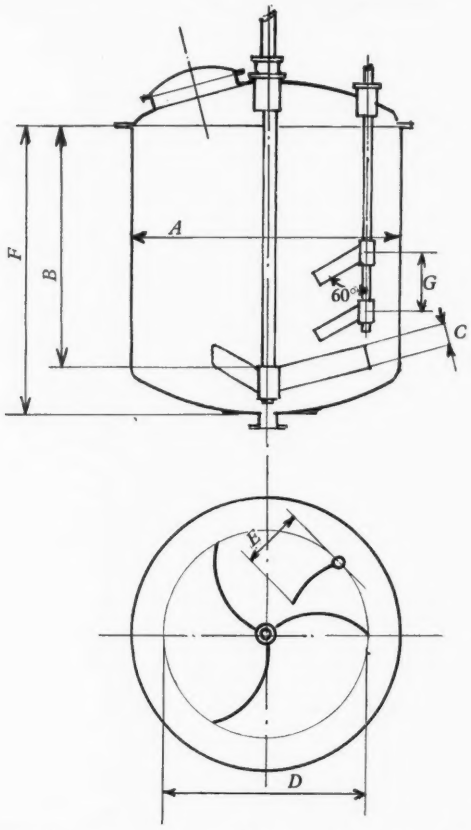

FIGURE 7. Experimental arrangement used for testing scaling-up relations in author's experiments. Dimensions in mm.

	A	*B*	*C*	*D*	*E*	*F*	*G*
Large vessel	1220	1064	102	914	274	1270	254
Small vessel	305	266	25·5	228·5	68·5	317·5	83·5

Vermeulen determined average droplet sizes in agitated dispersions indirectly by measuring the amount of light scattered. A wide range of different combinations of two liquids was studied. The concentration of the dispersed liquid was varied from 10 to 40 %.

Vermeulen's results were correlated by the following empirically derived equation

$$\rho N^2 D^{\frac{4}{3}} d^{\frac{5}{3}} \sigma^{-1} = 0{\cdot}016, \tag{17}$$

which is identical to equation (8) derived in the present paper analytically. The deviation of Vermeulen's experimental data from (17) was about $\pm 40\,\%$.

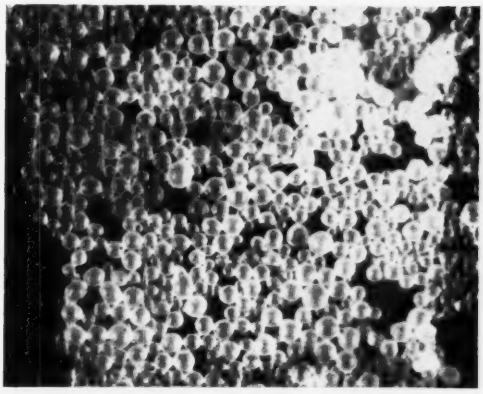

(*a*)

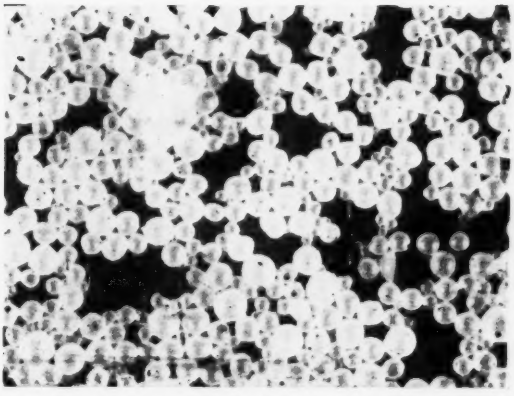

(*b*)

FIGURE 4. Photomicrograph of frozen samples of turbulence-stabilized dispersions; results of colour tracer tests (experimental conditions and results given in figure 6). Magnification $\times 20$. (*a*) Dispersion agitated at 220 r.p.m. 4 hr. after addition of red-coloured wax. (*b*) Same dispersion as in (*a*), agitated at 156 r.p.m. 4 hr after addition of red-coloured wax.

However, the comparatively large scatter could be explained if it is borne in mind that a number of these tests were carried out at conditions where the above theory does not apply (relatively low Reynolds numbers, high concentration of the dispersed phase, etc.). If only dilute dispersions of liquids of low viscosity are considered, the scatter of the experimental results is found to be much reduced. Some typical results are given in figure 9. The curve of d *vs* N on the log-log plot

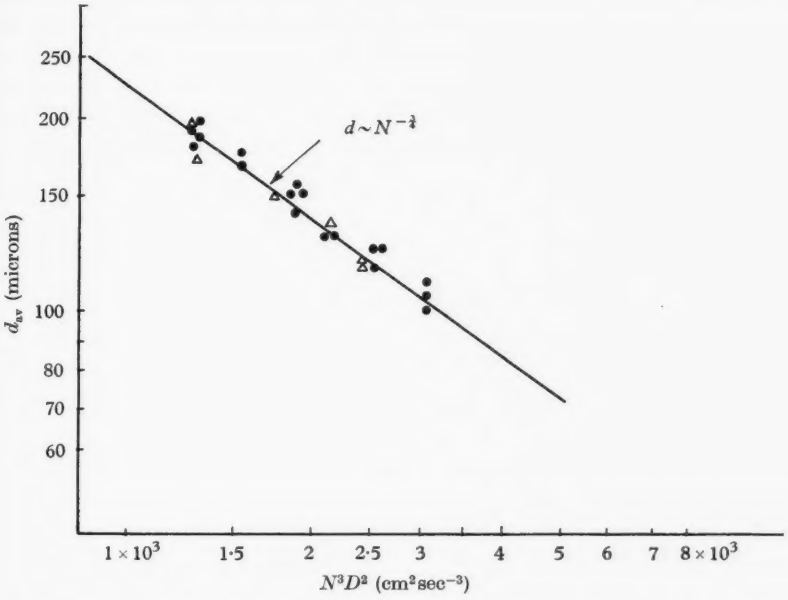

FIGURE 8. Average droplet size in mixing vessels of various sizes for a turbulence-stabilized dispersion. Dimensions of both vessels and agitators given in figure 7. Dispersion used: 5% molten wax (Shellwax 700) in water containing 3% polyvinylalcohol (Du Pont Elvanol 50–42 high molecular weight). All points were tested by colour tracer method and no visible intermixing could be detected after 2 hr. ●, Small vessel; △, large vessel.

is seen to be concave upwards at low agitator speeds. For all liquids agreement with (17) is better at higher speeds. The extension of Vermeulen's tests to cover a large range of mixing-vessel dimensions and the measurement of droplet size distributions (instead of average droplet sizes only) should be of great interest. Rodger, Trice & Rushton (1956) measured droplet sizes in agitated liquid-liquid dispersions, using equal volumes of both liquids. Technique and experimental conditions were similar to Vermeulen's, but both agitator and mixing-vessel dimensions were varied. A complicated equation relating droplet size to agitator speed, liquid properties and the dimensions of both agitator and vessel was empirically derived from these tests. This equation is quite different from the correlation proposed by Vermeulen. For any one pair of liquids and geometrically similar agitators this equation reverts practically to (16). Rodger's formula predicts droplet sizes to be a function of $N^{-\frac{12}{25}}$ as compared to $N^{-\frac{3}{4}}$ in (16). In

geometrically similar vessels of different dimensions, equal droplet sizes are predicted approximately at equal energy input per unit mass; this applies only to the range over which experiments were actually performed.

A possible explanation for the difference in the experimental results obtained by Vermeulen and Rodger could be that, in the first set of experiments, break-up of droplets is the determining factor, whereas in the second set slowing up of coalescence due to turbulence controls droplet size. Though it is questionable whether (16) is applicable to concentrated dispersions, as used by Rodger, the agreement with (16) is interesting to note.

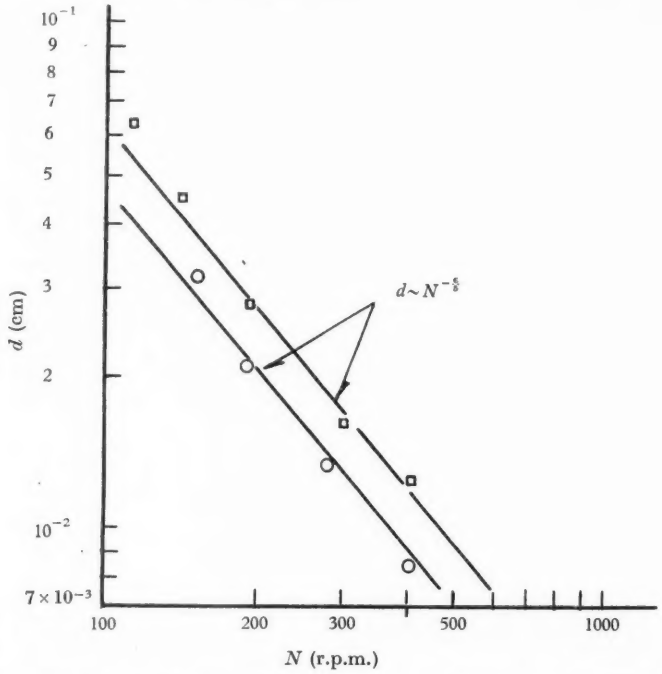

FIGURE 9. Droplet size as a function of agitator speed, d controlled by break-up. Data from Vermeulen *et al.* □, 10 % dispersion of kerosene in water; ○, 10 % dispersion of an iso-octanol carbon tetrachloride mixture in water.

Magnusson (1954) studied agitation power requirements for oil-in-water dispersions in mixing vessels of various sizes and found the energy per unit mass needed to be approximately constant. However, droplet sizes were not determined directly. The time needed for coalescence of a sample of each dispersion was used as a criterion for the state of mixing. Comparison with other data is therefore difficult.

Equation (7) for break-up was applied by Kolmogoroff (1949) to droplet sizes in a pipe in order to provide experimental evidence for his theory of local isotropy. The data were obtained at relatively low Reynolds numbers and were found to be non-conclusive, as droplet diameter was found to be proportional to U^{-1}

and not to $U^{-\frac{2}{3}}$ (here U is the mean bulk velocity). Hinze (1955) applied equation (7) to Clay's data (1940) on dispersions agitated between rotating cylinders, but again the scatter is much larger than in Vermeulen's tests.

There is as yet no experimental evidence justifying the application of equation (10) to dispersions in which $d \ll \eta$. It is therefore interesting to note that (10) describes to a good approximation the equilibrium size distribution of gas bubbles in a liquid agitated by a turbine agitator. In such a case the size distribution of the gas bubbles reaches an equilibrium value which depends on the intensity of the agitation and the physical properties of the system. Vermeulen *et al.* (1955) measured bubble sizes of different gases in water and other liquids with the same experimental arrangement used to measure droplet sizes in agitated liquid-liquid dispersions, and obtained the following dimensionless correlation

$$\frac{N^{\frac{3}{2}} D d \rho_c^{\frac{1}{2}} \mu_d^{\frac{3}{4}}}{\sigma \mu_c^{\frac{1}{4}}} = \text{constant}. \tag{18}$$

This may be rewritten as

$$\frac{N^{\frac{3}{2}} D d \mu_c}{\nu_c^{\frac{1}{2}} \sigma} \propto \left(\frac{\mu_c}{\mu_d}\right)^{\frac{3}{4}}. \tag{18}$$

Equation (18) is identical with (10). However, this problem is of much greater complexity, because of the large difference in densities of the two fluids, and no definite conclusions can be drawn at the present stage.

The author is indebted to Mr Z. Rotem for reading the manuscript and for some useful suggestions.

REFERENCES

Batchelor, G. K. 1947 *Proc. Camb. Phil. Soc.* **43**, 533; **47**, 359.

Batchelor, G. K. 1953 *The Theory of Homogeneous Turbulence*. Cambridge University Press.

Bradley, R. S. 1932 *Phil. Mag.* **13**, 853.

Clay, P. H. 1940 *Proc. K. Akad. Wet. Amst.* **43**, 852 and 979.

Deryaguin, B. *et al.* 1934 *Kolloidzschr.* **69**, 135.

Hinze, J. O. 1955 *Amer. Inst. Chem. Eng. J.* **1**, 289.

Kolmogoroff, A. M. 1941 *C.R. Acad. Sci. U.R.S.S.* **30**, 301 and **32**, 16.

Kolmogoroff, A. M. 1949 *Dokl. Akad. Nauk, S.S.S.R.* **66**, 825.

Magnusson, K. 1954 *Chem. Proc. Engng*, **35**, 276.

Rodger, W. A., Trice, V. G. & Rushton, J. H. 1956 *Chem. Engng Progr.* **52**, 515.

Rushton, J. H. & Sachs, J. P. 1954 *Chem. Engng Progr.* **50**, 597.

Rushton, J. H. *et al.* 1950 *Chem. Engng Progr.* **46**, 395–497.

Schuichi, Aiba 1958 *Amer. Inst. Chem. Eng. J.* **4**, 485.

Shinnar, R. & Church, J. M. 1960 *Ind. Engng Chem.* **52**, 253.

Shinnar, R. & Church, J. M. 1961 (To be published.)

Shinnar, R. 1957 Doctoral thesis, Columbia University.

Taylor, G. I. 1932 *Proc. Roy. Soc.* A, **138**, 41.

Vermeulen, Th., Williams, G. M. & Langlois, G. E. 1955 *Chem. Engng Progr.* **51**, 85F.

A study of the magnetohydrodynamic boundary layer on a flat plate

By M. B. GLAUERT

Department of Mathematics, University of Manchester

(Received 21 October 1960)

This paper is concerned with the boundary layer on a semi-infinite flat plate in a uniform stream of conducting fluid, with a magnetic field in the stream direction such that the Alfvén speed is less than the undisturbed fluid speed. Series solutions are derived which are applicable for large and small values of the electrical conductivity, and which give a guide as to the validity and limitations of theories which assume the fluid to have infinite or zero conductivity.

1. Introduction

The subject of this paper is the derivation of solutions of the equations governing a certain problem in magnetohydrodynamics. This problem, discussed in detail by Greenspan & Carrier (1959) in a paper hereafter referred to as **I**, concerns the steady two-dimensional flow of a viscous incompressible electrically conducting fluid of constant properties past a semi-infinite rigid plate. The applied magnetic field is uniform and in the direction of the undisturbed stream, which is parallel to the plate and perpendicular to its edge.

As shown in **I** and recapitulated briefly in the Appendix to this paper, the boundary-layer equations governing the flow are

$$f''' + ff'' - \beta gg'' = 0, \tag{1.1}$$

$$g'' + \epsilon(fg' - f'g) = 0, \tag{1.2}$$

with boundary conditions

$$f(0) = f'(0) = g(0) = 0, \quad f'(\infty) = g'(\infty) = 2. \tag{1.3}$$

Here $\epsilon = \sigma\mu\nu$ is the ratio of the viscous to the magnetic diffusivity and is proportional to the conductivity of the fluid, and $\beta = \mu H_0^2/\rho U_0^2$ is the square of the ratio of the Alfvén speed to the fluid speed in the undisturbed flow. The fluid has density ρ, kinematic viscosity ν, electrical conductivity σ and magnetic permeability μ, and in the undisturbed stream the speed is U_0 and the magnetic field intensity is H_0. The functions $f(\eta)$ and $g(\eta)$ describe the velocity field and the magnetic field respectively, where

$$\eta = \tfrac{1}{2}(U_0/\nu x)^{\frac{1}{2}} y \tag{1.4}$$

is the usual Blasius non-dimensional variable, x and y being distances measured

along and perpendicular to the plate from its leading edge. The velocity components are

$$u = \tfrac{1}{2}U_0 f', \quad v = \tfrac{1}{2}(U_0\nu/x)^{\frac{1}{2}}(f - \eta f'), \tag{1.5}$$

and the magnetic field components are

$$H_x = \tfrac{1}{2}H_0 g', \quad H_y = \tfrac{1}{2}H_0(\nu/U_0 x)^{\frac{1}{2}}(g - \eta g'). \tag{1.6}$$

The method used in **I** to tackle the problem was to replace the fundamental equations by Oseen equations, linearized equations obtained by assuming that the convective velocity and magnetic fields may be replaced by their free-stream values. For $\beta < 1$ the method led to plausible results, although they did not agree very satisfactorily with certain numerical solutions of equations (1.1) and (1.2). For $\beta > 1$ the whole formulation of the problem breaks down. The Alfvén speed is then greater than the fluid speed and disturbances penetrate upstream ahead of the plate, so it is no longer possible to describe the flow completely in terms of the Blasius variable based on the leading edge. This was confirmed in **I** by a study of the Oseen equations applicable to a flat plate of finite length. The solutions for $\beta < 1$ obtained in **I**, and an investigation of the nature of the equations when $1-\beta$ is small and $\epsilon = 1$, were interpreted by the authors as indicating that the entire flow becomes 'plugged' or brought to rest at the critical value $\beta = 1$.

Further discussions of the problem by means of the Oseen equations have been given by Carrier & Greenspan (1960) and by Greenspan (1960). The former paper treats unsteady flow conditions and the latter the flow past a finite plate with $\beta > 1$.

The scope of the present paper is limited to the range $\beta < 1$, with $1-\beta$ not small. Two solutions in series of the full boundary-layer equations (1.1) and (1.2) are obtained, valid for large and for small values of ϵ respectively. Several terms are calculated explicitly, each depending in a simple manner on the parameter β. The physical reason why such series expansions are possible is that when ϵ is large the magnetic boundary layer is effectively much thinner than the velocity boundary layer and when ϵ is small it is much thicker. The situation has many points of similarity to the study of heat transfer in a laminar boundary layer of non-conducting fluid, as discussed by Morgan & Warner (1956) and by Morgan, Pipkin & Warner (1958). The temperature distribution function and the Prandtl number there take analogous places in the equations to the magnetic field function $g(\eta)$ and the conductivity parameter ϵ.

Our series solutions appear to give reliable numerical values for the ranges $\epsilon > 10$ and $\epsilon < 0{\cdot}001$. Most practical applications will probably be covered by one or other of these cases. If results are required for some specific values of ϵ outside these ranges they may be obtained without undue labour by use of an electronic computer, but the presence of two arbitrary parameters ϵ and β means that anything like a complete coverage is a formidable task. The equations have simple solutions for $\epsilon = \infty$ and for $\epsilon = 0$, and perhaps the chief point of interest is to see how these limiting values are approached, since in many problems in magnetohydrodynamics it is most helpful to be able to assume that the electrical conductivity is either infinite or zero.

2. Equations for large conductivity

When the electrical conductivity is large it is convenient to make a slight change of variables, in order that the functions to be calculated shall as far as possible be independent of the parameter β. We write

$$\eta = (1-\beta)^{-\frac{1}{2}}\theta, \quad f(\eta) = (1-\beta)^{-\frac{1}{2}}p(\theta), \quad g(\eta) = (1-\beta)^{-\frac{1}{2}}q(\theta), \tag{2.1}$$

and

$$\epsilon = (1-\beta)\lambda. \tag{2.2}$$

As stated above, $1-\beta$ is supposed to be positive and not small. Then

$$f'(\eta) = p'(\theta), \quad f''(\eta) = (1-\beta)^{\frac{1}{2}}p''(\theta), \quad \text{etc.},$$

and the equations (1.1) and (1.2) become

$$(1-\beta)p''' + pp'' - \beta qq'' = 0, \tag{2.3}$$

$$q'' + \lambda(pq' - p'q) = 0, \tag{2.4}$$

with boundary conditions

$$p(0) = p'(0) = q(0) = 0, \quad p'(\infty) = q'(\infty) = 2. \tag{2.5}$$

For a perfectly conducting fluid λ, like ϵ, is not only large but infinite. Equation (2.4) reduces to $pq' = p'q$ and the only solution satisfying (2.5) is

$$p(\theta) = q(\theta). \tag{2.6}$$

Equation (2.3) now becomes

$$p''' + pp'' = 0, \tag{2.7}$$

of which the required solution is

$$p(\theta) = B(\theta), \tag{2.8}$$

where $B(\theta)$ is the well-known Blasius function which governs the boundary layer on a flat plate in a non-conducting fluid.

If λ is finite this solution is incorrect in the vicinity of the plate. It implies that $q''(0) = B''(0)$, which is non-zero, while the boundary conditions (2.5) and equation (2.4) show that $q''(0) = 0$. It is clear that however large λ may be there is an inner part of the boundary layer in which the first term of (2.4) cannot be ignored. According to (2.8), when θ is small $p = O(\theta^2)$, $p' = O(\theta)$, $p'' = O(1)$ and similarly for $q(\theta)$, and so the terms of (2.4) become of comparable magnitudes when $\theta = O(\lambda^{-\frac{1}{3}})$. We must introduce an appropriately stretched co-ordinate to describe the inner layer. Since the transformed equation (2.4) must no longer contain λ explicitly we write

$$\theta = \lambda^{-\frac{1}{3}}\xi, \quad p(\theta) = \lambda^{-\frac{2}{3}}P(\xi), \quad q(\theta) = \lambda^{-\frac{2}{3}}Q(\xi). \tag{2.9}$$

It follows that $p'(\theta) = \lambda^{-\frac{1}{3}}P'(\xi)$, $p''(\theta) = P''(\xi)$, etc., and (2.3) and (2.4) become

$$\lambda(1-\beta)P''' + PP'' - \beta QQ'' = 0, \tag{2.10}$$

$$Q'' + PQ' - P'Q = 0, \tag{2.11}$$

with boundary conditions $P(0) = P'(0) = Q(0) = 0$. The boundary condition at $\theta = \infty$ is of no importance to the inner layer.

We may now seek solutions for p, q, P and Q in the form of series in descending powers of λ, and hope to be able to determine the arbitrary constants which arise in the integrations by matching the forms of the inner solutions for large ξ to the outer solutions for small θ. The form of the transformation (2.9) shows that it will be most convenient to carry out this matching by balancing corresponding second derivatives, since the relations between these do not involve λ explicitly.

3. Solutions for large conductivity

The first approximations $p_0(\theta)$, $q_0(\theta)$, $P_0(\xi)$, $Q_0(\xi)$ to the solutions are found by taking λ to be infinite in (2.3), (2.4), (2.10) and (2.11). As determined in (2.6) and (2.8)

$$p_0(\theta) = q_0(\theta) = B(\theta). \tag{3.1}$$

The form of the substitution (2.9) permits no change in the boundary conditions (2.5) at $\theta = 0$, if $P_0(\xi)$ and $Q_0(\xi)$ are to be independent of λ. Equation (2.10) becomes

$$P_0''' = 0, \tag{3.2}$$

and hence

$$P_0(\xi) = \tfrac{1}{2}A\xi^2, \tag{3.3}$$

where A is a constant. For small θ, $p_0'' \doteq B''(0)$ and the solutions will match as required if

$$A = B''(0) = 1{\cdot}32823. \tag{3.4}$$

Equation (2.11) now becomes

$$Q_0'' + \tfrac{1}{2}A\xi^2 Q_0' - A\xi Q_0 = 0, \tag{3.5}$$

and the solution for which $Q_0''(\infty) = A$, as required to match with q_0, is

$$Q_0(\xi) = K\xi\, {}_1F_1(-\tfrac{1}{3}, \tfrac{4}{3}, -\tfrac{1}{6}A\xi^3), \tag{3.6}$$

where ${}_1F_1$ is the confluent hypergeometric function and

$$K = \tfrac{1}{2}\frac{(\frac{2}{3})!}{(\frac{1}{3})!}A^{\frac{2}{3}}6^{\frac{1}{3}} = 1{\cdot}1098. \tag{3.7}$$

This shows that $Q_0'(0) = K$.

The asymptotic form of the confluent hypergeometric function for ξ large shows that

$$Q_0 \sim \tfrac{1}{2}A\xi^2 + \tfrac{2}{3}\xi^{-1} + \ldots, \tag{3.8}$$

which requires that for θ small

$$q = \tfrac{1}{2}A\theta^2 + \tfrac{2}{3}\lambda^{-1}\theta^{-1} + \ldots. \tag{3.9}$$

Likewise for θ small

$$B(\theta) = \tfrac{1}{2}A\theta^2 - \tfrac{1}{120}A^2\theta^5 + \ldots, \tag{3.10}$$

and hence for ξ large

$$P, Q \sim \tfrac{1}{2}A\xi^2 - \tfrac{1}{120}A^2\lambda^{-1}\xi^5 + \ldots. \tag{3.11}$$

These expressions indicate the nature of the extra terms which must be added to the inner and outer solutions in order to improve the matching. In fact rather more is needed. The appropriate expansions are

$$\left.\begin{aligned} p(\theta) &= p_0(\theta) + \lambda^{-1}\log\lambda\, p_1(\theta) + \lambda^{-1}p_2(\theta) + \ldots, \\ P(\xi) &= P_0(\xi) + \lambda^{-1}\log\lambda\, P_1(\xi) + \lambda^{-1}P_2(\xi) + \ldots, \end{aligned}\right\} \tag{3.12}$$

and similarly for $q(\theta)$ and $Q(\xi)$. The functions occurring in these expansions are independent of λ but do involve the parameter β. The necessity for including terms in $\lambda^{-1}\log\lambda$ is seen from a study of the appropriate equations, which are obtained by equating to zero the coefficients of successive powers of λ in (2.3), (2.4), (2.10) and (2.11). The equations are as follows:

$$(1-\beta)p_1'''+p_0p_1''+p_0''p_1-\beta q_0q_1''-\beta q_0''q_1=0, \tag{3.13}$$

$$p_0q_1'-p_0'q_1+p_1q_0'-p_1'q_0=0, \tag{3.14}$$

$$P_1'''=0, \tag{3.15}$$

$$Q_1''+P_0Q_1'-P_0'Q_1+P_1Q_0'-P_1'Q_0=0, \tag{3.16}$$

$$(1-\beta)p_2'''+p_0p_2''+p_0''p_2-\beta q_0q_2''-\beta q_0''q_2=0, \tag{3·17}$$

$$q_0''+p_0q_2'-p_0'q_2+p_2q_0'-p_2'q_0=0, \tag{3.18}$$

$$(1-\beta)P_2'''+P_0P_0''-\beta Q_0Q_0''=0, \tag{3.19}$$

$$Q_2''+P_0Q_2'-P_0'Q_2+P_2Q_0'-P_2'Q_0=0. \tag{3.20}$$

Let us examine the behaviour of (3.19) for large ξ. From (3.3) and (3.8),

$$P_0P_0''-\beta Q_0Q_0''\sim\tfrac{1}{2}A^2(1-\beta)\xi^2-\tfrac{4}{3}A\beta\xi^{-1}$$

and hence

$$P_2''\sim-\tfrac{1}{6}A^2\xi^3+\tfrac{4}{3}A\frac{\beta}{1-\beta}\log\xi+C_2, \tag{3.21}$$

where C_2 is a constant. The first term is precisely as demanded by (3.11). A similar inspection of (3.20) reveals that Q_2 must also contain a logarithmic term. Use of (3.3), (3.8) and (3.21) shows that for large ξ

$$Q_2''\sim-\tfrac{1}{6}A^2\xi^3+\left(\frac{4}{3}\frac{\beta}{1-\beta}+\frac{8}{15}\right)A\log\xi+D_2. \tag{3.22}$$

Without the presence of the term in $\log\xi$ the coefficient of ξ^3 in (3.20) cannot be zero. Studies of (3.17) and (3.18) show in the same way that for θ small

$$p_2''\simeq\tfrac{4}{3}A\frac{\beta}{1-\beta}\log\theta+c_2, \tag{3.23}$$

$$q_2''\simeq\tfrac{4}{3}\theta^{-3}+\left(\frac{4}{3}\frac{\beta}{1-\beta}+\frac{8}{15}\right)A\log\theta+d_2. \tag{3.24}$$

The first term of (3.24) is in agreement with (3.9). The implication of (3.23) is that for ξ large $P''(\xi)$ must have a contribution

$$\left\{\tfrac{4}{3}A\frac{\beta}{1-\beta}(\log\xi-\tfrac{1}{3}\log\lambda)+c_2\right\}\lambda^{-1}=-\tfrac{4}{9}A\frac{\beta}{1-\beta}\lambda^{-1}\log\lambda+\left(\tfrac{4}{3}A\frac{\beta}{1-\beta}\log\xi+c_2\right)\lambda^{-1}. \tag{3.25}$$

The first term demonstrates that the expansion must include terms in $\lambda^{-1}\log\lambda$ if the inner and outer solutions are to balance. The last term is satisfied by (3.21) provided that $C_2=c_2$. Similarly, we deduce from (3.24) that $D_2=d_2$, and that $Q''(\xi)$ must have a contribution

$$-\left(\frac{4}{9}\frac{\beta}{1-\beta}+\frac{8}{45}\right)A\lambda^{-1}\log\lambda. \tag{3.26}$$

We now turn to equations (3.13) to (3.16). The only solution of (3.13) and (3.14) satisfying the boundary conditions is $p_1 = q_1 = 0$. The solution of (3.15) which is in agreement with (3.25) is

$$P_1 = -\tfrac{2}{9}A\frac{\beta}{1-\beta}\xi^2. \tag{3.27}$$

Equation (3.16) may then be written as

$$Q_1'' + \tfrac{1}{2}A\xi^2 Q_1' - A\xi Q_1 = \frac{4}{9}\frac{\beta}{1-\beta}Q_0'', \tag{3.28}$$

using (3.5). A particular integral of (3.28) is

$$Q_1 = \frac{4}{27}\frac{\beta}{1-\beta}\xi Q_0',$$

and a complementary function is $Q_1 = Q_0$. Both of these satisfy the boundary condition $Q_1(0) = 0$, and in view of (3.26) the required solution is

$$Q_1 = \frac{4}{27}\frac{\beta}{1-\beta}(\xi Q_0' - 5Q_0) - \tfrac{8}{45}Q_0, \tag{3.29}$$

so that

$$Q_1'(0) = -\left(\frac{16}{27}\frac{\beta}{1-\beta} + \frac{8}{45}\right)K. \tag{3.30}$$

To complete this stage of the approximation the equations (3.17) to (3.20) were integrated numerically. Care was needed owing to the logarithmic behaviour of the functions, but the expressions (3.21) to (3.24) were of great assistance, and the work was shortened by the fact that all the equations have simple complementary functions. The integration of (3.17) and (3.18) under the boundary conditions

$$p_2(0) = p_2'(0) = q_2(0) = p_2'(\infty) = q_2'(\infty) = 0$$

determined the constants c_2 and d_2, and (3.19) and (3.20) were then integrated with boundary conditions

$$P_2(0) = P_2'(0) = Q_2(0) = 0, \quad P_2''(\infty) = c_2, \quad Q_2''(\infty) = d_2.$$

The results of chief importance were

$$P_2''(0) = 0{\cdot}577\frac{\beta}{1-\beta}A, \tag{3.31}$$

$$Q_2'(0) = \left(0{\cdot}557\frac{\beta}{1-\beta} - 0{\cdot}026\right)K. \tag{3.32}$$

Finally we may inquire what is the dependence on λ of the next most important terms in the expansion (3.12). It is clear that contributions in $\lambda^{-2}\log^2\lambda$ are present in equations (2.10) and (2.11), so the next terms must be of at least this order of magnitude. An inspection of the equations which govern these terms reveals no logarithmic or other awkward behaviour, so we conclude that the next terms in (3.12) are indeed multiples of $\lambda^{-2}\log^2\lambda$.

The most important physical quantities to be estimated from our analysis

are the skin friction τ_W at the plate and the surface value H_l of the tangential component of magnetic intensity. The results are

$$\tau_W = \nu\rho\left(\frac{\partial u}{\partial y}\right)_{y=0} = \tfrac{1}{4}\rho\left(\frac{U_0^3\nu}{x}\right)^{\frac{1}{2}} f''(0) = \tfrac{1}{4}\rho\left(\frac{U_0^3\nu}{x}\right)^{\frac{1}{2}} (1-\beta)^{\frac{1}{2}} P''(0)$$

$$= 0{\cdot}33206\rho\left(\frac{U_0^3\nu}{x}\right)^{\frac{1}{2}} (1-\beta)^{\frac{1}{2}} \left\{1 - 0{\cdot}4444\,\frac{\beta}{1-\beta}\lambda^{-1}\log\lambda + 0{\cdot}577\,\frac{\beta}{1-\beta}\lambda^{-1} + O(\lambda^{-2}\log^2\lambda)\right\}$$

$$= 0{\cdot}33206\rho\left(\frac{U_0^3\nu}{x}\right)^{\frac{1}{2}} (1-\beta)^{\frac{1}{2}} \left\{1 - 0{\cdot}4444\beta\epsilon^{-1}\log\frac{\epsilon}{1-\beta} + 0{\cdot}577\beta\epsilon^{-1} + O(\epsilon^{-2}\log^2\epsilon)\right\}, \tag{3.33}$$

$$H_l = \tfrac{1}{2}H_0 g'(0) = \tfrac{1}{2}H_0\lambda^{-\frac{1}{3}}Q'(0)$$

$$= 0{\cdot}5549H_0\lambda^{-\frac{1}{3}}\left\{1 - \left(0{\cdot}5926\,\frac{\beta}{1-\beta} + 0{\cdot}1778\right)\lambda^{-1}\log\lambda + \left(0{\cdot}557\,\frac{\beta}{1-\beta} - 0{\cdot}026\right)\lambda^{-1} + O(\lambda^{-2}\log^2\lambda)\right\}$$

$$= 0{\cdot}5549H_0(1-\beta)^{\frac{1}{3}}\epsilon^{-\frac{1}{3}}\left\{1 - (0{\cdot}4148\beta + 0{\cdot}1778)\,\epsilon^{-1}\log\frac{\epsilon}{1-\beta} + (0{\cdot}583\beta - 0{\cdot}026)\,\epsilon^{-1} + O(\epsilon^{-2}\log^2\epsilon)\right\}. \tag{3.34}$$

4. Equations for small conductivity

When the electrical conductivity is such that ϵ is small compared with unity a completely fresh start is necessary, though it will be observed that the steps in the analysis have strong points of resemblance to what has gone before. The preliminary transformation of variables given by (2.1) and (2.2) is no longer required, and we revert to the original forms of equations (1.1) and (1.2).

For a non-conducting fluid in which ϵ is zero the solution of (1.2) satisfying the boundary conditions (1.3) is

$$g(\eta) = 2\eta, \tag{4.1}$$

and (1.1) becomes $f''' + ff'' = 0$. As before the required solution is given by the Blasius function

$$f(\eta) = B(\eta). \tag{4.2}$$

When ϵ is small but non-zero (1.2) is not satisfied by (4.1) and (4.2) for large values of η. The asymptotic form of $B(\eta)$ shows that

$$f \sim 2\eta - c \tag{4.3}$$

for η large, where $c = 1{\cdot}7208$. Consequently the second term of (1.2) has the limiting value $-2c\epsilon$, while (1.3) insists that $g''(\infty) = 0$. It is clear that we must introduce a new co-ordinate to discuss the outer part of the boundary layer. Throughout this outer layer f' and g' remain of order unity, in view of (1.3), but the terms of (1.2) must be of comparable magnitude for arbitrarily small ϵ. Accordingly we write

$$\eta = \epsilon^{-\frac{1}{2}}\zeta, \quad f(\eta) = \epsilon^{-\frac{1}{2}}F(\zeta), \quad g(\eta) = \epsilon^{-\frac{1}{2}}G(\zeta). \tag{4.4}$$

Then $f'(\eta) = F'(\zeta), f''(\eta) = \epsilon^{\frac{1}{2}} F''(\zeta)$, etc., and (1.1) and (1.2) become

$$\epsilon F''' + FF'' - \beta GG'' = 0, \tag{4.5}$$

$$G'' + FG' - F'G = 0, \tag{4.6}$$

with boundary conditions $F'(\infty) = G'(\infty) = 2$. When ζ is small the values of F and G must be in accord with the values of f and g for η large, matching being carried out as for the case of large conductivity. The only difference is that the form of transformation given above shows that now it is the first derivatives of the corresponding inner and outer functions which must balance at each stage of the series expansion.

5. Solutions for small conductivity

The first approximations $f_0(\eta)$, $g_0(\eta)$, $F_0(\zeta)$ and $G_0(\zeta)$ are found by taking ϵ to be zero in (1.1), (1.2), (4.5) and (4.6). The required solutions of (4.5) and (4.6) are seen at once to be

$$F_0 = G_0 = 2\zeta. \tag{5.1}$$

Matching these solutions requires no change in the boundary conditions (1.3) at $\eta = \infty$, so, as in (4.1) and (4.2),

$$f_0 = B(\eta), \quad g_0 = 2\eta. \tag{5.2}$$

The only one of these four functions which gives a contribution to later stages of the matching is f_0. As in (4.3), $f_0 \sim 2\eta - c$ and this implies that

$$F = 2\zeta - c\epsilon^{\frac{1}{2}} + \ldots \tag{5.3}$$

for ζ small.

Appropriate forms of expansion turn out to be

$$\left.\begin{aligned} f(\eta) &= f_0(\eta) + \epsilon^{\frac{1}{2}} f_1(\eta) + \epsilon \log \epsilon f_2(\eta) + \epsilon f_3(\eta) + \ldots, \\ F(\zeta) &= F_0(\zeta) + \epsilon^{\frac{1}{2}} F_1(\zeta) + \epsilon \log \epsilon F_2(\zeta) + \epsilon F_3(\zeta) + \ldots, \end{aligned}\right\} \tag{5.4}$$

and similarly for $g(\eta)$ and $G(\zeta)$. The presence of the logarithmic terms will be proved in due course. The terms in $\epsilon^{\frac{1}{2}}$ in (1.1), (1.2), (4.5) and (4.6) lead to the equations

$$f_1''' + f_0 f_1'' + f_0'' f_1 - \beta g_0 g_1'' - \beta g_0'' g_1 = 0, \tag{5.5}$$

$$g_1'' = 0, \tag{5.6}$$

$$F_0 F_1'' + F_0'' F_1 - \beta G_0 G_1'' - \beta G_0'' G_1 = 0, \tag{5.7}$$

$$G_1'' + F_0 G_1' - F_0' G_1 + F_1 G_0' - F_1' G_0 = 0. \tag{5.8}$$

Using (5.1) we can write (5.7) as

$$2\zeta(F_1'' - \beta G_1'') = 0. \tag{5.9}$$

Now $F_1'(\infty) = G_1'(\infty) = 0$, and by (5.3), $F_1(0) = -c$, $G_1(0) = 0$, so (5.9) may be integrated twice to give

$$F_1 = \beta G_1 - c. \tag{5.10}$$

Substituting this result in (5.8) we obtain

$$G_1'' + 2(1-\beta)\zeta G_1' - 2(1-\beta) G_1 = 2c. \tag{5.11}$$

A particular integral of this equation is $G_1 = -c/(1-\beta)$, and the complementary functions are

$$G_1 = \zeta \quad \text{and} \quad G_1 = \exp[-(1-\beta)\zeta^2] - 2(1-\beta)^{\frac{1}{2}}\zeta \operatorname{erfc}(1-\beta)^{\frac{1}{2}}\zeta,$$

where

$$\operatorname{erfc} x = \int_x^\infty e^{-u^2}\,du.$$

The boundary conditions show that the required solution of (5.11) is

$$G_1 = \frac{c}{1-\beta}\{-1 + \exp[-(1-\beta)\zeta^2] - 2(1-\beta)^{\frac{1}{2}}\zeta \operatorname{erfc}(1-\beta)^{\frac{1}{2}}\zeta\}, \tag{5.12}$$

and hence

$$F_1 = \frac{c}{1-\beta}\{-1 + \beta\exp[-(1-\beta)\zeta^2] - 2\beta(1-\beta)^{\frac{1}{2}}\zeta \operatorname{erfc}(1-\beta)^{\frac{1}{2}}\zeta\}. \tag{5.13}$$

Then

$$F_1' = \beta G_1' = -\frac{2c\beta}{(1-\beta)^{\frac{1}{2}}} \operatorname{erfc}(1-\beta)^{\frac{1}{2}}\zeta, \tag{5.14}$$

and in particular

$$F_1'(0) = \beta G_1'(0) = -\frac{\pi^{\frac{1}{2}}c\beta}{(1-\beta)^{\frac{1}{2}}} \tag{5.15}$$

since $\operatorname{erfc} 0 = \frac{1}{2}\pi^{\frac{1}{2}}$. The solution of (5.6) to give the necessary matching is

$$g_1 = -\frac{\pi^{\frac{1}{2}}c\eta}{(1-\beta)^{\frac{1}{2}}}. \tag{5.16}$$

Equation (5.5) reduces to $f_1''' + Bf_1'' + B''f_1 = 0$, and the required solution is

$$f_1 = -\frac{\pi^{\frac{1}{2}}c\beta}{4(1-\beta)^{\frac{1}{2}}}(B + \eta B'). \tag{5.17}$$

We note that

$$g_1'(0) = -\frac{\pi^{\frac{1}{2}}c}{(1-\beta)^{\frac{1}{2}}}, \quad f_1''(0) = -\frac{3}{4}\frac{\pi^{\frac{1}{2}}c\beta}{(1-\beta)^{\frac{1}{2}}}A, \tag{5.18}$$

where A is given by (3.4). The contributions to later terms of the series implied by these results are that for ζ small F has a term $\frac{1}{4}\pi^{\frac{1}{2}}c^2\beta(1-\beta)^{-\frac{1}{2}}\epsilon$, and for η large f has a term $c\beta\eta^2\epsilon$ and g a term $c\eta^2\epsilon$. The last two results follow from the fact that $F_1''(0) = \beta G_1''(0) = 2c\beta$.

The equations which determine the next batch of functions are:

$$f_2''' + f_0 f_2'' + f_0'' f_2 - \beta g_0 g_2'' - \beta g_0'' g_2 = 0, \tag{5.19}$$

$$g_2'' = 0, \tag{5.20}$$

$$F_0 F_2'' + F_0'' F_2 - \beta G_0 G_2'' - \beta G_0'' G_2 = 0, \tag{5.21}$$

$$G_2'' + F_0 G_2' - F_0' G_2 + F_2 G_0' - F_2' G_0 = 0, \tag{5.22}$$

$$f_3''' + f_0 f_3'' + f_0'' f_3 - \beta g_0 g_3'' - \beta g_0'' g_3 + f_1 f_1'' - \beta g_1 g_1'' = 0, \tag{5.23}$$

$$g_3'' + f_0 g_0' - f_0' g_0 = 0, \tag{5.24}$$

$$F_0''' + F_0 F_3'' + F_0'' F_3 - \beta G_0 G_3'' - \beta G_0'' G_3 + F_1 F_1'' - \beta G_1 G_1'' = 0, \tag{5.25}$$

$$G_3'' + F_0 G_3' - F_0' G_3 + F_3 G_0' - F_3' G_0 + F_1 G_1' - F_1' G_1 = 0. \tag{5.26}$$

Equation (5.24) is $g_3'' + 2B - 2\eta B' = 0$, which shows that when η is large $g_3 \sim c\eta^2$,

as predicted above. For large η, (5.23) now gives $f_3''' + (2\eta - c) f_3'' - 4c\beta\eta \sim 0$ which can only be satisfied if $f_3'' \sim 2c\beta + c^2\beta\eta^{-1}$ and hence

$$f_3' \sim 2c\beta\eta + c^2\beta \log \eta. \tag{5.27}$$

The first term is as required for the matching and the second proves (in the same way as for large ϵ) that logarithmic terms must be present in the expansions. Similarly, a study of (5.25) and (5.26) shows that when ζ is small

$$F_3' \doteq c^2\beta \log \zeta, \tag{5.28}$$

but G_3' is bounded. Now $\log \zeta = \log \eta + \frac{1}{2} \log \epsilon$, and so (5.28) implies that an additional contribution

$$f'(\eta) \doteq \tfrac{1}{2} c^2 \beta \epsilon \log \epsilon \tag{5.29}$$

for η large is required to balance the inner and outer solutions.

The only solutions of (5.21) and (5.22) which satisfy the boundary conditions are $F_2 = G_2 = 0$. Also since g_3 and G_3 have no logarithmic terms the required solution of (5.20) is $g_2 = 0$. Equation (5.19) reduces to $f_2''' + Bf_2'' + B''f_2 = 0$, and in view of (5.29) the appropriate solution is

$$f_2 = \tfrac{1}{8} c^2 \beta (B + \eta B'), \tag{5.30}$$

which shows that

$$f_2''(0) = \tfrac{3}{8} c^2 \beta A. \tag{5.31}$$

In the set of equations corresponding to the next stage of the approximation (5.25) and (5.26) can be integrated explicitly, using the known boundary conditions

$$F_3(0) = \tfrac{1}{4}\pi^{\frac{1}{2}} c^2 \beta (1-\beta)^{-\frac{1}{2}}, \quad G_3(0) = F_3'(\infty) = G_3'(\infty) = 0.$$

The values of $F_3'(0)$ and $G_3'(0)$ thus obtained, together with the conditions $f_3(0) = f_3'(0) = g_3(0) = 0$, suffice to determine the required solutions of (5.23) and (5.24), but here, as at the corresponding stage of the work for large conductivity, numerical integration is needed for the first time. As before, simple complementary functions are available. The integrations gave the values

$$f_3''(0) = \left[11{\cdot}814 + 0{\cdot}606 \frac{\beta}{1-\beta} + \tfrac{3}{8} c^2 \log (1-\beta)\right] \beta A, \tag{5.32}$$

$$g_3'(0) = 6{\cdot}056 - 0{\cdot}354 \frac{\beta}{1-\beta}. \tag{5.33}$$

Further terms in the expansions could be calculated if required, but it seems unlikely that the range of values of ϵ for which the series solution gives useful information could be extended significantly without considerable labour. An inspection of the equations governing the next terms of the expansion shows that these are not of greater order of magnitude than $\epsilon^{\frac{3}{2}} \log \epsilon$.

The formulae for τ_W and H_l which follow from the analysis are

$$\begin{aligned} \tau_W &= \tfrac{1}{4}\rho \left(\frac{U_0^3 \nu}{x}\right)^{\frac{1}{2}} f''(0) \\ &= 0{\cdot}33206 \rho \left(\frac{U_0^3 \nu}{x}\right)^{\frac{1}{2}} \left\{1 - 2{\cdot}2875 \frac{\beta}{(1-\beta)^{\frac{1}{2}}} \epsilon^{\frac{1}{2}} + 1{\cdot}1104 \beta\epsilon \log (1-\beta)\epsilon \right. \\ &\qquad \left. + 11{\cdot}814 \beta\epsilon + 0{\cdot}606 \frac{\beta^2}{1-\beta} \epsilon + O(\epsilon^{\frac{3}{2}} \log \epsilon)\right\}, \end{aligned} \tag{5.34}$$

$$\begin{aligned} H_l &= \tfrac{1}{2} H_0 g'(0) \\ &= H_0 \left\{1 - 1{\cdot}5250 (1-\beta)^{-\frac{1}{2}} \epsilon^{\frac{1}{2}} + 3{\cdot}028\epsilon - 0{\cdot}177 \frac{\beta}{1-\beta} \epsilon + O(\epsilon^{\frac{3}{2}} \log \epsilon)\right\}. \end{aligned} \tag{5.35}$$

6. Discussion of results

The chief results of the analysis are contained in equations (3.33), (3.34), (5.34) and (5.35). These give the skin-friction τ_W and the surface value H_t of the tangential component of magnetic intensity as functions of the parameters ϵ and β. As shown in the Appendix the current flow in the boundary layer per unit length of the plate is $H_t - H_0$, so this important quantity is also determined by H_t.

Probably the main interest centres on the forms of the leading terms of each expansion, since these indicate to what extent theories which assume the conductivity to be either infinite or zero are likely to be reliable. The perfect conductivity solutions (2.6) and (2.8) give the correct limiting skin-friction as from (3.33), and give $H_t = 0$. Since the leading term of (3.34) is proportional only to $\epsilon^{-\frac{1}{3}}$ this last result may be inadequate except at very large conductivities. For zero conductivity the solutions (4.1) and (4.2) give correctly the leading terms of (5.34) and (5.35). In each case the first correction term is proportional to $\epsilon^{\frac{1}{2}}$.

For large conductivity the values given by (3.33) and (3.34) should be adequate for all practical purposes (say within 1 %) for $\epsilon > 10$, and should provide useful estimates (say within 10 %) for $\epsilon > 3$. For $\epsilon = 10$, (3.33) gives values of τ_W which are indistinguishable from those shown in figure 2 of **I**, which were obtained by direct numerical integration. The series for small conductivity (5.34) and (5.35) are less efficient. The ratio of the magnitudes of successive groups of terms is $\epsilon^{\frac{1}{2}}$ (ignoring logarithmic factors) compared with ϵ^{-1} for large conductivity, and in addition the numerical coefficients increase rapidly. The series should, however, be entirely adequate for $\epsilon < 0{\cdot}001$ and useful for $\epsilon < 0{\cdot}01$. A comparison with the computed values of τ_W in figure 2 of **I** for $\epsilon = 0{\cdot}005$ shows detectable but small discrepancies.

The formulae (3.33), (3.34), (5.34) and (5.35) each have a singular behaviour at $\beta = 1$, but it would be rash to draw too precise conclusions since in the analysis $1-\beta$ was assumed not to be small. A direct study of the original equations is informative. For any value of ϵ it follows from (1.2) and (1.3) that when η is large $f \sim g \sim 2(\eta - a)$, where a is some constant, and from (1.1) and (1.2) it is now readily shown that

$$f'' \sim b\, e^{-c(\eta-a)^2}, \quad g'' \sim d\, e^{-c(\eta-a)^2}, \tag{6.1}$$

where b and d are constants and c is the algebraically smaller root of the equation

$$c^2 - (1+\epsilon)\, c + (1-\beta)\, \epsilon = 0. \tag{6.2}$$

Both roots are positive for $\beta > 1$, and when $1-\beta$ is small the smaller root is approximately $c = (1-\beta)\,\epsilon/(1+\epsilon)$. This shows that the width of the boundary layer is given by $(1-\beta)\,(\eta-a)^2 = O(1)$, or

$$\frac{y}{x} = O[(1-\beta)^{-\frac{1}{2}} R^{-\frac{1}{2}}], \tag{6.3}$$

where R is the Reynolds number $U_0 x/\nu$. The boundary-layer equations are valid only if y/x is small within the boundary layer, and consequently they cease to hold when $1-\beta = O(R^{-1})$. Incidentally the asymptotic forms given above show

clearly that solutions of the present type cannot exist for $\beta > 1$. Equation (6.2) would then imply that for η large, f'' and g'' increase exponentially with η, which is impossible.

A point which troubled the authors of **I** was that the Oseen analysis predicted that for large finite ϵ the value of τ_W exceeds that for $\epsilon = \infty$, at the same value of β, while their numerical integrations of the full equations showed that in fact τ_W is reduced. The leading correction term in (3.33), that multiplied by $\epsilon^{-1}\log\epsilon$, clearly acts to reduce τ_W. Actually an inspection of the results of the Oseen analysis given in **I** shows that they are very inaccurate for all ϵ, large and small. However, the authors state that their numerical values could be improved by supposing that the convective velocity and magnetic fields, instead of being equal to their free-stream values, are suitably chosen fractions of them. It is not evident that a major improvement over the whole range of the parameters can be achieved in this way, particularly in view of the involved forms of the solutions found above. Failing such an improvement, it seems that the linearized method of analysis is not to be relied on in a problem of this complexity.

Appendix. Derivation of the boundary-layer equations

The equations governing steady incompressible magnetohydrodynamic flow are

$$(\mathbf{q}.\nabla)\,\mathbf{q} = -\frac{1}{\rho}\nabla p + \nu\nabla^2\mathbf{q} + \frac{\mu}{\rho}\mathbf{j}\wedge\mathbf{H}, \tag{A 1}$$

$$\frac{1}{\sigma}\mathbf{j} = \mathbf{E} + \mu\mathbf{q}\wedge\mathbf{H}, \tag{A 2}$$

$$\mathbf{j} = \operatorname{curl}\mathbf{H}, \tag{A 3}$$

$$\operatorname{div}\mathbf{q} = \operatorname{div}\mathbf{H} = \operatorname{div}\mathbf{E} = \operatorname{curl}\mathbf{E} = 0, \tag{A 4}$$

in m.k.s. units, where p is the pressure, $\mathbf{q}$ the velocity, $\mathbf{j}$ the current, and $\mathbf{H}$ and $\mathbf{E}$ the magnetic and electric intensities. The boundary conditions in our problem are that $\mathbf{q} = 0$ and $H_y = 0$ on the plate $y = 0$, $x > 0$, and at a large distance $p = p_0$, $\mathbf{q} = U_0\mathbf{i}$, $\mathbf{H} = H_0\mathbf{i}$. (Some comments on the plate condition $H_y = 0$ are made below.) The electric field $\mathbf{E}$ may be taken to be zero everywhere, and using (A 3) equations (A 1) and (A 2) may be written as

$$(\mathbf{q}.\nabla)\,\mathbf{q} = -\frac{1}{\rho}\nabla(p + \tfrac{1}{2}\mu\mathbf{H}^2) + \nu\nabla^2\mathbf{q} + \frac{\mu}{\rho}(\mathbf{H}.\nabla)\,\mathbf{H}, \tag{A 5}$$

$$\mathbf{q}\wedge\mathbf{H} = \frac{1}{\sigma\mu}\operatorname{curl}\mathbf{H}. \tag{A 6}$$

We require two-dimensional solutions and in view of (A 4) we may look for these in the forms

$$\mathbf{q} = \operatorname{curl}\psi(x,y)\,\mathbf{k}, \quad \mathbf{H} = \operatorname{curl}A(x,y)\,\mathbf{k}, \tag{A 7}$$

where $\mathbf{k}$ is a unit vector in the z-direction.

On the usual boundary-layer assumption that a rate of change in the y-direction is of a greater order of magnitude than one in the x-direction, the y-component of (A 5) shows that $p + \frac{1}{2}\mu\mathbf{H}^2$ has negligible variation across the boundary layer, and so may be taken to have the constant value $p_0 + \frac{1}{2}\mu H_0^2$ everywhere.

The boundary-layer approximations to the x-component of (A 5) and to (A 6) then give

$$\frac{\partial\psi}{\partial y}\frac{\partial^2\psi}{\partial x\partial y}-\frac{\partial\psi}{\partial x}\frac{\partial^2\psi}{\partial y^2}=\nu\frac{\partial^3\psi}{\partial y^3}+\frac{\mu}{\rho}\left(\frac{\partial A}{\partial y}\frac{\partial^2 A}{\partial x\partial y}-\frac{\partial A}{\partial x}\frac{\partial^2 A}{\partial y^2}\right), \tag{A 8}$$

$$\frac{\partial\psi}{\partial y}\frac{\partial A}{\partial x}-\frac{\partial\psi}{\partial x}\frac{\partial A}{\partial y}=\frac{1}{\sigma\mu}\frac{\partial^2 A}{\partial y^2}. \tag{A 9}$$

Guided by the form of the Blasius solution for a non-conducting fluid we next write

$$\psi=(U_0\nu x)^{\frac{1}{2}}f(\eta),\quad A=H_0(\nu x/U_0)^{\frac{1}{2}}g(\eta), \tag{A 10}$$

where $\eta=\frac{1}{2}(U_0/\nu x)^{\frac{1}{2}}y$. Equations (A 8) and (A 9) become ordinary differential equations in η, with the forms given in (1.1) and (1.2). We see also from (A 7) and (A 10) that the velocity and magnetic field components are as given in (1.5) and (1.6), and that the boundary conditions stated above imply the conditions (1.3). The boundary-layer approximation to (A 3) is that $\mathbf{j}=j\mathbf{k}$, where

$$j=-\frac{\partial^2 A}{\partial y^2}=-\tfrac{1}{4}H_0\left(\frac{U_0}{\nu x}\right)^{\frac{1}{2}}g''(\eta), \tag{A 11}$$

and the total current in the boundary layer, flowing parallel to the edge of the plate, is

$$\int_0^\infty j\,dy=\left[-\frac{\partial A}{\partial y}\right]_0^\infty=H_l-H_0 \tag{A 12}$$

per unit distance in the x-direction, where H_l is the value of H_x at the plate $y=0$.

The boundary condition $H_y=0$ on $y=0$, $x>0$ is obviously essential for an infinitely thin plate with a similar boundary layer on its lower side. By symmetry the values of H_y at $y=0$ on the upper and lower surfaces are equal and opposite, and the necessary continuity of μH_y across the plate surfaces can be achieved only if $H_y=0$ at the plate. But in fact the resulting form of solution is of wider applicability. Equation (1.6) shows that when $y=0$, $H_x=H_l=\frac{1}{2}H_0g'(0)$ which is independent of x. Consequently for a plate of arbitrary thickness all the magnetic equations are satisfied if $\mathbf{H}$ has the constant value $H_l\mathbf{i}$ throughout the plate.

Finally it may be noted that for the boundary-layer approximation to be appropriate it is not sufficient that the Reynolds number $R=U_0x/\nu$ shall be large. By comparing the forms of (A 9) and (A 8), or by studying the width of the outer layer for small conductivity as found in § 5, we see that it is also necessary that the magnetic Reynolds number $R_M=\epsilon R=U_0x\sigma\mu$ shall be large compared with unity. This sets a lower limit to the conductivities for which the results of this paper are applicable.

REFERENCES

Carrier, G. F. & Greenspan, H. P. 1960 *J. Fluid Mech.* **7**, 22.

Greenspan, H. P. 1960 *Phys. Fluids* **3**, 581.

Greenspan, H. P. & Carrier, G. F. 1959 *J. Fluid Mech.* **6**, 77 (**I**).

Morgan, G. W., Pipkin, A. C. & Warner, W. H. 1958 *J. Aero. Sci.* **25**, 173.

Morgan, G. W. & Warner, W. H. 1956 *J. Aero. Sci.* **23**, 937.

Singularities of attached shock waves in steady axially symmetric flow

By HENRI CABANNES

Professeur à la Faculté des Sciences de Paris

AND CLAUDE STAEL

Ingénieur des Arts et Manufactures

(Received 17 October 1960)

An I.B.M. 704 electronic computer was used to integrate the differential equations, which determine the shock singularity, when the velocity after the shock on a body is subsonic. The results are given in twenty-two cases corresponding to three different bodies; the procedure followed was outlined in a previous paper (Cabannes 1952).

1. Introduction

We consider a body of revolution placed in a compressible fluid; the viscosity and thermal conductivity are neglected. The fluid is moving at infinity with a uniform supersonic velocity $\bar{q}$ parallel to the axis of revolution Ox. A shock wave is formed in front of the obstacle; it limits the region in which the flow is uniform. We assume that the nose of the body is a cone of revolution with semi-angle at the apex θ_s, and that the angle θ_s has been chosen such that a shock wave could be attached at the point 0 of the body. For small values of Mach number, $M < M_0(\theta_s)$, the shock wave is detached; for large values of Mach number, $M \geqslant M^{**}(\theta_s)$, the flow after the shock is supersonic; for intermediary values, $M_0(\theta_s) \leqslant M < M^{**}(\theta_s)$, the flow after the shock is subsonic, partially or totally.

When the body is an infinite cone of revolution, the flow after the shock is conical and the shock wave is itself an infinite cone of revolution. Since we assume that only the nose of the body is a cone, the body meridian possesses a rectilinear segment OI, up to the point I, at which point the slope of the tangent, or one of the higher derivatives, is discontinuous; the presence of the discontinuity perturbs the conical flow. Two cases are to be distinguished.

(1) When the speed on the cone is subsonic, that is, for $M_0(\theta_s) \leqslant M < M^{**}(\theta_s)$, the perturbation is propagated in all the region of subsonic flow and then in all the supersonic region if the latter exists. The conical flow is not produced in any region of space and the meridian of the shock wave does not possess a rectilinear segment.

(2) When the speed on the cone is supersonic, that is, for $M^{**}(\theta_s) < M$, the perturbation is propagated along a characteristic IA which meets the shock wave meridian at a point A; this meridian possesses a rectilinear segment OA and a region of space in which conical flow exists.

In the work which follows, we consider only the first case. We locate the position of a point P in a semi-meridian plane by the polar co-ordinates $OP = r$ and $xOP = \theta$ (see figure 1). By means of these co-ordinates, the equation of the semi-cone in which the body terminates is written in the form (1), and the equation of the shock wave in the neighbourhood of the point O is written in the form (2). Thus

$$\text{(body)} \quad \theta = \theta_s, \tag{1}$$

$$\text{(shock)} \quad \theta = \theta_w + Ar^m + \ldots. \tag{2}$$

The angle θ_w is determined by the theory of axially symmetric flow (Kopal 1947); it depends on the Mach number M and the angle θ_s. The purpose of the following tables is to determine the value of the exponent m; this exponent depends similarly on the Mach number M and the angle θ_s.

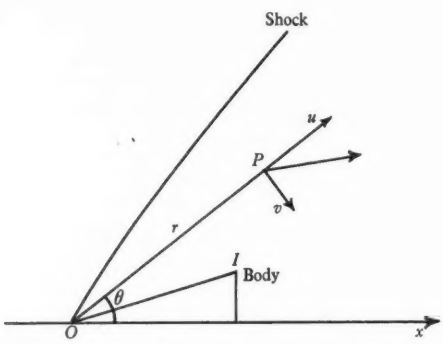

FIGURE 1. Definition of polar co-ordinates.

2. Equations of motion

We designate by u and v the components, in the directions θ and $\theta + \frac{1}{2}\pi$, of the fluid velocity at a point P, by p and ρ the pressure and density of the fluid at this point, and by γ the ratio of the specific heats of the fluid. The four functions u, v, p and ρ of the two variables r and θ satisfy the following partial differential equations which express the fundamental law of dynamics, the conservation of mass and the conservation of energy:

$$\left.\begin{aligned} u\frac{\partial u}{\partial r} + \frac{v}{r}\frac{\partial u}{\partial \theta} - \frac{v^2}{r} + \frac{1}{\rho}\frac{\partial p}{\partial r} &= 0, \\ u\frac{\partial v}{\partial r} + \frac{v}{r}\frac{\partial v}{\partial \theta} + \frac{uv}{r} + \frac{1}{r\rho}\frac{\partial p}{\partial \theta} &= 0, \\ \frac{\partial}{\partial r}(r^2\rho u \sin\theta) + \frac{\partial}{\partial \theta}(r\rho v \sin\theta) &= 0, \\ u\frac{\partial}{\partial r}(p\rho^{-\gamma}) + \frac{v}{r}\frac{\partial}{\partial \theta}(p\rho^{-\gamma}) &= 0. \end{aligned}\right\} \tag{3}$$

We attempt to satisfy the preceding equations using functions expanded in series of increasing powers of r; the coefficients depend only on θ. Thus

$$\left.\begin{aligned} u(r,\theta) &= u_0(\theta)+2Ar^m u_m(\theta)+\ldots,\\ v(r,\theta) &= v_0(\theta)+2Ar^m v_m(\theta)+\ldots,\\ p(r,\theta) &= p_0(\theta)+2Ar^m p_m(\theta)+\ldots,\\ \rho(r,\theta) &= \rho_0(\theta)+2Ar^m \rho_m(\theta)+\ldots. \end{aligned}\right\} \tag{4}$$

By substitution of the preceding expansions into equations (3) and by identification according to successive powers of r, one obtains an infinite set of differential equations. The equations (3) permit a first integral deduced from the theorem of Bernoulli. Since the limiting speed q_m is constant in front of the shock and continuous across the shock, one can take the following equation to be valid throughout the fluid

$$\frac{2\gamma}{\gamma-1}\frac{p}{\rho}+u^2+v^2=q_m^2. \tag{5}$$

We now introduce the positive function $a_0(\theta)$ defined by

$$a_0^2=\frac{\gamma p_0}{\rho_0}=\tfrac{1}{2}(\gamma-1)\,(q_m^2-u_0^2-v_0^2). \tag{6}$$

The differential equations deduced from equations (3) can be written in the following form. Using given initial conditions, the functions with index 0 can be calculated from equations (7) below, whereas the functions with index m can then be calculated, when m has been chosen, from equations (8); the prime indicates differentiation with respect to θ;

$$\left.\begin{aligned} u_0'-v_0&=0,\\ v_0'\left(1-\frac{a_0^2}{v_0^2}\right)+u_0\left(1-2\frac{a_0^2}{v_0^2}\right)-\frac{a_0^2}{v_0}\cot\theta&=0,\\ \frac{\rho_0'}{\rho_0}\left(1-\frac{a_0^2}{v_0^2}\right)+\frac{u_0}{v_0}+\cot\theta&=0,\\ \frac{p_0'}{p_0}=\gamma\frac{\rho_0'}{\rho_0}&=0; \end{aligned}\right\} \tag{7}$$

$$\left.\begin{aligned} u_m'v_0+mu_mu_0-v_mv_0+m\frac{a_0^2}{\gamma}\frac{p_m}{p_0}&=0,\\ v_m'+v_0\left(\frac{\rho_m}{\rho_0}\right)'+(m+2)\,u_m+\left(\cot\theta+\frac{\rho_0'}{\rho_0}\right)v_m+mu_0\frac{\rho_m}{\rho_0}&=0,\\ mu_0\left(\frac{p_m}{p_0}-\gamma\frac{\rho_m}{\rho_0}\right)+v_0\left(\frac{p_m}{p_0}-\gamma\frac{\rho_m}{\rho_0}\right)'&=0,\\ \frac{p_m}{p_0}-\frac{\rho_m}{\rho_0}+(\gamma-1)\frac{u_0u_m+v_0v_m}{a_0^2}&=0. \end{aligned}\right\} \tag{8}$$

3. Conditions on the body

The body is formed by the stream surface extending from the point 0. By requiring that the differential equation of the stream surfaces

$$\frac{dr}{u}=\frac{r\,d\theta}{v} \tag{9}$$

be satisfied by the function (1), one obtains the conditions

$$v_0(\theta_s) = 0, \tag{10a}$$

$$v_m(\theta_s) = 0. \tag{10b}$$

4. Conditions on the shock wave

A certain number of conditions must be satisfied across the shock wave. These conditions which express the law of conservation of mass and conservation of energy are stated by the following equations, in which $\bar{c}$, $\bar{p}$ and $\bar{\rho}$ denote the speed of sound, the pressure and density before shock, β the angle which the tangent to the shock wave meridian makes with the axis of revolution, and $\mathscr{M}$ denotes the normal Mach number $M\sin\beta$:

$$\left.\begin{aligned} u &= \bar{q}\cos\theta + \frac{2\bar{c}}{\gamma+1}\left(\mathscr{M}-\frac{1}{\mathscr{M}}\right)\sin(\beta-\theta),\\ v &= -\bar{q}\sin\theta - \frac{2\bar{c}}{\gamma+1}\left(\mathscr{M}-\frac{1}{\mathscr{M}}\right)\cos(\beta-\theta),\\ \frac{p}{\bar{p}} &= \frac{2\gamma}{\gamma+1}\mathscr{M}^2 - \frac{\gamma-1}{\gamma+1},\\ \frac{\bar{\rho}}{\rho} &= \frac{2}{\gamma+1}\frac{1}{\mathscr{M}^2} + \frac{\gamma-1}{\gamma+1}. \end{aligned}\right\} \tag{11}$$

The Mach number M is expressed as a function of the speed $\bar{q}$ by

$$M^2 = \frac{2}{\gamma-1}\frac{\bar{q}^2}{q_m^2-\bar{q}^2}. \tag{12}$$

By considering that the relations (11) are satisfied identically on the shock wave, one obtains, for $\theta = \theta_w$,

$$\left.\begin{aligned} u_0(\theta_w) &= \bar{q}\cos\theta_w,\\ v_0(\theta_w) &= \frac{\gamma-1}{\gamma+1}\frac{\bar{q}^2\cos^2\theta_w - q_m^2}{\bar{q}\sin\theta_w},\\ \frac{p_0(\theta_w)}{\bar{p}} &= \frac{2\gamma}{\gamma+1}M^2\sin^2\theta_w - \frac{\gamma-1}{\gamma+1},\\ \frac{\bar{\rho}}{\rho_0(\theta_w)} &= \frac{2}{\gamma+1}\frac{1}{M^2\sin^2\theta_w} + \frac{\gamma-1}{\gamma+1}, \end{aligned}\right\} \tag{13}$$

$$\left.\begin{aligned} 2u_m + (m+1)\,u_0\tan\theta_w + (m+1)\,v_0 &= 0,\\ 2v_m + \frac{m(\gamma-3)-4}{\gamma+1}u_0 + \frac{m(\gamma+1)+2}{\gamma+1}v_0\cot\theta_w &= 0,\\ \frac{p_m}{p_0} &= \frac{\gamma}{\gamma+1}\cot\theta_w - (m+1)\frac{2\gamma}{\gamma+1}\frac{u_0 v_0}{a_0^2},\\ \frac{\rho_m}{\rho_0} &= \frac{m(\gamma+1)+\gamma+2}{\gamma+1}\cot\theta_w + (m+1)\frac{\gamma-1}{\gamma+1}\frac{u_0}{v_0}. \end{aligned}\right\} \tag{14}$$

5. Method of integration

The system (8) has two first integrals, which can be written in the following form, where α denotes a constant, determined by the conditions on the shock wave,

$$\left.\begin{aligned}\frac{p_m}{p_0} &= -\gamma\frac{u_0u_m+v_0v_m}{a_0^2}-\alpha\exp\left\{\int_\theta^{\theta_w}\frac{mu_0}{v_0}d\theta\right\},\\ \frac{\rho_m}{\rho_0} &= -\frac{u_0u_m+v_0v_m}{a_0^2}-\alpha\exp\left\{\int_\theta^{\theta_w}\frac{mu_0}{v_0}d\theta\right\},\end{aligned}\right\} \tag{15}$$

with

$$\frac{\alpha}{\gamma(m+1)}=\frac{u_0^2(\theta_w)}{q_m^2-u_0^2(\theta_w)}\frac{\tan\theta_w}{\gamma-1}-\frac{\gamma+3}{\gamma+1}\frac{\cot\theta_w}{\gamma+1}.$$

Thus the system (8) is reduced to a system of two linear non-homogeneous differential equations, that is,

$$\left.\begin{aligned}u_m'-(m+1)v_m &= \frac{m}{\gamma}\frac{a_0^2}{v_0}\alpha\exp\left\{\int_\theta^{\theta_w}\frac{mu_0}{v_0}d\theta\right\},\\ \left(1-\frac{v_0^2}{a_0^2}\right)v_m'+Au_m+Bv_m &= \frac{m}{\gamma}u_0\alpha\exp\left\{\int_\theta^{\theta_w}\frac{mu_0}{v_0}d\theta\right\},\end{aligned}\right\} \tag{16}$$

where

$$\left.\begin{aligned}A &= m+2-\frac{mu_0^2+v_0^2}{a_0^2}+(\gamma-1)\frac{u_0v_0^2}{a_0^2}\frac{u_0+v_0\cot\theta}{a_0^2-v_0^2},\\ B &= \frac{2u_0v_0+(a_0^2+v_0^2)\cot\theta}{a_0^2-v_0^2}+(\gamma-1)\frac{v_0^3}{a_0^2}\frac{u_0+v_0\cot\theta}{a_0^2-v_0^2}-2m\frac{u_0v_0}{a_0^2}.\end{aligned}\right\} \tag{17}$$

The general solution is the sum of a particular solution of the complete system plus the general solution of the homogeneous system. For the homogeneous system, all the points of the interval $\theta_s\leqslant\theta\leqslant\theta_w$ are ordinary points; the right-hand sides of (16) are infinite at the extremity $\theta=\theta_s$ of the interval.

In the neighbourhood of the body, we can write the following series expansions

$$\begin{aligned}u_0(\theta) &= u_0(\theta_s)\left\{1-(\theta-\theta_s)^2+\cot\theta_s\frac{(\theta-\theta_s)^3}{3}+\ldots\right\},\\ v_0(\theta) &= u_0(\theta_s)\{-2(\theta-\theta_s)+\cot\theta_s(\theta-\theta_s)^2+\ldots\},\\ \exp\left\{\int_\theta^{\theta_w}\frac{mu_0}{v_0}d\theta\right\} &= O(\theta-\theta_s)^{\frac{1}{2}m},\\ u_m(\theta) &= O(\theta-\theta_s)^{\frac{1}{2}m},\\ v_m(\theta) &= O(\theta-\theta_s)^{\frac{1}{2}m}.\end{aligned}$$

For positive values of the exponent m, the functions u_m, v_m, p_m and ρ_m therefore have finite values on the body. Thus the presence of the singularity in the system (8) for $\theta=\theta_s$ does not introduce any complication in the numerical integration. This singularity was studied by Shen & Lin (1951) for the case $m=1$. Because they neglected the existence of one of the first integrals, they were led to an indicial equation of third degree which had a double root, and therefore they found a logarithmic term. In reality, the indicial equation is of second degree with two distinct roots. Lin has shown in a private communication that the coefficient of the logarithmic term is zero, which brings the results of Shen & Lin (1951) into accord with those of Cabannes (1951*b*).

To begin the calculations for fixed γ, the angle θ_s of the body is assumed and the two first equations of (7) are integrated starting from $\theta = \theta_s$, taking $v_0(\theta_s) = 0$ and selecting an arbitrary value of $u_0(\theta_s)$. The shock wave is reached when

$$\frac{\gamma-1}{\gamma+1}(q_m^2 - u_0^2) + u_0 v_0 \tan\theta = 0; \tag{18}$$

at this point we have $\theta = \theta_w$, and the Mach number M before the shock is given by the relation

$$M^2 = \frac{2}{\gamma-1}\frac{u_0^2(\theta_w)}{q_m^2\cos^2\theta_w - u_0^2(\theta_w)}. \tag{19}$$

The functions p_0 and ρ_0 are computed starting from the shock conditions by means of the relation (6) and the first integral $p_0\rho_0^{-\gamma} = \text{const.}$ The functions of index zero being known, the functions of index m are calculated, for an assumed

θ_s	$\frac{u_0(\theta_s)}{q_m}$	θ_w	M	m
10°	0·37	80·056	1·05398	−0·25869
	0·38	75·790	1·05639	0·84264
	0·39	71·640	1·07239	4·18764
	0·40	67·958	1·09481	18·293
20°	0·33	72·869	1·21221	−0·16049
	0·34	70·477	1·21171	0·15595
	0·35	68·096	1·21866	0·61447
	0·36	65·787	1·23144	1·30671
	0·37	63·584	1·24873	2·42736
	0·38	61·500	1·26954	4·45732
	0·39	59·539	1·29315	8·93831
	0·40	57·697	1·31906	25·10423
30°	0·31	69·419	1·48062	−0·04791
	0·32	67·763	1·48228	0·18019
	0·33	66·146	1·48959	0·47582
	0·34	64·577	1·50171	0·86948
	0·35	63·068	1·51792	1·41366
	0·36	61·622	1·53768	2·20664
	0·37	60·241	1·56053	3·45348
	0·38	58·924	1·58613	5·65570
	0·39	57·670	1·61418	10·41496
	0·40	56·477	1·64449	27·46310

TABLE 1

value of m, by integrating the system (8), starting from the relations (14) which are valid for $\theta = \theta_w$. The computation is completed when the value θ_s is reached; the value $v_m(\theta_s)$ thus obtained is in general different from zero. The computation is repeated with the same values of θ_s, $u_0(\theta_s)$ and γ, and a different value of m; successive approximations are used to obtain the value of m for which $v_m(\theta_s) = 0$. We thus define the exponent m as a function of the angle θ_s, the Mach number M, and the adiabatic constant γ. The computations have been carried out with the help of the I.B.M. 704 electronic computer. The numerical integrations were made by the fourth-order Runge–Kutta method; the step length for the integration was chosen to be equal to one-twentieth of a degree.

6. Numerical results

In the computations, the adiabatic constant was taken to be $\gamma = 1{\cdot}4$. Three cones have been considered with $\theta_s = 10°$, $20°$ and $30°$. The results are given in table 1, the angles θ_w being expressed in degrees, and the results are also plotted in figure 2.

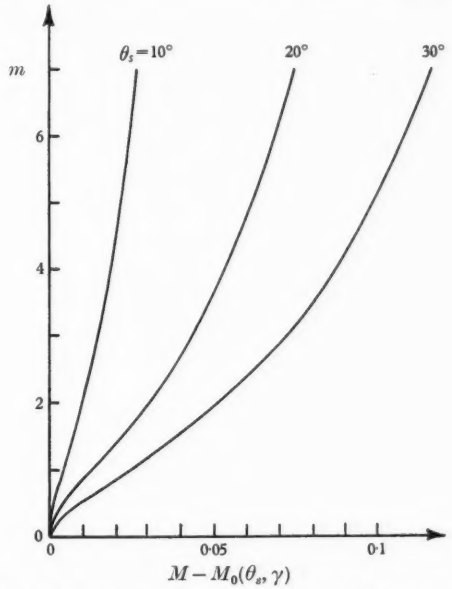

FIGURE 2. Variations of the exponent m for axially symmetric flow.

7. Comparison with the results for plane flow

In the case of plane flow it is possible to calculate the exponent m by means of formulae in finite terms (Cabannes 1951*a*). In the cross-sectional plane of the wedge the axis of symmetry of the wedge is taken as the polar axis and θ_w is the angle between the shock and the polar axis. The equation of the shock in the neighbourhood of the vertex of the wedge can be written, in polar co-ordinates, in the form

$$\theta = \theta_w + Ar^m + \ldots. \tag{20}$$

The exponent m is implicitly defined as a function of the wedge angle θ_s, the Mach number M and the adiabatic constant γ by the formulae

$$\left.\begin{aligned}
\Delta \tan m\phi &= \frac{\gamma+1}{4\sin(\theta_w-\theta_s)\cos(\theta_w-\theta_s)} - \frac{\gamma-1}{2}\cot(\theta_w-\theta_s) - \frac{\gamma+1}{4}(\tan\theta_w - \cot\theta_w),\\
\tan\phi &= \Delta\tan(\theta_w-\theta_s),\\
\frac{1}{1-\Delta^2} &= \sin(\theta_w-\theta_s)\cos(\theta_w-\theta_s)\left\{\frac{\gamma+1}{2}\tan\theta_w - \frac{\gamma-1}{2}\tan(\theta_w-\theta_s)\right\},\\
M^2\sin^2\theta_w &= \frac{\tan\theta_w}{\frac{1}{2}(\gamma+1)\tan(\theta_w-\theta_s) - \frac{1}{2}(\gamma-1)\tan\theta_w}.
\end{aligned}\right\} \tag{21}$$

Thirty-five cases have been computed with $\gamma = 1{\cdot}4$. The results are presented in table 2.

This work was made possible by a research grant, made available to us by the 'Centre Européen de Calcul Scientifique', to whom we wish to express our appreciation.

θ_s	θ_w	M	m
10°	67° 26′	1·4210	0·0000
	67°	1·4211	0·1349
	66°	1·4226	0·5536
	65°	1·4255	1·2697
	65°	1·4297	2·8570
	63°	1·4354	14·7041
	62° 52′	1·4363	∞
20°	64° 54′	1·8400	0·0000
	64° 30′	1·8402	0·1915
	64°	1·8411	0·5080
	63° 30′	1·8426	0·9472
	63°	1·8447	1·5999
	62° 30′	1·8474	2·6812
	62°	1·8507	4·8916
	61° 30′	1·8549	13·6217
	61° 19′	1·8591	∞
30°	64° 48′	2·5192	0·0000
	64° 40′	2·5193	0·1357
	64° 30′	2·5195	0·3362
	64° 20′	2·5198	0·5757
	64° 10′	2·5203	0·8661
	64°	2·5210	1·2255
	63° 50′	2·5218	1·6819
	63° 40′	2·5228	2·2792
	63° 30′	2·5239	3·0979
	63° 20′	2·5252	4·2893
	63° 10′	2·5266	5·3123
	63°	2·5282	9·8407
	62° 50′	2·5299	20·6164
	62° 43′	2·5312	∞
40°	66°	4·4473	0·0000
	65° 55′	4·4481	0·5369
	65° 50′	4·4492	1·0597
	65° 45′	4·4504	2·2032
	65° 41′	4·4514	∞

TABLE 2

REFERENCES

CABANNES, H. 1951*a* Détermination de l'onde de choc attachée lorsque la vitesse aval à la pointe est subsonique. *Publ. Scient. et Tech. du Ministère de l'Air*, **250**, 181–95.

CABANNES, H. 1951*b* Etude de l'onde de choc attachée dans les écoulements de révolution. I. Cas d'un obstacle terminé par une ogive. *Rech. aéro.* **24**, 17–23.

CABANNES, H. 1952 Etude de l'onde de choc attachée dans les écoulements de révolution. II. Cas d'un obstacle terminé par un cône. *Rech. aéro.* **27**, 7–16.

KOPAL, Z. 1947 *Tables of Supersonic Flow Around Cones.* Massachusetts Institute of Technology.

SHEN, S. F. & LIN, C. C. 1951 On the attached curved shock in front of a sharp-nosed symmetrical body placed in a uniform stream. *N.A.C.A. Tech. Note* 2505.

A study of the behaviour of a thin sheet of moving liquid

By D. R. BROWN

The British Iron and Steel Research Association, South Wales Laboratories, Swansea

(Received 10 March 1960 and in revised form 25 October 1960)

An investigation has been carried out on the behaviour of a thin sheet of liquid in connexion with the new method of lacquer application known as 'curtain coating'. A method is described for measuring the velocity of the sheet and an equation deduced for calculating this for a liquid of any viscosity. The minimum liquid flow rate required to maintain a stable sheet is discussed, and some effects of the impingement of the sheet on a rapidly moving surface are described.

1. Introduction

When considering the possible methods of applying protective organic coatings at high speed to continuous steel or tinplate strip, the relatively new process of curtain coating appears very attractive. This process as used at present, for example in the furniture trade, consists of pumping the coating material from a supply tank to a precision built head which has a narrow slot along its lower face; the liquid passes through this slot and is formed into a continuous sheet or curtain which falls on to the work pieces as they travel underneath. The coating weight applied varies with the speed of travel of the article through the curtain. For further details of the process see Stein & Podmore (1959) or Bardin (1958).

It was observed that in order to maintain a stable curtain, the rate of flow of liquid through the slot must be above a certain minimum value, hence tending to limit the process to application of thick coatings at reasonable speeds. One objective of this investigation was to determine the physical factors on which the minimum flow rate depends, as well as to study the general behaviour of a liquid in this rather unusual form of a thin moving sheet.

Some interesting work on the disintegration of liquid sheets has recently been carried out by Taylor (1959) and also by Dombrowski & Fraser (1954) and Fraser, Eisenklam & Dombrowski (1957), the latter in connexion with the production of efficient sprays for use in chemical and combustion engineering and agriculture.

2. Experimental technique

The investigation fell naturally into three parts; a study of the behaviour of the liquid in the slot, in the curtain itself, and finally as it impinges on a rapidly moving surface. To study these an adjustable slot of 12 cm length was constructed and a system for pumping liquid through it built up as shown in figure 1. The arrangement was such that the curtain could either fall on to a stationary trough conveniently shaped to allow the liquid to be collected in a flask, or on to the

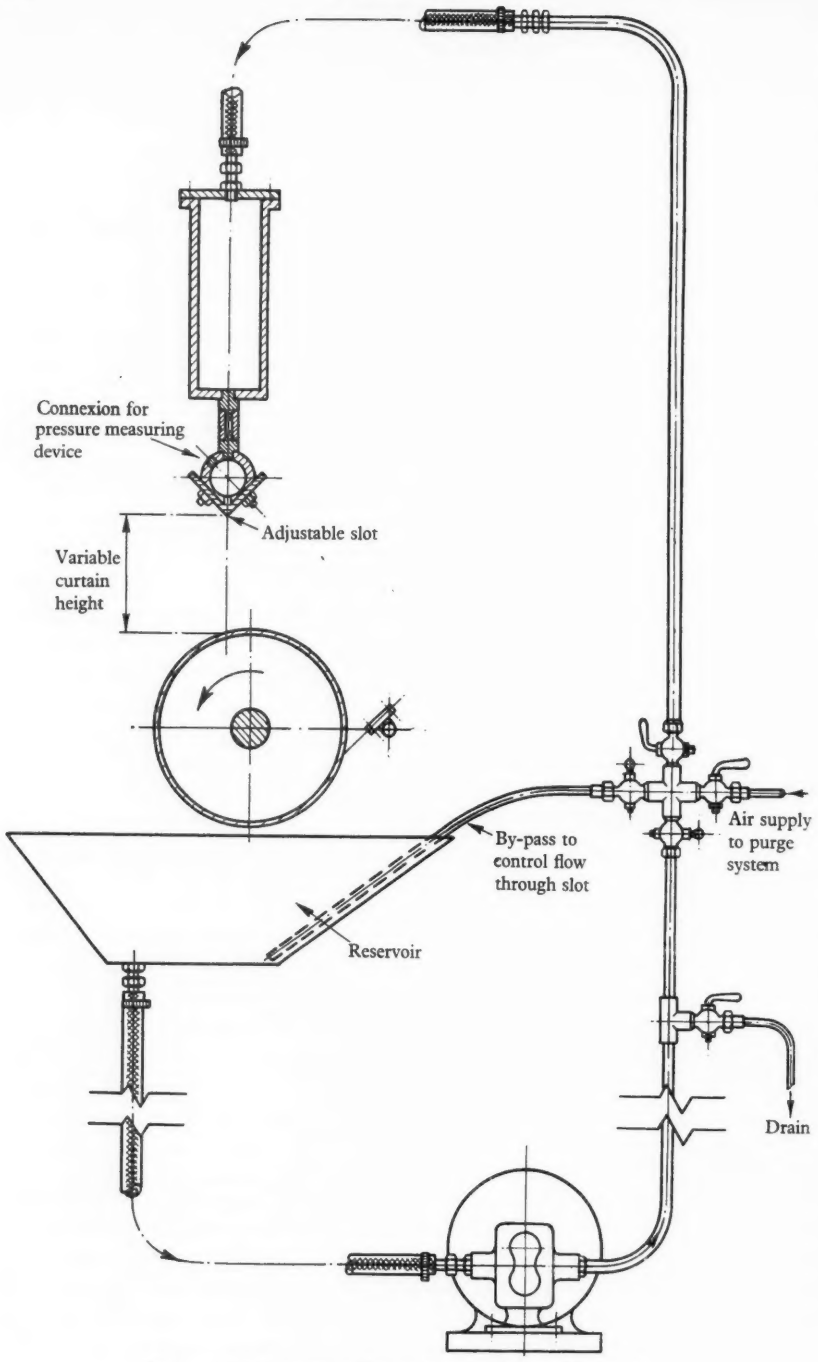

FIGURE 1. Apparatus for producing the liquid curtain.

surface of a roll which could be rotated at peripheral speeds up to 600 cm/sec, and fitted with a scraper blade to remove the liquid.

The liquid used in this work was a lacquer with high solids content, which was thinned to the required viscosity with a high boiling point solvent such as diacetone alcohol. By use of this material a 10:1 range of viscosities was conveniently available. The viscosity was measured by a Ferranti rotation viscometer reading directly in poise and the surface tension by a Cambridge Du Noüy tensiometer calibrated in dyn/cm. As the density of the liquid, determined by a hydrometer, was approximately unity, no more precise measurements were considered necessary and this value was assumed throughout.

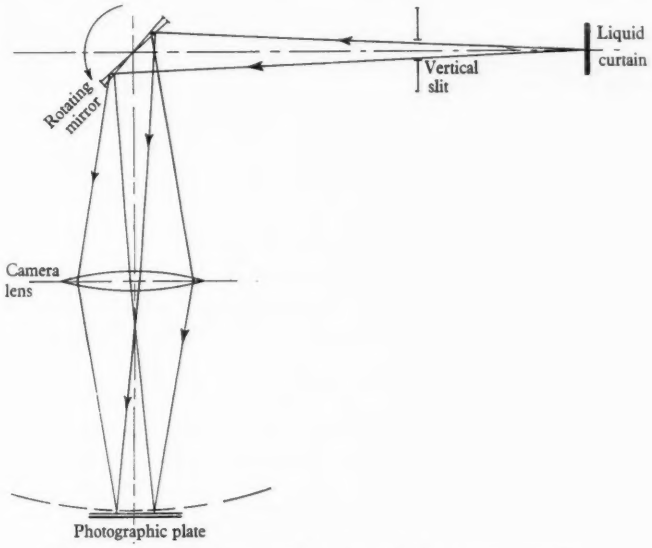

FIGURE 2. Optical system for the velocity measurements.

The flow rate and pressure drop across the slot for various slot widths and liquid viscosities were measured, and also the velocity of the liquid flowing in the curtain under various conditions. Some observations of the behaviour of the liquid as it impinged on the moving roll surface were recorded photographically.

The flow rate was determined by weighing the liquid collected in a weighed flask in a measured time, and the pressure drop by means of a Bourdon gauge calibrated against a mercury manometer, or for the lower pressures by means of a water manometer. The slot width was determined using a feeler gauge. The method used to measure the velocity of the liquid in the curtain was to photograph small air bubbles carried down with the curtain via a rotating plane mirror whose axis of rotation was in a vertical plane parallel with the curtain. In this way curves were obtained on the photographic plate, and from their slope the velocity of the bubble was calculated. This optical system is shown diagrammatically in figure 2 and typical photographic traces, which are effectively graphs of distance against time, are shown in figure 4, plate 1. The mirror was very care-

fully mounted on a platform running in ball-races and driven at approximately 4 r.p.m. by a geared motor, the essential object being to obtain a smooth rotation at constant speed. Attached to this platform was a cam arranged to trigger a relay which operated the camera shutter at the appropriate instant. The bubbles were illuminated by two photoflood lamps carefully arranged so as to produce traces that were as clear as possible, and in order to reduce the distortion on the plates due to the curved path of the image (as can be seen from figure 2) the object and image distance were made as large as possible compatible with the supplementary camera lenses available. By ensuring that the mirror and camera were correctly set up and aligned, a horizontal reference line was also traced on the plate from a small suitably illuminated object. Measurements were made directly from the plates using a Cambridge Universal Measuring Machine. As a check on the method, some photographs were taken of a $\frac{1}{16}$ in. steel ball-bearing freely falling from rest in air, an example of these being shown in figure 3, plate 1. The velocities at various depths obtained from the slopes of these traces were in close agreement with calculated values.

3. Results and discussion

3.1 *Properties of the liquid*

The density ρ of the liquid was 0·98 g/cm^3 and is taken as unity for the purpose of the following calculations. The surface tension T was measured to be 30 dyn/cm. As explained above, the viscosity η was varied over a wide range during the experiments.

3.2 *Pressure and flow-rate measurements*

For the range of viscosities, the pressure drops p required to achieve certain mean velocities u of the liquid through the slot (depth L) for various gap widths b were found to be in good agreement with values calculated from the following equation (see Lamb 1932, p. 582), which applies to the steady flow of liquid between two parallel planes:

$$p = \frac{12\eta L u}{b^2}. \tag{1}$$

In the present case $L = 0{\cdot}9$ cm. Expressing the velocity in terms of the mass flow rate Q per unit span in g/sec per cm, and writing p' for the pressure measured in cm of mercury, we have

$$p' = 8{\cdot}1 \times 10^{-4} \frac{\eta Q}{\rho b^3}, \tag{2}$$

with η in poise and b in cm, and with $\rho \div 1$.

Thus, knowing the dimensions of the slot, assuming it has parallel sides, we can obtain the flow rate directly from the pressure drop across it for a liquid of any viscosity and density. The presence of the curtain does not significantly affect the behaviour of the liquid flowing through such a slot.

3.3 *Velocity measurements*

Some traces obtained by the rotating mirror method are shown in figures 3 and 4, plate 1. Figure 3 shows the trace of a freely falling ball-bearing, and figure 4 typical bubble traces in curtains of low and high viscosity liquid, the slot velocity

in these latter cases being similar. Comparison of these photographs shows that with a liquid of low viscosity the velocity at a given depth is approximately that which would be expected from free fall under gravity, but for higher viscosities it is lower.

This difference at higher viscosities is shown more clearly in table 1 where the velocity as measured at a depth of 5 cm below the slot is compared with that calculated assuming free fall with an initial velocity equal to that of the liquid in the slot (the mean slot velocities were calculated from the flow rates and slot widths). To determine more generally the magnitude of this viscosity effect, the velocities u at various distances x below the slot were measured from the

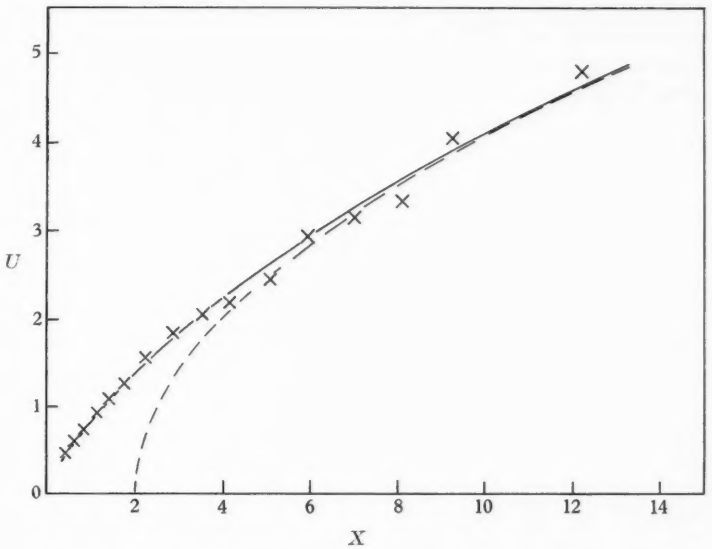

FIGURE 5. Graph of curtain velocity against distance from the slot; ×, experimental results; ---, free-fall parabola.

plates, and the values converted into the dimensionless forms U and X respectively by use of the following expressions (see Appendix):

$$U = \left[\frac{\rho}{4\eta g}\right]^{\frac{1}{3}} u, \tag{3}$$

$$X = \left[\frac{\rho}{4\eta}\right]^{\frac{2}{3}} g^{\frac{1}{3}} x. \tag{4}$$

The curves of U against X obtained from these figures were of the form shown in figure 5, which is for the particular case of a liquid of viscosity 2·6 poise passing through the slot with negligibly small velocity. These curves agree closely with a curve Maruo (1958) obtained by numerical solution of Sir Geoffrey Taylor's equation for a falling sheet of viscous fluid, equation (12) in the Appendix. The curve corresponding to free fall from rest, i.e.

$$U^2 = 2X, \tag{5}$$

was then superimposed on these experimental curves and found to coincide in general with them, for other than small values of X, after displacing its origin to $X = 2$, and making due allowance for the initial slot velocity. This curve is shown as the broken line in figure 5. This means that the velocity attained by the liquid in the curtain after travelling a distance x is that which would have been attained by a body falling freely through a distance $(X-2)$. Converting into cm, we have that this equivalent distance $x_{\text{equiv.}}$ is less than the true distance x travelled by an amount

$$x - x_{\text{equiv.}} = 2(4\eta/\rho)^{\frac{2}{3}} g^{-\frac{1}{3}} \doteq 0{\cdot}5\,(\eta/\rho)^{\frac{2}{3}}. \tag{6}$$

Thus the velocity u at a depth x in the curtain for a liquid passing through the slot with a mean velocity u_0 can be expressed by

$$u^2 = u_0^2 + 2g\,[x - 0{\cdot}5\,(\eta/\rho)^{\frac{2}{3}}]. \tag{7}$$

Some values of u calculated from equation (7) for $x = 5$ are given in table 1 and can be seen to agree quite well with the experimental values.

Viscosity (poise)	Slot width (mm)	Mean slot velocity (cm/sec)	Velocity at 5 cm below slot (cm/sec): Experimental	Velocity at 5 cm below slot (cm/sec): Assuming free fall	Velocity at 5 cm below slot (cm/sec): Calculated from equation (7)	Qu at base of curtain (17·8 cm long)
1·2	0·6	18	96	101	95	200
1·5	0·6	56	110	114	108	645
1·95	0·2	38	100	106	99	142
2·0	0·2	47	109	110	102	177
2·6	0·6	18	97	101	91	197
2·7	0·3	33	93	104	95	183
2·8	0·3	13	87	100	90	71
3·45	0·6	6	86	99	87	65
3·7	1·5	5	86	99	86	136
5·3	1·5	12	85	100	83	322
9·9	0·6	8	75	99	73	85

TABLE 1

3.4 *Flow rate and stability of curtain in contact with a moving surface*

For a free edge of a thin sheet of moving liquid to exist, equilibrium must be maintained at the edge between the surface tension and the inertia forces of the liquid. Let AB (figure 6) represent such a free edge between a liquid and air. Considering a unit length CD of the edge whose thickness is t, let the velocity of the liquid at the boundary in the direction normal to AB be u. The mass of liquid arriving at CD per second is Q, and its momentum $\rho u^2 t$ (since $Q = \rho u t$). As this momentum is destroyed at the boundary there is a resultant force $\rho u^2 t$, which for equilibrium must be balanced by the surface tension force; i.e.

$$\rho u^2 t = 2T, \tag{8}$$

or

$$Qu = 2T. \tag{9}$$

These equations give the limiting condition for 'stability' at any point in the curtain, in the sense that if a free edge appears by the formation of a hole in the

curtain, then if Qu is greater than $2T$ such a hole will not grow but will be carried away with the curtain, whereas if Qu is less than $2T$ it will grow and disrupt the curtain.

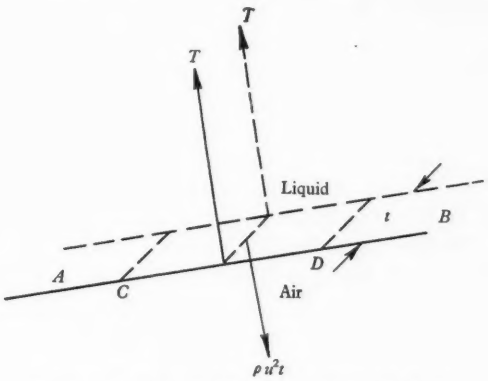

FIGURE 6. Forces at free edge of liquid sheet.

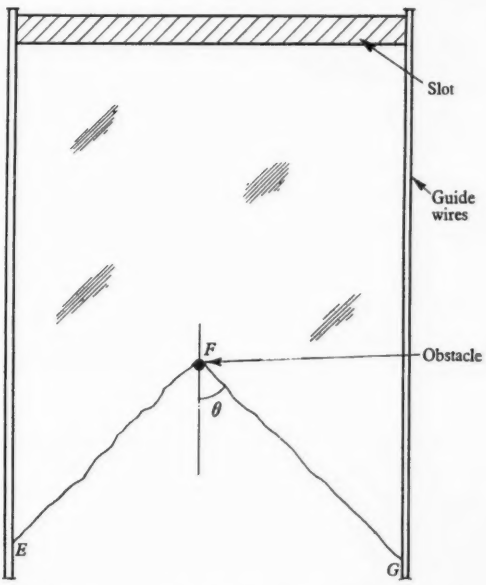

FIGURE 7. Breaking of the curtain round an obstacle.

The theory may be illustrated by introducing an obstacle such as a rod into the curtain and making the liquid flow past it as indicated in figure 7. The component of the velocity, across unit length of the boundary EFG, at any point is $u \sin\theta$ (where u is the velocity in the vertical direction); and hence, from equation (9),

$$\sin\theta = 2T/Qu.$$

In the limit, i.e. when $\theta = 90°$, we have again $Qu = 2T$.

That Qu should be greater than $2T$ near the line of impingement of the curtain with some object is illustrated by the figures in the last column of table 1; the runs in this set with viscosities 2·8, 3·45 and 9·9 poise being with the flow rate near the minimum value ($2T = 60$). For the curtain to be completely stable, that is, free of any tendency for holes to appear spontaneously, Qu must everywhere be greater than $2T$; it was found, however, that a curtain in which Qu was less than $2T$ over a *limited* region near the slot could apparently remain intact, though clearly any hole formed in this metastable region will grow and break the curtain.

By allowing the curtain to fall on to the rotating roll, it was found that under suitable conditions a continuous film could be uniformly laid down on a rapidly moving surface. These conditions are as follows.

(i) For a moderate length curtain such as would be employed industrially, the value of Qu should be greater than $2T$ near the line of impingement of the curtain with the moving surface, since otherwise the disturbance of the flow at the point of impingement will break the curtain.

(ii) The curtain should be protected from air currents carried along with the moving surface. Figure 8 (*a*), plate 2, shows the film being disturbed by such an air current, and figure 8 (*b*) how this can be obviated by the presence of a screen held in contact with the surface immediately behind the curtain. The sharpness of the line of contact of the curtain with the moving surface is remarkable, as can be seen in figure 8 (*b*), and it seemed little affected by the speed of the surface up to 600 cm/sec; at lower surface speeds the air disturbance was less obvious, as might be expected.

(iii) The impingement velocity of the curtain should be above a certain value (of the order of 130 cm/sec) which is apparently independent of the speed of the surface. In figure 8, plate 2, the impingement velocity was 140 cm/sec, but on reducing this to 100 cm/sec, by decreasing the curtain height, it was not possible to obtain a sharp line of contact on the moving surface. This is shown in figure 9, plate 2. Under these conditions the air screen had little effect.

4. Conclusions

(i) A thin curtain of liquid produced by pumping the liquid through a slot suffers from inherent instability in the region near the slot unless the velocity everywhere outside the slot is greater than $2T/Q$. This instability can be avoided by sufficiently increasing the flow rate.

(ii) Small-scale experiments indicate that it is possible to lay down a thin continuous film of liquid on to a rapidly moving surface from a curtain which may be in a metastable condition over a limited region near the slot.

The author is indebted to Sir Geoffrey Taylor for considerable help and encouragement in carrying out this work.

FIGURE 3. Rotating mirror photograph of freely falling ball-bearing.

(*a*)

(*b*)

FIGURE 4. Rotating mirror photographs of bubbles in a curtain of (*a*) low viscosity liquid, and (*b*) high viscosity liquid.

(*Facing p.* 304)

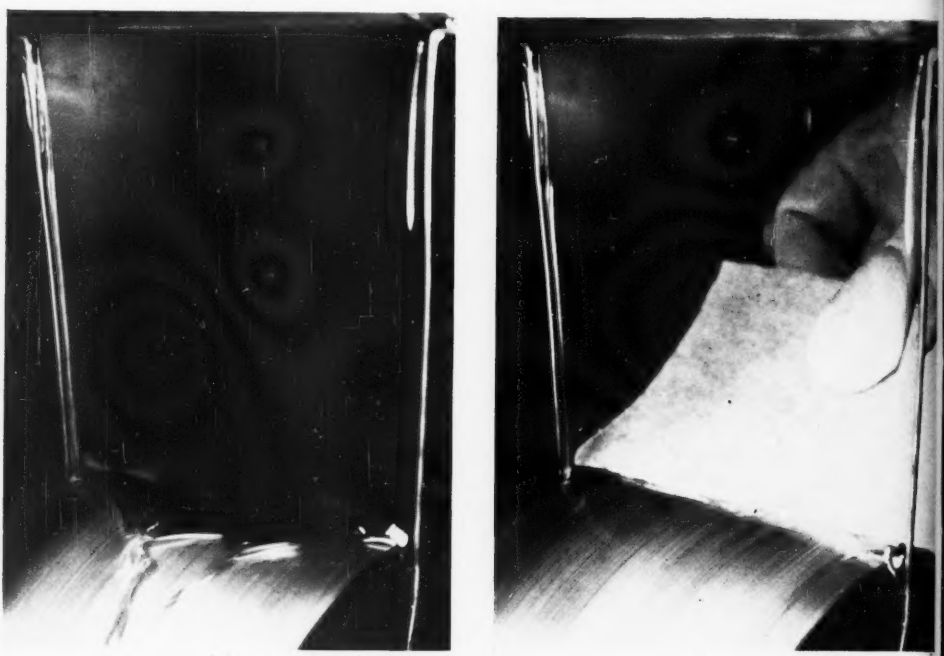

(*a*) (*b*)

FIGURE 8. Effect of the 'air screen'; curtain falling on to a surface moving at 500 cm/sec with an impingement velocity of 140 cm/sec.

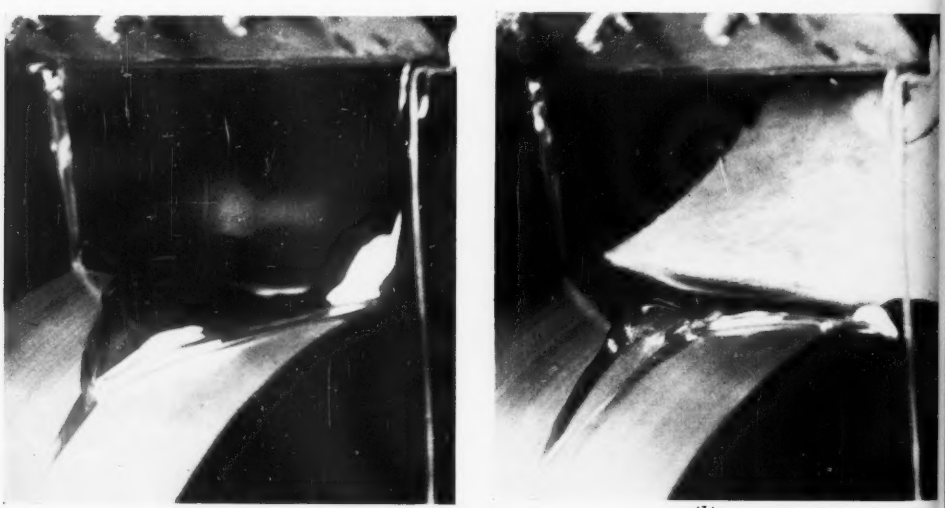

(*a*) (*b*)

FIGURE 9. Effect of reducing the impingement velocity of the curtain; curtain falling on to a surface moving at 500 cm/sec with an impingement velocity of 100 cm/sec.

Appendix

Calculation by Sir Geoffrey Taylor

When the liquid comes down from the slot, the velocity of the flow increases according to the acceleration of gravity. If only the inertia of the liquid is taken into account, the velocity is proportional to the square root of the distance through which the liquid has come down. Since the flux through any section of the jet must be constant, a contraction of the jet is observed which gives a deformation of the liquid resulting in a viscous stress. This stress has an effect upon the velocity of the flow and may be calculated as follows.

Taking the x-axis in the direction of the flow, we have that the stress components are

$$X_x = -p + 2\eta \frac{\partial u}{\partial x}, \quad Y_y = -p + 2\eta \frac{\partial v}{\partial y}, \quad Z_z = -p,$$

where $p = -\frac{1}{3}(X_x + Y_y + Z_z)$ is pressure and it is assumed that $W \equiv 0$ everywhere, because of the guide wires. If the effect of surface tension is neglected and it is assumed that everywhere $u \gg v$, then $Y_y = \text{const.}$, so that, if the atmospheric pressure is p_0, $Y_y = -p_0$. Since

$$\frac{\partial u}{\partial x} = -\frac{\partial v}{\partial y},$$

then

$$X_x = -p_0 + 4\eta \frac{\partial u}{\partial x}. \tag{10}$$

Let the thickness of the sheet be t at a depth x from a fixed level. Then

$$\rho u t = Q = \text{const.} \tag{11}$$

The equation of motion becomes

$$Q \frac{\partial u}{\partial x} = \frac{\partial}{\partial x}(tX_x) + t\rho g,$$

or, on substitution of (10) and (11) and division by Q,

$$\frac{\partial u}{\partial x} = \frac{4\eta}{\rho} \frac{\partial}{\partial x}\left(\frac{1}{u}\frac{\partial u}{\partial x}\right) + \frac{g}{u}.$$

This equation can be put into non-dimensional form by substituting the following expressions:

$$u = \left(\frac{4\eta g}{\rho}\right)^{\frac{1}{3}} U, \quad x = \left(\frac{4\eta}{\rho}\right)^{\frac{2}{3}} g^{-\frac{1}{3}} X.$$

On rearrangement this gives

$$\frac{d}{dx}\left(\frac{1}{U}\frac{dU}{dX}\right) + \frac{1}{U} - \frac{dU}{dX} = 0. \tag{12}$$

REFERENCES

Bardin, P. C. 1958 *Industr. Finish (Mag.), Sept.*, p. 8.

Dombrowski, N. & Fraser, R. P. 1954 *Phil. Trans.* A, **247**, 101.

Fraser, R. P., Eisenklam, P. & Dombrowski, N. 1957 *Brit. Chem. Eng.* **2**, 414.

Lamb, H. 1932 *Hydrodynamics*, 6th ed. Cambridge University Press.

Maruo, H. 1958 Private communication from Sir Geoffrey Taylor.

Stein, W. & Podmore, E. 1959 *Sheet Metal Ind.* **381**, 44.

Taylor, G. I. 1959 *Proc. Roy. Soc.* A, **253**, 313.

Slow flow past ellipsoids of revolution

By D. R. BREACH
Department of Mathematics, University of Melbourne*

(Received 28 June 1960 and in revised form 11 November 1960)

The results of Proudman & Pearson (1957) for a sphere are generalized to apply to all ellipsoids of revolution both prolate and oblate.

1. Introduction

The two classical methods, those of Stokes (1851) and Oseen (1910), for finding approximations to viscous streaming at low Reynolds numbers have both been applied to the problem of determining the flow past an ellipsoid in a uniform stream. By using the first method Oberbeck (1876) obtained a first approximation for any ellipsoid at any orientation to a uniform stream. For the particular cases of bodies with rotational symmetry about an axis parallel to the stream the results can be expressed in terms of a Stokes stream function, ψ. Thus, for a prolate spheroid of eccentricity e and with semi-major axis of unit length in a stream of velocity U, Oberbeck's result becomes

$$\psi = \tfrac{1}{2}U\left\{(r^2-e^2) - \frac{\left[e(1-e^2)r - \tfrac{1}{2}(1+e^2)(r^2-e^2)\log\left(\frac{r+e}{r-e}\right)\right]}{\left[e - \tfrac{1}{2}(1+e^2)\log\left(\frac{r+e}{r-e}\right)\right]}\right\}\sin^2\theta, \quad (1.1)$$

where (r, θ, ϕ) are prolate spheroidal coordinates. Oseen's method was applied by him to many similar cases the results for which are collected in his book of 1927. This paper gives the results of attempting to find higher approximations for slow flow past ellipsoids of revolution by a technique which combines Stokes's and Oseen's methods. This technique has been used by Proudman & Pearson (1957) and Kaplun & Lagerstrom (1957) to obtain higher approximations to the flow past a sphere and circular cylinder.

The Stokes approximation breaks down in the outer region where the neglected inertia terms are comparable in magnitude with the retained viscous terms. On moving away from the body this region is reached when $Rr = O(1)$, where R is the Reynolds number. In the technique mentioned above the co-ordinate system is then strained by taking new variables $\rho = Rr$ and $\Psi(\rho, \cos\theta) = R^2\psi(\rho, \cos\theta)$. Ψ is chosen so that there are no first-order terms in R in the transformed equations of motion. Expansions of the forms

$$\psi = \sum_{n=0}^{\infty} f_n(R)\,\psi_n(r, \cos\theta) \quad \text{and} \quad \Psi = \sum_{n=0}^{\infty} F_n(R)\,\Psi_n(\rho, \cos\theta), \quad (1.2)$$

where

$$\frac{f_{n+1}(R)}{f_n(R)} \to 0 \quad \text{and} \quad \frac{F_{n+1}(R)}{F_n(R)} \to 0 \quad \text{as} \quad R \to 0, \quad (1.3)$$

* Now at the Department of Applied Mathematics, University of Sheffield.

and F_0 and f_0 can be taken as bounded for small R, are assumed for ψ and Ψ. These are called the Stokes and Oseen expansions, respectively, after the leading terms in each. The no-slip condition on the body partially determines the ψ_n. The condition that the solution must tend to the uniform stream far out partially determines the Ψ_n. The ψ_n and Ψ_n are completely determined by matching the expansions (1.2) in orders of R as ρ becomes small and r becomes large. For this matching to be possible there must exist a region where the Oseen expansion and the Stokes expansion overlap. The existence of such a region is discussed by Kaplun & Lagerstrom (1957).

For a prolate spheroid with its axis along the uniform stream the following results in terms of non-dimensional variables have been found

$$\Psi = \tfrac{1}{2}\rho^2(1-\mu^2) - R\frac{B}{6}\{1-\exp[-\tfrac{1}{2}\rho(1-\mu)]\}(1+\mu) + O(R^2) \tag{1.4}$$

and

$$\psi = \left\{\tfrac{1}{2} + R\frac{B}{48} + R^2\log R\frac{B^2}{720}\right\}\left\{(r^2-e^2) - \frac{Br}{6} + \frac{B(1+e^2)}{6e}V_1(r/e)\right\}(1-\mu^2) + R\sum_{m=1}^{\infty} X_{2m}(r,e)\,U_{2m}(\mu) + O(R^2), \tag{1.5}$$

where

$$B = 24e^3\left\{(1+e^2)\log\left(\frac{1+e}{1-e}\right) - 2e\right\}^{-1}, \tag{1.6}$$

$\mu = \cos\theta$ and the Reynolds number, R, is Ua/ν, where ν is the kinematic viscosity and a is the semi-major axis of the ellipsoid. The functions $U_n(x)$ and $V_n(x)$ are defined by

$$U_n(x) = \int_1^x P_n(y)\,dy \quad \text{and} \quad V_n(x) = \int_x^\infty Q_n(y)\,dy, \tag{1.7}$$

where $P_n(y)$ and $Q_n(y)$ are Legendre's functions of the first and second kind of the nth degree. X_{2m} is a complicated function of r and e which is $O(r^{-2m+4})$ for large r. Its structure is given more explicitly below in §4.

2. The equations of motion and the Oseen terms

Prolate spheroidal coordinates are related to rectangular cartesian coordinates by the equations

$$\left.\begin{aligned} x &= \sqrt{(r^2-d^2)}\sin\theta\cos\phi, \\ y &= \sqrt{(r^2-d^2)}\sin\theta\sin\phi, \\ z &= r\cos\theta, \end{aligned}\right\} \tag{2.1}$$

where r is the semi-major axis of the prolate spheroid which passes through (x,y,z) and θ is the eccentric angle of that point with respect to the ellipse in which a plane through the axis of symmetry cuts the spheroid. ϕ corresponds to the azimuthal angle of spherical polars. The spheroids are confocal with foci $(0, 0, \pm d)$.

If the flow under consideration is that past a stationary prolate spheroid of semi-major axis a and eccentricity e with its centre at the origin and its axis of symmetry parallel to an otherwise undisturbed uniform stream of velocity U, then non-dimensional (primed) variables can be defined by

$$r = ar', \quad \psi = a^2U\psi', \quad \mu = \mu'. \tag{2.2}$$

Further, if the foci of the ellipsoid coincide with the foci of the coordinate system then $d = ae$. The Navier–Stokes equations for incompressible, steady, viscous flow then yield, on dropping the primes and introducing a new dependent variable l,

$$E_r^2 \psi = -(r^2 - e^2)(r^2 - e^2\mu^2)(1-\mu^2) l \tag{2.3}$$

and

$$\bar{E}_r^2 l = R \frac{\partial(\psi, l)}{\partial(r, \mu)}, \tag{2.4}$$

where

$$E_r^2 \equiv (r^2 - e^2)\frac{\partial^2}{\partial r^2} + (1-\mu^2)\frac{\partial^2}{\partial \mu^2} \tag{2.5}$$

and $\bar{E}_r^2$ is the adjoint operator

$$(r^2 - e^2)\frac{\partial^2}{\partial r^2} + (1-\mu^2)\frac{\partial^2}{\partial \mu^2} + 4r\frac{\partial}{\partial r} - 4\mu\frac{\partial}{\partial \mu}. \tag{2.6}$$

The variables in these equations are called Stokes variables. The dependent variable l which has been introduced for convenience in solving the equations of motion can be identified physically as the vorticity at a point divided by the distance of that point from the axis of symmetry and may thus be called ring vorticity strength. It will have an expansion of the form

$$l = \sum_{n=0}^{\infty} f_n(R)\, l_n(r, \mu). \tag{2.7}$$

If the Oseen variables, ρ, L, Ψ given by

$$\rho = Rr, \quad \Psi = R^2\psi, \quad L = l \tag{2.8}$$

are used then the equations of motion become

$$(\rho^2 - R^2e^2)\frac{\partial^2 \Psi}{\partial \rho^2} + (1-\mu^2)\frac{\partial^2 \Psi}{\partial \mu^2} = -(\rho^2 - R^2e^2)(\rho^2 - R^2e^2\mu^2)(1-\mu^2) R^{-2} L \tag{2.9}$$

and

$$(\rho^2 - R^2e^2)\frac{\partial^2 L}{\partial \rho^2} + 4\rho\frac{\partial L}{\partial \rho} + (1-\mu^2)\frac{\partial^2 L}{\partial \mu^2} - 4\mu\frac{\partial L}{\partial \mu} = \frac{\partial(\Psi, L)}{\partial(\rho, \mu)}. \tag{2.10}$$

By noting that terms in R^2e^2 in (2.9) and (2.10) may be neglected if a solution correct to $O(R)$ in R is sought, the analysis for the first two Oseen terms reduces to that for the sphere case. The constant B appears in (1.4) as a result of matching with the Stokes expansion. The Oseen terms will therefore not be further discussed.

3. The leading Stokes terms

If $f_0(R) = 1$ then from (1.2), (2.3) and (2.4) an appropriate general solution for l_0 finite on $\mu = \pm 1$ and bounded for small R at large values of r is

$$l_0 = \sum_{n=1}^{\infty} \frac{B_n V_n(\tau)\, U_n(\mu)}{e^4(\tau^2 - 1)(1-\mu^2)}, \tag{3.1}$$

where $\tau = re^{-1}$ and the B_n are constants. By use of the recurrence relationship

$$(2n+1)\mu U_n(\mu) = (n+2)\, U_{n+1}(\mu) + (n-1)\, U_{n-1}(\mu) \tag{3.2}$$

and the variation-of-parameters technique this leads to

$$\psi_0 = \sum_{n=1}^{\infty} \left\{ U_n(\tau) \left[\frac{B_{n+2} v_n^2(\tau)}{(2n+5)(2n+3)} - \frac{2B_n v_n^0(\tau)}{(2n+3)(2n-1)} + \frac{B_{n-2} v_n^{-2}(\tau)}{(2n-1)(2n-3)} \right.\right.$$
$$\left. - B_n \int_{e^{-1}}^{\tau} \frac{[V_n(x)]^2}{n(n+1)}\, dx \right] - V_n(\tau) \left[\frac{B_{n+2} u_n^2(\tau)}{(2n+5)(2n+3)} - \frac{2B_n u_n^0(\tau)}{(2n+3)(2n-1)} \right.$$
$$\left.\left. + \frac{B_{n-2} u_n^{-2}(\tau)}{(2n-1)(2n-3)} - B_n \int_{e^{-1}}^{\tau} \frac{U_n(x) V_n(x)}{n(n+1)}\, dx \right] \right\} n^2(n+1)^2 U_n(\mu), \quad (3.3)$$

where
$$v_n^m(\tau) = \int_{e^{-1}}^{\tau} \frac{V_n(x) V_m(x)}{(x^2-1)}\, dx,$$

$$u_n^m(\tau) = \int_{e^{-1}}^{\tau} \frac{U_n(x) V_m(x)}{(x^2-1)}\, dx$$

and $B_0 = B_{-1} = B_{-2} = 0$.

This satisfies the boundary conditions $\psi = \psi_r = 0$ on $r = 1$. Because of the behaviour of $V_n(\tau)$ at infinity the integrals $v_n^m(\tau)$, $u_n^2(\tau)$ and $\int_{e^{-1}}^{\tau} [V_n(x)]^2\, dx$ are convergent as $\tau \to \infty$. The integrals u_n^0, u_n^{-2} and $\int_{e^{-1}}^{\tau} U_n(x) V_n(x)\, dx$ are of orders $\log \tau$, τ^2 and τ^2, respectively. However, in (3.3) they are multiplied by $V_n(\tau)$ which is $O(\tau^{-n})$ and therefore far out the product of $V_n(\tau)$ and its cofactor in (3.3) is $O(\tau^{-2n+4})$.

When the integrals in the cofactor of $U_n(\tau)$ in (3.3) are evaluated at their upper limits the result is a function which is $O(\tau^{-2n+1})$ for large τ. When this is multiplied by $U_n(\tau)$, which is $O(\tau^{n+1})$, the resulting contribution to ψ_0 is a term $O(\tau^{-n+2})$ and this is not large enough to affect the matching process. However, when the integrals in the cofactor of $U_n(\tau)$ are evaluated at their lower limits the result is a constant. This implies that if ψ_0 is expressed in Oseen variables then the function $U_n(\tau)$ with its cofactor will contribute a term $O(R^{-n+1})$ to Ψ. But $\Psi = O(1)$ for small R. Therefore the constant must be zero for $n > 1$. Hence

$$\frac{B_{n+2} v_n^2(\infty)}{(2n+5)(2n+3)} - \frac{2B_n v_n^0(\infty)}{(2n+3)(2n-1)} + \frac{B_{n-2} v_n^{-2}(\infty)}{(2n-1)(2n-3)}$$
$$- B_n \int_{e^{-1}}^{\infty} \frac{[V_n(x)]^2}{n(n+1)}\, dx = 0 \quad (n \geqslant 2), \quad (3.4)$$

since all the integrals vanish at the upper limit if that limit is infinite.

Clearly the infinite set of linear equations (3.4) can be divided into two independent subsets, one involving all the odd B_n's only and the other involving all the even B_n's only. The set for the odd B_n's is not complete because the contribution of Ψ_0 to ψ, namely $\frac{1}{2}r^2(1-\mu^2)$, has not yet been matched to $O(1)$ in R with ψ_0. When this is done a further equation for B_1 and B_3 is obtained. This is

$$\int_{e^{-1}}^{\infty} \{(5x^2-1) V_1(x) B_1 - \tfrac{2}{7} V_3(x) B_3\} \frac{V_1(x)}{(x^2-1)}\, dx = 5e^2. \quad (3.5)$$

When the help of the recurrence relationship (3.2), which is true in general for $V_n(\tau)$, the case $n = 1$ being exceptional, it can now be shown that for the odd B_n's

$$B_{2m+1} = (2m+2)(2m+1)(4m+3)\left\{\frac{B_1}{6} - M\sum_{s=0}^{m-1}\frac{(2s)!\,(4s+5)}{(2s+4)!\,v_{2m+1}^2(\infty)}\right\},$$

where
$$M = \frac{B_1}{5}\int_{e^{-1}}^{\infty}\{(5x^2-1)V_1(x) - 4V_3(x)\}\frac{V_1(x)}{(x^2-1)}\,dx - e^2.$$

An investigation of the convergence of the odd terms of l_0 shows that the only solution which remains bounded in the field of the flow is that for which $M = 0$. It then follows that

$$B_1 = eB \quad \text{and} \quad B_{2m+1} = (2m+2)(2m+1)(4m+3)\frac{B_1}{6}. \tag{3.6}$$

A similar investigation for the even B_n's shows that the only possible solution to fit the physical conditions is

$$B_{2m} = 0. \tag{3.7}$$

The cofactor of $U_n(\tau)$ in (3.3) then vanishes identically for $n \geqslant 2$ by (3.6), (3.7) and (3.2). The same is true of the cofactor of $V_n(\tau)$ $(n \geqslant 2)$ and by the special case of the recurrence relationship for $V_n(\tau)$ when $n = 1$ it is found that

$$\psi_0 = \frac{1}{2}\left\{(r^2-e^2) - \frac{Br}{6} + \frac{B}{6e}(1+e^2)V_1(r/e)\right\}(1-\mu^2), \tag{3.8}$$

which, since

$$V_1(\tau) = \frac{1}{2}\left\{\tau - \tfrac{1}{2}(\tau^2-1)\log\left(\frac{\tau+1}{\tau-1}\right)\right\},$$

agrees with Oberbeck's result (1.1). Further, as $e \to 0$, $B \to 9$ and $e^{-1}V_1(\tau) \to \frac{1}{3}r$, so when the eccentricity is zero and the body is a sphere (3.8) simplifies to the classical Stokes result,

$$\psi_0 = \frac{1}{4}\left(2r^2 - 3r + \frac{1}{r}\right)(1-\mu^2). \tag{3.9}$$

4. The second Stokes terms

If it assumed that $f_1(R) = R$ then the equation for l_1 is

$$\bar{E}_r^2 l_1 = \frac{\partial(\psi_0, l_0)}{\partial(r,\mu)}. \tag{4.1}$$

If $\psi_0 = T(\tau)(1-\mu^2)$ then the Jacobian in (4.1) can be written

$$\frac{B}{6e^2}\sum_{m=1}^{\infty} 2m(2m+1)(4m+1)\frac{W_{2m}(\tau)}{(\tau^2-1)}\frac{U_{2m}(\mu)}{(1-\mu^2)},$$

where
$$W_{2m}(\tau) = 2(\tau^2-1)V_{2m}(\tau)\frac{d}{d\tau}\left\{\frac{\tau T(\tau)}{(\tau^2-1)}\right\} + V_{2m}'(\tau)\frac{d}{d\tau}\{(\tau^2-1)T(\tau)\}. \tag{4.2}$$

The appropriate general solution for l_1 is then found by variation of parameters to be

$$l_1 = \sum_{n=1}^{\infty}\{C_n V_n(\tau) + Y_n(\tau)\}\frac{U_n(\mu)}{e^4(\tau^2-1)(1-\mu^2)}, \tag{4.3}$$

where $C_{\pm}$ is a constant and $Y_n(\tau)$ is such that

$$Y_{2m}(\tau) = \frac{B}{6}(2m)^2(2m+1)^2(4m+1)\left\{U_{2m}(\tau)\int_{\infty}^{\tau}\frac{W_{2m}(x)V_{2m}(x)}{(x^2-1)}\,dx - V_{2m}(\tau)\int_{e^{-1}}^{\tau}\frac{W_{2m}(x)U_{2m}(x)}{(x^2-1)}\,dx\right\}$$

and
$$Y_{2m+1}(\tau) = 0. \tag{4.4}$$

For large τ, $Y_{2m}(\tau) = O(\tau^{-2m+2})$.

The general solution for ψ_1 satisfying the boundary conditions on the body is then

$$\begin{aligned}\psi_1 = \sum_{n=1}^{\infty}\Bigg\{&U_n(\tau)\left[\frac{C_{n+2}v_n^2(\tau)+y_n^2(\tau)}{(2n+5)(2n+3)} - \frac{2C_n v_n^0(\tau)+2y_n^0(\tau)}{(2n+3)(2n-1)}\right.\\ &\left.+\frac{C_{n-2}v_n^{-2}(\tau)+y_n^{-2}(\tau)}{(2n-1)(2n-3)} - C_n\int_{e^{-1}}^{\tau}\frac{[V_n(x)]^2}{n(n+1)}\,dx\right]\\ &-V_n(\tau)\left[\frac{C_{n+2}u_n^2(\tau)+z_n^2(\tau)}{(2n+5)(2n+3)} - \frac{2C_n u_n^0(\tau)+2z_n^0(\tau)}{(2n+3)(2n+1)}\right.\\ &\left.+\frac{C_{n-2}u_n^{-2}(\tau)+z_n^{-2}(\tau)}{(2n-1)(2n-3)} - C_n\int_{e^{-1}}^{\tau}\frac{U_n(x)V_n(x)}{n(n+1)}\,dx\right]\Bigg\}n^2(n+1)^2U_n(\mu),\end{aligned} \tag{4.5}$$

where
$$y_n^m(\tau) = \int_{e^{-1}}^{\tau}\frac{V_n(x)Y_m(x)}{(x^2-1)}\,dx,$$

$$z_n^m(\tau) = \int_{e^{-1}}^{\tau}\frac{U_n(x)Y_m(x)}{(x^2-1)}\,dx$$

and $C_0 = C_{-1} = C_{-2} = 0$.

As in ψ_0 the constant arising from the evaluation of the integrals in the cofactor of $U_n(\tau)$ in (4.5) at their lower limits must be zero for otherwise ψ_1 would contain terms $O(\tau^{2m+1})$ and would therefore contribute terms $O(R^{-2m+1})$ for small R to Ψ. This again leads to two infinite sets of linear equations for the constants C_n, one for the odd C_n's and one for the even ones. For the latter the only solution for which l_0 remains bounded near the body is given by

$$\begin{aligned}C_{2m+2} - \frac{(2m+3)(2m+2)(4m+5)}{(2m+1)(2m)(4m+1)}C_{2m} &= -y_{2m}^2(\infty) + \frac{(2m+3)(2m+2)(4m+5)}{(2m+1)(2m)(4m+1)}y_{2m+2}^{-2}(\infty)\\ \text{and}\qquad C_2\int_{e^{-1}}^{\infty}V_2(x)\,dx &= -y_2^0(\infty).\end{aligned} \tag{4.6}$$

By definition $Y_{2m+1}(\tau) = 0$ which means that the odd C_n's satisfy the same equations in general as do the odd B_n's in ψ_0. There is a further equation for B_1 and B_3 which comes from matching the term in ρ^2 in ψ_1 when expressed in Oseen variables with the term in ρ^2 in $F_1(R)\Psi_1$. This gives

$$C_1\int_{e^{-1}}^{\infty}(5x^2-1)V_1(x)\,dx - \tfrac{2}{7}C_3v_1^2(\infty) = \tfrac{5}{48}e^2B. \tag{4.7}$$

It is then found that the only solution for the odd C's is

$$C_1 = \frac{eB^2}{24} \quad \text{and} \quad C_{2m+1} = (2m+2)(2m+1)(4m+3)\frac{C_1}{6}. \tag{4.8}$$

The equation (4.5) then becomes

$$\psi_1 = \frac{B}{48}\left\{(r^2-e^2) - \frac{Br}{6} + \frac{B(1+e^2)}{6e}V_1(r/e)\right\}(1-\mu^2) + \sum_{m=1}^{\infty} X_{2m}(r,e)\,U_{2m}(\mu), \tag{4.9}$$

where $X_{2m}(r,e)$ stands for the coefficient of $U_{2m}(\mu)$ in (4.5).

5. The third Stokes terms

Proudman & Pearson in their treatment of the sphere case show that the assumption $f_2(R) = R^2$ leads to a particular integral for ψ_2 containing a term in $r^2 \log r U_1(\mu)$. They infer from this that the assumption about $f_2(R)$ should be amended to

$$f_2(R) = R^2 \log R \tag{5.1}$$

and that ψ_2 is then a multiple of ψ_0. It is easy to show by differentiation that if the particular integral for ψ_2 contains a term in $r^2 \log r U_1(\mu)$ then this term arises from a term in $r^{-2}U_1(\mu)(1-\mu^2)^{-1}$ on the right-hand side of the inhomogeneous equation for l_2 and only from a term of this form there. This suggests that in the present case it is necessary to expand the right-hand side of

$$\bar{E}_r^2 l_2 = \frac{\partial(\psi_0, l_1)}{\partial(r,\mu)} + \frac{\partial(\psi_1, l_0)}{\partial(r,\mu)} \tag{5.2}$$

(which equation arises if $f_2(R) = R^2$) in powers of τ and to select the term in $\tau^{-2}U_1(\mu)(1-\mu^2)^{-1}$, a knowledge of whose numerical coefficient enables one to determine what multiple of ψ_0 the term ψ_2 must be.

On performing the expansion it is found that the right-hand side of (5.2) contains the term

$$\frac{-B^2}{120e^2\tau^2}\frac{U_1(\mu)}{(1-\mu^2)} \tag{5.3}$$

and therefore, if $f_2(R) = R^2$, the general solution for ψ_2 will be of the form

$$\left\{D_1 U_1(\tau) - \frac{e^2B^2}{720}\tau^2 \log \tau\right\}(1-\mu^2) + \left\{\begin{matrix}\text{other functions of } \mu \text{ and } \tau \text{ not involving} \\ \text{the combination } \tau^2 \log \tau (1-\mu^2)\end{matrix}\right\}, \tag{5.4}$$

where D_1 is a constant.

But when this is expressed in Oseen variables it will contribute a term of order $R^2 \log R$ to Ψ and there are no such terms in the expansion of Ψ for small ρ. If there were such terms there would be terms of order $R \log R$ in L and these terms could not be matched since there are no terms of order $R \log R$ in l. Therefore

$$D_1 = -\frac{e^2B^2}{720}\log R + O(1) \tag{5.5}$$

and it must be assumed not that $f_2(R) = R^2$ but that (5.1) holds. ψ_2 is then a multiple of ψ_0 and by (5.5)

$$\psi_2 = \frac{B^2}{720}\left\{(r^2-e^2) - \frac{Br}{6} + \frac{B(1+e^2)}{6}V_1(r/e)\right\}(1-\mu^2). \tag{5.6}$$

6. Oblate spheroids

The equations of motion for an oblate spheroid can be derived from those for the prolate case by replacing r with ir. The appropriate general solutions then involve $U_n(i\tau)$ and $V_n(i\tau)$ which, from considerations of parity, are either real or purely imaginary. The boundary conditions on the surface of an oblate spheroid will be slightly different from those in the prolate case if the original definition of the Reynolds number is to be maintained throughout. The major axis of the axial section of an oblate spheroid is normal to the axis of symmetry whereas in the prolate case it is coincident with it. The member of the confocal family whose semi-major axis is unity is specified by $r = \sqrt{(1-e^2)}$ and consequently the boundary conditions on the body become

$$\psi = \frac{\partial \psi}{\partial r} = 0 \quad \text{on} \quad r = \sqrt{(1-e^2)}. \tag{6.1}$$

e	B (prolate)	b (oblate)
0·0	9·00	9·00
0·1	8·96	8·99
0·2	8·85	8·96
0·3	8·67	8·93
0·4	8·40	8·85
0·5	8·04	8·76
0·6	7·56	8·64
0·7	6·95	8·50
0·8	6·13	8·32
0·9	4·96	8·09
1·0	0·00	7·64

TABLE 1. Values of B and b.

With these modifications the analysis can proceed as before to give

$$\psi_0 = \frac{1}{2}\left\{(r^2+e^2) - \frac{br}{6} + \frac{ib}{6e} V_1(ir/e)\right\}(1-\mu^2), \tag{6.2}$$

where

$$b = 12e^3\left\{e\sqrt{(1-e^2)} + (2e^2-1)\arctan\frac{e}{\sqrt{(1-e^2)}}\right\}^{-1}. \tag{6.3}$$

When $e \to 0$, $b \to 9$ and the Stokes result is recovered as before.

One can proceed to higher approximations as in the prolate case the only essential difference in the analysis being the value of the constant b and the change in the lower limits of the particular integrals in the Stokes solutions due to the change in boundary conditions on the surface.

It is of some interest to calculate the constants B and b, for these give a rough indication of the degree of departure of the flow from that about a sphere taken as a norm. Values of B and b are given in table 1.

7. The drag coefficient

By observing that ψ_2 is a multiple of ψ_0 and that ψ_1 consists of a multiple of ψ_0 plus a function which is odd in μ and which therefore makes no contribution to the drag, the calculation of the drag coefficient C_0 is greatly simplified. It is found that for the prolate case

$$C_0 = \frac{2\pi B}{(1-e^2)R}\left\{1+\frac{BR}{24}+\frac{B^2}{360}R^2\log R+O(R^2)\right\} \tag{7.1}$$

and for the oblate case

$$C_0 = \frac{2\pi b}{3R}\left\{1+\frac{bR}{24}+\frac{b^2}{360}R^2\log R+O(R^2)\right\}. \tag{7.2}$$

The first two terms in each of these were given by Oseen (1927).

The oblate case $e = 1$ corresponds to a circular disk broadside on to the stream. If $e \to 1$ in (7.2) then the drag coefficient for this disk is

$$C_0 = \frac{16}{R}\left\{1+\frac{R}{\pi}+\frac{8R^2}{5\pi^2}\log R+O(R^2)\right\}. \tag{7.3}$$

For prolate bodies the case $e = 1$ corresponds to a needle of length two units lying along the axis of symmetry. From (7.1) the drag on this needle is predicted to be zero. This is a rather surprising result for it implies that although the fluid is brought to rest along a finite line segment by the imposition of the boundary conditions this has no effect on the uniform stream as a whole. Looked at in another way this means that any number of these needles could be placed in and parallel to a uniform stream without disturbing it. Of course, this needle is a highly idealized case, being an entity of finite length but no breadth. Further, for a body whose greatest diameter is comparable with the distance between neighbouring molecules of the fluid, the original equations of motion can scarcely be expected to hold but should be replaced by equations taking into account the properties of the medium considered as a collection of particles rather than as a homogeneous fluid.

This work was done with the aid of an Australian Commonwealth Post-Graduate Research Scholarship and a Research Grant from the University of Melbourne. I am particularly grateful for the impetus and inspiration given by Dr A. F. Pillow in the earlier part of my research period and for the criticism and advice given by Dr W. W. Wood later on and, more recently, by the referees.

REFERENCES

Kaplun, S. & Lagerstrom, P. 1957 *J. Math. Mech.* **6**, 585.
Kaplun, S. 1957 *J. Math. Mech.* **6**, 595.
Oberbeck, A. 1876 *Crelle*, **81**, 62.
Oseen, C. W. 1910 *Ark. Mat.* **6**, 29.
Oseen, C. W. 1927 *Hydrodynamik*. Leipzig: Akademische Verlagsgesellschaft.
Stokes, G. G. 1851 *Camb. Trans.* **9**, 8.
Proudman, I. & Pearson, J. R. A. 1957 *J. Fluid Mech.* **2**, 237.

REVIEWS

Non-Newtonian Fluids. By W. L. Wilkinson. London: Pergamon Press, 1960. 138 pp. 37*s.* 6*d.*

The need to study and explain the behaviour of anomalous, or non-Newtonian, fluids has been evident for many years. Nevertheless this study has so far remained almost a backwater of mechanics, and finds no place in formal teaching courses. This has been largely because of the great difficulties inherent in the mathematical formulation of the behaviour of any non-Newtonian fluid system; lack of a suitable theoretical background has hampered the systematic collection of experimental evidence on which the validity of any theory must ultimately rest.

The situation is further complicated by the enormous range of types of anomalous behaviour that have been observed, and by the variety of effects that result. The distinction between solids and fluids ceases to have any clear-cut significance. Hence categorization and suitable specialization become problems in themselves. This circumstance cannot be avoided by any author attempting to treat the subject, even though the normal restrictions of space may cause him to treat fully only a limited selection of individual topics.

The book under review has been written by a chemical engineer for students of chemical engineering. As such it fulfils its purpose very adequately; it will also be found very useful by non-specialists as an introduction to the simpler concepts and elementary mechanical principles of non-Newtonian flow. These obvious merits imply in this case a degree of superficiality: because of the undoubted problems that arise in a more comprehensive mechanical treatment of non-Newtonian flow, a critical account of the several chapters of this book is given below.

The first chapter is concerned, necessarily, with the classification of non-Newtonian fluids. The terminology adopted is as conventional as it could be, given the present stage of development of the subject; but this does not mean that it is a satisfactory terminology or that it is exhaustive. In particular, the author limits himself to a discussion of stress *vs* rate of strain laws for various bodies in *plane shear* only. Unfortunately this method fails to distinguish between many fluids of very different mechanical properties, properties—such as 'cross-elasticity'—which give rise to very different behaviour in more general types of flow (e.g. flow with a free surface, or flow past an obstruction). This severe limitation is maintained throughout the book; it is perhaps arguable that such a restriction is justified in a monograph for chemical engineering students, where the main application is to pipe flow, but the author should have made abundantly clear its restrictive nature. Mention should have been made of the results, if not the methods, of Oldroyd (*Proc. Roy. Soc.* A, **200**, 1950, 253), Truesdell (*J. Rat. Mech. Anal.* **1**, 1952, 125) and Rivlin (*J. Rat. Mech. Anal.* **4**, 1955, 681). That their work is of a highly complex mathematical nature does not absolve any would-be author from considering it, for their results are of fundamental

importance in the subject. The general dynamics of any fluid system must be based on tensor equations of state. Nothing less will do.

The treatment of visco-elastic fluids is rather unsatisfying. Only once, and then on page 37, long after the topic has been developed, is it explicitly stated that only the linear case is being considered. In other words only the 'Newtonian' approximation for fluids with a 'memory' is discussed. Much of the analytical discussion connecting creep functions and relaxation functions with generalized Maxwell or Voigt models is practically significant only for visco-elastic *solids* (i.e. materials for which the initial undeformed body geometry is crucially relevant throughout any experiment—and this is not in any sense an experiment into fluid behaviour). A further criticism is that many of the references are out of date, as a glance at the bibliography by anybody familiar with the literature will show. (For example the analysis of experimental data for visco-elastic systems in terms of linear Maxwell–Voigt models has been taken much further than the author suggests.)

The second chapter, on the experimental characterization of non-Newtonian fluids, provides a fairly comprehensive picture of the methods available for investigating non-Newtonian fluids. (The analytic definitions given in the first chapter are of just sufficient complexity to explain the type of behaviour quoted in the second.) There is, however, one curious lapse when the recovery curve in a creep-recovery experiment is stated to be a mirror image of the creep curve; this is never strictly true.

The third chapter, on the flow of non-Newtonian fluids in pipes and channels, is the most satisfactory of the book. It presents in a straightforward and elementary fashion those aspects of non-Newtonian flow that are relevant to pipe design. Friction factors and velocity profiles for steady laminar flow are given diagrammatically. The section on turbulent flow in pipes gives a good survey of recent work on the subject, in particular that of Metzner and co-workers. Here the author is evidently on familiar ground. The shorter sections on the extrusion of polymer melts and the rolling of plastics show less familiarity with the subject of polymer flow. The idealization chosen for flow in a single-screw extruder is an incorrect (and out-of-date) one in that it neglects the cross-flows (see, for example, *Industr. Engng Chem.* **51**, 1959, 765 and 841). Because of the critical effect of shear heating and of the shear and temperature-dependence of apparent viscosity, this error leads to major inaccuracies.

The following chapters, on heat-transfer and mixing characteristics, are a little sketchy but this only reflects the lack of good theoretical or experimental work on the subject. The final chapter is on viscometric measurements and apparatus.

A general impression given by parts of this book is of a lot of slightly undigested material being rather uncritically reported. This is a pity because it detracts from the merit of the more carefully written parts. The need for text-books on all the varied aspects of non-Newtonian flow has been felt for so long that any author attempting to fill the gaps is to be congratulated. Dr Wilkinson may not have produced a classical text on the mechanics of non-Newtonian fluids, but he has produced a book that should serve quite well as an introduction to the subject for students of engineering or chemical engineering. It is, moreover, pleasingly free from typographical errors.

J. R. A. Pearson

Heat Transfer. By ALAN J. CHAPMAN. The Macmillan Company, New York. 1960. 452 pp. 63*s*.

In the last few years many textbooks have been published which, like the one reviewed here, present the elements of heat transfer to senior undergraduate and first-year graduate students of engineering. One of the earliest, that by Eckert, has been widely imitated, both on content and in manner of treatment; the present book conforms to the same type. This reviewer greeted Eckert's book enthusiastically, and has welcomed, though with diminishing fervour, its emulators. Surfeit has, however, now produced its accustomed effect, and the reviewer proposes, with apologies to Professor Chapman for using his book as the occasion, to begin the review with some remarks which apply more or less to the whole class of books referred to.

The subject is presented as consisting of three sections: conduction, convection and radiation. On a superficial view it might seem that a review for the *Journal of Fluid Mechanics* could be restricted to the second of these. While pondering whether to make this restriction, the reviewer hit on one of the reasons for his growing dissatisfaction with the conventional treatment. It is that the books in question either obscure, or at least fail to exploit, the close relations which exist between the theory of heat conduction and the theory of momentum and heat transfer in the fluid-mechanical boundary layer.

These relations derive of course from similarities in the governing differential equations, which are parabolic, linear in some cases, non-linear in others, and are as follows.

For one-dimensional transient heat conduction with a uniformly distributed heat source

$$c\rho\frac{\partial T}{\partial t}=\frac{\partial}{\partial y}\left(k\frac{\partial T}{\partial y}\right)+Q. \tag{1}$$

For the development of the steady two-dimensional velocity boundary layer

$$\rho u\frac{\partial u}{\partial x}=\rho u\frac{\partial}{\partial \Psi}\left(\mu\rho u\frac{\partial u}{\partial \Psi}\right)-\frac{dp}{dx}. \tag{2}$$

For the development of the steady two-dimensional thermal boundary layer with a uniformly distributed heat source

$$c\rho u\frac{\partial T}{\partial x}=\rho u\frac{\partial}{\partial \Psi}\left(k\rho u\frac{\partial T}{\partial \Psi}\right)+Q. \tag{3}$$

Q is the strength of the heat source, Ψ is the stream function and the other notation is conventional.

The similarity between the equations has often been noted. Why then are the solutions to equation (1) not used as stepping-stones to those of equations (2) and (3)? To see how this might be done, let us consider the simple case in which the heat-source and pressure-gradient terms are absent.

Equation (1), with boundary conditions appropriate to a semi-infinite medium with fixed wall temperature T_w, has the solution

$$\frac{T-T_w}{T_\infty-T_w}=f\left(\frac{y}{2\sqrt{(k_\infty t/c\rho)}}\right). \tag{4}$$

The function f involves the error function if k is a constant; when k depends on temperature, however, the function must normally be determined numerically. This much usually appears in the conduction section of the textbook.

Since equation (2), without the dp/dx term, has the same form, the student can now easily be led to appreciate that its solution must be

$$\frac{u}{u_\infty} = f\left(\frac{\psi}{2\sqrt{(\mu\rho u_\infty x)}}\right), \tag{5}$$

where now, due to the non-linearity of the right-hand side of the differential equation, numerical evaluation is *essential*. There is nothing else new in the situation whatsoever.

Equation (3) likewise has the solution

$$\frac{T-T_w}{T_\infty - T_w} = f\left(\frac{\psi}{2\sqrt{(k_\infty \rho u_\infty x/c)}}\right). \tag{6}$$

If the conductivity is independent of temperature, and the velocity can be taken as uniform through the thermal boundary layer as is the case for fluids of low Prandtl number, f is again the complementary error function; the student has obtained his first solution to a convective heat transfer problem at no extra trouble.

Of the many further relations which can be developed between conduction and convection it should suffice to mention two. First, in conduction theory, Duhamel's theorem is usually presented, permitting equation (4) to be used (for constant conductivity) for the evaluation of the temperature distribution and heat transfer rate when the wall temperature varies with *time*. Discussion of this theorem can pave the way for a presentation of methods, such as those of Tribus and Klein, for the calculation of convective heat transfer when the wall temperature varies with *position*. Secondly, when the conducting medium is finite in extent, textbooks on conduction show how the temperature distribution can be expressed as the sum of an infinite series of eigenfunctions. In simple cases these are sines and cosines. The same is true of heat transfer into a fluid confined in a duct, the sole difference being that there, because of the non-uniform velocity distribution, the eigenfunctions do not usually have such a simple form.

Once these relations and possibilities have been recognized, books such as that under review can be irritating. The author presents only the eigenfunction type of solution for the heat conduction equation; for convective heat transfer he presents only solutions like that of equation (6). Again, for convection he introduces approximate methods of the so-called 'integral' type, and readers who suspect that the same techniques might be valuable in conduction problems are given no encouragement. Dimensional analysis is introduced towards the end of the section on convection by way of illustrations drawn from elementary mechanics; the dimensionless groups which have cropped up on almost every page of the conduction chapters are not even mentioned in this connexion.

From this point of view therefore the book must be regarded as unimaginative; the author has kept closely to the paths trodden by his predecessors without looking to right or left. Within these limitations, however, he has done a careful and painstaking job. For example, his derivation of the equations of motion of the boundary layer is more rigorous than in most works of this character; and many of the detailed infelicities of earlier authors are avoided. Minor blemishes

remain; for example, figure 6.10 (*c*) illustrates a boundary layer on a cylinder having zero thickness at the forward stagnation line, and on page 261 the author recommends, without comment, formulae for the local Nusselt number on cones which contain no mention of the cone angle.

In conclusion, the reviewer would like to suggest to publishers that the market for the present class of book is now saturated. What seem to be required in future are, on the one hand books which unify and so simplify the whole field of heat transfer, and on the other books which select one aspect of the subject and treat it much more thoroughly than has been attempted hitherto. D. B. SPALDING

Turbulence. An Introduction to Its Mechanism and Theory. By J. O. HINZE. New York: McGraw-Hill, 1959. 586 pp. $15.00 or £5. 16*s*. 6*d*.

A book on turbulence written for the beginner and also for many others who have their primary interest in the applications has been long awaited. The two excellent Cambridge Monographs (Batchelor 1953 and Townsend 1956) do not serve this purpose, since both were written more for an audience already familiar with the field and interested more in the inner workings of turbulence than in its gross effects on the mean values of the flow parameters.

Professor Hinze's book fills this demand largely, although not quite completely. The book is, of course, much longer than either of the above two monographs and the topics are handled with more attention to detail and to intermediate steps so it is easier reading for those who encounter the subject for the first time. It has certain value as a text-book, especially if used in a course on fluid mechanics for chemical engineers.

The author explains in the introduction that the book grew out of a lecture series given by him at the Royal Dutch Shell Laboratory in 1950. Most of the features of the book that may be criticized are a direct consequence of its origin. First, there is a great emphasis on phenomena important to chemical engineering; secondly, much more space is dedicated to the 'state of the art' as it was known before 1950 than to the later developments since that time.

The problem of turbulence in a compressible medium is almost completely ignored throughout. (There are some short remarks about 'effects of compressibility' but apparently these have been added only as an afterthought.) At one place (p. 131), the strange notion is proposed that turbulent density fluctuations in a compressible flow are uniquely related to the fluctuations of the velocity component in the mean flow direction and this is obviously wrong.

The reviewer also regrets that a vast array of applications in fields other than chemical engineering have not been included. More than anything else, this omission limits the usefulness of the book to serve as the principal text in a course on turbulence given for a group of graduate students as yet uncommitted to a more narrow field of specialization. Such a book is still awaited by those who have an active interest in teaching turbulence, both in theory and in applications. The interaction of turbulence with sound and some astrophysical or meteorological applications would have added much to the breadth of the book.

On the credit side, it must be acknowledged that the treatments of those topics that the author has decided to include are quite clear and skilful. The

book is non-partisan in the sense that Professor Hinze does not attempt to force some personal bias on the reader, and he does not attempt to promote his own favoured theories or interpretations. The chapters are distinct, some of them almost monographs in themselves, and each one merits a short separate account.

I. General introduction and concepts (69 pages). It introduces the statistical concepts such as correlation function, one-dimensional spectrum, and deals clearly with the difference between Lagrangian and Eulerian representations. It is well presented and easy to read even by the uninitiated.

II. Measurement of turbulent flows (68 pages). The author here gives a survey dealing mostly with the hot-wire anemometer. It is intended to familiarize the reader with the problem of turbulence measurement, but it does not serve as a text for the design of equipment or even for the performance of experiments with existing equipment without further study of other sources. The electronic circuitry is not treated at all and the measurements are concerned only with low-speed flows (both incompressible and slightly heated).

III. Isotropic turbulence (103 pages). This is a good, well-detailed account of this classical subject, and for the beginner it may be even easier reading than Batchelor's 1953 monograph.

IV. Non-isotropic turbulence (22 pages). This short chapter deals with homogeneous shear flow and its significance is minor.

V. Transport processes: turbulent flows (100 pages). This chapter in a way provides the *raison d'être* of the book. The material collected here is quite valuable as it is hard to find it elsewhere except scattered in the original publications. Naturally, often the treatment is still based on mixing-length concepts and there are many crude engineering approximations. It may be safely predicted, however, that it will become one of the sources quoted most often in the chemical engineering community as far as turbulence is concerned.

VI. Non-isotropic free turbulence (70 pages). VII. Non-isotropic wall turbulence (70 pages). Both of these chapters deal with shear flow turbulence. Although the flow configurations are largely identical with those treated in Townsend's 1956 book, the approach is quite different. Professor Hinze emphasizes the prediction of the effect of turbulence on mean qualities (diffusion and shear) and not as much the inner workings of the turbulent flow itself. Chapter VI deals with wakes and jets; chapter VII deals with boundary layers (with no pressure gradient) and turbulent pipe flow. From the point of view of applications to aerodynamics it would have been extremely useful to include the treatment of the turbulent boundary layer with a pressure gradient.

There is an appendix on Cartesian tensors and it is quite useful.

Probably the most important function of a book review is to allow the prospective reader to judge whether or not he should acquire the book. For those who use fluid mechanics in an applied field and want to learn something about turbulence, the book is quite valuable especially for those with chemical engineering leanings. For the student of turbulence it is quite useful as a reference on many applications. Professor Hinze has been quite successful in introducing turbulence to a new and growing group of engineering students.

L. S. G. Kovasznay

ARCHIVE
FOR
RATIONAL MECHANICS AND ANALYSIS

EDITED BY C. TRUESDELL

Editorial Board: R. Berker, L. Cesari, L. Collatz, A. Erdélyi, J. L. Ericksen, G. Fichera, R. Finn, Hilda Geiringer, H. Görtler, D. Graffi, A. E. Green, J. Hadamard, L. Hörmander, M. Kac, E. Leimanis, A. Lichnerowicz, C. C. Lin, W. Magnus, G. C. McVittie, J. Meixner, C. Miranda, C. B. Morrey, C. Müller, W. Noll, A. Ostrowski, R. S. Rivlin, M. M. Schiffer, J. Serrin, E. Sternberg, R. Timman, R. A. Toupin, C. Truesdell, H. Villat.

This journal fosters mathematical studies of fluid mechanics: On the one hand, researches on the newer theories of non-linear response, both for liquids and for gases, and of visco-elastic and memory effects, whether by phenomenological or by statistical methods; on the other hand, analytical problems arising in the classical theories of perfect or viscous or magnetised fluids. Now in its seventh volume, it has published such studies by A. E. Green, R. S. Rivlin, A. J. M. Spencer, J. Serrin, R. Finn, W. Noll, J. L. Ericksen, B. D. Coleman, C. C. Lin, G. S. S. Ludford, K. Nickel, H. Gloistehn, E. Ikenberry, J. Wolska-Bolchenek, to mention a few. Included are many of the sources cited in the articles on fluids in Flügge's "Encyclopedia of Physics".

About ten numbers, or two volumes are published per year.

The price is DM 96 per volume.

May be obtained through any scientific bookseller.

SPRINGER-VERLAG

BERLIN · GÖTTINGEN · HEIDELBERG

JOURNAL OF FLUID MECHANICS

Volume 10, Part 2 March 1961

CONTENTS

Deposition of a viscous fluid on the wall of a tube
by G. I. TAYLOR *page* 161

The motion of long bubbles in tubes
by F. P. BRETHERTON 166

The wave drag of wind over water
by R. W. STEWART 189

Unsteady interaction of a shock wave with a cellular vortex field
by J. E. WERNER 195

A non-linear theory for oscillations in a parallel flow
by D. J. BENNEY 209

The theory of the jet-flap for unsteady motion
by D. A. SPENCE 237

On the behaviour of liquid dispersions in mixing vessels
by REUEL SHINNAR 259

A study of the magnetohydrodynamic boundary layer on a flat plate
by M. B. GLAUERT 276

Singularities of attached shock waves in steady axially symmetric flow
by HENRI CABANNES and CLAUDE STAEL 289

A study of the behaviour of a thin sheet of moving liquid
by D. R. BROWN 297

Slow flow past ellipsoids of revolution
by D. R. BREACH 306

REVIEWS

Non-Newtonian Fluids 315

Heat Transfer 317

Turbulence. An Introduction to Its Mechanism and Theory 319

Printed in Great Britain at the University Press, Cambridge
(Brooke Crutchley, University Printer)